Technical Report Documentation Page

1. Report No.	2. Government Accession No.	3. Recipient's Catalog No.
TX-98/2911-4	-	

4. Title and Subtitle	5. Report Date
HIGH EARLY STRENGTH CONCRETE OVERLAY DESIGNS AND CONSTRUCTION METHODS FOR REHABILITATION OF CRCP	November 1996
	6. Performing Organization Code

7. Author(s)	8. Performing Organization Report No.
Norbert J. Delatte, Jr., David W. Fowler, and B. Frank McCullough	2911-4

9. Performing Organization Name and Address	10. Work Unit No. (TRAIS)
Center for Transportation Research The University of Texas at Austin 3208 Red River, Suite 200 Austin, TX 78705-2650	11. Contract or Grant No. 7-2911

12. Sponsoring Agency Name and Address	13. Type of Report and Period Covered
Texas Department of Transportation Research and Technology Transfer Section/Construction Division P.O. Box 5080 Austin, TX 78763-5080	Research Report (9/95 — 8/96)
	14. Sponsoring Agency Code

15. Supplementary Notes

Project conducted in cooperation with the Texas Department of Transportation.

16. Abstract

For rehabilitation of concrete pavements, resurfacing with a bonded concrete overlay (BCO) may provide significantly longer life and reduced maintenance costs. Two important issues are bonding and rapid reopening of resurfaced sections. The project objective was to determine a method or methods for constructing a bonded concrete overlay under extreme weather conditions in El Paso, Texas, that would ensure early opening to traffic and achieve design requirements for long-term performance, and to investigate methods of detecting and mapping delaminations nondestructively. A BCO test slab was designed and constructed for a full-scale test of feasible design and construction alternatives. The month of June was selected for the test because severe environmental conditions were expected. The experimental variables encompassed in eight test sections were reinforcement of concrete (plain, polypropylene fiber reinforced, and steel fiber reinforced), use of shear connectors (nails and anchors), reinforcement, surface preparation, and day or night construction. A weather station was used to record air temperature, relative humidity, and wind speed. By combining these data with concrete temperatures, evaporation rates could be calculated. Several nondestructive testing methods were used to detect and map delaminations. The results developed from the test are presented in terms of observations during construction, weather and slab temperatures, coring and pull-off testing, delamination detection, cracking, and slab loading. The early-age behavior and long-term performance of BCOs is reviewed, along with materials selection and mix design criteria. Recommendations are made for construction and quality control of BCOs for early opening to traffic.

17. Key Words	18. Distribution Statement
Bonded concrete overlays, early-age behavior of concrete, IH 10, El Paso, CRCP, long-term performance	No restrictions. This document is available to the public through the National Technical Information Service, Springfield, Virginia 22161.

19. Security Classif. (of report)	20. Security Classif. (of this page)	21. No. of pages	22. Price
Unclassified	Unclassified	218	

Form DOT F 1700.7 (8-72) Reproduction of completed page authorized

HIGH EARLY STRENGTH BONDED CONCRETE OVERLAY DESIGNS AND CONSTRUCTION METHODS FOR REHABILITATION OF CRCP

by

Norbert Joseph Delatte, Jr.
David W. Fowler
B. F. McCullough

Research Report 2911-4

Research Project 7-2911
Project Title: *Full-Scale Bonded Concrete Overlay on IH-10 in El Paso*

Conducted for the

TEXAS DEPARTMENT OF TRANSPORTATION

by the

CENTER FOR TRANSPORTATION RESEARCH
Bureau of Engineering Research
THE UNIVERSITY OF TEXAS AT AUSTIN

November 1996

IMPLEMENTATION RECOMMENDATIONS

The results of the research presented in this report may be used:

1. to recommend specifications for expedited bonded concrete overlays, and
2. to develop criteria for opening the overlayed sections to traffic.

The laboratory and field testing demonstrated that bonded concrete overlays may be opened to traffic as early as 12 hours after casting without damage to the overlay.

Several nondestructive testing methods for locating and mapping delaminations were investigated. Currently the most reliable method for thicker overlays is the impulse-response method. However, it is not suitable for large-scale sampling.

Sample specification recommendations and a monitoring and testing plan for IH-10 bonded concrete overlay construction are included in the appendices.

Prepared in cooperation with the Texas Department of Transportation.

DISCLAIMERS

The contents of this report reflect the views of the authors, who are responsible for the facts and the accuracy of the data presented herein. The contents do not necessarily reflect the official views or policies of the Texas Department of Transportation. This report does not constitute a standard, specification, or regulation.

There was no invention or discovery conceived or first actually reduced to practice in the course of or under this contract, including any art, method, process, machine, manufacture, design or composition of matter, or any new and useful improvement thereof, or any variety of plant, which is or may be patentable under the patent laws of the United States of America or any foreign country.

NOT INTENDED FOR CONSTRUCTION,
BIDDING, OR PERMIT PURPOSES

B. F. McCullough, P.E. (Texas No. 19914)
Research Supervisor

TABLE OF CONTENTS

SUMMARY

For rehabilitation of concrete pavements, resurfacing with a bonded concrete overlay (BCO) may provide significantly longer life and reduced maintenance costs. Two important issues are bonding and rapid reopening of resurfaced sections. The project objective was to determine a method or methods for constructing a bonded concrete overlay under extreme weather conditions in El Paso, Texas, that would ensure early opening to traffic and achieve design requirements for long-term performance, and to investigate methods of detecting and mapping delaminations nondestructively. A BCO test slab was designed and constructed for a full-scale test of feasible design and construction alternatives. The month of June was selected for the test because severe environmental conditions were expected. The experimental variables encompassed in eight test sections were reinforcement of concrete (plain, polypropylene fiber reinforced, and steel fiber reinforced), use of shear connectors (nails and anchors), reinforcement, surface preparation, and day or night construction. A weather station was used to record air temperature, relative humidity, and wind speed. By combining these data with concrete temperatures, evaporation rates could be calculated. Several nondestructive testing methods were used to detect and map delaminations. The results developed from the test are presented in terms of observations during construction, weather and slab temperatures, coring and pull-off testing, delamination detection, cracking, and slab loading. The early-age behavior and long-term performance of BCOs are reviewed, along with materials selection and mix design criteria. Recommendations are made for construction and quality control of BCOs for early opening to traffic.

CHAPTER 1. INTRODUCTION

Concrete pavements are subjected to traffic and environmental loadings that will, over time, cause distress and lead to a need for rehabilitation. Rehabilitation may be necessary because of structural inadequacy (inability to carry further loading) or functional inadequacy (poor ride quality). Alternatives for rehabilitation include removal and replacement of the pavement structure or placing an asphalt or concrete overlay. Overlays are generally much more economical than removal and replacement. Although asphalt overlays may have a lower initial cost, concrete overlays are more durable and may, thus, be more economical when life cycle costs and user costs are considered.

Concrete overlays may be of three types: unbonded, bonded, or partially bonded (Ref 1). An unbonded overlay is generally constructed over a badly deteriorated pavement, with a bond breaker used to prevent damage from the original pavement from causing similar cracking in the overlay or *reflecting* cracking in the overlay. In effect, the original pavement is used as high-quality support for the overlay, and the overlay becomes a new pavement. Thus, an unbonded overlay is designed as a pavement and will generally have to be as thick as, or thicker than, the original pavement. However, it may be possible for the designer to use the support provided by the original pavement to reduce the overlay thickness.

A bonded concrete overlay (BCO) is used to increase the thickness of the original pavement, thereby increasing stiffness and reducing pavement deflections and stresses. The stiffness of a concrete pavement is directly proportional to the cube of its thickness, and pavement stresses are inversely proportional to stiffness (Ref 2). Thus, a 25 percent increase in pavement thickness will lead to nearly doubling the pavement stiffness and reducing stresses by about one-half. This can be achieved by overlaying a 200 mm thick pavement with a 50 mm thick BCO. Since BCOs make full use of the remaining structural capacity of the original pavement, they are generally thinner than unbonded overlays. BCOs only 50 mm thick have been constructed. Thinner BCOs are often termed thin-bonded concrete overlays (TBCOs), although there is no general agreement on what the upper limit of thickness is for a TBCO.

For a BCO, the bond of the overlay to the original pavement is very important. If the bond is not achieved, the section will not behave compositely, and deflections and stresses will be higher than desired. Thus, the BCO may not achieve its design life. Problems with overlay delamination in the past have made some agencies reluctant to use BCOs (Refs 3, 4). Moreover, it is important to repair significant damage to the original pavement before placing a BCO; otherwise, the damage is likely to reflect through the BCO (Ref 5).

For partially bonded concrete overlays, no particular effort is made to either prevent or achieve bond. Although these are easier to construct than either unbonded overlays or BCOs, they may combine the worst features of both, and recent use of partially bonded concrete overlays has been limited.

There has been a significant increase in the use of BCOs, starting in the early 1970s, particularly in the states of Iowa, South Dakota, Texas, Kansas, Minnesota, and Missouri. Two important issues are bonding and rapid reopening of resurfaced sections. The use of BCOs can be expected to increase, particularly as the research becomes available to convince

transportation officials that bond can be ensured, and resurfaced pavements can be opened quickly to traffic (Ref 6).

1.1 RESEARCH OBJECTIVE

Research has been conducted at The University of Texas at Austin (UT) for the Texas Department of Transportation for a bonded concrete overlay for an 0.8 km section of IH-10 in downtown El Paso, Texas. The BCO is only 46 percent of the length of the rehabilitation; bridge clearance difficulties made full-depth replacement of the pavement in other parts of the project necessary. The original continuously reinforced concrete pavement (CRCP) was constructed in 1965 and has three lanes in each direction. In 1992, the average daily traffic was over 90,000 vehicles in each direction, with about 35 percent trucks. Since IH-10 is an important east-west route and El Paso is a major border city, a substantial number of heavy trucks pass through this downtown section (Ref 7). Traffic is expected to increase significantly with the adoption of the North American Free Trade Agreement.

Initially, a feasibility study (Ref 7) was conducted by the Center for Transportation Research (CTR) that concluded that a BCO was the optimum solution. Since the project was located in a mountain pass, alternate routes were not available. Thus, rapid opening to traffic was explored.

The project objective is to determine a method or methods for constructing a bonded concrete overlay under extreme weather conditions in El Paso, Texas, that would ensure early opening to traffic and achieve design requirements for long-term performance, and to investigate methods of detecting and mapping delaminations nondestructively.

To ensure satisfactory performance of a BCO, it is important to eliminate or limit cracking or, if cracking cannot be prevented, to prevent delamination. Previous research (Refs 3, 8, 9) has indicated that delamination probably begins within 48 hours of construction before traffic is allowed on the overlay. Thus, delamination is probably initiated by environmental effects.

The primary variables affecting performance of a BCO are the concrete mix design, the overlay thickness, the surface preparation, the reinforcement, placement and curing methods, and environmental conditions during placement and curing.

1.2 OBJECTIVE OF THIS REPORT

The objective of this report is to investigate concrete materials selection and mix design considerations, as well as construction methods, for high early strength BCOs for rehabilitation of CRCP. High early strength BCOs allow traffic to be returned to the pavement in 24 hours or less. To achieve this objective, six tasks had to be accomplished:

1. determine what concrete properties are desirable for the successful performance of expedited BCOs (early opening to traffic);
2. determine how concrete mixes should be engineered to achieve the required concrete properties for El Paso construction;

3. determine how flexural, compressive, bond strength, and thermal and shrinkage strains of these concrete mixes develop at early ages;
4. develop criteria based on material properties for early opening of BCOs to traffic;
5. develop one or more combinations of surface preparation, reinforcement, and curing to ensure successful performance of an accelerated construction BCO under hot and dry conditions; and
6. develop a mechanistic model for predicting performance based on material properties.

1.3 SCOPE

The scope of this investigation is limited to methods of constructing BCOs on continuously reinforced concrete pavement. Jointed pavements are not considered. However, some of the results of this research will be applicable to jointed pavements.

1.4 RESEARCH PLAN

This research study concentrated on five areas:

1. developing a mix design for BCO construction in El Paso,
2. investigating the bond and fatigue strength development of the mix design,
3. constructing and analyzing eight full-scale BCO test sections in El Paso,
4. modeling early-age behavior and long-term performance of BCOs, and
5. developing recommendations for high early strength mix designs.

1.5 FORMAT

This document is divided into thirteen chapters. Chapter 1 provides the introduction. Chapter 2 reviews previous research in expedited paving, BCOs, and expedited BCOs. Chapter 3 discusses the research leading up to the full-scale test. In Chapter 4, the experimental design of the full-scale test is summarized. Observations made during construction of the base slab for the BCO test sections are documented in Chapter 5. Results from the BCO test sections are presented in Chapter 6 and discussed along with results from the base slab in Chapter 7.

Chapter 8 reviews the behavior of BCOs at early ages, and Chapter 9 discusses long-term performance of BCOs. Materials selection and mix design criteria for improving BCO performance are presented in Chapters 10 and 11, respectively. Recommendations for IH-10 BCO construction are reviewed in Chapter 12. The summary, conclusions, and recommendations are contained in Chapter 13. Sample specifications and monitoring and testing recommendations for El Paso BCO construction are given in Appendices A and B. Some nondestructive test results are presented in Appendix C. Appendix D contains acronyms.

CHAPTER 2. REVIEW OF PREVIOUS RESEARCH

2.1 INTRODUCTION

In this chapter, previous research pertaining to expedited construction of bonded concrete overlays (BCOs) is reviewed. Many projects have incorporated either expedited construction or BCOs, but not both, so these are covered in separate sections. Those projects incorporating both technologies are discussed in the last section.

2.2 EXPEDITED CONCRETE PAVING

Concrete pavements that need rehabilitation often carry heavy traffic. In order to reduce the disruption to highway users, many agencies have used expedited paving methods (Refs 10, 11, 12). This technology is sometimes referred to as fast track paving. However, a better term may be expedited concrete paving, to clarify that construction and not design is being accelerated. Construction windows as narrow as 12 hours for an intersection have been used (Ref 10). On a thin-bonded overlay project, Virginia attempted to limit lane closure to 48 hours, but 58 were required (Refs 1, 13). Two issues must be addressed for successful expedited paving. The first is materials—concrete mix designs that gain strength rapidly. The second is the construction process.

The strength development of concrete paving mixes is usually measured using center-point or third-point flexural beam testing. For example, for a full-depth pavement the Iowa Department of Transportation specified flexural strengths of 2,750 kPa for mainline pavement and 2,400 kPa for intersections before allowing traffic on the new pavement (Ref 9). Compression testing and nondestructive testing have also been considered for measuring strength development (Ref 11).

"Fast track concrete pavement is essentially an adaptation of high-early strength concrete used in other applications" (Ref 11). Methods of achieving high early strength include use of special cements, admixtures, or accelerated curing methods. Special cements include Type III (Refs 11, 12) or Pyrament Blended Cement® (Refs 12, 14). Admixtures such as high-range water reducers (superplasticizers) and pozzolanas may be used to produce high early strength concrete.

2.2.1 American Concrete Paving Association Technical Bulletin 004.0 IT, 1989 (Ref 11)

This publication by the American Concrete Pavement Association (ACPA) provides an overview of expedited portland cement concrete paving methods. It was noted that Types I, II, and III cement had been successfully used for expedited paving. If Type I or II cement is used, admixtures must be used to promote early and long-term strength gain. A water-cement ratio of less than 0.43 was recommended for low permeability and good durability. Additives such as fly ash have also been used. Admixtures may be water reducers or accelerators. Twelve-hour flexural strengths of 2,170 to 3,790 kPa have been developed for a number of

expedited projects. All eight of these mixtures used air entraining and water-reducing admixtures.

2.2.2 New Brunswick Canada, 1993 (Ref 12)

This research evaluated the performance of three high early strength (HES) concrete mixes for use in New Brunswick, Canada. Three mix designs were evaluated for cost and strength development.

The first alternative evaluated was Type III portland cement with Master Builders® admixtures. The admixtures used were Rheobuild 1000® superplasticizer and Pozzolith 122® pozzolana. At approximately 12 hours, a flexural strength of 4,610 kPa and a compressive strength of 38.1 MPa were achieved. At just over 6 hours, a flexural strength of 2,960 kPa was achieved.

A second alternative investigated was Pyrament Blended Cement® (PBC-XT) concrete. At 12 hours, a flexural strength of 3,624 kPa and a compressive strength of 23.4 MPa were reached. Six-hour strength was similar to the Master Builders® mix (2,910 to 3,160 kPa).

The final mix used Type III cement with no admixtures. Twelve-hour strengths were 3,362 kPa (flexural) and 17.3 MPa (compressive). Thompson concluded that the mix with Master Builders admixtures produced the same strength gain as the Pyrament® concrete at about half the cost, and recommended use of high-performance concrete made with Master Builders® admixtures for expedited paving.

2.2.3 Synthesis of Current and Projected Concrete Highway Technology, SHRP-C-345, 1993 (Ref 6, pages 146 to 150)

This reference reviewed the state of the art of fast track paving as of 1993. It was noted that use of expedited paving materials could reduce opening times for new construction to 6 to 24 hours from 5 to 14 days. By using conventional cements and aggregates with a high cement content and a low water-cement ratio, beam flexural strengths in excess of 2,750 kPa at 12 hours could be achieved. Typically, Type III cements or Type I or II cements with admixtures were used. Type C fly ash was also often used as a partial replacement for cement or as an additive. It was pointed out that entrained air should be limited to the recommended amounts, because excessive entrained air reduced the strength of the concrete. More careful control of aggregate gradation was recommended.

Two examples of expedited concrete mixes were given, both developed by the Iowa DOT. The Iowa Fast Track I Mix contained 421 kilograms per cubic meter of Type III cement, and developed a center point flexural strength of 2,750 kPa in less than 12 hours. The Fast Track II Mix used 488 kilograms per cubic meter of the same cement and achieved a center-point flexural strength of 2,400 kPa in 7 hours. Iowa considered this strength (2,400 kPa) adequate for opening the new pavement to traffic.

It was noted that although no special equipment or procedures were required for expedited paving, the curing of these pavements required more attention. High early strength requires retention of moisture and heat. Recommended methods included applying curing compound at 1.5 times the normal rate and/or using curing blankets.

The authors stated that several problems remained to be solved before expedited concrete paving could realize its full potential. They included the drop-off at the edge of the slab that prevents traffic from using the newly paved lane, paving equipment projecting into adjacent traffic lanes, lack of efficient and accurate methods to predict slab strength in the field, and establishing the minimum strength of concrete for opening the pavement to traffic for various applications.

2.2.4 Strength Gain of Rapid Concrete Repairs, 1994 (Ref 15)

This study investigated the strength gain of two mixtures (termed *very early strength* and *fast track*) as measured using maturity and pulse velocity techniques. The mixtures cured within 4 to 12 hours. The repair mixtures investigated used accelerators, water-reducers, and/or superplasticizers, as well as air-entraining admixtures. The two mixtures were used for full-depth pavement repairs on test sections in Georgia. The length of pavement repaired ranged from 1.8 to 9.1 meters.

The authors concluded that with proper calibration, nondestructive techniques can be used to monitor and predict early strength gain, and the predictions of these techniques correlated well with cores extracted from the test sections. The maturity method was judged to offer a better, although often overly conservative, measure of strength gain.

2.2.5 Accelerated Rigid Paving Techniques, State of the Art Report, 1994, (Ref 16), Flexural Strength Criteria for Opening Concrete Roadways to Traffic, 1995 (Ref 17)

These studies were conducted under Federal Highway Administration (FHWA) Special Project 201, a collaborative effort between FHWA and the ACPA. Case studies were gathered throughout the United States. The entire paving process was analyzed to determine ways to save time.

Issues addressed included materials, specifications, paving equipment capabilities, edge drop-off, dowels, curing compounds and blankets, joint sawing and sealing, smoothness, incentives/disincentives, and rapid field tests. Concretes for expedited paving may be formulated with commonly available materials. Specifications that give the contractor greater responsibility can potentially lead to greater innovation; however, it may also be efficient for the state to assist with evaluating trial batches. Zero clearance or minimum clearance pavers make faster paving possible; further efficiencies can be achieved with tining, curing, blanketing, and other processes. Drop-offs should be kept within 50 mm at lane edges. Dowels may be placed with baskets or inserters. The case studies reviewed all used blankets, although they made sawing and sealing more difficult. Potentially, use of curing compounds could accelerate paving and opening to traffic. Joint sawing and sealing could also be expedited with appropriate technologies and materials. Expedited paving should achieve the same smoothness as other projects. Incentives and disincentives may be used to motivate contractors. Rapid field tests should be used to determine when the pavement is ready for traffic.

Criteria for opening new concrete pavements to traffic may be based on minimum time or minimum concrete strength. Since strength is influenced by many factors other than time, strength should be used. Strength may be determined by nondestructive methods

(maturity, pulse velocity, pullout, or breakoff methods), cylinders, or beams. Cylinders or beams should be made and stored in the field. Flexural strength may be correlated to compressive strength or nondestructive testing.

For most paving applications, opening criteria should be based on flexural strength. However, since BCOs are in compression, opening criteria for BCOs should probably be based on compressive strength or shear strength at the interface of the BCO and the existing concrete. At early ages, the interface is also subjected to shear and direct tension due to moisture and temperature variations.

The required flexural strength of new pavement is based on traffic loading (magnitude and number of loads), location of applied loads, moisture and temperature gradients, foundation support, and pavement thickness. Required flexural strengths for opening ranged from 2,060 to 3,170 kPa for construction traffic; 2,060 to 4,340 kPa for municipal streets; and 2,060 to 3,240 kPa for highways. For some pavements, dowel bar bearing strength is also important.

Different state transportation agencies use different criteria for early opening of pavements to traffic. They include compressive strength (17.2 to 27.6 MPa), third-point flexural strength (2,580 to 4,480 kPa), center-point flexural strength (3,445 kPa), splitting tensile strength (2,060 to 2,400 kPa), time (24 hours to 14 days), or a combination of criteria.

The Special Project 201 State-of-the-Art Report (Ref 16) notes that for opening BCOs to traffic at early ages, several questions remain to be answered. They include:

1. Can bond strength be related to overlay concrete strength at early ages?
2. How much temperature gradient can be tolerated in early ages before bond strength is affected?
3. How do early curing conditions affect bond strength?
4. Is some minimum time of acceptable temperature gradient and moisture loss prevention needed to assure adequate bond?
5. When and how much thermal differential can be tolerated if insulating blankets are suddenly removed from the surface of a bonded concrete overlay?
6. What temperature (maximum or minimum) of the existing slab can be tolerated at time of placement?
7. How should bond strength be determined?
8. How much bond strength is required to open traffic (Ref 16, p. 24)?

Three case studies from successful accelerated BCOs used either compressive strength of 20.7 MPa at 24 hours or center-point flexural strength of 2,400 kPa for overlays 89 to 100 mm thick in Virginia, Kansas, and Iowa.

2.2.6 "Fast Track Paving," 1995 (Ref 18)

To shorten pavement construction time, planning, concrete materials, jointing/sealing, concrete curing and temperature, strength testing, and traffic opening criteria should all be

addressed. Planning should consider traffic handling, incentives and disincentives including lane rental, and project specifications that allow innovative technologies and materials. Concrete materials should be carefully selected and proportioned to achieve both satisfactory properties in the plastic state and the required strength gain. Jointing and sealing should be done as early as possible. Concrete curing and temperature management are also important; higher application rates of curing compounds or blanket insulation should be used. For traffic opening criteria, reference is made to the paper reviewed in 2.25 (Ref 16). Addressing these issues can significantly reduce construction time.

2.3 BONDED CONCRETE OVERLAYS

2.3.1 National Cooperative Highway Research Program Synthesis of Highway Practice 99, 1982 (Ref 19)

This study reviewed the state of the art of resurfacing with PCC. Overlays had been constructed on portland cement and asphalt concrete roads, highways, and airfields. Projects built since 1913 were reviewed.

The synthesis reviewed bonded, partially bonded, and unbonded overlays. Only bonded overlays are of interest to this study. Bonding had been facilitated by adequate surface preparation and use of bonding agents. Methods of surface preparation included milling/scarifying, sandblasting, shotblasting, high-pressure water blasting, high-pressure water blasting with abrasives, and others with more limited applications. The method of surface preparation is usually specified by the state department of transportation or other agency. The most common bonding agents used were sand-cement and water-cement grouts (with a water-cement ratio of approximately 0.62). Epoxy and latex bonding agents had been used for patching small areas.

Concrete used for overlays was plain, reinforced, or continuously reinforced, with limited use of steel fiber reinforced concrete (SFRC) and prestressed overlays. Mix proportions were similar to conventional paving concretes with the exception of higher cement contents and smaller maximum aggregate sizes. Low-slump mixtures with superplasticizers had been used for several projects. Placement, finishing, and curing process were similar to those for pavements. Concrete was usually placed by slip-forming. In hot weather, high temperatures on the surface to be overlaid could lead to problems. Wetting the surface or paving at night were two solutions suggested. The importance of proper curing to prevent debonding stresses was noted. The synthesis also addressed design issues and the importance of considering traffic delays when evaluating resurfacing options.

2.3.2 IH-80 near Truckee, California, 1981, (Ref 20)

In 1981 a 2.4-kilometer section of three-lane roadway was overlaid with a thin BCO on IH-80 near Truckee, California. The existing pavement, constructed in 1964, had been subjected to numerous freeze-thaw cycles and had experienced considerable loss of wearing

surface. It was 200 mm thick over 100 mm thick cement-treated base (CTB). The joints were skewed with staggered spacings. The roadway was considered structurally adequate, so the purpose of the BCO was to restore riding quality.

The test section was on a 5 percent grade at approximately 2,195 meters of elevation. A 75 mm thickness of overlay was selected. The surface of the existing concrete was sandblasted. Cold milling was used to remove rubberized asphalt and taper the transitions to the overlay. Large spalled areas were patched with fast-setting magnesium phosphate concrete. A neat cement grout was used as a bonding agent.

Paving of the first two lanes began June 25. Problems were encountered with excessive slump loss due to highly absorptive aggregate. The slump of the mix design was increased. The surface was hand floated, supplemented by bull floating, burlap dragged, and tined. A resin-based curing compound was applied. Evaporation was high due to high temperatures (27°C to 30°C), low humidity (10 to 15 percent) and high wind (19 to 29 kph). Fogging was specified, but wind made it less effective.

Guillotine shear tests performed on 100 mm cores at 2 to 3 weeks indicated bond values of 2,400 to 3,800 kPa, which is generally considered adequate. Compressive strength tests of the core sections indicated 34.5 to 41.3 MPa for the BCO and 41.3 to 55.1 MPa for the original pavement.

Most of the overlay slabs were found to have transverse cracks at the pavement edges. Cracks were thin but numerous, with spacings as low as 0.3 meters. It was noted that cracking was probably due to volume change of the BCO at an early age, due to high evaporation rate (up to 1.5 $kg/m^2/hr$), the differential between fresh concrete and base concrete temperatures, high temperature drop from day to night (28°C ambient temperature differential plus 22°C concrete surface temperature differential), high-shrinkage concrete due to the highly absorptive aggregates used, and inadequate fogging. Cracking was not associated with the time of day or ambient temperature when the concrete was placed, wind direction, or pavement superelevation, cut, or fill.

After discovery of problems in the first two lanes, procedures were changed for constructing the third lane. The coarse aggregate stockpile was kept wet, and the pavement was fogged longer. No problems were encountered while paving the third lane, which was done in 3 days in July.

On August 6 a core was taken near a crack and a joint in lane two and was found to be unbonded. Another core taken 10 feet away had satisfactory bond (2,800 kPa). Sounding with a hammer revealed extensive unbonded areas in this slab and throughout the section. All three lanes were surveyed for delamination between August 11 and September 22. Delamination in individual sections ranged from 5 percent to 88 percent. During the survey, delamination progressed in some areas but not in others. To repair slabs, epoxy injection was attempted but was too time consuming to be satisfactory. The entire project was overlaid with asphalt concrete.

A thorough investigation of the bond failure was made. The grout may have dried before the overlay was placed in some areas, but where this was observed, fresh grout had been sprayed on. Sandblasting may not have adequately prepared the existing pavement for the BCO. In lanes where large amounts of aggregate had been exposed from surface attrition there was less delamination.

A laboratory testing program was undertaken to investigate delamination. Slabs 0.3 by 2.4 meters by 75 mm thick were cast using the same materials that had been used on the project. Strain gages and thermocouples were installed. Seven days after casting, both ends of the first specimen were found to be delaminated from 250 to 300 mm at the ends. A week later delamination on each end had progressed another 300 mm. Delamination was greatest along the edges of the slab. The debonding was attributed to a temperature differential of up to 7.2°C between the overlay and the base.

Another overlay was tested with one end of the base well sandblasted. No delamination was detected during the first 14 days. A tent with heat lamps was then set up over the slab to cycle it from a low of 2° to 7°C to a high of 27° to 38°C. After 3 days of cycling, delamination was detected. Delamination progressed from both ends, although slightly slower on the sandblasted end.

Four more overlays were placed, with half of the base sandblasted and the other half roughened with a chipping hammer. All delaminated with either natural weathering or heating and cooling. The latter two overlays used less absorptive aggregates with lower shrinkage characteristics, but still delaminated. Three 0.9 m by 0.9 m overlays were placed to determine if the size and shape of the slab affected delamination. All overlays debonded at all four corners. All tests ended in delamination. It was recommended that no thin-bonded portland cement concrete (PCC) overlays using cement grout be constructed in California until the debonding problem could be solved.

2.3.3 US 61 in Louisiana, 1981 (Ref 21)

In April 1981, a two-lane, 1.28 km section of jointed concrete pavement was overlaid with a 100 mm thick BCO on US 61 north of Baton Rouge, Louisiana. The existing pavement was 230 mm thick over 150 mm of sand and had been originally constructed in 1959. Joints were doweled and spaced 6.1 meters apart. The pavement was in good structural condition and required only 8.4 square meters of repairs over the section before the BCO was constructed.

The overlay was made of limestone aggregate concrete with 324 kilograms of cement per cubic meter. No reinforcement was used except for deformed steel tie-bars placed across some slab cracks. No difference in overlay crack reflection was noted between cracks with tie-bars across them and those without.

The pavement was shotblasted and a water-cement grout was used as a bonding agent. Particular care was taken to ensure that motor oil drippings, asphalt concrete, and surface dirt were completely removed before the BCO was placed. Polyethylene sheeting was placed under concrete trucks to catch oil drippings. A shotblaster with a 2.4-meter width removed

less than 3 mm of the pavement surface. Compressed air was used to clean the pavement before grout application. A slip-form paver was used to place the BCO. A white pigmented curing compound was applied at 1 1/2 times the normal rate. Joints were sawn within 24 hours of paving. Bond was evaluated using a guillotine test previously used by the Iowa DOT.

Four months later (August 1981) some debonding was noted adjacent to the sawn joints. Approximately 16 percent of exterior slab corners were debonded. Under traffic loading, the damage continued, and four years later 12 percent of the debonded corners had cracked. A total of 0.3 percent of the total surface area of the project debonded. Debonded sections were repaired using high-modulus epoxy resin.

Possible causes of debonding proposed by the authors were difficulties with the grout, excess air content of the mix, and excessive stress buildup at relief joints. The grout cured rapidly, so if the paving train was delayed the grout could act as a bond breaker. The report recommended not using grout during the summer months in Louisiana.

During construction, 61 linear meters of concrete had to be removed because excessive air entraining agent greatly reduced concrete strength. The strength of the contaminated concrete was 13.8 MPa, compared to 27.6 MPa in adjacent sections. The authors suggested that some sections of concrete that were not removed might also have had excessive entrained air and low compressive strength, and thus low bond strength.

Prior to BCO construction 100 mm relief joints were cut in the existing pavement. Before the overlay was placed, these joints had closed to about 50 mm wide. The overlay was placed and relief joints were installed using two sawcuts 50 mm apart. The joints were sealed with neoprene compression seals. The joints closed another 19 mm, and since the BCO was now more compressed than the existing pavement, this could have caused the overlay to debond near the cracks.

The performance of the BCO was satisfactory, and after 4 years of service there was no reflective cracking. The cost of construction with a BCO was about $29 per square meter, compared to an estimated $25 per square meter for an asphalt concrete overlay.

2.3.4 South Loop IH-610, Houston, 1983 (Refs 22, 23, 24, 25, 26)

To assist the Texas State Department of Highways and Public Transportation (now TxDOT) in establishing criteria for using thin-bonded concrete overlays (TBCOs) to rehabilitate pavements, a series of laboratory and field tests were conducted. Objectives of the study were to find a suitable bonding agent, an optimum treatment for the original pavement surface, and to determine whether or not the position of the steel affected the bonding characteristics of the TBCO. Three types of overlay were considered — plain concrete (50 mm thick), reinforced concrete (50 and 75 mm thick), and SFRC (50 and 75 mm thick). A four-lane 305-meter-long test section on IH-610 in Houston was selected for field study.

The surface was prepared by rotomilling 6 mm deep, followed by surface brooming, sandblasting to remove contaminants, and air blasting. A grout with a water-cement ratio of

0.62 with a superplasticizer was used as a bonding agent. The grout was uniformly broomed. The plain concrete had 390 kilograms of cement per cubic yard, and the SFRC had 446 kilograms of cement per cubic meter. A white pigmented impervious curing compound was applied to the overlays. The fiber reinforced concrete was easily cast and surface finished.

No significant debonding was noted in the test sections. Some cracks reflected through from the continuously reinforced concrete (CRCP), but they remained hairline cracks. More cracking along longitudinal joints was noted in the sections with welded wire fabric (WWF) reinforcement than with the steel fibers; in time, this may lead to spalling. It was noted that "fibrous concrete is a more resilient material than steel mat reinforced concrete" (Ref 23). A section 6.1 meters long of the 50 mm WWF section was placed without bonding grout. No adverse effect was noted.

Placing the WWF flat on the existing pavement did not interfere with the bond. Cement grout was noted to be a better bonding agent than epoxy. The bonding grout reduces the coefficient of variation of shear strength. Overlay placement temperature did not influence interface shear strength within the range of temperatures in this study. Three years later, no significant debonding was noted. "The fiber sections proved to be far superior in their ability to control longitudinal and transverse cracking" (Ref 23).

Average costs for the BCO were $35 per square meter for construction. Traffic handling cost an additional $9.60 per square meter, for a total agency cost of $44.60 per square meter. User costs were estimated at $108 per square meter with the USER-CST computer model. Thus, the estimated user costs were 70 percent of the total cost. The cost differential for fiber reinforced concrete over plain concrete was $7.88 per square meter for the 50 mm thick overlay. WWF-reinforced BCOs were cheaper, with a cost $2.25 per square meter more than plain concrete (Refs 22, 23, 24, 25).

Many studies were conducted by CTR in conjunction with this project. Reilley et al. (Ref 26) constructed and tested four half-scale model slabs of BCOs on jointed concrete pavement (JCP) and CRCP. It proved to be very difficult to cause substantial damage to BCOs on CRCP, even when very high fatigue loads (up to 89 kN) were applied. The BCOs on JCP failed in punchout, while the BCOs on CRCP suffered cracking but no other distress (Ref 24).

In another study, the effects of construction variables on CRCP overlays cast over old CRCP were considered. The variables investigated were surface preparation, vibration level, grout, location of cores, and seasonal variations. Both laboratory and field studies were made.

Methods of surface preparation studied included acid etching, water blasting, sandblasting, shotblasting, and rotomilling. Only shotblasting and rotomilling were actually tested. The type and intensity of vibration needed to consolidate the overlay concrete were also examined. Use of grout as a bonding agent was evaluated. Cores were taken from the corners, sides, and interior of BCOs. Seasonal variations were considered.

Pavement texture was evaluated using the sand patch method (ASTM E965-83, Ref 27), the Text-ur-meter®, and the texture profile recorder. Bond between the overlay and substrate was tested with a direct shear test and a bond pullout test.

A 0.9 m by 0.9 m by 100 mm thick base slab was cast and sandblasted. Four 0.46 m by 0.46 m by 100 mm overlays were cast on the base. Cores 100 mm in diameter were tested for direct shear, density, and bond pullout strength.

The study concluded that the sand patch method was the best method for evaluating pavement texture. Higher vibration appeared to increase bond strength. For a shotblasted surface, a wet pavement gave lower interface shear strengths. Drier surfaces gave better bond and did not require grout (Ref 24).

Suh et al. (Ref 25) reviewed the previous work under Project 457 and made the following recommendations for construction of BCOs:

1. The overlay should be constructed before the existing pavement has failed.
2. Cracks with low load transfer should be repaired before the pavement is overlaid.
3. Shotblasting is preferred to cold milling because it gives better bond strength.
4. Grout should be used as a bonding agent regardless of moisture condition.
5. Grout should not be allowed to dry.
6. Time between surface preparation and overlay placement should be minimized.
7. Sufficient vibration to consolidate the concrete should be used, but not so much as to cause the concrete to segregate.
8. Reinforcing bars placed directly on the original surface will not lose bond with concrete.
9. BCOs with steel mat reinforcement should be used to reduce large pavement deflections.
10. BCOs with SFRC should be used to reduce cracking in the overlay (Ref 25).

2.3.5 Field Evaluation of Iowa BCOs (Ref 28)

A study conducted by Construction Technologies Laboratories and the Iowa Department of Transportation used field testing to measure strains and deflections in five pavements, four with BCOs. Four of the pavements were jointed reinforced concrete with thicknesses from 150 to 250 mm and joint spacings from 12 to 23.3 meters. The fifth was 200 mm thick CRCP.

The overlays were 75 or 100 mm thick plain concrete. Sandblasting and airblasting had been used as surface preparation, and sprayed cement grout had been used as a bonding agent. The overlays had been constructed between 1979 and 1985. The old pavements were 13 to 20 years old at the time of overlay. The sections were condition surveyed and cored

and then loaded with two trucks. An 89-kN nominal single axle load and 151-kN nominal tandem axle load were used for load testing.

Results indicated that the overlaid sections were behaving as monolithic pavements, with high interface shear strength. Some of the cracking from the existing pavement had not reflected through the overlay, and the cracks that reflected remained tightly closed even after almost seven years of service.

2.3.6 North Loop IH-610, Houston, 1985 (Refs 3, 4, 8, 9, 29, 30, 31, 32, 33)

Following the successful performance of the test sections on South Loop 610 in Houston, ten sections were placed on North Loop 610. The existing pavement was 200 mm thick CRCP. The variables considered in the study were overlay reinforcement and overlay aggregate. Eight sections were placed with welded wire fabric, and two with steel fiber reinforcement (50 kilograms per cubic meter of concrete). The aggregates tested were siliceous river gravel and limestone. All overlay sections were 100 mm thick. The total length of the project was 5.1 km.

One pavement condition survey was taken before the overlay was placed (May 1985) and three after (February and May 1986 and March 1987). No spalling or punchouts were observed in any of the test sections until the last condition survey. The BCO improved the stiffness of the pavement structure and load transfer across cracks, as well as the riding quality. The fiber and limestone sections showed good bond strength at the layer interface. The limestone sections had the least number of transverse cracks (Refs 29, 30).

As part of the preparations for BCO test sections on the South and North Loops of 610, a finite element computer program was developed to design BCOs. The effect of cracks in the original pavement on the required BCO thickness was considered. Stresses due to volume change were examined, as well as those due to pavement loading, braking tires, or snow removal equipment. The nature of bond and the respective contributions of chemical adhesion and mechanical properties were considered.

The results of cores taken from test sections on South Loop IH-610 (constructed July–August 1983) and North Loop 610 (constructed October 1985–May 1986) in Houston and tested in guillotine shear were compared. The North Loop cores gave higher bond strengths than the South Loop cores. The 50 mm thick BCOs had greater bond strength than the 75 mm thick sections. The effect of grout was found not to be significant. For the North Loop, bond strengths of cores drilled at 8 months were higher than those removed at 2 months. Overall strength of sixty-one samples averaged 1,560 kPa with a standard deviation of 681 kPa.

Computed stresses due to wheel loads were very low and probably did not affect the bond. Snow removal equipment could produce high stresses of up to 638 kPa. Stresses due to volume change were not calculated, although clearly they could be very important (Ref 31).

Some delamination occurred, and condition surveys were taken in March and August of 1987 and March of 1988. Delamination was detected and marked by sounding the overlay

with a length of 19 or 25 mm (US #6 or #8) rebar dropped onto the surface. This detection method was affected to some extent by the operator's hearing sensitivity. The cracks and delaminations were then logged using the automated road analyzer (ARAN).

Cores from the overlay were taken and tested. Lab tests included direct (guillotine) shear testing, density testing, indirect tensile testing (splitting tension), coefficient of thermal expansion testing, and petrographic study. Direct shear test bond strengths ranged from 2,320 to 3,200 kPa. Indirect tensile test results ranged from 5,320 to 5,500 kPa for plain concrete and 4,790 to 7,280 kPa for steel fiber reinforced concrete. Thermal coefficients measured were 8.1 x 10^{-6} mm/mm/°C for limestone coarse aggregate, 9.5 to 12.8 x 10^{-6} mm/mm/°C for siliceous river gravel, and 12.8 x 10^{-6} mm/mm/°C for fiber reinforced concrete with siliceous river gravel aggregate.

Methods considered for detecting the delaminations were spectral analysis of surface wave (SASW), sounding, coring, and radar. Ultrasonic transmission and infrared thermography were considered but not tried because they did not seem promising given the conditions on IH-610 North Loop. Manual soundings with steel bars, hammers, or chains were made during the March 1987 and March 1988 condition surveys. SASW was used on a 0.74 square meter area during the March 1987 survey. Although the method was able to detect delaminations it was very slow and labor intensive (4 hours for the small section investigated). Ground penetrating radar was tried in April 1988; data did not show any clear differences between delaminated and bonded areas. Only manual sounding was judged to be accurate and rapid enough for large-scale surveys. Overlays placed with limestone aggregate and WWF or siliceous river gravel (SRG) had less delamination than those placed with SRG and WWF (Refs 3, 4).

Attempts were made to repair the delaminated sections, but they were generally unsuccessful. Only two methods worked reasonably well. The first was monomer injection without water or compressed air flushing. The second was to sawcut and remove the overlay, then sandblast, than fill the gap with polymer concrete. The long-term success of these procedures was not verified.

It was concluded that BCOs performed generally well. Delamination correlated well with higher evaporation rates (0.7 to 1.0 kg/m^2/hr). Delamination occurred where the temperature dropped more than 14°C between the time the concrete was placed and the next day. Using grout as a bonding agent gave higher bond strength than ungrouted sections, and ungrouted sections had a higher percentage of delamination. The direct shear tests did not give easily reproducible results. Delamination was easier to detect in warm months. After delamination was detected, the percentage did not increase except for the ungrouted sections.

Recommendations for BCO construction were to avoid placement when the evaporation rate exceeded 1.0 kg/m^2/hr, use blankets or a double application of curing compound, avoid placement when the temperature is expected to drop 14°C or more over the next 24 hours, use cold milling for surface preparation, use steel fiber for primary

reinforcement, use limestone coarse aggregate, to limit the alkali reactivity of the cement to 0.6 or less, and use grout as a bonding agent (Ref 32).

A finite element model (NSLIP) was developed to analyze behavior of BCOs under wheel and environmental stresses, particularly at early ages. Existing BCO design procedures were reviewed. Project objectives included modeling behavior observed on overlays in Houston, particularly cracking and delamination, analyzing BCO behavior, establishing a rational method to determine when a BCO is the best rehabilitation alternative, develop a BCO design procedure, and predict long-term performance of BCOs (Ref 33).

The model was used to investigate mechanisms that initiate delamination and develop recommendations for construction and materials specifications and procedures to prevent debonding. Debonding significantly increases pavement stresses and thus reduces predicted pavement life. Delamination may be initiated at early ages (before loading) or after traffic is allowed on the BCO, but only the former was considered. Delamination is caused by the differential changes occurring between the BCO and original pavement. These changes induce tensile or shear stresses that exceed the bond strength at the interface, resulting in delamination. Volume changes are caused by temperature changes or shrinkage of the curing BCO. Using NSLIP, tensile and shear stresses were calculated near cracks and edges. Maximum thermal stresses calculated were 276 kPa, which was less than half of predicted interface strengths. Environmental conditions leading to evaporation in excess of 1.0 $kg/m^2/hr$ or substantial temperature drops following BCO placement should be avoided (Refs 3, 4).

The observed delaminations were often detected within 24 hours after overlay placement. In all cases where delamination occurred on IH-610 South or North Loop it was located next to a joint or crack. The delaminations did not appear to be progressive over three years of observations. Analysis of cracking showed that cracks in the original pavement did not always reflect through, but pavement made with SRG had more cracking than that made with crushed limestone aggregate. Between surveys, transverse cracks increased in delaminated areas but not in nondelaminated areas. Analysis of both South and North Loop IH-610 data led to the conclusion that reinforcing type, thickness, and aggregate are important to BCO transverse crack development and thus to interface stress development at early ages (Ref 8).

As part of this study, the effects of bonding agents and application rates, moisture, substrate surface texture, interval between bonding agent application and overlay, and substrate temperature on bond performance of BCOs was investigated. A laboratory study with over 150 1 m by 1 m by 127 mm thick slabs was undertaken, followed by a field study under more typical construction and weather conditions. Bonding agents considered were portland cement slurry (water-cement ratio approximately 0.98), latex, epoxy, and water. In addition, placement of BCO with no bonding agent was evaluated. Methods of surface preparation investigated were coldmilling and shotblasting with three surface textures (Type I with an average texture depth of 0.6 mm, Type II with an average of 2 mm, and heavy with

an average of 9.5 mm as measured by test method 436A and ASTM E965-83, [Ref 27]). High, medium, and low substrate temperatures (52–60°C, 32–38°C, and 10–16°C) were considered. Variables that affect evaporation (concrete temperature, ambient temperature, humidity, and wind velocity) were recorded and analyzed.

Three different methods of measuring substrate texture were considered: the sand-patch method, the Texas texture meter method, and the RTV silicone casting method. Only the former was judged to be satisfactory. Several methods for testing bond strength in the laboratory and in the field were evaluated.

The study concluded that most debonding occurred at low stresses (less than 350 kPa) while the overlay was in an early curing stage. Bond was adequate under most conditions while the overlay was curing. Early debonding problems occurred only when environmental conditions caused significant combinations of stresses at the interface at very early ages. Debonding also occurred when latex, used as a bonding agent, set prematurely. The latex then became a bond breaker.

Once the overlay had attained enough strength to be cored and tested, it had probably either developed enough strength or debonded. Consequently, the bond testing methods used only verified that the bond had formed. Several conditions were judged to adversely affect bond, including high substrate temperatures (over 52°C), ambient temperature drops of more than 14°C during the 24-hour period immediately following the placement of the overlay, and evaporation rates exceeding 1.0 $kg/m^2/hr$. Under conditions where adverse environmental conditions cause a significant debonding risk, either epoxy bonding agent or severe shotblasting was recommended for use (Ref 9).

2.3.7 West Montreal, Canada, 1986 (Ref 34)

In late October 1986 a BCO was placed on a section of Autoroute 40 in West Montreal. A unique feature of this test was the use of 38 mm long concrete nails partially embedded in the old pavement to improve bond. These nails were placed 0.3 to 0.45 meters on center and driven halfway into the old pavement.

Eighteen different construction conditions were investigated. The existing pavement surface was prepared by sandblasting in some sections and by scarifying with a diamond saw in others. Three different steel fibers were investigated: Dramix®, Eurosteel, and Xorex™. For one lane, a thin cement grout was used as a bonding agent; the other two lanes used the steel nails. The test took place in cold weather, with temperatures reaching freezing nearly every night.

The slump of the concrete mixes was 38 mm and the air content was 5 to 7 percent. For the steel fiber sections, steel fibers were added at a rate of either 0.35 percent or 0.5 percent by volume (22 to 34 kg/m^3). The lower percentages were used to keep the concrete economical and workable. Superplasticizer was also added at the jobsite to achieve workable concrete. Curing compound was spread over the BCO 10 to 15 minutes after the concrete was placed. The concrete was completely covered with curing blankets at night.

The performance of the slabs made with plain concrete was very poor, although in the sections with nails the mechanical bonding was beneficial. The steel fiber reinforced sections had much less cracking. The influence of the nails was less evident. After eight months, the cracks in the SFRC had stabilized, although they continued to propagate in the plain concrete. The nonreinforced overlay exhibited distress and debonding, and had to be replaced after 18 months of service.

To examine the bond between the BCO and the old pavement, full-depth core samples were drilled at different locations. With the plain concrete, it proved impossible to recover a complete core. However, in the SFRC sections, none of the cores exhibited interface failure during extraction, even when a cracked area was cored. The investigators noted that "the presence of the steel fibers inhibit crack propagation and reduce the intensity of the tangential stress along the interface, thereby preventing delamination (Ref 34)." Their load-deflection tests also showed that Dramix® fibers held higher levels of load after cracking than Eurosteel or Xorex™.

2.3.8 Mori Bypass Highway, Japan, 1984 (Ref 35)

The first successful thin BCOs in Japan were constructed in 1983. In 1984, an experimental thin BCO was constructed on the Mori Bypass Highway on Hokkaido's National Highway Route Number 5. The existing pavement was a plain jointed concrete pavement (1,600 meters long, about 230 mm thick) and CRCP (1,000 meters long, about 200 mm thick), constructed in 1972. The existing pavement had been severely damaged by studded tires, with an average abrasion loss of from 23 to 28 mm.

The old pavement was undersealed by injecting a colloid cement grout, and then the top 30 mm of surface was removed with a heavy cold planer. The surface was prepared by steel shotblasting with 1.4 mm diameter steel balls. Placing the overlay directly on the freshly shotblasted surface, without using a bonding agent, gave the best results. Both plain concrete and steel fiber reinforced concrete were used for overlays. The aggregate was selected to minimize abrasion loss due to steel studded tires, based on the Los Angeles Abrasion Test.

The study compared the bond strength of five different surface preparations: cement paste coating, epoxy resin coating, shotblasting, shotblasting plus cement paste coating, and polymer cement paste coating. Cores were made through the BCO layer, a cap was bolted or glued to the top of the core, and then the core was pulled off with a hydraulic jack. Shotblasting gave the highest pull-off strengths.

Cracking in the steel fiber reinforced overlay sections was approximately 10 percent of that in the plain concrete sections. The cracks occurring in the SFRC BCO were tiny (widths less than or equal to 0.6 mm) and had no effect on pavement serviceability.

2.3.9 Belgium (Ref 36)

Twelve concrete overlays were constructed in Belgium, but only two were bonded to an existing concrete pavement. The other ten were either placed over asphalt concrete or

over portland cement concrete with an asphalt bond breaking layer. All of the overlays were constructed at different sites.

The two bonded concrete overlays were constructed at Gent and Viersest. Surface preparation was either simple cleaning or milling, with and without grout. The overlays were constructed of SFRC with Bekaert Dramix® fibers.

Results were poor. At Gent considerable debonding was observed, and the Vierset overlay exhibited considerable shrinkage cracking. It was suggested that had a proper bond been achieved, there would have been no advantage to using steel fibers. The grout did not appear to aid the bond, and it was noted that shotblasting would perhaps be a better surface preparation than milling, and simple surface cleaning was clearly inadequate.

2.3.10 Long-Term Evaluation of CRCP Overlay, Greene County, Iowa (Ref 37)

In October 1973 a comprehensive study of SFRC overlays on concrete pavements was made. Study variables included cement content, steel fiber content and type, overlay thickness, and type of bonding. Cement contents investigated were 356 or 445 kg/m^3 of Type I cement, 297 kg/m^3 of Type I cement and 139 kg/m^3 of fly ash (type not specified), and 445 kg/m^3 of Chem Comp expansive cement. Steel fibers 25 and 64 mm long were used at 36, 59, and 95 kg/m^3. Overlays were 50 mm or 76 mm thick. Sections were intended to be fully bonded (with cement paste as a bonding agent on a wetted surface), partially bonded, or unbonded. A total of thirty-three SFRC sections and eight control-reinforced concrete sections was constructed. Performance evaluations were made at 5, 10, and 15 years of service.

The best performance was provided by control sections of 100 mm thick nonfibrous mesh reinforced CRCP and 125 mm deformed bar reinforced concrete. Of the SFRC sections, best performance was provided by sections with the greatest amount of fibers (95 kg/m^3). Type of fiber had no significant effect. The SFRC overlays had substantial deterioration at 5 years, but performance remained acceptable at 10 and 15 years. Increasing cement content did not significantly improve overlay performance. Thicker overlays performed substantially better than thinner. The bonded sections did not bond, so all sections were in fact unbonded. The study concluded that the extra cost of SFRC could not be justified because the more economical but thicker nonfibrous sections had better performance.

2.3.11 Iowa Route 141 (Ref 38)

A 7.2 km section of Iowa Route 141 was overlaid with unreinforced 76 to 110 mm BCO in 1983. The existing pavement was 43 years old, 190 mm thick JCP, in good condition except for some transverse midpanel cracking. The pavement surface was prepared by shotblasting, and a sand-cement-water grout was used as a bonding agent. A white-pigmented curing compound was applied after texturing. Weather was cool during construction.

Testing in 1984 with a Delamtect showed no delamination. "The Delamtect is an instrument capable of determining delamination occurring beneath the pavement surface. The instrument sends sound waves through the concrete and measures the time needed for the wave to reflect back to the surface. Delaminations in the concrete will cause the wave to reflect back at the point of delamination. The resulting shorter travel time is then registered as a delaminated area on the instrument printout (p. 7, Ref 39)." In 1986, Delamtect testing revealed 11.6 lineal meters of delamination (less than 1 percent). Testing in 1989 still showed less than 1 percent delamination (14 lineal meters). Cores for shear testing gave strengths of 4,550; 3,790; and 4,000 kPa in 1986 and 4,350; 3,350; 4,050; and 1,850 kPa in 1987.

The project was successful except for some reflective cracking through the overlay. It was recommended that TBCOs be at least 100 mm thick.

2.3.12 Nongrouted BCO, County Road T61, Iowa (Ref 39)

In 1985, two 76.2 m long 100 mm thick BCO test sections were constructed in Iowa to evaluate the feasibility of omitting bonding agents. The rest of the project was constructed using pressure-sprayed grout. Shotblasting was used for surface preparation.

Cores were removed from the BCO soon after construction and at later intervals, and tested for shear strength. At 14 days, average shear strengths of ungrouted sections (4,370 and 4,570 kPa) were higher than at adjacent grouted sections (2,070 and 3,280 kPa). Over the following 6 years, strengths in the ungrouted sections leveled off or decreased, while strengths in the grouted sections increased to 4,320 and 7,050 kPa. However, in all cases the minimum bond strength was higher than the Iowa Dot specification of 1,380 kPa.

Delamtect tests of ungrouted sections indicated some delaminations at transverse joints in one section. Debonding did not subsequently increase. In the other section, no evidence of debonding was found. The study concluded that adequate bond can be achieved without grout. Although limited debonding occurred in one test section, it does not appear to have progressed.

2.3.13 SFRC on IH-10, Louisiana (Ref 40)

An experimental overlay to assess the long-term performance of SFRC with a high cement content placed on a shotblasted surface, using edge bond reinforcement and tied shoulders, was constructed on IH-10 south of Baton Rouge. The BCO was 3.5 km long and 100 mm thick over 200 mm thick, 16-year-old CRCP. The existing pavement was patched and then prepared by shotblasting to a specified average texture depth of 1.15 mm. The mean texture depth achieved was 1.5 mm with a standard deviation of 0.23 mm. It was further required that old pavement markings be completely removed. The BCO edge was reinforced to discourage debonding, using curb-type bars epoxied into the existing slab surface. The bars were inverted U-shaped 16 mm diameter (US #5) 1.2-meters long and placed on 2.4 m centers 100 mm from the pavement edge. The bars were high enough above the pavement to allow the concrete to be vibrated under them. A stiff, slurry grout was applied as a bonding

agent. The concrete used contained 418 kg/m^3 of cement with a maximum water-cement ratio of 0.40 and 50 kg/m^3 of steel fibers. The aggregate was a river gravel with a maximum size limited to 12.7 mm.

The concrete temperature was limited to a maximum of 32°C. The overlay surface was tined and a white-pigmented curing compound was applied at 1 1/2 times the normal rate. BCO bond strength was measured using two methods. A guillotine shear test similar to that used by the Iowa DOT gave average values of 6,500 kPa, greatly exceeding the Iowa Dot recommended value of 1,380 kPa. The ACI tension pull test gave average values of 880 kPa, greater than the 689 kPa minimum used by ACI to evaluate multicomponent epoxy adhesives. When the pull test was used in the field, the specimen always failed at the overlay or in the original pavement.

Although after 3 years of service 35 percent of the cracks in the original pavement had reflected through the BCO, the cracks were tight and were not expected to lead to performance problems. A performance evaluation revealed only two small areas of debonding of 3.3 and 6.7 square meters adjacent to construction joints. Load carrying capacity of the roadway was significantly enhanced. As a result of the success of this test, three further projects using the same methods and specifications were planned.

2.3.14 U.S. Army Corps of Engineers Survey of Overlays (Ref 41)

Case histories of thirty-three Corps of Engineers overlay projects from 1973 through 1992 were reviewed. Most were overlays of stilling basins and locks; only four bridge overlays and four roadway overlays were examined. In most cases, the overlays were required to repair severe abrasion. To reduce shrinkage and reflective cracks in the bonded overlays, use of polymer-modified concretes and concretes containing polypropylene fibers was suggested. Methods of surface preparation included shotblasting, sandblasting, or mechanical abrading, followed by waterblasting or air blasting. Bond agents included mortar and epoxy. For some of these applications unbonded overlays had fewer and smaller cracks than bonded overlays.

2.3.15 National Cooperative Highway Research Program Synthesis of Highway Practice 204, 1994 (Ref 1)

In 1994 the NCHRP followed up its 1982 synthesis (Ref 19) reviewed above. The number of cataloged projects had grown from 375 in 1982 to over 700 by 1993. One of the trends noted was increasing use of expedited construction to reduce lane closure times. Few bonded CRC overlays of CRCP were reported, and these had often not performed well. Use of SFRC overlays was also limited.

For bonded overlays, PCC slurry or grout was usually used as a bonding agent, although some BCOs were places without agent directly on clean, dry substrates. Most PCC overlays used conventional concrete, occasionally with a high cement factor, although SFRC, synthetic fiber reinforced concrete (SnFRC), and chemically modified concretes have been used.

For BCOs, it is important that the original pavement be structurally sound and that areas of deterioration are repaired, or the distress is likely to reflect through the overlay. Although cold milling was widely used as a surface preparation technique in the past, some engineers suggested that it could cause microcracking. Shotblasting and sandblasting are now more widely used. Suggested average texture depths were 3 mm or 6 mm.

Performance of BCOs has been mixed. Some have performed well for more than 20 years, and some have deteriorated appreciably within the first year or two. In most cases, poor performance was linked to an excessively deteriorated underlying pavement. Loss of bond does not necessarily lead to BCO failure; some overlays have performed well for 15 years or more although the overlay may have never been bonded to the substrate.

2.4 EXPEDITED BONDED CONCRETE OVERLAYS

2.4.1 Iowa, 1986 (Ref 42)

A 100 mm thick BCO using high early strength concrete mixes to allow early opening of the pavement to traffic was constructed by the Iowa Department of Transportation in 1986. Twelve kilometers of US 71 in Buena Vista County were resurfaced. The original pavement had been constructed in 1937 and was considered to be in good condition. As part of the project, the pavement was widened from 6.1 to 7.3 meters.

The overlay concrete was batched with 380 kilograms of special Type III cement and 41 kilograms of Type C fly ash per cubic meter. The project specifications required that the cement meet AASHTO M-85 Type III standards, as well as attaining a compressive mortar strength of 8,960 kPa when tested under ASTM C309. The concrete had about 6.5 percent entrained air. The concrete temperature at placement was about 32°C.

The mix achieved strengths of 2,690 kPa flexural and 13.1 MPa compressive at 8 hours, 4,134 kPa flexural and 24.1 MPa compressive at 24 hours, and 14-day strengths of 5,650 kPa flexural and 36.5 MPa compressive. Flexural strengths were measured using 152 mm by 152 mm by 508 mm beams loaded at the center point. Compressive strengths were measured using 152 mm by 305 mm cylinders. The bond was measured at 2,070 kPa, but details of the test used were not given. Some of the concrete used for driveways and county road intersections had calcium chloride added and developed higher strengths. Thermal curing blankets were used to accelerate strength gain.

The only reinforcement in the overlay was 16 mm (US #5) epoxy-coated rebars placed across cracks to reduce reflective cracking. The 910 mm long bars were spaced 760 mm on center. Surface spalls were corrected by milling and placing partial depth patches. This led to problems because the concrete trucks bent the reinforcing steel in the open holes, and the paver dropped into the holes, increasing pavement roughness. The authors concluded that the patches should have been completely filled before the BCO was placed.

The contractor was given the option of either milling or shotblasting to remove paints, oil drippings, rubber, and other contaminants. Shotblasting was selected and a 1.22 m wide machine was used. The report noted that the operation was quiet and dust free, but did not

remove asphalt well. Sandblasting and airblasting were used to clean the pavement immediately in front of the paver. New specifications in Iowa may require the shotblasting equipment to operate immediately in front of the paver.

Grout was used as a bonding agent over all the pavement except for two sections. The authors note "this was a qualified success" (Ref 42, page 6). The BCO was placed using a 3.66 m wide Rex paver, and some problems with achieving the required smoothness of the pavement were noted. A liquid curing compound was applied as soon as the surface was finished. Transverse sawcuts over old expansion joints were made 3 to 4 hours after the BCO was placed. The sawcut was made through the full depth of the overlay. Thermal blankets were then placed. Debonding tape was used to control reflective cracking and transform a crack in the old pavement into a straight sawed joint in the overlay. The tape was 0.1 mm plastic, 100 mm wide with adhesive on one side.

Difficulties were encountered in bonding the overlay to the old pavement. Two possible causes were identified. The first was the difficulty of keeping the roadway clean in front of the paver. The second was that the grout was too thin. Proposed new specifications would target a water-cement ratio of 0.6 with a maximum of 0.7.

The project was evaluated one year after construction and no apparent distress due to traffic or weather was noted. A small amount of additional transverse cracking was sawed out and sealed with Sof Seal joint sealant (about 1,100 meters). There was a tendency for minor debonding in midpanel cracks.

The cause of debonding was thought to be related to cracks closing in compression. On previous projects, overlays had buckled and debonded, and considerable effort was taken to ensure pressure relief joints were installed immediately after placement of the overlay. Delamination percentages were 0.05 percent on 28 October 1986 and 0.68 percent on 14 April 1987. The debonding was considered minor and not a cause for concern.

Direct shear testing at the bond line of the overlay showed that average bond strength had decreased slightly. Overlays placed with Type I grout averaged 2,180 kPa, with Type III grout averaged 2,380 kPa, and without grout averaged 1,480. Only eight specimens were tested, and there was considerable variation in results. Although the bond strength was less than anticipated, it was considered satisfactory.

The results of using debonding tape to control reflective cracking were encouraging. Overall the test was successful. It was pointed out that expedited paving must overcome contractor fears associated with working with very rapid setting concretes.

2.4.2 US Route 13, Northampton County, Virginia, 1990 (Ref 13)

In June 1990 an attempt was made to overlay 1.6 km of concrete pavement in 48 hours. Although the construction in fact took 58 hours, the potential of expedited BCO construction to reduce lane closure times was clearly demonstrated. The original pavement was 200 mm thick JCP with undowelled joints, constructed in 1965. The old pavement had joint faulting and spalling and some longitudinal cracking. An 89 mm thick BCO was selected. Considerable care was taken to design a concrete mixture that would achieve a

compressive strength of 20.7 MPa and a tension bond strength of 1,380 kPa at 24 hours. A cement content of 445 kg/m^3 was used with a water-cement ratio of 0.42. Half of the overlay was placed without bonding agent, and half with a grout with a water-cement ratio of 0.53. It was demonstrated in both laboratory and field tests that the same bond strengths could be achieved with and without grout.

Shotblasting machines were used to prepare the original pavement surface. Exposure of coarse aggregate particles was specified. After concrete placement, liquid membrane curing compound and curing blankets were used. Due to mild environmental conditions, curing was not a problem for this test.

Early performance of the project was excellent. There was no difficulty in achieving the required strengths, which were monitored using maturity and pulse velocity techniques. The study concluded that bonding grout may be omitted, and expedited construction of BCOs is feasible.

2.5 SUMMARY

A summary of projects and studies is given in Table 2.1. Expedited construction of BCOs is certainly feasible. However, problems that have been noted in the past with BCOs in California, Louisiana, Texas, Iowa, and Belgium make it clear that bond cannot be ensured under all conditions. Overlays with SFRC have performed well; however, cost is often an obstacle to use of SFRC. Many methods of surface preparation have been used, with varying degrees of success. The current standard method is shotblasting. On two occasions (Refs 34, 40), some sort of nailing or edge reinforcement was used to help the BCO adhere to the substrate.

Table 2.1 Summary of expedited paving, BCO, and expedited BCO projects and studies

Project or Study	Year	Reference	Comment
Expedited Concrete Paving			
ACPA Technical Bulletin 004.0 IT	1989	11	Overview of Methods
New Brunswick, Canada	1993	12	Laboratory tests of three high early strength paving mixes
SHRP Synthesis C-345	1993	6	Overview of methods and projects
Strength gain of rapid concrete repairs	1994	15	Laboratory and field monitoring of strength gain using maturity and pulse-velocity
FHWA Special Project 201 State of the Art Report, Review of Opening Criteria	1994, 1995	16, 17	Overview of criteria for opening concrete pavements to traffic; considered opening criteria for BCOs
Fast track paving	1995	18	Discussion of construction and scheduling issues
Bonded Concrete Overlays			
NCHRP Synthesis 99	1982	19	Review of overlay techniques and projects
IH-80 near Truckee, California	1983	20	Project report on a BCO that delaminated, and subsequent forensic laboratory work

Project or Study	Year	Reference	Comment
Bonded Concrete Overlays (continued)			
US 61 in Louisiana	1981	21	Unreinforced BCO with some debonding, repaired with epoxy
South Loop IH-610, Houston	1983	22, 23, 24, 25, 26	Plain, reinforced, and SFRC BCO test sections, with considerable monitoring and laboratory investigation
Field Evaluation of Iowa BCOs	1979 - 1985, 1988	28	Load testing and strain and deflection measurement of four BCOs in service. All were well bonded.
North Loop IH-610, Houston	1985	3, 4, 8, 9, 29, 30, 31, 32	Ten BCO test sections placed, some of which had delaminations. Laboratory work and finite element modeling of BCO behavior were used to investigate results.
West Montreal, Canada	1986	34	Plain and SFRC BCO test sections, some with concrete nails to improve bond
Mori Bypass Highway, Japan	1989	35	BCO test sections with five surface preparation methods. Shotblasting gave highest pull-off strengths.
Belgium	1989	36	Two SFRC BCOs showed considerable debonding and shrinkage cracking
Long-term evaluation, Greene County, Iowa	1989	37	Evaluation of BCOs at 15 years of service found widespread debonding, but acceptable performance
Iowa Route 141	1990	38	BCO on JCP with shotblasting and grout. Less than 1 % delamination.
Nongrouted BCO, Iowa	1992	39	Comparison of grouted and ungrouted BCOs; both performed well
IH-10, Louisiana	1992	40	SFRC BCO with excellent crack control and very little delamination. Edges were tied with reinforcing steel bars.
Army Corps of Engineers Survey	1994	41	Survey of overlay projects, mostly of locks, some using polymer concretes and SnFRC
NCHRP Synthesis 204	1994	1	Follow-up to 1982 synthesis. Noted that poor BCO performance often linked to poor condition of base pavement
Expedited Bonded Concrete Overlays			
US 71, Iowa	1986	42	Grouted high early strength BCO demonstration project. Achieved 24.1 MPa compressive strength at 24 hours
US Route 13, Virginia	1990	13	BCO 1.6 km long placed in 58 hours total lane closure time.

CHAPTER 3. PRELIMINARY WORK

3.1 INTRODUCTION

Prior to performing this test in El Paso, a considerable amount of research was performed by the Center for Transportation Research (CTR) and the Construction Materials Research Group at The University of Texas at Austin. Initially, a feasibility study was made to select a method for rehabilitating a section of IH-10 (Ref 7). This study included collecting traffic data and environmental information, surveying and documenting the current pavement conditions, and a preliminary design.

Subsequently, twenty-six cores of the existing pavement were obtained, measured for pavement thickness, and tested for compressive strength, splitting tensile strength, and modulus of elasticity. These measured properties were compared to those predicted using the falling weight deflectometer (FWD) and values calculated in the feasibility study.

Next, a concrete mix was designed that gave high early strength in compression, flexure, and bond. The development of compressive and bond strength with time and maturity was also investigated (Ref 43). Using the measured properties of the existing pavement and the overlay concrete, an overlay thickness of 165 mm was selected (Ref 44). Since some test sections would use steel fiber reinforced concrete (SFRC), a test program was undertaken to select the type and amount of steel fiber. Some test sections employed a power-driven shear connector (Ref 45).

Several half-scale models of bonded concrete overlays (BCOs) were loaded at early ages to determine whether early traffic loading would decrease fatigue life (Ref 46). It was then decided as a preliminary step to construct eight 3.66 m by 15.2 m one-lane test sections to compare the performance of different overlay designs and construction methods.

Analysis of climate data from July 1992 to June 1994 indicated that during the month of June extremely harsh environmental conditions can be expected. For example, it is usually recommended that special precautions be taken when the projected evaporation rate of water from concrete exceeds 1.0 $kg/m^2/hr$ (Ref 46). During the month of June, the evaporation at any time during the day is rarely less than this value and on occasion may rise as high as 3.4 $kg/m^2/hr$. The combination of high concrete and air temperatures, low humidity, and high winds cause severe danger of plastic shrinkage cracking. Thus, the month of June was selected for the test.

3.2 CHARACTERIZATION OF EXISTING PAVEMENT

Twenty-six cores of the existing pavement were taken. Before testing, the length of each core was measured. Although the pavement was nominally 203 mm thick, actual thicknesses varied from 178 mm to 248 mm, with a mean of 209 mm and a standard deviation of 15 mm. Fourteen cores were tested for modulus of elasticity, six were tested for coefficient of thermal expansion, seven were tested for splitting tensile strength, and seven were tested for compressive strength. Cores tested for modulus of elasticity were subsequently tested for compressive or splitting tensile strength. Six cores were reserved in case any tests had to be repeated. Results of the testing are given in Table 3.1.

3.2.1 Modulus of Elasticity

Modulus testing of the cores received from El Paso was performed using strain gauges. The ends of each of the cores tested were first sawcut to provide a uniform end perpendicular to the longitudinal axis. Since the cores varied in length, they were all cut to a uniform length of 165 mm. Next, four areas on each core were prepared for the application of the strain gauges. This preparation included applying a base layer of 5-minute, quick-set epoxy over each of the four 25 mm by 100 mm gauge areas in order to fill surface voids. This layer of epoxy was then sanded down smooth to the original surface. After wiping the area with a damp cloth and letting it dry thoroughly, the strain gauges were applied to the core surface with additional quick-set epoxy. In order to ensure no bubbles were trapped underneath the gauges, a thin layer of epoxy was also applied to the contact side of the gauges. The four gauges were then pressed firmly to the core and smoothed with a plastic strip.

Each of the four gauges was oriented on the core in a full-bridge pattern, with two horizontal strips on opposite sides of the diameter and two vertical strips on opposite sides of the longitudinal axis. The leads of the four gauges were connected in proper sequence to a data logger machine. The actual testing procedure involved loading the cores in compression while the data logger read the bridge resistance in microvolts. Readings of resistance and load were taken at constant load intervals until approximately forty percent of ultimate core strength was reached. The readings were then converted into stress and strain values which, in turn, were used to compute the modulus values for each core. The strain conversion formula took into account the full-bridge correlation as well as the individual strain gauge factors.

Table 3.1 Properties of existing pavement

Property	Mean	Standard Deviation	Coefficient of Variation	Highest Value	Lowest Value	Number of Specimens Tested
Pavement Thickness	209 mm	15 mm	0.072	248 mm	178 mm	26
Modulus of Elasticity	35.8 GPa	5.72 GPa	0.160	41.3 GPa	25.5 GPa	14
Coefficient of Thermal Expansion	7.6×10^{-6} mm/mm°C	0.92×10^{-6} mm/mm°C	0.121	8.8×10^{-6} mm/mm°C	6.5×10^{-6} mm/mm°C	5 (only 4 used)
Splitting Tensile Strength	4,354 kPa	358 kPa	0.082	4,950 kPa	3,850 kPa	7
Compressive Strength	44.1 MPa	8.07 MPa	0.183	56.5 MPa	35.5 MPa	7
Predicted Compressive Strength	51.9 MPa	9.49 MPa	0.183	66.5 MPa	41.8 MPa	-
Predicted Modulus of Elasticity	34.1 GPa	-	-	38.6 GPa	30.6 GPa	-

Measured core moduli varied from 25.5 to 41.3 GPa. The mean value was 35.8 GPa, the standard deviation was 5.72 GPa, and the coefficient of variation was 0.160. Values of elastic modulus varying from 9.4 GPa to 40.6 GPa had previously been reported (Ref 7). Five of the earlier values were lower than the lowest value measured. Since in the previous testing some cores were known to be cracked (Ref 7), and the cores tested in this study were not, this is a reasonable result. It is believed that the current results are more representative of the pavement.

Elastic moduli were measured from cores in 1992 and 1994 and predicted from back calculation using FWD data in July 1992 and December 1993. There was concern that the FWD data indicated a considerable loss of stiffness between the two times; in July 1992, only 56 percent of backcalculated moduli were less than 31 GPa, whereas in December 1993, 78 percent of the moduli were less than this value. However, the moduli measured in the laboratory in 1994 were higher.

Backcalculation results were improved by using the actual pavement thicknesses measured from cores. Since the stiffness of a rigid pavement is directly proportional to the elastic modulus but proportional to the cube of the pavement thickness (Ref 2, page 83), any error in measurement in the thickness of a pavement introduces considerable error into the prediction of the pavement's modulus of elasticity.

3.2.2 Coefficient of Thermal Expansion

Each of the cores selected for thermal expansion testing had both ends sawcut. This ensured that all the cores were of the same length and the ends of the cores were perpendicular to the longitudinal axis. Holes were drilled at the center of the ends of the cores, and gauge studs were epoxied to each end, so that approximately half of each of the gauge studs extended out of both ends of the core. The lengths of the gauge studs extending out of the core and the lengths of the cores were measured at room temperature.

After the epoxy bonding of the gauge studs to the cores was sufficiently cured, the cores were placed in an oven and heated overnight. Actual testing of all the cores was done in two cycles to reduce error. The changes in temperature for the two cycles were 93°C and 96°C. The change in length of the steel gauge studs and the change in length of the core were measured. The change in temperature and the change in length of the concrete cores were then used to obtain the coefficient of thermal expansion for each core. The results obtained for each core during both cycles were then averaged to obtain one overall thermal coefficient.

The coefficient of thermal expansion of the cores tested varied from 6.5×10^{-6} mm/mm°C to 8.8×10^{-6} mm/mm°C. The mean value was 7.6×10^{-6} mm/mm°C for both cycles, the standard deviation was 0.92×10^{-6} mm/mm°C, and the coefficient of variation was 0.121. Results from cycle 1 were not used, since those are considered to be less stable than subsequent cycles. The values for core number 2 were not used in determining the thermal coefficient average since the gauge stud imbedded in this core was not aligned properly with the longitudinal axis of the specimen.

3.2.3 Splitting Tensile Strength

Half of the cores used in performing modulus of elasticity tests were used in conducting splitting tensile tests. Splitting tensile tests were performed according to ASTM C496-90 (Ref 27). The diameter and length of each core were measured prior to testing. These values, along with the failure loads, were used in determining the splitting tensile strength of each core tested. Testing was performed on a 534 kN capacity Tinius Olsen testing machine at slow loading rate.

Splitting tensile strength varied from 3,850 to 4,950 kPa. The mean value was 4,350 kPa, the standard deviation was 358 kPa, and the coefficient of variation was 0.082. This corresponds to a flexural strength (modulus of rupture) of at least 5,500 kPa (Ref 48). The splitting tensile tests conducted under the feasibility study (Ref 7) produced twelve values from 2,950 to 5,450 kPa, with a mean of 4,078 kPa. This is only 276 kPa less than the mean value presented above. The previous tests show greater variability; this may be due to the fact that some of the earlier cores were cracked or contained reinforcing steel.

3.2.4 Compressive Strength

Each of the cores used in performing compressive strength tests was tested in accordance with ASTM C39-86 (Ref 27). Half of the cores used in performing modulus of elasticity tests were used in conducting compressive strength tests. Therefore, the lengths of the cores used in performing this test were shorter than the standard 200 mm specimen. Testing was performed on a 2,670 kN capacity Forney Cylinder Testing Machine at a loading rate of 178 to 276 kN per minute.

Compressive strength varied from 35.5 to 56.5 MPa. The mean value was 44.1 MPa, the standard deviation was 8.07 MPa, and the coefficient of variation (COV) was 0.183. Normally core compressive strength is expected to be approximately 85 percent of cylinder strength, so $f'c$ can be predicted by dividing core strength by 0.85 (Ref 48). Similarly, the elastic modulus in GPa may be predicted by multiplying 4.73 times the square root of the predicted cylinder strength in MPa (Ref 48). The mean value predicted is 34.1 GPa, and the mean value measured is 35.8 GPa. Although the means are nearly the same, the measured values show more variability. The measured modulus of elasticity should be more reliable than the predicted modulus.

The measured values showed considerable scatter, with coefficients of variation ranging from 0.072 to 0.183. As a result of this variation, conservative values were adopted for design.

3.3 MATERIALS SELECTION AND CONCRETE MIX DESIGN

The intent of the materials selection and mix design procedure was to develop concrete mixes for BCOs that would permit traffic in 8 to 24 hours.

3.3.1 Materials Selection

Samples of coarse and fine aggregates and Type I/II cement were obtained from Jobe Concrete Products in El Paso. Initially a mix of two coarse aggregates was considered, with the larger aggregate having a nominal maximum size of 37.5 mm. This aggregate was

rejected because it could lead to difficulty placing the concrete for thinner overlays. The coarse aggregate used was TxDOT grade 6 (ASTM C33 grade 67) with a maximum size of 19 mm (Ref 49). It was a crushed dense dolomitic Cambrian limestone, with a specific gravity of 2.70 and a dry rodded unit weight of 1,474 kg per cubic meter. The fine aggregate used had a specific gravity of 2.60 and a fineness modulus of 2.80.

Pyrament PBC-XT90 blended cement provided by Lone Star Industries was also tested. Type K expansive cement was also investigated; due to the difficulty of controlling expansion and the high cost of this cement, it was not considered further. Rapid Set cement was also considered and rejected due to excessive cost. Subsequently, Type V cement and 35 percent cement replacement with Monex Dealy Class C fly ash were investigated to reduce the heat buildup of the BCO. Type I/II and V cements were considered because of potential sulfate reactivity problems in the El Paso area.

Admixtures used were Grace Darex II air-entraining agent and Master Builders superplasticizers. Two Master Builders superplasticizers were evaluated for high early strength concrete overlay mixes. Use of Rheobuild 1000 high-range water reducer (superplasticizer) led to high early strength at a very low-dosage rate (262 ml per hundred kilograms of cement). A higher dosage rate of Polyheed 997 medium range water reducer, however, produced inferior strength to the Rheobuild mix. Therefore, Polyheed 997 was not considered further in this study.

3.3.2 Mix Design Alternatives Considered

The mix design alternatives considered in this study were a standard TxDOT CO mix (Ref 49), two high early strength mixes using Master Builders superplasticizers, and a high early strength mix using Pyrament PBC-XT90 blended cement.

The initial mix was based on the 1995 TxDOT specification for CO class concrete (Ref 48), shown in Table 3.2. However, the air content was reduced to 5 percent, based on previous research for TxDOT on air-entrainment requirements for high-performance concrete (Ref 50). It was anticipated that a concrete paver would be used to construct the BCO. As a result, the slump of the concrete had to be between 25 mm and 75 mm.

Table 3.2 TxDOT Specification for CO Class paving concrete (Ref 50)

Minimum cement content:	390 kg/m^3
Minimum 28-day cylinder compressive strength	32 MPa
Minimum 7-day flexural strength:	4,410 kPa
Maximum water/cement ratio:	0.40 L/kg
Coarse aggregate grade number:	6
Slump requirements (section 421.8, table 3) for concrete pavement:	
	Desired slump 40 mm
	Maximum slump 75 mm
Entrained air (section 421.8)	7% ± 1 1/2%

The CO mix was proportioned to achieve 4,410 kPa flexural strength at 7 days. Mix constituents are shown in Table 3.3 and mix characteristics are shown in Table 3.4. The cement content was slightly less than normally specified, but concrete strength was adequate. Mixes were designed using the absolute volume method (Refs 47, 51). A high early strength mix using Pyrament blended cement with a set time of 90 minutes was evaluated. No admixtures were used with the Pyrament mix. The Rheobuild 1000 mix used Rheobuild 1000 superplasticizer.

Table 3.3 Mix constituents

	CO Mix	Rheobuild 1000 Mix	Pyrament Mix
Constituents in kg/m^3			
Water	151	151	93.7
Type I/II Cement	379	520	-
Pyrament PBC-XT	-	-	446
Coarse Aggregate	1,105	1,061	1,120
Fine Aggregate	673	652	817
Admixtures ml/ 100 kg cement			
Darex II air-entrainer	131	78.5	-
Rheobuild 1000 superplasticizer	-	262	-

Table 3.4 Mix characteristics

	Baseline Mix	Rheobuild 1000 Mix	Pyrament Mix
W/C Ratio	0.40	0.29	0.21
Slump (mm)	25 - 75	25 - 75	25 - 75
Air Content	6%	4.5%	2.5%

All 1- and 3-day specimens were cured outside under wet burlap and plastic wrap. This was done in an attempt to simulate field-curing conditions in order to not overestimate early age specimen strengths. Seven and 28-day specimens were taken inside after 3 days and placed in lime saturated water at 21°C to finish curing.

3.3.3 Development of Flexural and Compressive Strength

The development of flexural and compressive strength at 8 hours, 1 day, 3 days, 7 days, and 28 days is shown in Figures 3.1 and 3.2 for the three mixes under consideration. Flexural strengths were determined according to ASTM C78 (Ref 27) using a Reinhart Beam Tester and third-point loading. Beam specimens were standard size (152 mm by 152 mm by 508 mm). Compressive strengths were determined according to ASTM C39 (Ref 27) using 100 mm by 200 mm cylinders, with the procedure described in 3.1.4, above.

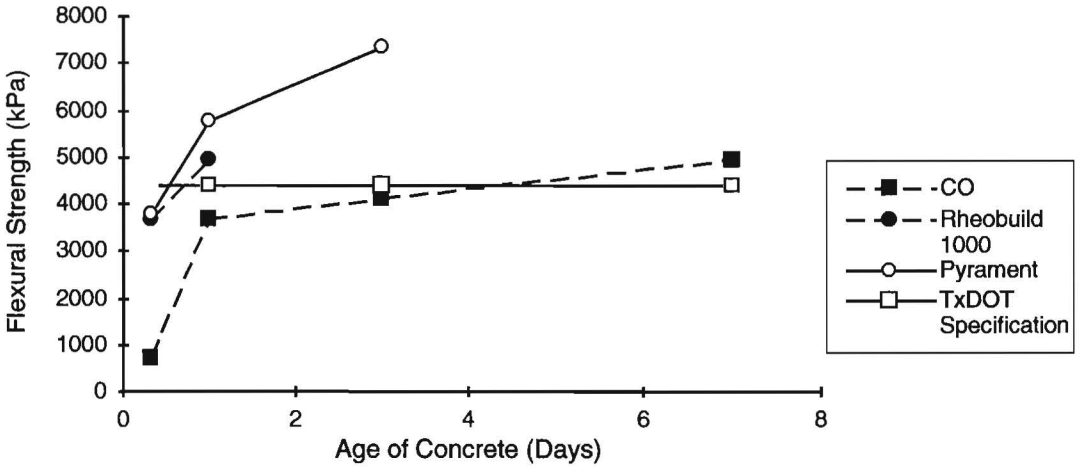

Figure 3.1 Flexural strength development

The CO mix achieved the TxDOT specified flexural strength (4,410 kPa) at 7 days of curing. The Rheobuild 1000 and Pyrament mixes achieved the desired strength within the first 24 hours. Both mixes subsequently developed considerably higher strength, which would lead to a stronger and more durable overlay.

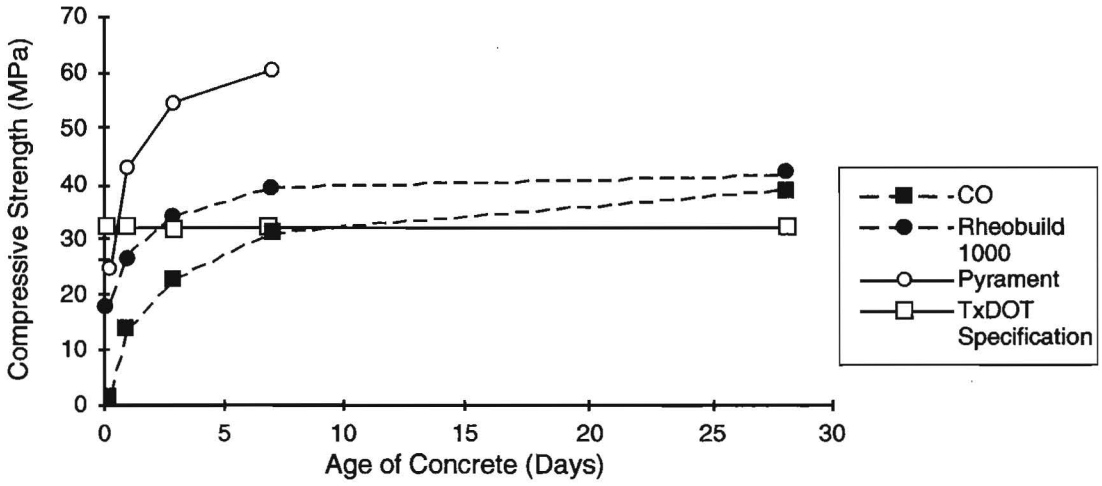

Figure 3.2 Compressive strength development

The CO mix achieved the TxDOT specified compressive strength (32 MPa), with an excess of 6.9 MPa, at 28 days. The Rheobuild 1000 mix achieved 34.2 MPa at 3 days, and the Pyrament mix achieved 42.3 MPa at 1 day.

3.3.4 Development of Bond Strength

Concrete-to-concrete bond strength was measured using an in-situ push-off test procedure developed by Choi at The University of Texas at Austin (Ref 45), shown in Figure 3.3. First, the base substrate was cleaned and roughened using a Blastrac® portable blast cleaning system 1-8D Unit MK4 shotblaster, with S460 steel shot. This was intended to simulate the shotblasting procedure that specified for actual construction of the overlay. Next, a 380 mm by 610 mm by 130 mm overlay specimen was cast on the substrate. A 9.5 mm foam core board with a 150 mm by 300 mm opening was used to ensure that the overlay did not bond to the substrate except at the opening. A pair of 25 mm diameter PVC pipes were cast in the overlay for the rods which pull off the specimen.

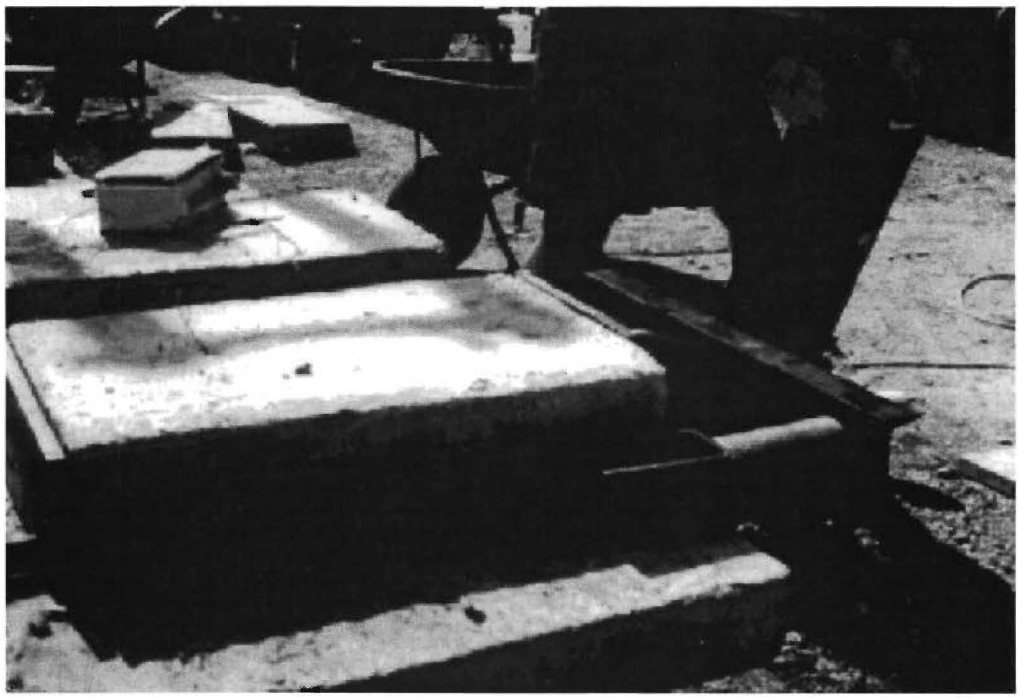

Figure 3.3 In situ push-off test

The overlay was pulled off the substrate using a hydraulic pump with two rams. Due to the 25 mm eccentricity of the load above the bond interface, a moment was induced. Thus, the test produced a lower bound of the bond strength that can be developed between the overlay and substrate. This loading simulates the stress state that is considered to be most

likely to cause overlay debonding; that is, a combination of shrinkage or thermally induced tensile and shear stresses.

Due to time and material constraints, only the Rheobuild 1000 high early strength mix was tested for development of bond strength at three time intervals. At 8 hours, a shear stress of 860 kPa was developed. At 24 hours, 3,150 kPa was attained, but at 72 hours only 2,700 kPa was measured. Only one specimen was tested at each age. The apparent drop in strength at 72 hours may be due to experimental error or due to the inherent variability of the development of bond strength. Previous research has indicated that shrinkage and thermal effects will induce shear stresses on the order of 200 and 80 kPa, respectively (Ref 8). Therefore, these 24- and 72-hour bond strengths should be satisfactory to prevent overlay debonding if earlier debonding can be prevented.

For the CO and Pyrament mixes, bond testing was performed with a single 24-hour specimen for each mix. Compared to the Rheobuild 1000 high early strength mix bond stress of 3,150 kPa, the CO mix achieved 2,832 kPa and the Pyrament mix only reached 985 kPa. It should be noted that the baseline mix for the bond test yielded 24-hour compressive strengths roughly 50 percent higher than that of earlier trials.

3.3.5 Cost Comparison

Costs per cubic meter of concrete at the batch plant were estimated to be $78 for the CO mix, $94 for the Rheobuild 1000 high early strength mix, and $165 for the Pyrament mix.

3.3.6 Concrete Mix Selection

The Rheobuild 1000 high early strength mix was clearly superior for a expedited BCO. It was not significantly more expensive than the baseline mix, yet it achieved higher strength at much earlier ages. Because of the higher cost, the Pyrament mix did not appear promising for a BCO. It would, however, be attractive for a full-depth pavement replacement where either traffic must be put quickly on the replacement pavement, or restrictions on pavement cross-section thickness mandated a very high flexural strength (Refs 43, 46).

3.4 BCO THICKNESS DESIGN

With the materials properties measured above (Sections 3.1 and 3.2), the computer program BCOCAD was used to select the BCO thickness. The program uses both the American Association of State Highway and Transportation Officials (AASHTO) and rigid pavement rehabilitation design system (RPRDS) to design BCO thickness. RPRDS was developed by CTR. The BCO thickness was designed at five eastbound and five westbound locations. Estimates of remaining pavement life at these locations ranged from 41 percent to 81 percent. The elastic modulus of CRCP ranged from 20.7 to 34.5 GPa, the subbase modulus was 520 to 1,000 MPa, and a constant subgrade modulus of 140 MPa was used. The AASHTO procedure gave design thicknesses of 91 to 142 mm, and the RPRDS procedure required thicknesses of 140 mm to 254 mm. A thickness of 165 mm was selected for the project (Ref 44).

3.5 DEVELOPMENT OF BOND STRENGTH

Using the high early strength concrete mix design developed above, Wade investigated factors affecting bond at early ages (Ref 43). In addition to the testing described in Section 3.2.4 above, fifty-four specimens were cast and tested in direct (guillotine) shear. Half cylinders (100 mm in diameter by 100 mm long) were cast, the surface was roughened with a wire brush, and the cylinders were cured. This substrate concrete averaged 44.8 MPa in compressive strength at 28 days. Overlay specimens were then cast in cylinder molds on top of the half-cylinder substrate specimens. Experimental variables were age of concrete at testing (8, 24, and 72 hours), ambient temperature (4°C, 21°C, or 38°C), and evaporation (moist curing or uncovered with forced air circulation).

Moist cured specimens attained higher strengths than specimens with forced air circulation (2,758 versus 2,413 kPa). Effects of substrate temperature were less clear, with no significant differences in strength development. Bond strength at 8 hours was highly variable (ranging from 680 to 2,585 kPa), but all specimens showed strengths equal to or greater than 2,400 kPa at 24 hours. It was suggested that traffic should not be allowed on an overlay until 24 hours after placement to allow for sufficient bond development. Maturity testing of the proposed BCO concrete mix showed that at least 2,400 kPa can be achieved at 600°C-hours, so this value could be used as a criterion to open a BCO to traffic (Ref 43).

3.6 FIBER SELECTION FOR SFRC AND SnFRC

While many steel and polypropylene fibers are available, it was not possible to test more than one of each type. The selection of fibers to consider in this study is discussed below.

3.6.1 Steel Fiber Selection for SFRC

Testing was undertaken to select a type of fiber for steel fiber reinforced concrete (SFRC) for El Paso BCO construction, and to select the quantity of fiber per cubic meter to be used. Although many steel fibers were available, Novocon Xorex™ and Bekaert Dramix® fibers had a proven track record for this type of construction. As a result only these fibers were investigated. The Xorex™ fibers are relatively thick (about 1 mm) and wavy to resist pullout, whereas the Dramix® fibers are thinner with hooked ends.

3.6.1.1 Basis for Mix Design. When an existing concrete mix is adjusted for the inclusion of steel fibers, the coarse aggregate content is reduced and the fine aggregate content is increased. On the advice of Rick Smith of Novocon, an intermediate aggregate was added. Mix proportions are shown in Table 3.5. For the selection of the type of steel fiber, 44.5 kilograms per cubic meter of each fiber was used. Fibers just less than one-third the thickness of the overlay were used (51 mm for Xorex™ and 60 mm for Dramix®).

3.6.1.2 Selection of Type of Fiber. The type of fiber was selected on the basis of the toughness of a third-point loading beam (152 mm by 152 mm by 508 mm) after 7 days of curing. Four Xorex™ beams and three Dramix® beams were made. The load-deflection

curves for one of each type of beam are attached (Figures 3.4 and 3.5); others were similar. The deflection at the first load increment (8.9 kN) probably also reflects play in the testing apparatus.

Table 3.5 SFRC mix constituents

Constituents in kg/m^3:	
Water	151
Cement, type I/II	520
Grade 67 coarse aggregate	606
Grade 8 intermediate aggregate	404
Fine aggregate	652
Novocon Xorex 50 mm or Bakaert Dramix® 60/80 steel fibers	44.5.
Admixtures ml/100 kg cement	
Darex II	78.5
Master Builders Rheobuild 1000	262

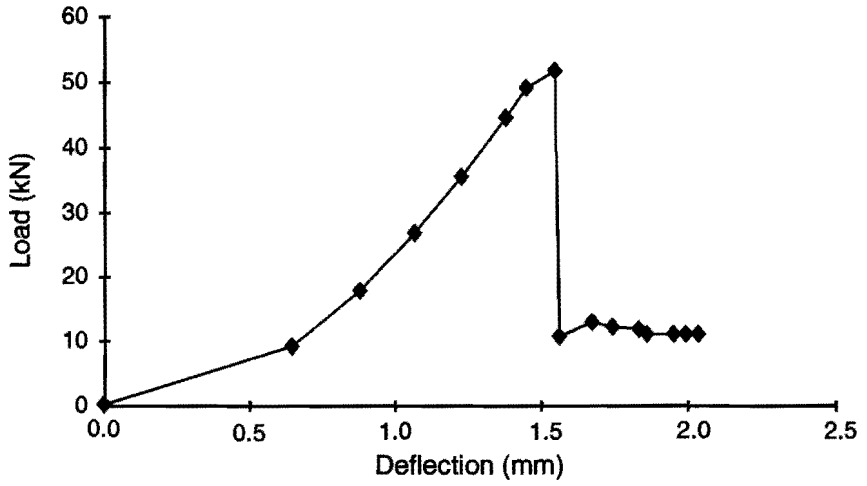

Figure 3.4 Load-deflection curve, Xorex™ Beam # 1

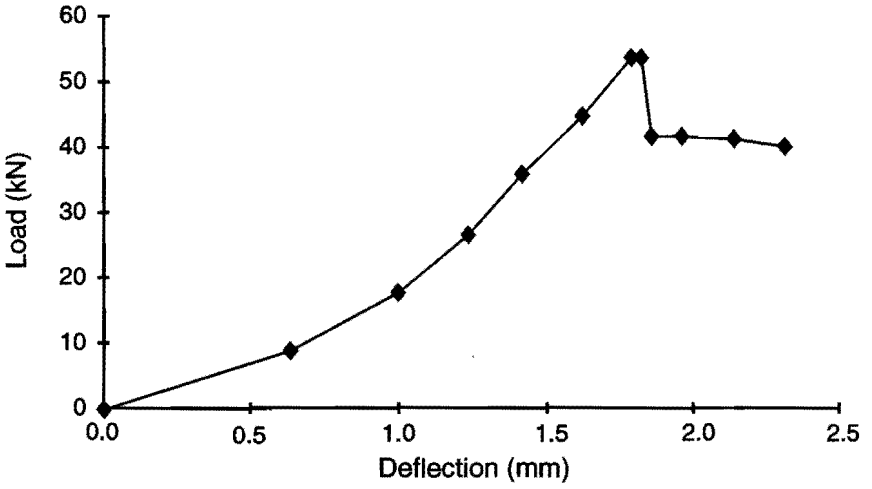

Figure 3.5 Load-deflection curve, Dramix® Beam # 1

In every case except one, the beam reached a cracking load of about 53.4 kN (6,890 kPa in flexure), and fell to a residual load after cracking. For one of the Xorex™ beams a cracking load of only 38.7 kN was reached. Two observations may be made:

a) The initial cracking load is not influenced by the presence or type of steel fibers (with the exception of one of the Xorex™ beams). This is consistent with previous research (Refs 34, 52).

b) In all cases, the residual load held by the Dramix® beams is considerably greater than that held by the Xorex™ beams (38.3 to 43.6 kN, versus 10.7 to 24.9 kN), for the same fiber content. This may be due to the fact that, since the Dramix® fibers are smaller, there are more individual fibers crossing the failure plane for a given weight of fibers.

All specimens are shown Table 3.6 below. Dramix® fibers were selected for further testing.

Table 3.6 Comparison of SFRC beams with different fiber types

Beam Number	Maximum (cracking) load, kN	Residual load, kN
Xorex™ #1	51.8	10.7 - 12.9
Xorex™ #2	53.0	11.6 - 14.2
Xorex™ #3	38.7	22.0 - 24.9
Xorex™ #4	54.3	16.0 - 18.9
Dramix® #1	53.6	40.1 - 41.4
Dramix® #2	55.2	38.3 - 40.1
Dramix® #3	58.2	42.7 - 43.6

3.6.1.3 Selection of Quantity of Fiber. Due to the high cost of steel fibers, the possibility of reducing the fiber content to 14.8 or 29.7 kg per cubic meter was investigated. Type V cement was substituted for Type I/II; since both achieved a flexural strength of about 6,890 at 7 days. This was not expected to affect results. The peak residual loads of the nine beams are shown in Figure 3.6. Three observations may be made:

a) As before, the fibers did not substantially influence the cracking load of the beams. As a result, the cracking loads are not shown.
b) The relationship between fiber content and peak residual load appears to be approximately linear for the specimens investigated.
c) Specimens with lower peak residual loads had greater variability of the peak residual load. This may be due to the difficulty of achieving a good distribution of fibers at low fiber contents using a laboratory mixer.

3.6.1.4 Discussion. Third-point flexure beams are commonly used to compare different types and quantities of fibers. They cannot, as yet, be used to directly predict the long-term performance of SFRC. Consequently, it would be useful to construct test sections and evaluate long-term performance, and then compare these results with third-point flexure beam predictions.

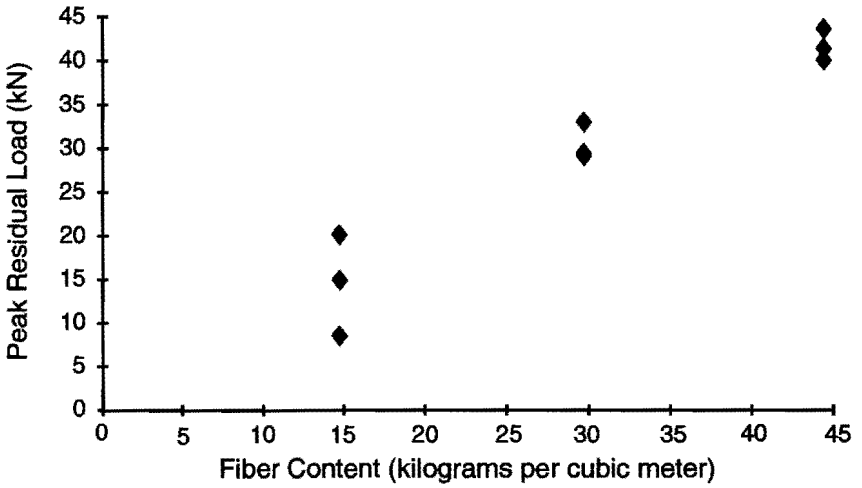

Figure 3.6 Comparison of SFRC beams at different fiber contents

For example, the residual load-carrying capacity provided by 14.8 kilograms per cubic meter of Dramix® fibers may be more than sufficient to hold cracks together if they form at early ages, before the concrete has developed much strength. Similarly, the thicker Xorex™ fibers may have some durability advantages.

3.6.1.5 Recommendation for SFRC. For the preliminary test sections, Dramix® steel fibers at 44.5 kg per cubic meter of concrete were used.

3.6.2 Synthetic Fiber Selection for SnFRC

Many different synthetic fibers are available. First generation fibers were polypropylene monofilaments. Subsequently, a second generation of collated fibrillated polypropylene (CFP) fibers was developed. CFP fibers are supplied in bundles that open during mixing, in contrast to the individual monofilaments. CFP fibers are easier to introduce and distribute within the concrete matrix than monofilaments. Some CFP fibers, such as Forta CR, have twisted fiber bundles. Twisted bundles eliminate fiber balling and accelerate the bundle opening process (Ref 53).

Commonly used CFP fibers are Forta CR and Fibermesh. For this study, Forta CR was selected because of previous experience on CTR projects with it (Ref 54). A fiber content of 1.78 kg/m^3, or approximately 0.2 percent by volume, was selected based on common practice.

3.7 USE OF SHEAR CONNECTORS (REF 45)

A research project was initiated in fall 1992 to characterize the shear strength of proprietary shear connectors for use in BCO construction. The pullout characteristics were also established. Three types of shear transfer test were conducted: direct shear transfer tests, early-age interface strength development tests, and beam tests for static and fatigue shear strength.

For direct shear transfer tests, small overlays were cast on top of base slabs. The Blastrac® shotblasting machine was used to prepare the substrate to three different surface roughness conditions as measured by the Sand Patch Method: low (0.27 to 0.36 mm average texture depth,), medium (0.47 to 0.54 mm), and high (0.64 to 0.77 mm). A smooth troweled finish was also tested. Other experimental variables were number of nails (0, 1, or 2), contact area (23,200, 46,500, or 69,700 mm^2), strength and type of substrate concrete, and age of overlay at testing.

The specimens failed in several different modes, making the ultimate strength difficult to characterize. However, the data indicated that nails added considerable strength to the interface. Since delaminations tend to initiate at boundaries (Refs 3, 4), it seemed appropriate to test the feasibility of arresting delamination by reinforcing boundaries with nails. For CRCP, boundaries are construction joints, contraction joints, and cracks. However, since the locations of cracks are not known in advance, only construction and contraction joints may be reinforced with nails. In a previous project in Louisiana (Ref 40), a similar reinforcement of the BCO was used. Performance of the BCO was excellent after 3 years of service.

3.8 FATIGUE (REF 46)

To investigate the effects of early traffic loading on the fatigue life of BCOs, Huddleston tested seven half-scale beam specimens under cyclic loading (Figure 3.7). The testing program was similar to that of Reilley (Ref 26), except that simply supported beams

rather than slabs supported on neoprene pads were loaded. Thus, the extremely high loads required by Reilley to produce failure were not required. The substrates for the beams tested were 406 mm wide by 1,829 mm long by 102 mm thick. Reinforcing steel percentage was 0.52 percent longitudinal and 0.083 percent transverse, matching that of IH-10 in El Paso. Compressive strength of the beam concrete at the time of testing was 38.8 MPa. The beams were cracked through their thickness at the center, so that by loading the BCO directly over the crack the potential for delamination and loss of structural stiffness would be increased. Finally, before the BCO was placed the substrate beams were shotblasted using the Blastrac® shotblaster with S460 shot (Section 3.2.4). The beams had an average texture depth of 1.15 mm as tested by the sand patch test. For one base beam, a section 152 mm wide adjacent to the crack was debonded using Dayton Superior Sure-Lift J6® debonding agent.

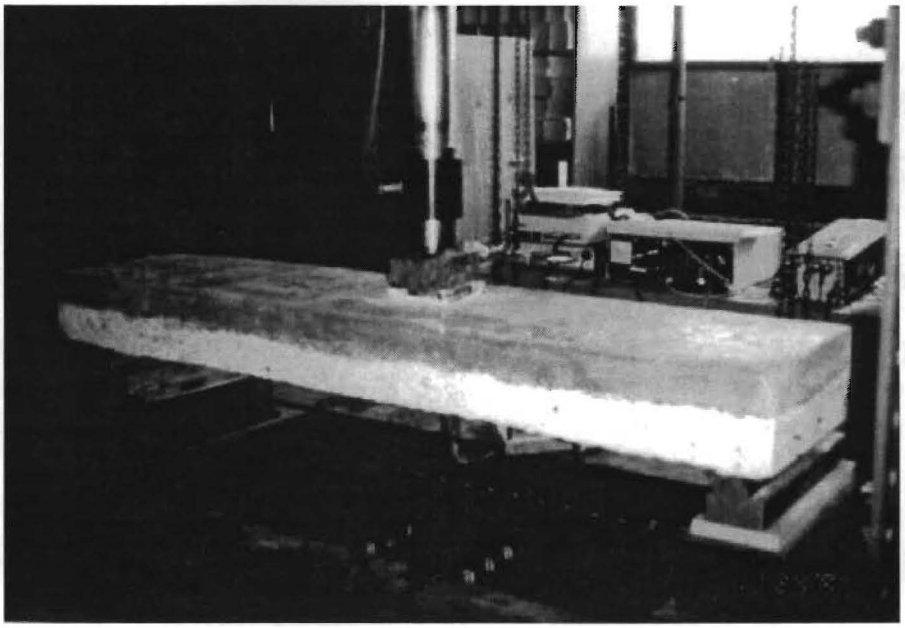

Figure 3.7 Fatigue testing of half-scale BCO beam (Ref 46)

Each beam was subjected to 2,000,000 load cycles at 18.2 kN. At every 250,000 cycles, the beam was loaded statically to 18.2 kN and the deflection was measured to determine the stiffness of the model pavement system.

First, two beams fully cured to a BCO compressive strength of 48.3 MPa were tested to establish a basis for comparison with beams loaded at early ages. The next two beams were loaded at a lower strength of 27.6 to 31.0 MPa. Finally, two beams were loaded when the BCO compressive strength was only 12.1 to 22.4 MPa. This strength was achieved at 8 to 12 hours with the high early strength concrete mixes under consideration. The seventh beam was loaded at 12.1 to 15.5 MPa and included a 152 mm debonded section. This simulated a BCO loaded at a very early age with a delamination near a crack, and thus

represented an extremely adverse loading condition for a newly constructed BCO. The delaminated region was approximately 13 percent of the span length.

In all cases, the static deflection after 2,000,000 cycles was 0.89 to 1.22 mm. Beams loaded at early ages had higher initial stiffness losses, but ultimate stiffnesses were similar to those for fully cured beams. After fatigue testing, an examination of the beams found no fatigue-induced delamination.

The beams were cored and the cores were tested in guillotine shear and direct tension. Guillotine shear strengths ranged from 934 to 10,211 kPa, and direct tension strengths were 878 kPa for a poorly shotblasted specimen and 1,372 to 2,032 kPa for all others.

The seven beams had been loaded at earlier and earlier ages in an attempt to induce a failure. However, the loss of stiffness and debonding associated with failure were never observed, despite much more rapid loading than could ever be imposed on a pavement by traffic. Even BCOs loaded at a compressive strength of only 13.5 MPa were able to carry 2,000,000 cycles with no loss of structural integrity. Thus, if bond is achieved BCOs can be loaded at very early ages without detrimental effects.

3.9 EVAPORATION

As mentioned previously, curing concrete environmental conditions that produce evaporation rates greater than 1.0 kg/m^2/hr. of water from the concrete surface should be avoided. High evaporation can lead to plastic shrinkage cracking. High evaporation is produced by high air temperatures, low humidity, high wind speeds, and high concrete temperatures (Refs 55, 56, 57, 58). Unfortunately, these conditions often occur in El Paso.

Menzel's equation for evaporation of water from a concrete surface may be written as (Ref 55):

$$W = \left[0.3115\left(0.253 + 0.06V\right)\right]\left(e_0 - e_a\right) \qquad \text{(Eq 3.1)}$$

where:

W = kg of water evaporated per square meter of concrete surface per hour,

V = wind velocity in kilometers per hour, which should be measured 0.5 m above the evaporating surface,

e_0 = pressure of saturated vapor in kPa at the temperature of the evaporating surface, and

e_a = vapor pressure of the air in kPa.

Although e_0 may be obtained in several ways, one method is by using Dilley's Equation (Ref 59):

$$e_0 = 0.61078\left[e^{\left(\frac{17.2694\,T_c}{T_c+237.30}\right)}\right] \qquad \text{(Eq 3.2)}$$

where:

T_c = concrete temperature in degrees Celsius.

Other prediction formulas are available but give similar results.

e_a is given by:

$$e_a = \frac{Rh}{100} e_{as} \qquad \text{(Eq 3.3)}$$

where:

RH = relative humidity in percent, and

e_{as} = pressure of saturated vapor in kPa at the air temperature. Again, e_{as} may be given by Dilley's equation:

$$e_{as} = 0.61078\left[e^{\left(\frac{17.2694\,T_a}{T_a+237.30}\right)}\right] \qquad \text{(Eq 3.4)}$$

where:

T_a = air temperature in degrees Celsius.

By substituting (3.2), (3.3), and (3.4) into (3.1);

$$W = \left[0.19026(0.253 + 0.06V)\right]\left\{e^{\left(\frac{17.2694T_c}{T_c+237.30}\right)} - \left[\frac{RH}{100}\right]e^{\left(\frac{17.2694T_a}{T_a+237.30}\right)}\right\} \qquad \text{(Eq 3.5)}$$

and where all variables are as previously defined.

This relationship is often presented in the form of a nomograph (Figure 3.8), which makes it easier to visualize the effects of the variables on the evaporation rate (Refs 46, 47, 55). Concrete bleeding rates for usual conditions of slab construction lie in a range of about 0.5 to 1.5 kg/m^2/hr. When evaporation exceeds bleeding, there is a severe danger of plastic shrinkage cracking, and precautions must be taken (Refs 54, 55, 56, 57). Possible corrective measures include dampening the subgrade and forms, lowering concrete temperature, improving curing, erecting windbreaks, or providing sunshades (Ref 57).

Hourly weather readings for El Paso from June 1992 through May 1994 were obtained from the National Climactic Data Center. Air temperature, wind speed and direction, and relative humidity were given. Concrete temperature, however, had to be assumed. Concrete temperatures for each month were selected based on plant records from Jobe Concrete Products, and ranged from a minimum of 10°C in January and February to a maximum of 32°C in June and July.

Average monthly evaporation rates ranged from 0.15 to 0.29 kg/m^2/hr. in January and February to 1.12 to 1.46 kg/m^2/hr. in June and July. In June 1992 and 1993, evaporation rates as high as 3.0 to 3.5 kg/m^2/hr. were calculated (Ref 43). Therefore, the best time to investigate methods of constructing BCOs under El Paso's most adverse conditions is in

June. Evaporation rates for all months investigated as calculated in Wade et al. (Ref 43) are shown in Table 3.7.

Evaporation varies considerably during the day. Mean and high evaporation rates for the months of May through August, as well as means for four daily time periods (early morning, 4 a.m. to noon; day, 6 a.m. to 6 p.m.; afternoon, 3 p.m. to 12 p.m.; and night, 6 p.m. to 6 a.m.) are shown in Table 3.8. The values in Table 3.8 are higher than those calculated by Wade et al. (Ref 43) and shown in Table 3.7 because a higher concrete temperature of 32°C was assumed.

Wade's analysis of wind direction indicated that the strongest winds tend to be from the west. This is of interest for this project because the section of IH-10 to be overlaid was a depressed section running east-west; thus, the topography will tend to create a funnel and increase the speed of winds from the west.

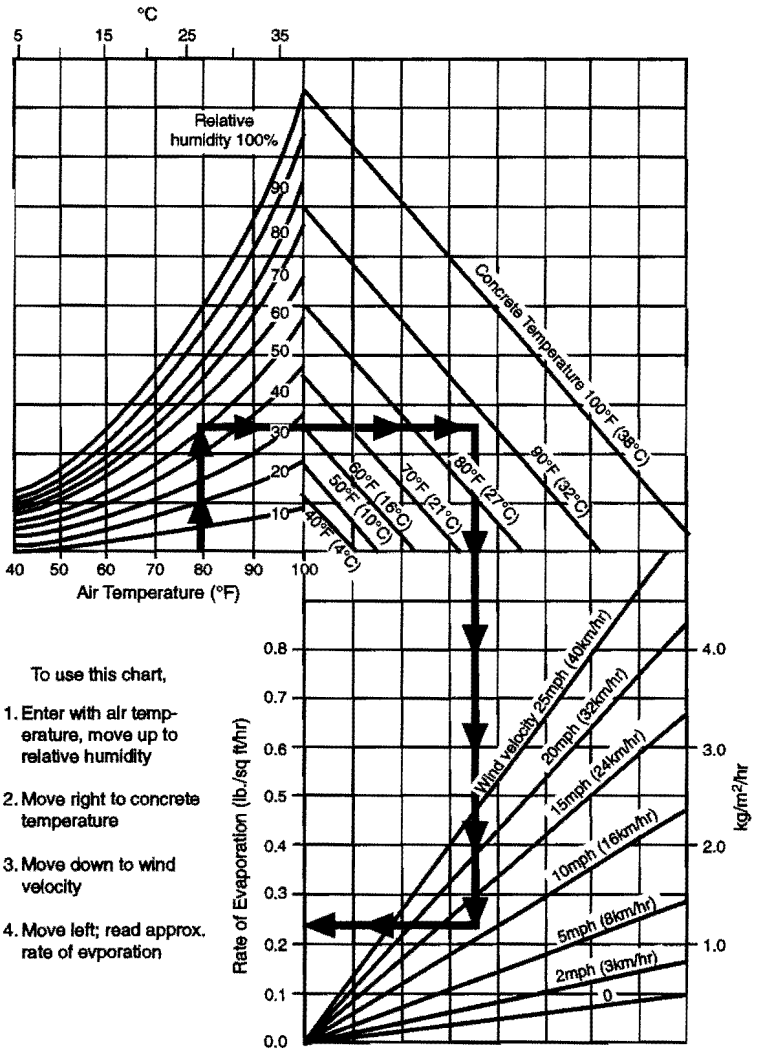

Figure 3.8 Evaporation prediction nomograph (Refs 46, 47, 55)

Table 3.7 Mean evaporation by month, El Paso, June 1992 to May 1994 (Ref 43)

Month	Mean Evaporation ($kg/m^2/hr$)
January	0.20
February	0.27
March	0.51
April	0.88
May	1.08
June	1.41
July	1.17
August	0.71
September	0.44
October	0.57
November	0.71
December	0.39

Table 3.8 Evaporation by time of day, El Paso, May–August ($kg/m^2/hr$)

Month	May	June	July	August
Mean Evaporation ($kg/m^2/hr$)	1.32	1.22	1.07	0.93
Highest Evaporation ($kg/m^2/hr$)	3.56	3.52	2.73	2.54
Mean evaporation, morning, 4 a.m. – noon ($kg/m^2/hr$)	1.17	1.07	1.00	0.88
Mean evaporation, day, 6 a.m. – 6 p.m. ($kg/m^2/hr$)	1.37	1.27	1.12	0.93
Mean evaporation, afternoon, 3 – 12 p.m. ($kg/m^2/hr$)	1.46	1.42	1.17	1.00
Mean evaporation, night, 6 p.m. – 6 a.m. ($kg/m^2/hr$)	1.27	1.22	1.07	0.88

Weather cannot be controlled, but adverse conditions for evaporation may be avoided by paving at times during the day when air temperatures are lower, humidity is higher, and winds are calmer. Moreover, concrete temperatures may be lowered by wetting aggregate stockpiles, use of ice or liquid nitrogen, use of retarders, use of cements with low heat of hydration (Type II or V), and cement replacement with fly ash. After batching, concrete temperatures increase as hydration proceeds. However, after the concrete sets, the temperature is no longer relevant for evaporation predictions because water is no longer evaporating from the concrete. Thus, the concrete temperature that is input into Equation 3.5 should be between that measured when the concrete is delivered to the job site and the temperature of the concrete when it sets.

CHAPTER 4. EXPERIMENTAL DESIGN

4.1 BACKGROUND

The objective of the experiment was to find one or more construction methods that would ensure good bonded concrete overlay (BCO) performance even under the most extreme environmental conditions. A secondary objective was to determine if any costly construction steps, such as shotblasting or installation of wire mesh, could be safely omitted.

A concrete mix design that performs satisfactorily in the laboratory may not perform well for construction of a BCO in the field. This is because thermal and shrinkage cracks are not likely to form in small laboratory specimens, but may affect long-term performance of a pavement. These cracks introduce discontinuities in the pavement structure that lead to stress concentrations, which may in turn initiate overlay debonding. Moreover, the reinforcement in the concrete greatly affects the formation and pattern of thermal and shrinkage cracks. This is virtually impossible to duplicate in the laboratory.

Several different designs for overlay test sections were constructed on an aggregate plant haul road in El Paso, Texas, on June 22, 1995. On May 1, 1995, a continuously reinforced concrete pavement base slab 137.2 m in length was constructed to simulate the existing condition of IH-10. The pavement was 200 mm thick and 3.66 m wide. The original mix design was duplicated as closely as possible with the available cement and aggregates. During base slab construction several different curing methods were tested, with the idea of using the most successful for the overlay construction. However, the humidity was unseasonably high and the wind speed was low, so evaporation was not severe (0.64 to 1.90 $kg/m^2/hr$).

Aggregate trucks were allowed to use the pavement over the next month before the BCO was cast in an attempt to induce fatigue damage. The BCO was one-lane wide, 121.9 m long, and 165 mm thick.

The following sections detail the experimental variables investigated, the construction specifications, and monitoring and instrumentation used and specimens prepared for strength testing for both the substrate slab and the BCO.

4.2 EXPERIMENTAL VARIABLES

4.2.1 Substrate Slab

The substrate slab placement was used to compare nine different curing methods. The slab was divided into eight 15.2 m long sections. Two curing methods were used on the first section. Curing methods investigated were wet mats or burlap with or without black plastic, Master Builders Confilm® Evaporation Reducer with and without curing compounds, and two different TxDOT-approved white pigmented membrane-forming curing compounds at normal and double application rates. The two curing compounds investigated were resin based (Secure THD Type II) and water based (Sealtight 2210 White Texas Type II). Although Confilm® is intended to be used with another curing method, one section was cured with Confilm® only. Curing methods for test sections are given in Table 4.1.

Table 4.1 Curing methods tested

Section	Method
1a	Wet mats/ burlap with water replenishment, covered with black plastic
1b	Wet mats/ burlap with water replenishment, no black plastic
2	Master Builders Confilm® at 4.9 m^2/L
3	Master Builders Confilm® at 4.9 m^2/L with Secure THD Type II at 3.7 m^2/L
4	Master Builders Confilm® at 4.9 m^2/L with Sealtight 2210 White Texas Type II at 3.7 m^2/L
5	Secure THD Type II at 3.7 m^2/L
6	Secure THD Type II at 1.8 m^2/L
7	Sealtight 2210 White Texas Type II at 3.7 m^2/L
8	Sealtight 2210 White Texas Type II at 1.8 m^2/L

4.2.2 BCO

The experimental variables encompassed in eight test sections were reinforcement of concrete (plain, polypropylene fiber reinforced, and steel fiber reinforced), use of shear connectors (nails and anchors), reinforcement, surface preparation, and day or night construction, as shown in Table 4.2.

4.2.2.1 Concrete. Two concrete mixes were used, with proportions as shown in Tables 3.3 and 3.5. For two sections, a plain concrete mix was used, as shown in Table 3.3, with one of the sections using 1.78 kg/m^3 of fibrillated polypropylene fibers (SnFRC). For the remaining six sections, concrete reinforced with 44.5 kg/m^3 of 60 mm steel fibers with hooked ends was used (SFRC). The water-cement ratio of both mix designs was 0.29 by weight. Superplasticizer was added at the batch plant, and additional superplasticizer was added at the job site as needed for workability. A superplasticizer with retarder (Monex Mighty RD-1) was substituted for the Rheobuild 1000 that had been used in the laboratory.

4.2.2.2 Shear Connectors. Two different types of shear connectors were tested in two test sections to explore possibilities of their use when a high probability of delamination exists. One type of connector used was a power-driven large nail (Figure 4.1). Each nail was installed into a predrilled hole with a powder-driven actuator. This connector was investigated in the laboratory work reviewed in Section 3.6. The second type of connector, a bolt, was epoxied into a predrilled hole (Figure 4.2).

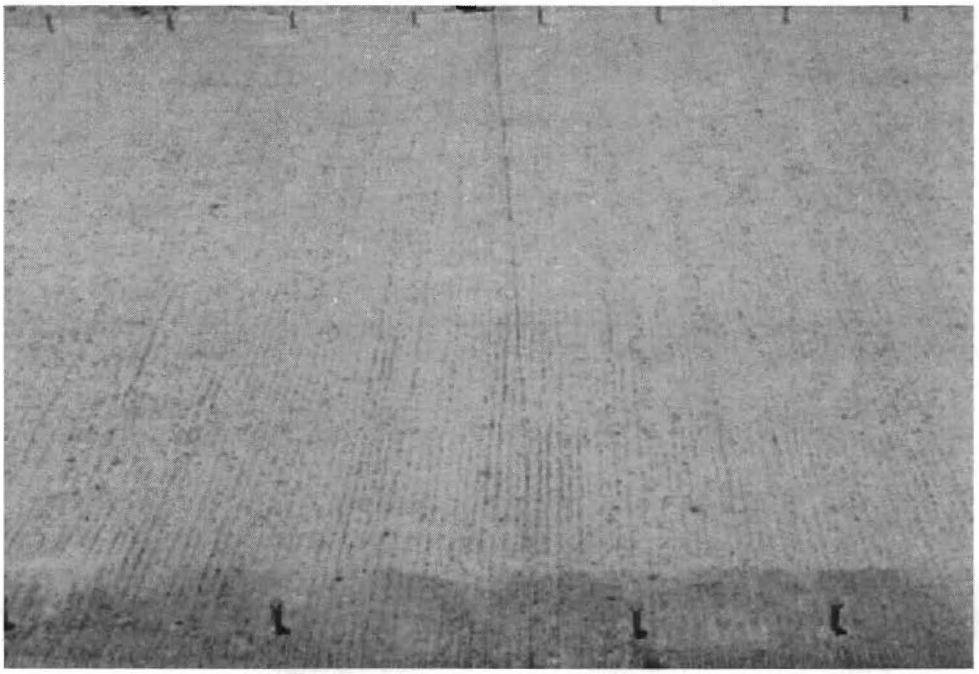

Figure 4.1 Installed nail shear connectors

Figure 4.2 Epoxied bolt shear connectors

The nails protruded approximately 55 mm above the base slab while the bolts protruded approximately 80 mm above the base slab. All shear connectors were installed along the longitudinal edges of two test sections, 152 mm from each edge, since delaminations generally start at a discontinuity. Nails were installed at spacings of 381 mm, 508 mm, and 762 mm. Bolts were installed at 508 mm on center. All four of these designs were tested in each of the two test sections containing nails.

4.2.2.3 Reinforcement. For four sections, the longitudinal steel was 12.7 mm bars (US #4), 152 mm on center and was not continuous between sections. Transverse steel was 12.7 mm bars (US #4), 457 mm on center (Figure 4.3). These steel percentages were selected to match the amount of steel in the base CRCP. Steel was placed directly on the base slab, without chairs. No steel was placed in the remaining four sections.

Figure 4.3 Installed nails and reinforcement with formwork

4.2.2.4 Surface Preparation of the Base Slab. In the past, several methods of preparing the base slab had been used, including shotblasting, cold milling, sandblasting, waterblasting, and airblasting. Cold milling may damage aggregate and create a plane of weakness in the base slab (Ref 6). The prepared surface is usually specified in terms of an average texture depth; for example, for an overlay in Louisiana, a texture depth of at least 1.14 mm was specified (Ref 40).

Hydrocleaning was investigated to determine whether it would produce an acceptable surface for overlay construction (Figure 4.4). Seven sections were shotblasted (Figure 4.5), and one section was hydrocleaned. Ideally, the pavement should be shotblasted or hydrocleaned immediately before paving, to avoid contamination of the surface in the interim. In this case this

was not possible, because the bond breaker, shear connectors, and formwork had to be installed. After these activities were completed, the surface was pressure washed to remove contamination.

Figure 4.4 Hydrocleaning equipment

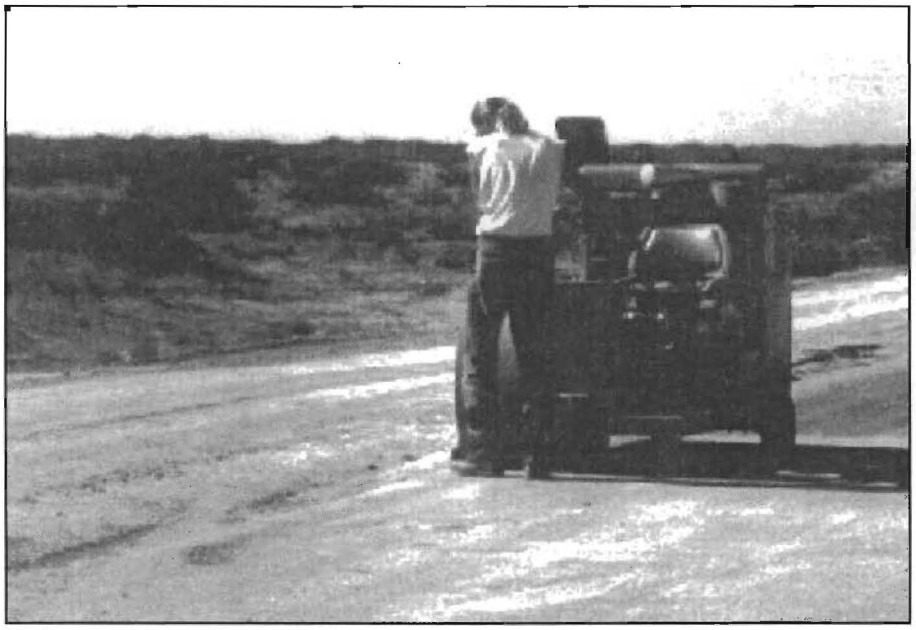

Figure 4.5 Shotblasting equipment used

4.2.2.5 Day/Night Construction. If a bonded concrete overlay is constructed early in the day, increasing air temperatures and solar radiation combined with the heat generated by a high early strength concrete mix can cause significant heat buildup in the slab. Subsequent cooling, combined with shrinkage, can induce severe tensile stresses in the slab, possibly exceeding the tensile strength of the concrete and causing cracking. BCO studies in Houston found that delaminations did not occur on days when the daily air temperature differentials were less than 14°C.

One section was constructed at night from 9:30 to 10:30 p.m. to investigate offsetting the concrete's heat of hydration with falling air temperatures. The other placement sections were constructed between 4:45 and 11:50 a.m. on June 22.

4.2.2.6 Test Sections. There were thirty-two possible combinations of the experimental variables listed above, all of which could not be investigated. The sections constructed are shown in Table 4.2.

Table 4.2 Test section specifications

Section	Surface Preparation	Nails	Reinforcement	Concrete Mix	Day/Night
1	Shotblast	No	Steel	Plain	Day
2	Shotblast	No	Steel	SnFRC	Day
3	Shotblast	No	Steel	SFRC	Day
4	Shotblast	Yes	Steel	SFRC	Day
5	Shotblast	Yes	None	SFRC	Day
6	Shotblast	No	None	SFRC	Day
7	Hydroclean	No	None	SFRC	Day
8	Shotblast	No	None	SFRC	Night

In effect, there are two basic cases. The first was a BCO constructed during the day using shotblasting and no shear connectors, and under these conditions the behavior of slabs with four different reinforcement schemes was compared. The second basic case was a BCO with steel fibers but no welded wire fabric. Under this set of parameters, the use of shear connectors, hydrocleaning, and nighttime construction on the performance of this type of pavement was investigated.

4.3 SPECIFICATIONS

4.3.1 Substrate Slab

4.3.1.1 Concrete. The concrete used was intended to duplicate IH-10 as constructed in 1964. The mix proportions were as shown in Table 4.3. The mix was designed with 5 percent air and TxDOT Grade 2 coarse aggregate (37.5 mm maximum size, ASTM Grade 467) (Ref 48). The surface was tined.

Table 4.3 Substrate slab mix constituents

Constituents	kg/m^3
Water	148
Type I/II Cement	279
Coarse Aggregate	1,142
Fine Aggregate	786
Admixtures ml/100 kg cement	
Air entrainer	132
Water reducer	195

4.3.1.2 Steel. Longitudinal steel was 16 mm bars (US #5). The outer two bars were placed 75 mm from the edge of the pavement, the next two were 133 mm inside the edge, and the rest were 190 mm on center. Transverse bars were 13 mm bars (US #4) placed 457 mm on center.

4.3.1.3 Terminal Anchors. Because of concerns that cracking would not develop in the base slab unless the ends were restrained, three terminal anchors were installed at each end.

4.3.1.4 Crack Sawing. Prior to surface preparation, transverse cracks 50 mm deep were sawed across the width of the pavement, spaced approximately 2 m apart.

4.3.2 BCO

4.3.2.1 No Bonding Agent. Although common practice is to use a bonding agent such as a grout or an epoxy (Ref 6), previous CTR research (Ref 9) found that under most conditions satisfactory bond could be achieved with a clean, dry, shotblasted surface. Thus, no bonding agent was used for this test.

4.3.2.2 Construction joints. Construction joints were placed between each section. Where used, reinforcing steel was not continuous between adjacent sections (Sections 1 through 4).

4.3.2.3 Finishing and Curing. All sections were broom finished and tined, then cured with TxDOT-approved Sealtight 2210 White Type II membrane forming curing compound at approximately 3.9 m^2/L.

4.3.2.4 Debonding Agent. Dayton Superior Sure-Lift J-6® was sprayed on as a debonding agent in certain parts of the test section. A 0.3 m strip of the north edge was debonded, as well as a 0.6 m strip between sections 1 and 2; 3 and 4; 5 and 6; and 7 and 8 (Figure 4.6). The agent was applied after shotblasting and hydrocleaning but before shear connectors were installed. The purpose of applying the debonding agent was to induce local delaminations for two purposes. The first was to investigate how well nondestructive testing methods could detect delaminations. The second was to determine whether the delaminations would spread under traffic and environmental loading.

4.4 MONITORING, INSTRUMENTATION, AND SPECIMEN PREPARATION

4.4.1 Substrate Slab

For substrate slab placement, data recorded included the development of strength with age of the concrete, the maturity and temperature history of the concrete slab, the weather, and surface cracking. Observations were also made during construction.

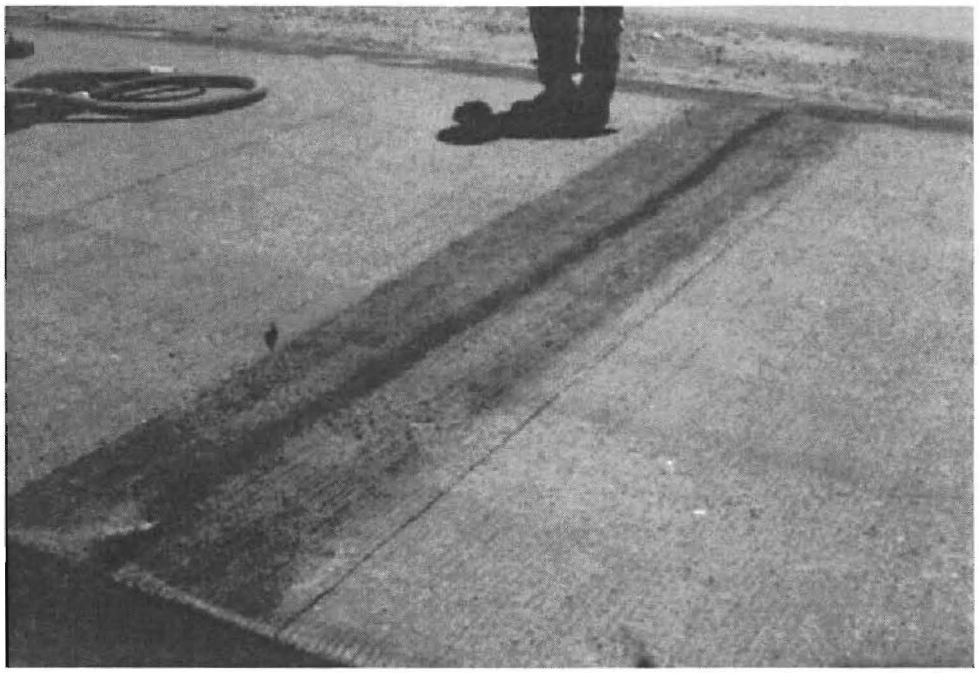

Figure 4.6 Debonding agent between sections

4.4.1.1 Strength. A total of thirty-five 152 mm by 305 mm cylinders was cast. Eleven were cured in the laboratory, and twenty-four were cured on site — three next to each test section and using the same curing method as that test section.

4.4.1.2 Maturity. The temperatures and maturities of the concrete slabs were measured using SDS Model 4101 Concrete Maturity Meters. These meters recorded data every 30 minutes. A thermocouple was tied to the steel in the center of each section.

4.4.1.3 Weather. Weather data were collected and recorded using a Campbell Scientific, Inc. tripod mounted weather station with a CR-10 datalogger (Figure 4.7). The weather station recorded air temperature, concrete temperature, wind speed, and relative humidity every 5 minutes. Concrete evaporation rates could be calculated from this data. In addition, the weather was compared to that recorded by the National Weather Service at the El Paso airport that day.

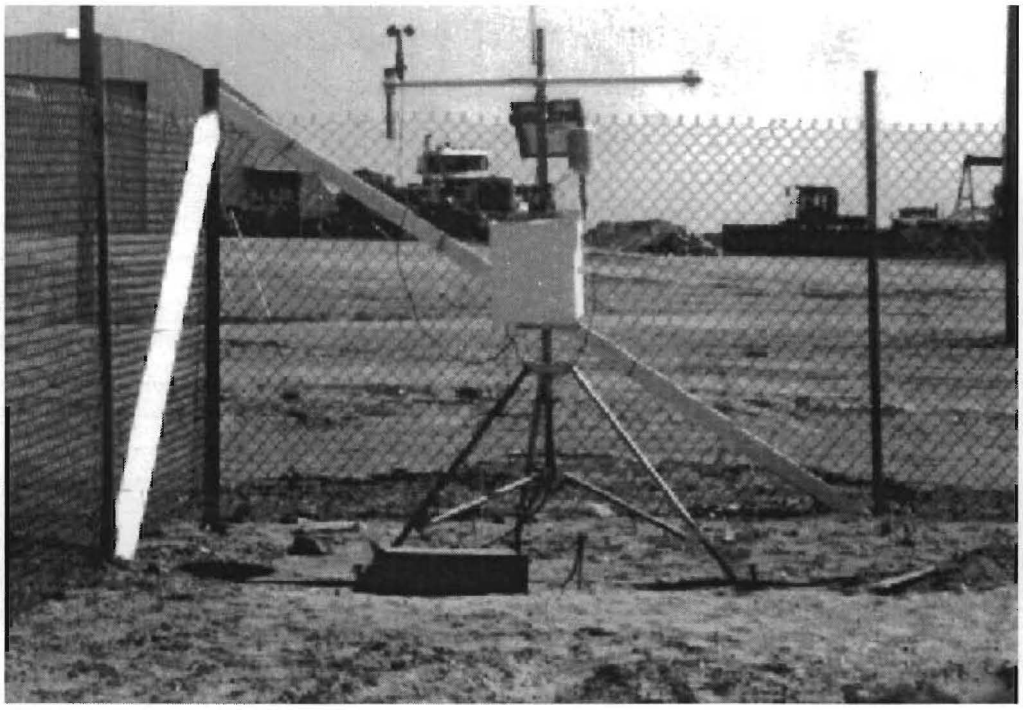

Figure 4.7 Tripod-mounted weather station

4.4.1.4 Cracking. It was also intended that cracking in each section would be recorded based on visual observations.

4.4.2 BCO

For BCO placement, all of the data above was gathered. In addition, the surface roughness of the prepared base slab was measured, nondestructive testing methods were used to attempt to detect and map delaminations, different strength specimens were made, BCO pull-off tests were made, thermal and moisture gradients were measured, and pavement strains were measured. The testing schedule is shown in Table 4.4.

4.4.2.1 Surface Roughness. The surface roughness of each section was measured using the sand patch method (test method Tex 436A, Figure 4.8).

4.4.2.2 Strength Testing and Bond Testing. The development of flexural, compressive, and bond strength of the concrete used was measured by casting beams and cylinders and testing them according to ASTM C-78 and C-39 (Ref 27), and by coring and testing bond specimens. For testing in compression and splitting tension, 100 mm x 200 mm cylinders were cast, and 152 mm x 152 mm x 508 mm beams were cast for flexural testing. Beams were also made from SFRC. Cores were drilled at 8, 16, 24, and 48 hours for testing in tension with a pull-off tester (Figure 4.9), and in shear with a guillotine-testing apparatus. Before the pull-off tester could be used, a steel cap was epoxied to the core. Cored specimens were intended to be tested with both a guillotine apparatus and a pull-off tester. However, owing to the thickness of the BCO it

proved to be impossible to extract any specimens for guillotine testing. Subsequently, pull-off tests were made at 3 and 5 months. Spectral Analysis of Surface Wave (SASW) (Refs 58, 59, 60) (Figure 4.10) and the Rolling Dynamic Deflectometer (RDD) (Figure 4.11) were also used to attempt to monitor pavement strength and stiffness development nondestructively.

Table 4.4 Testing schedule

Time interval	Type of test/ monitoring					
	Weather	Maturity	Coring	Compressive	Splitting Tension	Flexural
Continuous	Yes	Yes				
8 hours			8	2	2	1
16 hours			8	2	2	1
24 hours			8	2	2	1
48 hours			16	2	2	1
7 days				2		1
28 days				2	2	

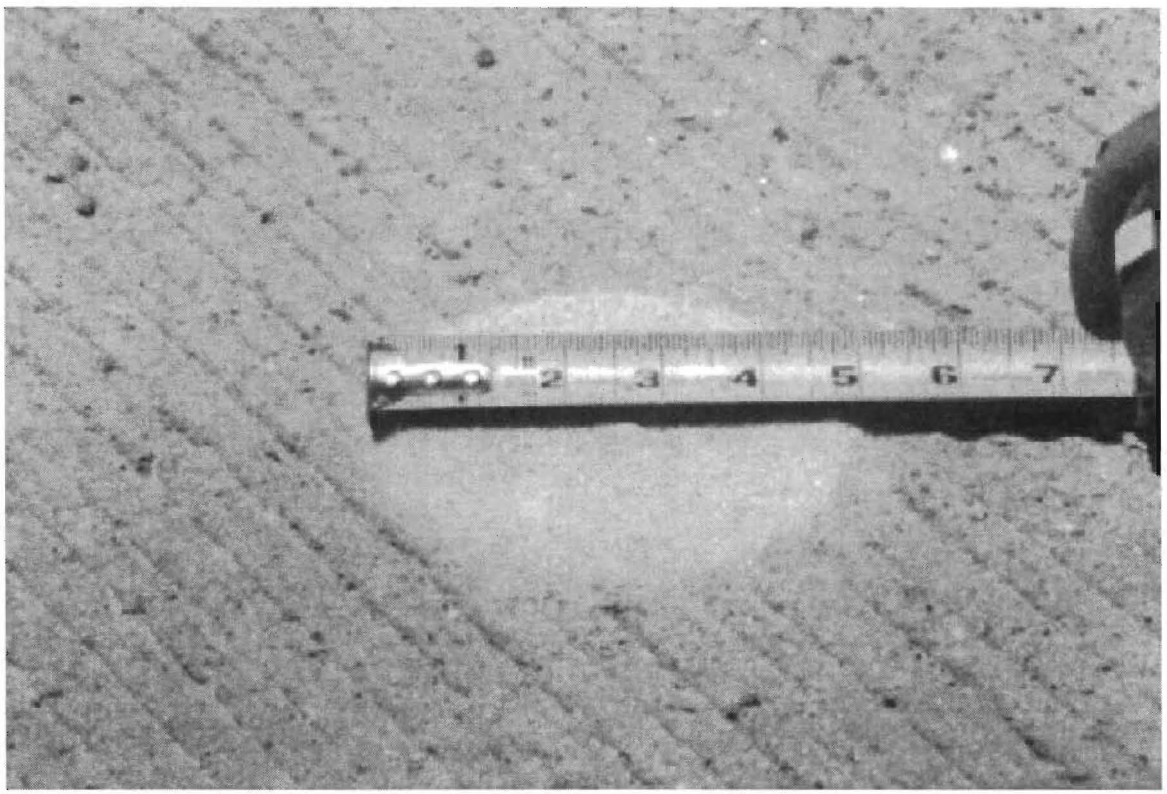

Figure 4.8 Sand patch method

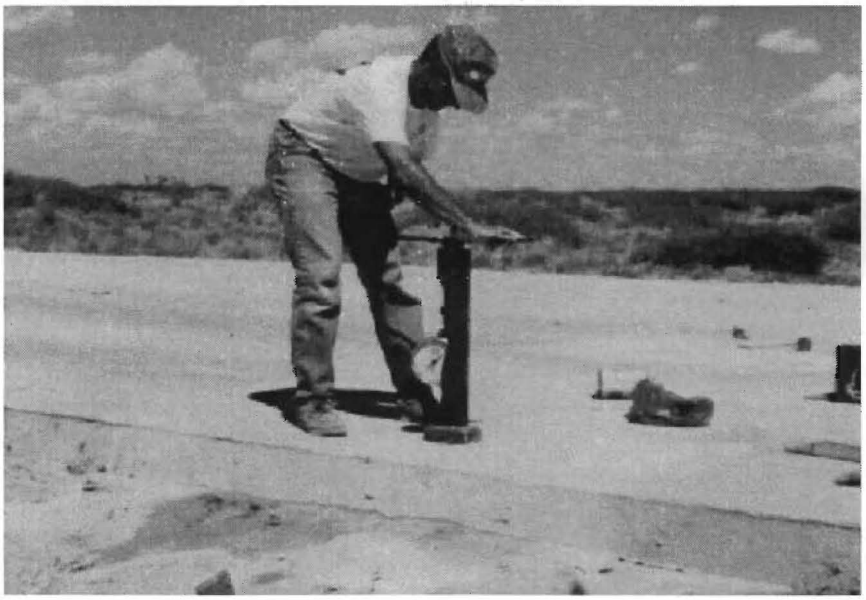

Figure 4.9 Pull-off testing procedure

4.4.2.3 Maturity, Thermal and Moisture Gradients, and Pavement Strains. Maturity meters were used to record slab temperatures and maturities as above. The thermocouple was placed at the center of each section, just above the interface between the overlay and the base slab. These maturity meters sampled at 30-minute intervals for the first 48 hours and at 1-hour intervals thereafter.

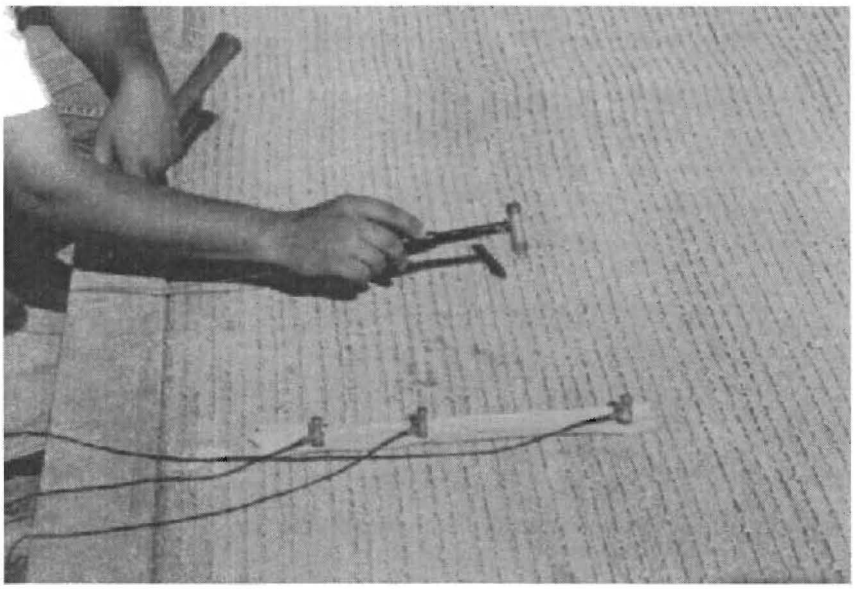

Figure 4.10 Spectral analysis of surface wave testing

Figure 4.11 Rolling Dynamic Deflectometer (RDD)

Data on thermal and moisture gradients and pavement strains were collected at several locations as shown in Table 4.5. To measure thermal gradients, four thermocouples were spaced equally through the depth of the BCO. Thermocouples were read every 30 minutes for the first 3 hours, hourly for the next 3 hours, and every 6 hours thereafter. Moisture data in the form of wet and dry bulb temperatures, which could be converted to relative humidity values, were recorded at three locations at different depths in the overlay. Moisture gauges were read every 2 hours for the first 12 hours and every 6 hours thereafter. Three vibrating wire strain gauges were installed at one location in the BCO. The gauges were oriented longitudinally at the top, middle, and bottom of the overlay. Strain gauges were read at the same time as the thermocouples.

Table 4.5 Location of thermal and moisture gradient and pavement strain instrumentation

Location	Section	Distance North within section (m)	Distance West (m)	Purpose
Thermocouple set 1	1	8.1	3.5	Start of day placement
Thermocouple set 2	6	7.2	3.5	At sawcuts in base slab
Thermocouple set 3	7	5.9	3.5	End of day placement
Thermocouple set 4	8	9.4	3.5	Night placement
Moisture meter set 1	6	7.6	3.5	At sawcuts in base slab
Moisture meter set 2	8	8.9	3.5	Night placement
Vibrating wire strain gauges (3)	6	5.8	3.5	At sawcuts in base slab

4.4.2.4 Weather. Weather data was recorded as above.

4.4.2.5 Cracking. It proved to be very difficult to detect cracking on a tined slab surface. As a result, when the formwork was removed from the north side of the slab, the edge was left exposed, and cracking was visually detected and measured along that smooth edge.

4.4.2.6 Delamination Detection. Several electronic and nonelectronic, nondestructive testing methods were used in an attempt to detect and map delaminations. They were SASW (Refs 62, 63, 64) (Figure 4.10), three different impact-echo devices (Figures 4.12, 4.13, 4.14) including the Defect Orientation Confirmation Tester (DOCter) (Figure 4.14) (Ref. 65), impulse-response (Figure 4.15), the Rolling Dynamic Deflectometer (RDD), and the falling weight deflectometer (FWD) (Figure 4.16).

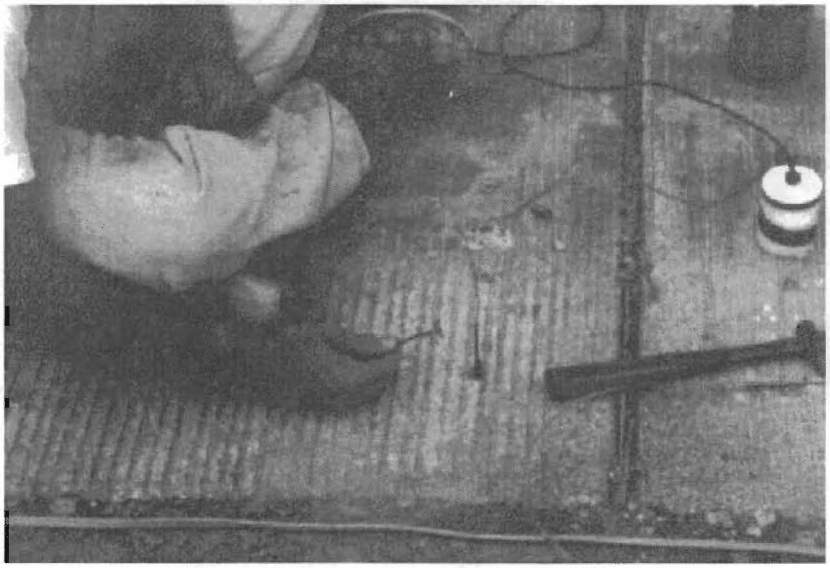

Figure 4.12 Impact-echo testing

Figure 4.13 Impact-echo testing using equipment supplied by Olson Engineering

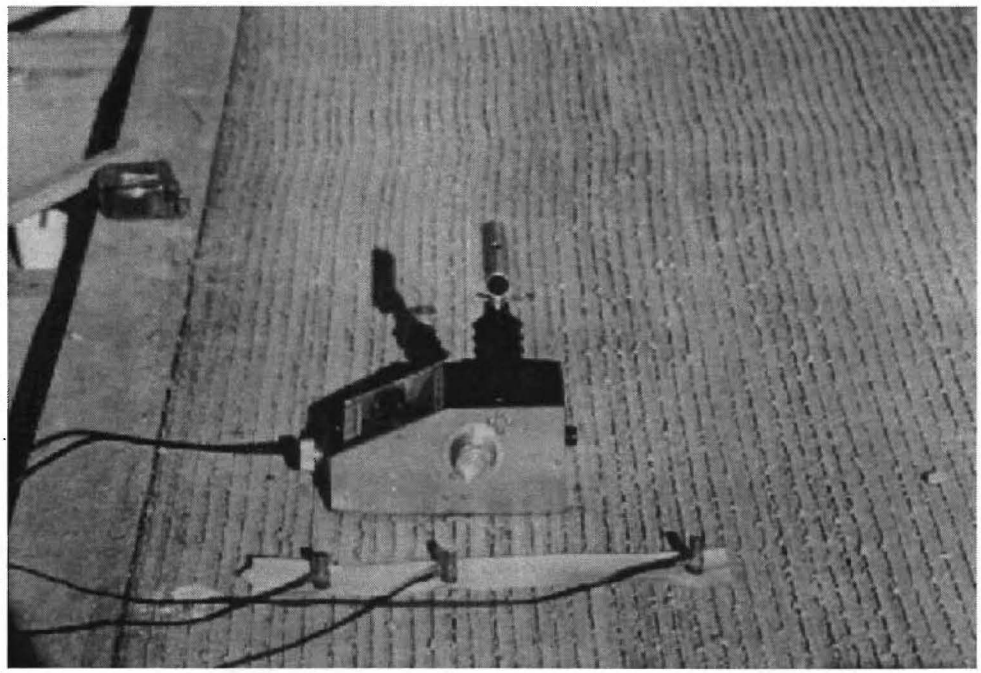

Figure 4.14 Impact-echo testing using the DOCter

Figure 4.15 Impulse-response testing

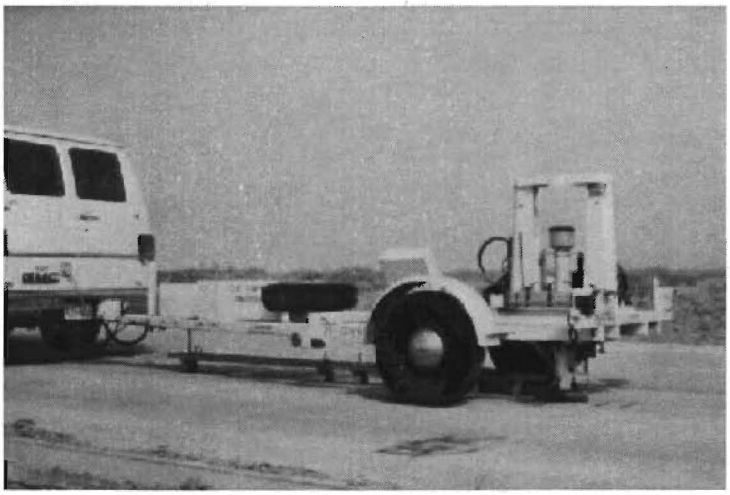

Figure 4.16 Falling Weight Deflectometer (FWD)

a. Nonelectronic Methods. Rebar sounding and the impact (Schmidt) hammer were used.

1. Rebar sounding. In this method a piece of reinforcing steel 10 to 20 mm in diameter and 1 to 1.5 meters long is dropped on the overlay from a height of 100 to 300 mm (Figure 4.17). Rebar dropped on the overlay over a delamination sounds *hollow* compared to a sounding made in the interior of the slab, where the BCO is presumably well bonded. Also, it is possible for the operator to feel vibrations in his feet when the rebar is dropped over a delamination. This method is subjective and dependent upon the skill of the operator.

Figure 4.17 Rebar sounding

2. Impact (Schmidt) hammer. It was theorized that impact hammer readings over delaminations might be less than readings over fully bonded BCOs due to greater flexibility of the pavement structure. However, no significant differences were noted, at least for a BCO of this thickness (165 mm).

b. Description of Electronic Methods. SASW, impact-echo, impulse-response, the RDD, and the FWD were used. All used the same analyzer (Figure 4.18) and stored the responses on disks. The methods are compared in Table 4.6.

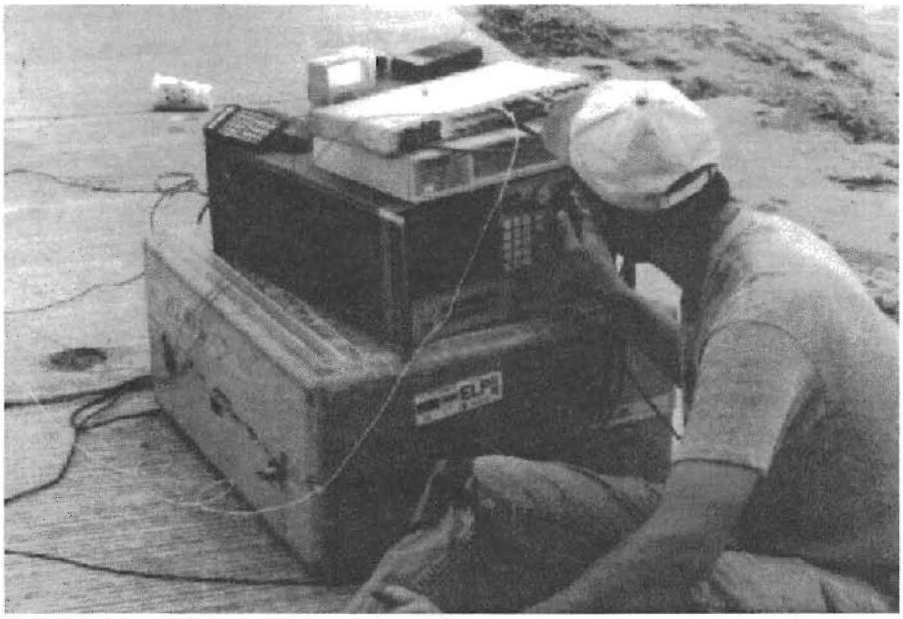

Figure 4.18 Analyzer used for electronic testing methods

1. SASW. In this method the BCO is struck with a small hammer and two accelerometers (acceleration transducers) pick up surface wave arrivals (Figure 4.9). A phase diagram is plotted on the analyzer. Delamination is indicated by a loss of low-frequency energy. This indicates that surface waves with amplitudes greater than 165 mm (the depth of the interface) are not propagating. Small steel washers were epoxied to the pavement and the transducers were magnetically attached to them.
2. Impact-Echo. A very small hammer with a load cell is used to impact the pavement next to an accelerometer (Figure 4.11). The accelerometer is one of the two used for SASW. The return energy is plotted in the frequency domain. Delamination is indicated by a lack of a return at a specific frequency. For example, with the pavement thicknesses used in this experiment a well-bonded overlay shows returns at 12 kHz (the interface between the BCO and the original pavement) and 5 kHz (the bottom of the original pavement). In a delaminated region the impulse is not transmitted past the interface and the 5 kHz return is not present. Two other types of impact-echo equipment were also used (Figures 4.12 and 4.13).

Table 4.6 Comparison of electronic nondestructive testing methods

Method	SASW	Impact-Echo	Impulse-Response
Excitation	Hammer	Small hammer with load cell	Large hammer with load cell
Measurement by	2 accelerometers	1 accelerometer	1 geophone
Measures	Surface wave arrivals	Return energy	Return energy
Plots	Phase diagram between surface wave arrivals in the frequency domain	Return energy in the frequency domain	Return energy in the frequency domain
Delamination indicated by	Loss of low frequency wave transmissions	Lack of return from bottom of original pavement	Lower flexural stiffness

3. Impulse-Response. This method is similar to impact-echo but a much larger hammer is used, producing much lower frequency impulses, and the return is measured with a geophone (velocity transducer) (Figure 4.14). A delaminated BCO would be less stiff flexurally than a well-bonded overlay.
4. RDD. The RDD excited the pavement with two aluminum loading wheels, and measured responses with displacement transducers. The RDD was rolled along the pavement at 0.6 to 1 meter per second. Deflection responses to inputs at 20 and 40 Hz were measured.
5. FWD. The FWD trailer drops a weight on the pavement from four different heights, and deflections are recorded by seven geophones. Both peak responses and dynamic response history were recorded. The FWD was positioned at four or six locations in each of the test sections, for a total of forty test locations.

CHAPTER 5. CONSTRUCTION AND MONITORING OF THE CRCP BASE SLAB

The results developed from the substrate slab are presented in terms of observations during construction, strength testing, weather and slab temperatures, and cracking.

5.1 OBSERVATIONS DURING CONSTRUCTION

The construction began at the west end of the slab at 2:27 p.m. and ended at 5:50 p.m. on May 1, 1995. Concrete temperatures and slump were measured for four of the fourteen trucks. Concrete temperatures ranged from 27°C to 28°C, and slumps were 44 mm to 100 mm. The different curing methods in the different sections are shown in Figure 5.1.

5.2 STRENGTH TESTING

A total of thirty-five 152 mm by 305 mm cylinders was cast. Eleven were cured in the laboratory, and twenty-four were cured on site. Of the on-site cylinders, three were cured next to each test section using the same curing method as that test section. Strength is presented for laboratory-cured cylinders and field-cured cylinders. At 2, 7, and 29 days, three laboratory cylinders were tested. Average strengths are shown in Figure 5.2. Strengths of field cylinders at 29 days are shown in Table 5.1. Three cylinders were tested for each section, and the average is shown. The 29-day cylinder strength of 26.7 MPa was 39 percent lower than the 44.1 MPa average of the IH-10 cores.

5.3 MATURITY AND TEMPERATURE DATA

Test section and air temperatures are shown in Figure 5.3 for the first 19 hours after the test sections were cast. The maturity attained by each section during that period is plotted in Figure 5.4. The maturities attained were very similar. The maturity meters began recording at 1:30 p.m., but curing did not begin until after the concrete had set, between 3 and 6 p.m.

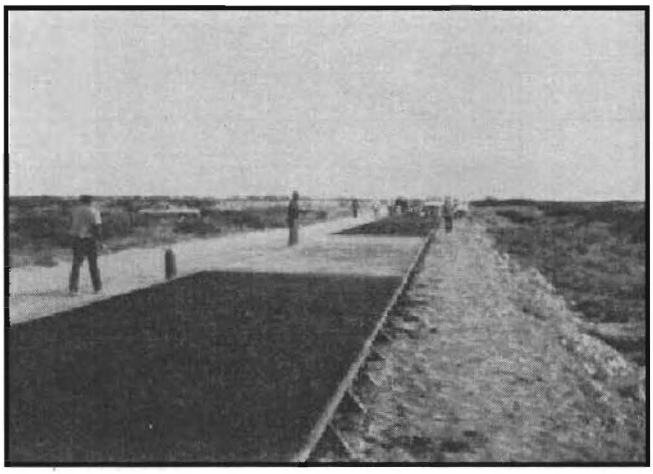

Figure 5.1 Comparison of curing methods

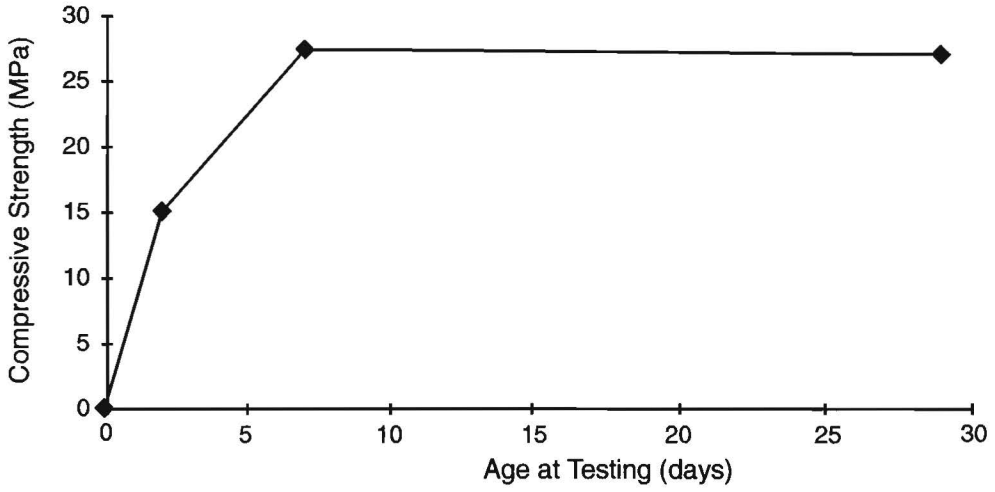

Figure 5.2 Development of substrate slab compressive strength based on laboratory curing

Table 5.1 29-day strength of field cylinders using different curing methods

Section	Type of Curing	Compressive Strength, MPa
1	Wet Mats/Plastic	20.2
2	Confilm	7.9
3	Confilm W/Secure	15.2
4	Confilm W/Sealtight	13.6
5	Secure @ 3.69 Sq M/L	9.1
6	Secure @ 1.84 Sq M/L	15.4
7	Sealtight @ 3.69 Sq M/L	9.4
8	Sealtight @ 1.84 Sq M/L	14.5

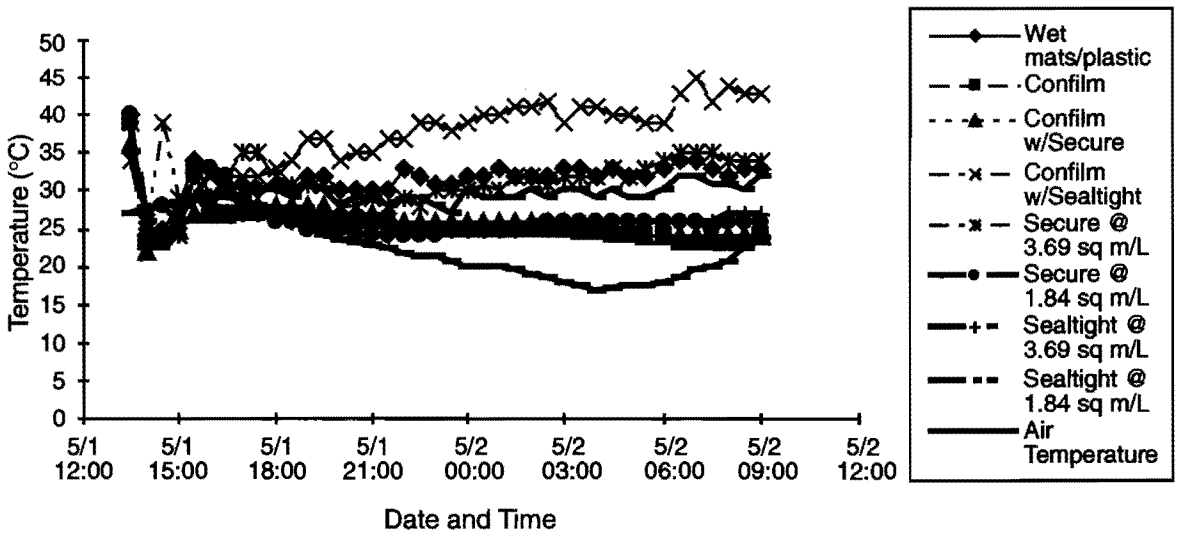

Figure 5.3 Slab and air temperatures during first 19 hours

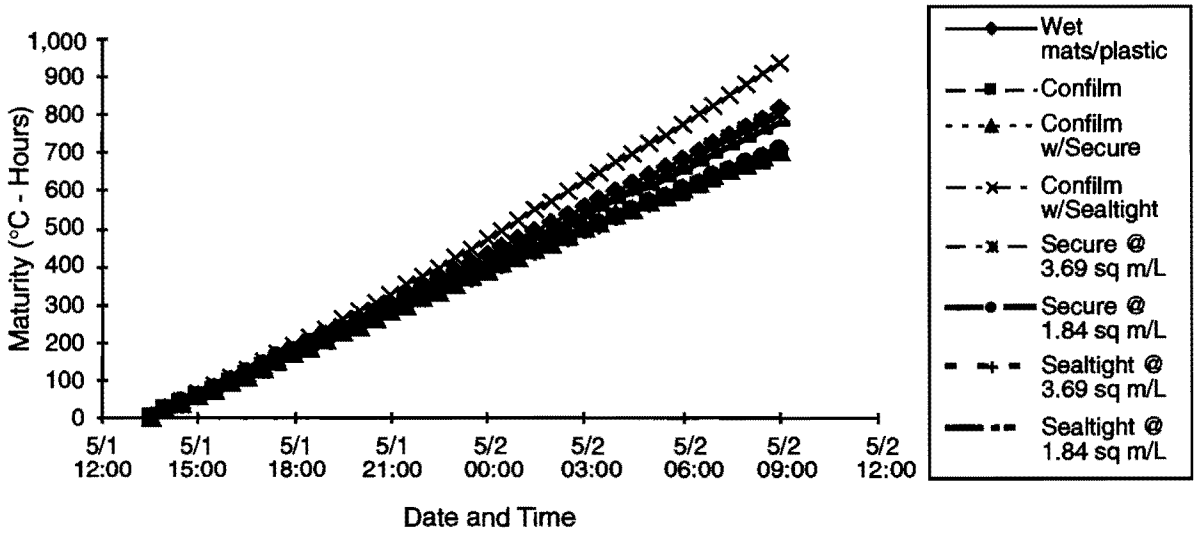

Figure 5.4 Maturity attained by each test section

5.4 WEATHER AND EVAPORATION

Weather data gathered by the Campbell Scientific Weather Station between 11:12 a.m. and 7 p.m. on May 1, 1995 are plotted in Figures 5.5 through 5.7.

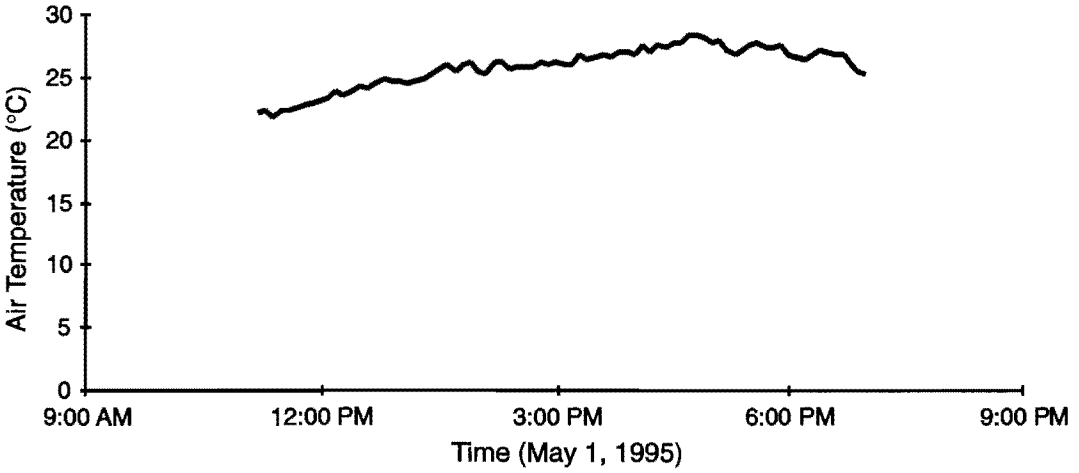

Figure 5.5 Air temperature during substrate slab construction

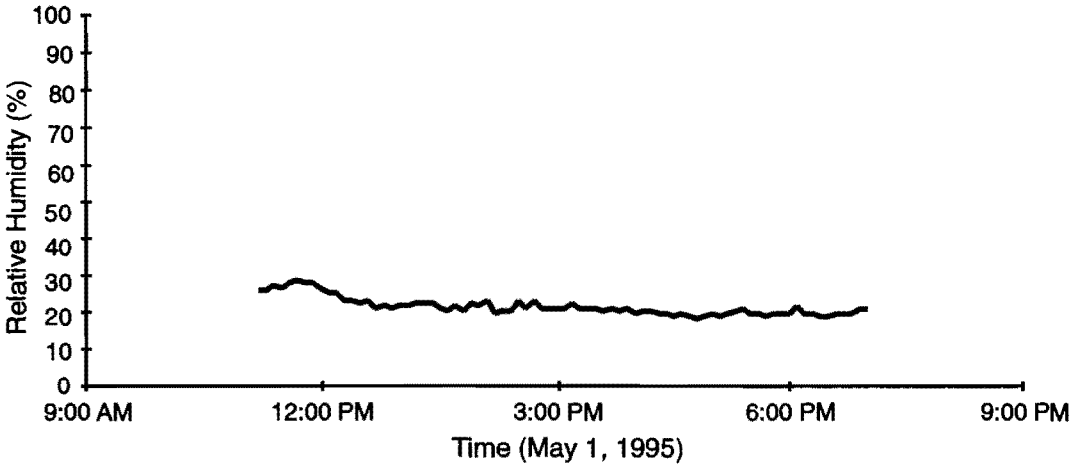

Figure 5.6 Relative humidity during substrate slab construction

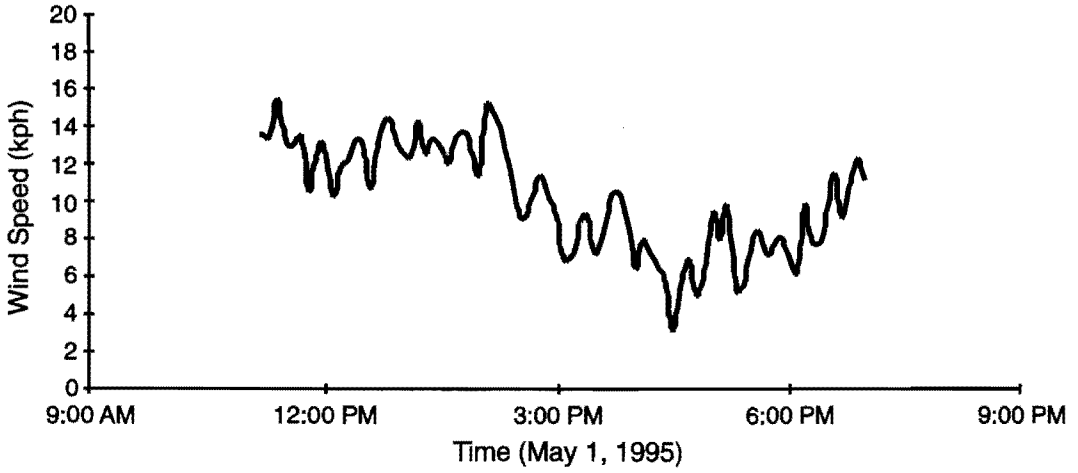

Figure 5.7 Wind speed during substrate slab construction

Evaporation predictions assuming a concrete temperature of 33°C are shown in Figure 5.8. The weather station is shown in Figure 4.7.

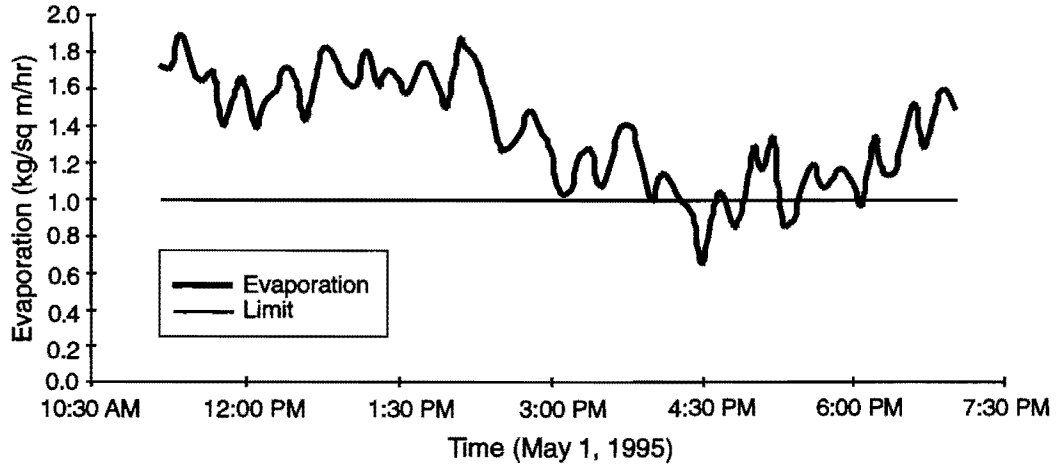

Figure 5.8 Evaporation predictions during substrate slab construction

The weather data gathered by the weather station were compared to that gathered at El Paso International Airport by the National Weather Service (NWS). Temperature, relative humidity, and wind speed data gathered by the weather station and the NWS on the afternoon of May 1, 1995 are compared in Table 5.2.

Table 5.2 Comparison of weather station and NWS data

	NWS Data			Weather Station (Nearest Sample Time)		
Time	Air Temperature, °C	Relative Humidity, Percent	Wind (Kph)	Air Temperature, °C	Relative Humidity, Percent	Wind (Kph)
11:52	24	24	20.3	23	27	15.5
12:53	26	22	22.1	25	20	16.7
1:53	26	23	18.4	26	21	15.5
2:53	28	21	12.9	26	20	12.5
3:50	28	20	14.7	27	19	12.9
4:50	29	20	9.2	28	17	6.0
5:51	29	20	18.4	27	18	9.9
6:51	27	22	14.7	26	19	13.9

Although the values and trends are similar, there is some variation in wind speed. For the NWS, the mean and standard deviation of the wind speed were 16.3 and 4.23 Kph, respectively, compared to 12.9 and 3.50 Kph measured at the weather station.

The evaporation rates predicted by weather station and NWS data, based on a concrete temperature of 33°C, are compared in Figure 5.9 below. Because the weather station data were only available on the hour, the corresponding weather station data alone are plotted in this figure. The trends of the weather station and NWS predictions are similar, and the evaporation was greater than 1.0 kg/m^2/hr for nearly the entire afternoon for both sets of data.

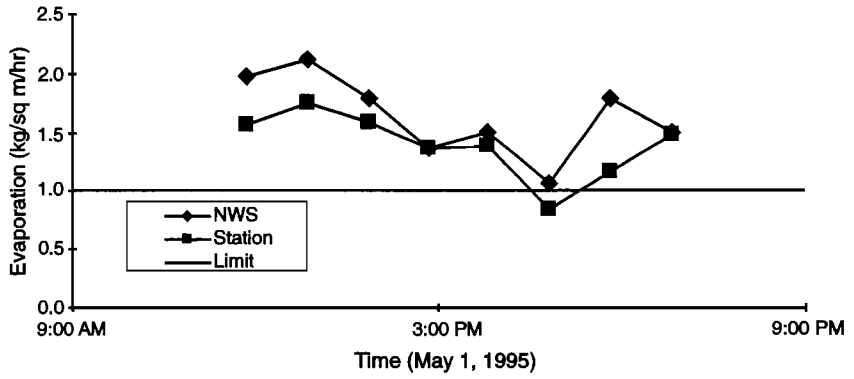

Figure 5.9 Comparison of evaporation predictions

5.5 CRACKING

It proved to be very difficult to detect cracking due to the tined surface of the test sections. With the exception of three cracks cut using a Sof-cut saw shortly after concrete placement, only one wide crack could be observed, near the midpoint of the section. As a result, cracks were sawcut 2 meters apart and 50 mm deep to duplicate the cracking on IH-10.

CHAPTER 6. BCO TEST SECTION RESULTS

For the bonded concrete overlay (BCO) test section, the results are presented in terms of comparing surface preparation methods, observations during construction, strength testing including coring and pull-off testing, maturity, temperature data, temperature and moisture gradients, pavement strains, weather and evaporation, cracking, nondestructive testing and delamination detection, and application of loading.

6.1 SURFACE PREPARATION

Using the sand patch method (Refs 27, 67) (Figure 4.8), the roughness of the shotblasted sections varied from 1 to 1.6 mm, with a mean and standard deviation of 1.30 mm and 0.15 mm, respectively. The sand patch method is subjective, and on two of the sections results varied by approximately 28 percent depending upon the person performing the test. The roughness of the hydrocleaned section varied from 1.5 to 2.0 mm, with a mean and standard deviation of 1.71 mm and 0.25 mm, respectively. Sand patch roughness values are shown in Table 6.1.

Table 6.1 Sand patch roughness values

Section	Roughness Measurements (mm)
1	1.27, 1.60
2	1.32, 1.52
3	1.32, 1.52
4	1.04, 1.19, 1.19, 1.19, 1.22, 1.27, 1.30, 1.32, 1.60
5	0.99, 1.12, 1.19, 1.19, 1.22, 1.22, 1.32, 1.32, 1.52
6	1.27, 1.52
7	1.52, 1.52, 1.85, 2.01
8	1.19, 1.42

The lowest roughness values for the hydrocleaned section were higher than the highest roughness values for the shotblasted section. Note that only three of the thirty-two tests would not have met a roughness standard of 1.14 mm, which was the specification recommendation first proposed for El Paso construction. This was the roughness specified for a steel fiber reinforced concrete (SFRC) BCO on IH-10 in Louisiana (Ref 40). The final recommendation for El Paso was 1.52 mm. Only ten of the thirty-two tests would have met this roughness standard.

For both methods of surface preparation, the roughness of the surface may be increased by slowing the pace of the machine. Each machine took about 30 to 45 minutes to prepare one 55.8-square-meter section. Hydrocleaning was a little slower, but produced a rougher surface. Production rates depend upon the desired surface roughness. Both methods cost approximately $1.50 per square meter, based on quotes from the Rampart Division, Flow International, and the Humble Equipment Company for hydrocleaning and shotblasting, respectively.

6.2 OBSERVATIONS DURING CONSTRUCTION

6.2.1 Workability

With such a low water-cement ratio, the mix was very difficult to work, even with a superplasticizer. The steel fibers also made the mix less workable. A small amount of additional water (19 to 56 liters) was added to each truckload, in addition to more superplasticizer.

6.2.2 Balling of Steel Fibers

The collated steel fibers, in sheets held together by a water-soluble glue, were supplied in 30 kg bags. For the first truck, the fibers were placed in the mixer before the concrete, leading to severe balling of the fibers in the mixer. The balls were approximately 200 to 250 mm in diameter and consisted of tightly interlocked fibers and paste. They could not be broken up and had to be removed from the fresh concrete.

Subsequently, the fibers were added to each truck, then a small amount of concrete, water, and superplasticizer was added and the mixture agitated. This led to satisfactory dispersion of the fibers, with only a few balls per truck. However, for a large project this would still be unsatisfactory, because the balls interfere with construction and rob the concrete of paste as well as fibers.

The manufacturer recommends that the fibers be added either to the coarse aggregate on a conveyor belt or placed by hand into the truck after the concrete, with the truck no more than 80 percent full. Both methods are labor intensive and impractical for large jobs demanding high production rates. If an aggregate bin is available, the best alternative would probably be to measure the fibers by weight along with the other mix constituents. Because water is needed to dissolve the glue holding the fibers together, a SFRC with a slightly higher water-cement ratio would be easier to work with. Neither the contractor nor the concrete supplier had worked with SFRC prior to this test.

6.2.3 Delay in Applying Curing Compound

Due to equipment problems, curing compound was not applied to the first section (Test Section 1) until the surface had begun to dry. Plastic shrinkage cracking subsequently appeared.

6.2.4 Finishing the SFRC

Prior to construction, concerns had been expressed that the SFRC would be hard to broom and tine finish, and steel fibers would protrude from the concrete to puncture tires. In fact, once the vibrating screed beam had leveled the concrete, the fibers were no longer visible, and no finishing problems were encountered.

6.2.5 Concrete Temperature for Night Placement

The night placement was intended to take advantage of falling air temperatures; however, this was offset in part because the concrete temperature was the highest recorded during the test. This was due to the fact that the mix constituents had been absorbing heat all day. This should be taken into account for concreting during the early evening.

6.3 STRENGTH TESTING

Compressive, flexural, and splitting tensile strength of the concrete were measured from prepared test specimens. Compressive and splitting tensile strengths were also measured from cores. Bond strengths were measured using pull-off tests of cores.

6.3.1 Prepared Test Specimens

At 8, 16, 24, and 48 hours and 7 days, two cylinders were tested in compression, two cylinders were tested in splitting tension, and one beam was tested in flexure. Two cylinders each were also tested in compression and splitting tension at 28 days. Strengths are plotted in Figure 6.1 and listed in Table 6.2. Two SFRC beams were tested at 7 days, cracking at an average of 5,710 kPa, and carrying 57 percent and 71 percent of the peak load after cracking. These concrete strengths were higher than those that had been obtained in the laboratory at similar ages were. The TxDOT specified strengths for CO class concrete (compressive strength of 32 MPa at 28 days and 4,410 kPa at 7 days (Ref 49)) were both exceeded by the time the concrete was 16 hours old.

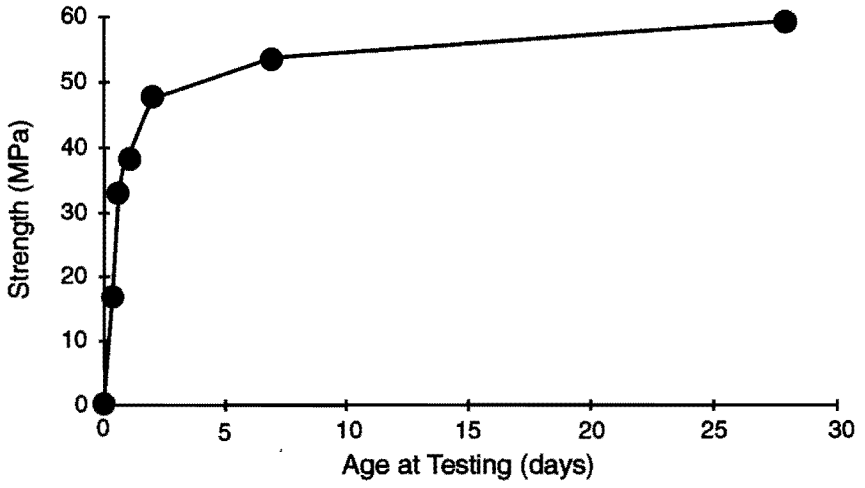

a. Compressive strength

Figure 6.1 Concrete strength gain

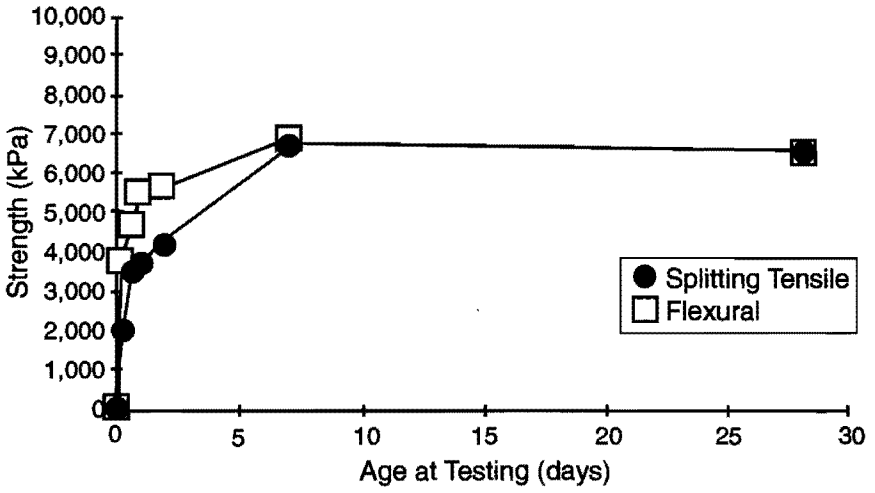

b. Flexural and splitting tensile strength

Figure 6.1 (continued) Concrete strength gain

Table 6.2 Concrete strength gain

Age at testing (days)	Compressive (MPa)	Splitting Tensile (kPa)	Flexural (kPa)
0.33	16.5	2,100	3,800
0.67	33.8	3,600	4,700
1	38.7	3,800	5,500
2	47.9	4,300	5,700
7	54.1	6,800	7,000
28	59.5	6,700	-
TxDOT Specification (Ref 48)	32 MPa @ 28 days	-	4,410 kPa @ 7 days

6.3.2 Cores

Cores were removed from the BCO immediately after placement, on September 18, and on November 22, 1995, in conjunction with pull-off testing. All cores were tested dry. Additional cores were also removed on December 9–11, 1995 and February 23 and 24, 1996. Since there had been little variation among previous cores, only a few cores from November and December were tested. None of the cores drilled in February 1996 was tested.

6.3.2.1 Cores drilled just after BCO placement. On August 10, 1995, nineteen cores drilled from the test sections were tested in the laboratory. These cores were 102 mm in diameter. Fourteen of the cores were tested in splitting tension, and five in compression.

The cores had been drilled between 16 and 50 hours after the BCO was cast. Four days after casting, they were placed in a moisture chamber. They were allowed to dry for one day before testing. The tests were performed when the concrete was 50 days old.

Lengths of the fourteen cores tested in splitting tension varied from 168 to 200 mm. Some cores were not straight, and thus broke at low strengths due to uneven bearing in the splitting tensile apparatus. Reinforcing steel, when present in the cores, did not cross the failure plane and thus did not affect strength. Strengths are tabulated in Table 6.3. If all cores are considered, the mean strength is 6,100 kPa, the standard deviation is 1,270 kPa, and the coefficient of variation (COV) is 0.21. If the cores that did not have even bearing along the sides (1, 2, 8, 11, and 14) are not considered, the new mean is 6,800, the standard deviation is 850, and the COV is 0.12. If cores do not have even bearing along the sides, the stress is not uniform, and the cores fail at a lower load. The latter values should be used for analysis. Of the nine cores used in the above calculations, only one (core 7) did not have steel fibers. Its strength (6,300) was within one standard deviation of the mean. The mean value of 6,800 kPa (disregarding cores with uneven bearing) is very close to the 7- and 28-day strengths measured from cylinders of 6,800 and 6,700 kPa.

Table 6.3 Splitting tensile strengths (cores removed directly after placement)

Core	Section (if known)	Steel rebar	Steel fibers	Polypropylene fibers	Stress, kPa
1	1	Yes			3,600
7	1	Yes			6,300
11	2	Yes		Yes	5,500
2	3	Yes	Yes		4,700
8	4		Yes		4,800
13	4		Yes		5,000
3	5		Yes		7,000
10	5				6,600
12	5		Yes		7,200
4	7		Yes		7,100
5	7		Yes		7,000
6	7		Yes		6,900
9	Unknown		Yes		8,200
14	Unknown				5,300

Five cores were tested in compression, as shown in Table 6.4. No reinforcing steel was present in any of the cores. Lengths varied from 162 to 175 mm after ends were sawn square. Compressive strength values are corrected for the lower aspect ratio by multiplying by 0.97 (as per ASTM C39-93a, Ref 27).

Table 6.4 Compressive strengths (cores removed directly after placement)

Core	Type	Stress, MPa
1	Polypropylene fiber	61.7
2	Plain	52.6
3	Steel fiber	53.5
4	Steel fiber	60.0
5	Steel fiber	55.7

All values appear reasonable. The mean strength is 56.7 MPa, the standard deviation is 4.0 kPa, and the COV is 0.07. This is within 4.7 percent of the 28-day cylinder strength of 59.5 MPa.

6.3.2.2 Cores drilled on September 18, 1995. Nine cores were tested in splitting tension in the laboratory (Table 6.5). Reinforcing steel did not cross failure planes. These cores were 108 mm in diameter.

Table 6.5 Splitting tensile strengths (cores removed after three months)

Core Number	Section	Steel Rebar	Steel Fibers	Polypropylene Fibers	Stress, kPa
3	2	Yes		Yes	6,500
5	4	Yes	Yes		7,200
8	5		Yes		6,200
9	5		Yes		6,800
10	5		Yes		7,200
11	5		Yes		8,000
13	5		Yes		9,000
15	6		Yes		6,000
18	6		Yes		5,300

The mean value of the splitting tensile strength of all nine cores was 6,900 kPa, with a standard deviation of 1,090 kPa and a COV of 0.16. If cores number 8 and 15 are disregarded, because of uneven bearing on the sides, the mean value becomes 7,100 kPa, the standard deviation 1,140 kPa, and the COV is also 0.16. This is 4.4 percent higher than the cylinder and previous core tests (6,800 kPa); however, the COV is greater (0.16 versus 0.12).

6.3.2.3 Cores drilled on November 22 and December 9–11, 1995. To verify the above results, three cores from Sections 5 and 6 were tested in compression. The mean compressive strength, multiplied by 0.97 to account for less than a 2:1 aspect ratio (Ref 27), was 56.6 MPa. This value is virtually identical to the mean compressive strength of the cores removed directly after BCO test section placement.

Four cores were tested in splitting tension, with strengths ranging from 5,300 to 6,300 kPa. This was lower than previously measured core strengths by 10 to 14 percent. However, it was within one standard deviation of previously measured values.

6.3.3 Coring and Pull-off Test Results

Coring and pull-off testing was performed within 50 hours after BCO placement, and at 3, 5, 6, and 8 months after BCO placement.

6.3.3.1 Cores drilled directly after BCO placement. The proposed testing and monitoring plan for the test sections envisioned drilling forty cores, half of which would be tested in tension (pull-off) and half of which would be tested in the guillotine direct shear apparatus. However, it proved to be impossible to extract any specimens suitable for guillotine testing with a 165 mm thick overlay. Only tensile pull-off tests were made, and these proved to be very difficult to perform. Tests were made within 50 hours after test section construction. Figures 4.9 and 6.2 illustrate the pull-off test procedure and a specimen after interface bond failure. Problems were encountered with coring and affixing steel caps to cores for testing. Coring difficulties were related to equipment failures and core barrels binding up in the overlay.

It was very difficult to secure steel caps to cores for pull-off testing. First, the curing compound had to be removed from the top of the cores since it was a bond breaker. Second, the tines at the surface of the concrete were weaker than the rest of the overlay. Two two-part quick curing epoxies were used. In many cases the specimen failed at the epoxy-concrete interface or at the top of the core, usually in the tines.

Figure 6.2 Pull-off test specimen after bond failure

Where the core failed at the surface, the results provide a lower bound for interface tensile strength. Two cores failed at lower loads in an accidental cold joint in Section 2. During paving, an air compressor had broken down and the delay led to the cold joint. Two others in Section 5 failed at low loads for no apparent reason. The interface was probably damaged during coring. In two cases, the core failed in the base slab, indicating excellent interface strength.

Disregarding unreasonably low results, an interface strength of at least 713 kPa was attained at 30 hours and 822 kPa was attained at 50 hours for cores that failed at the interface.

Bond testing done earlier in this study used either the in-situ pull-off test (Ref 45) or the guillotine test (Ref 43). Thus, results are not directly comparable, but seem lower than would be expected. Further testing is needed to establish the relationship between pull-off strengths and guillotine strengths. Results are shown in Table 6.6.

Table 6.6 Pull-off test results (cores removed directly after placement)

Section	Age, hours	Tensile stress, kPa	Remarks
7	16	877	
7	16	1151	
1	24	439	
5	30	1560	
5	30	713	
7	30	576	Core not straight
7	30	603+	Failed at surface
8	30	685+	Failed at surface
8	30	603+	Failed at surface
1	50	1206	Interface poorly shotblasted
2	50	603	Cold joint area
2	50	439	Cold joint area
3	50	1560	
4	50	822	
4	50	1070	Failed partially in base slab
5	50	219	
5	50	219	
6	50	932+	Failed at surface
6	50	493	Failed in base slab
7	50	658+	Failed at surface
7	50	822+	Failed at surface
8	50	822+	Failed at surface
8	50	877+	Failed at surface
8	50	1150+	Failed at surface

6.3.2.2 Cores drilled on September 18, 1995. Three months after test section construction, cores were drilled and tested to identify delaminations and measure bond strength. These results were later compared to data generated during nondestructive testing on September 16, 1995 (Section 5.2.7). Results are shown in Table 6.7.

Reinforcing steel was encountered while drilling cores 1 through 7. These may or may not have been delaminated before coring. The pull-off value for Core 9 may not be correct, since the core bound against the bottom of the pull-off tester during this test. Cores 12 and 17 failed above the interface in the paste at the top of the core. Thus, these values are lower bounds for interface strength at these locations. The mean value was 910 kPa with a standard deviation of 397 kPa and a COV of 0.44. In all cases where reinforcing steel was not encountered with drilling, cores in intentionally delaminated regions were found to be debonded, and those in other regions were found to be bonded.

Table 6.7 Pull-off test results (cores removed after 3 months)

Core Number	Section	Pull-off	
		Bonded	Tensile Stress, kPa
1	1	Delaminated	
2	1	Delaminated	
3	2	Delaminated	
4	3	Delaminated	
	4	Delaminated	
6	4	Delaminated	
7	4	Delaminated	
8	5	Delaminated	
9	5	Yes	97
10	5	Yes	1,020
11	5	Yes	1,410 +
12	5	Yes	1,510 +
13	5	Yes	1,040
14	6	Delaminated	
15	6	Delaminated	
16	6	Delaminated	
17	6	Yes	1,360
18	6	Yes	560
19	6	Yes	390
34	7	Yes	580 +

6.3.2.3 Cores drilled on November 22 December 9–11, 1995. At 5 months, fourteen cores were drilled for pull-off testing in Sections 5 and 6. Results are shown in Table 6.8. The mean pull-off strength was 550 kPa with a standard deviation of 290 kPa and a COV of 0.53. However, the three bonded cores in Section 5 had a mean pull-off strength of 900 kPa (with a standard deviation of 210 kPa and a COV of 0.23) and the seven in Section 6 had a mean of 400 kPa with a standard deviation of 170 kPa and COV of 0.43.

For all of the 3- and 5-month cores in Section 5 (disregarding core 9), the mean pull-off strength was 1,090 kPa, the standard deviation was 280 kPa, and the COV was 0.25. Strengths for all 3- and 5-month cores in Section 6 were lower, with a mean of 510 kPa, and standard deviation of 340 kPa and a COV of 0.66.

6.3.2.4 Cores drilled on February 23 and 24, 1996. After 8 months, twenty-one cores were removed from Sections 6, 7, and 8. Three cores were found to be unbonded, and two were found to be weakly bonded (less than 1,000 kPa). Of the remaining cores, one failed at the interface with a strength of 1,980 kPa, and the other fifteen failed at the surface. During this coring, the progress of delamination was investigated.

In all cases, where a delamination occurred near a corner, the delamination stopped within 250 mm of the corner. The mean strength (including surface failures) was 1,160 kPa, with a standard deviation of 420 kPa and a COV of 0.36. There were no significant differences in strength between Sections 6, 7, and 8. The mean strength of each section was within 70 kPa of the mean strength of all tests.

Table 6.8 Pull-off test results (cores removed after 5 and 6 months)

Core Number	Section	Pull-off	
		Bonded	Tensile Stress, kPa
20	5	Yes	1,140
21	5	Yes	790
22	5	Yes	760
23	5	Delaminated	
24	6	Delaminated	
25	6	Yes	480
26	6	Delaminated	
27	6	Delaminated	
28	6	Yes	520
29	6	Yes	450
30	6	Yes	620
31	6	Yes	240
32	6	Yes	340
33	6	Yes	140

6.3.2.5 Summary. Pull-off values for cores in Sections 5 through 8, at 3 through 8 months are shown in Figures 6.3 through 6.6. Debonded cores are indicated by blackened circles, poorly bonded cores (less than 1,000 kPa) by shaded circles, and well-bonded cores by open circles. Cracks of at least 0.4 mm in width are shown.

Low pull-off values tend to occur at intersections of cracks and edges, where delamination potential is high. In Table 6.9, all of the pull-off results at different ages are shown. In the 5-, 6-, and 8-month tests, some cores were found to be debonded outside of the intentionally delaminated regions. These were at intersections of cracks and edges where delamination potential is high. These delaminations did not occur in Section 7.

Table 6.9 Comparison of pull-off results at different ages

Age at testing	Number of samples	Mean strength, kPa	Standard deviation, kPa	Coefficient of variation
16–24 hours	3	822	360	0.44
30 hours	6	790	380	0.48
50 hours	15	790	370	0.47
3 months	9	890	500	0.56
3 months (disregarding core 9)	8	980	430	0.44
5 and 6 months	10	550	290	0.53
Section 5 at 3, 5, and 6 months, disregarding core 9	7	1,090	280	0.25
Section 6 at 3, 5, and 6 months	10	510	340	0.66
8 months	21	1,160	420	0.36

6.4 MATURITY, TEMPERATURE DATA, TEMPERATURE AND MOISTURE GRADIENTS, AND PAVEMENT STRAINS

6.4.1 Maturity

Maturity attained by Test Sections 2 through 7, from June 22–24, 1995 is shown in Figure 6.7, and the air and slab temperatures during that period are shown in Figure 6.8. The thermocouple wires in Test Sections 1 and 8 were too long, which led to excessive resistance in the wires and gave unreasonably high values. Thus, these data are not shown. The air temperature ranged from 36°C to 21°C during the first 24 hours. Slab heat buildup coincided with high air temperatures, so the overlay temperatures reached approximately 58°C at around 7 p.m.

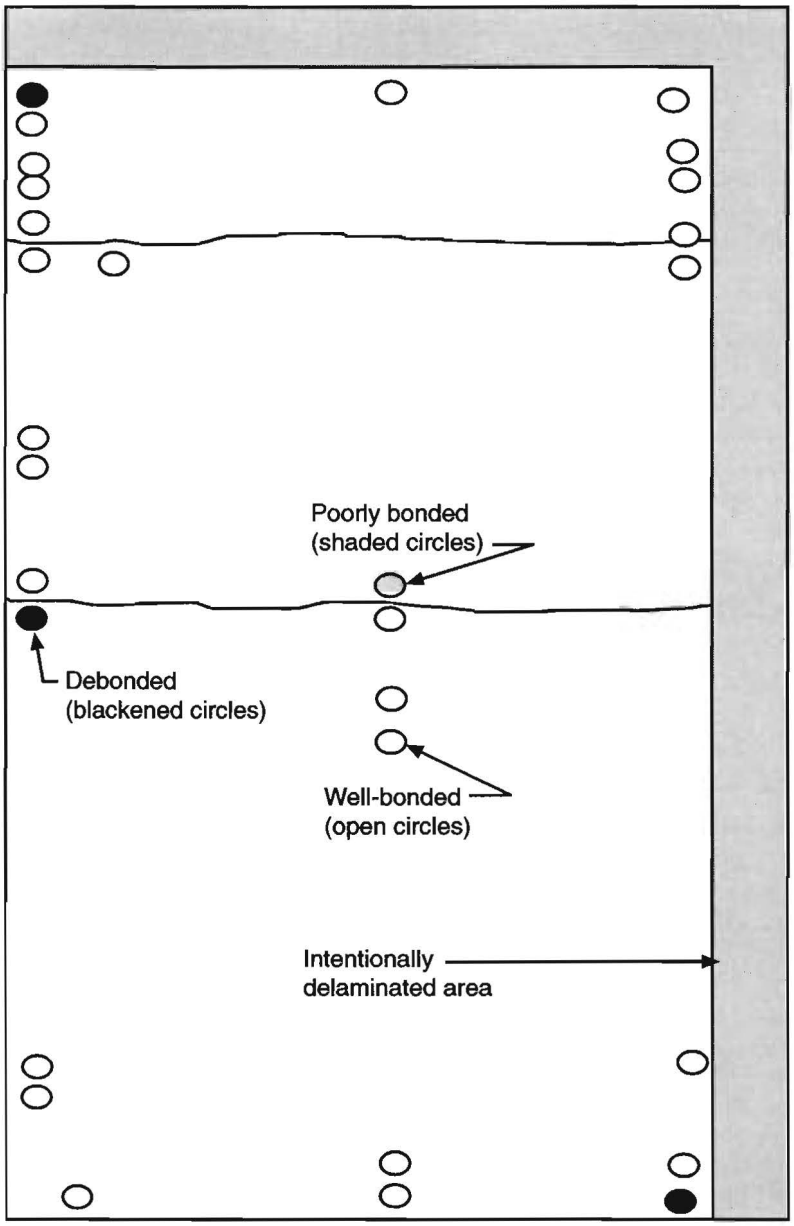

Figure 6.3 Pull-off test results in Section 5, November and December 1995 (Ref 45)

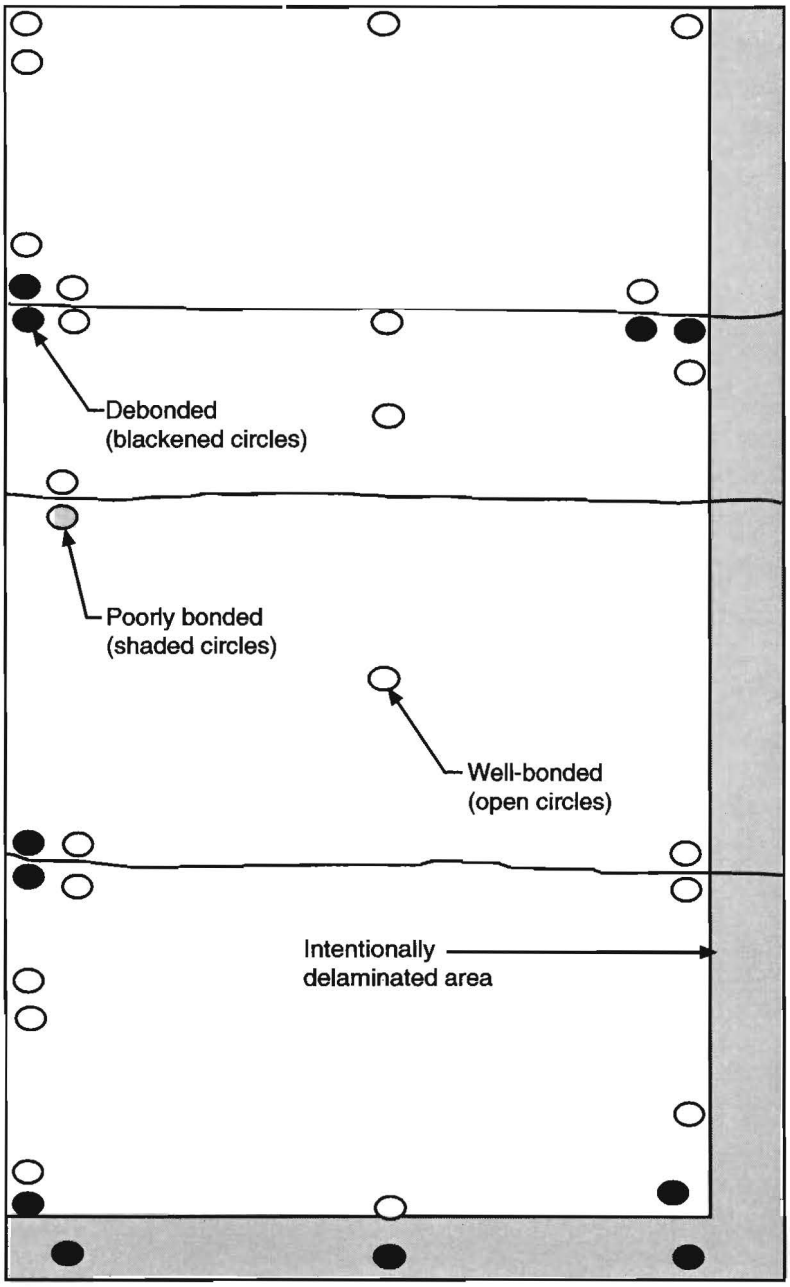

Figure 6.4 Pull-off test results in Section 6, November and December 1995 (Ref 45) and February 1996

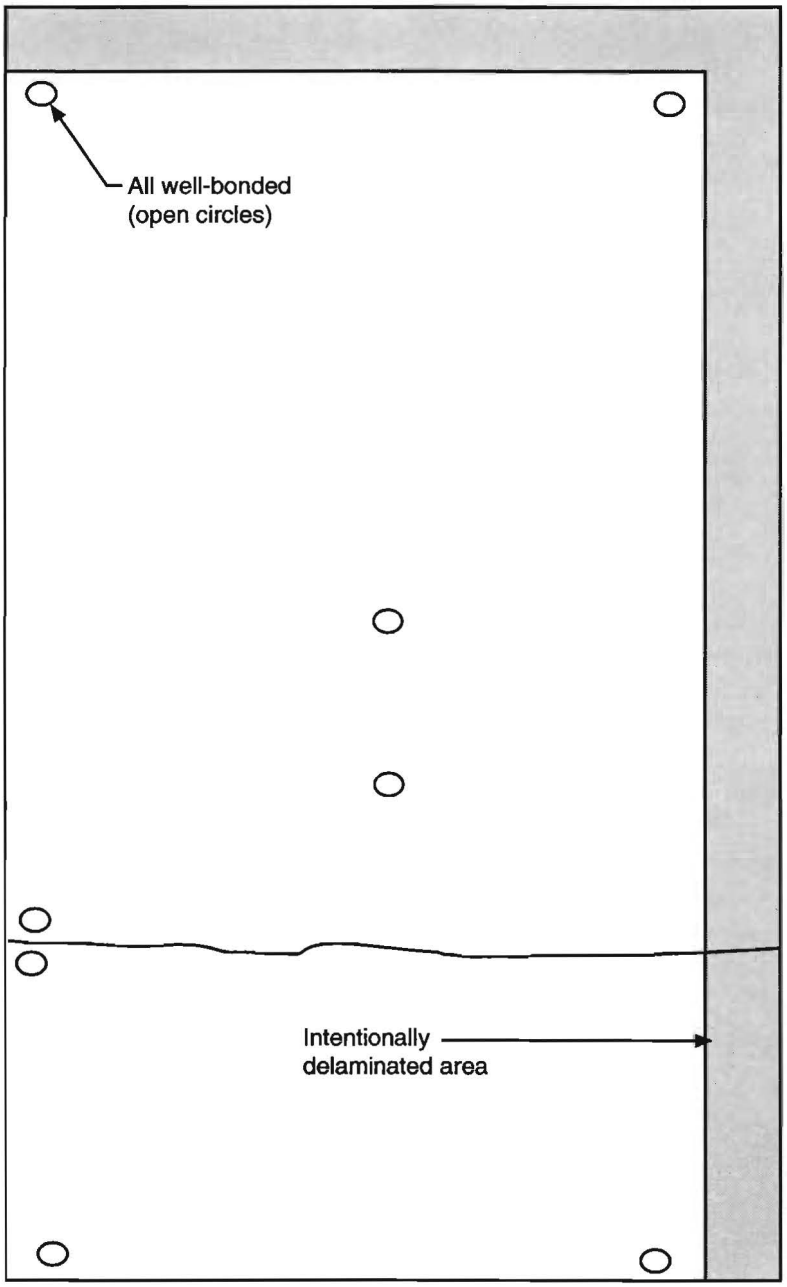

Figure 6.5 Pull-off test results in Section 7, February 1996

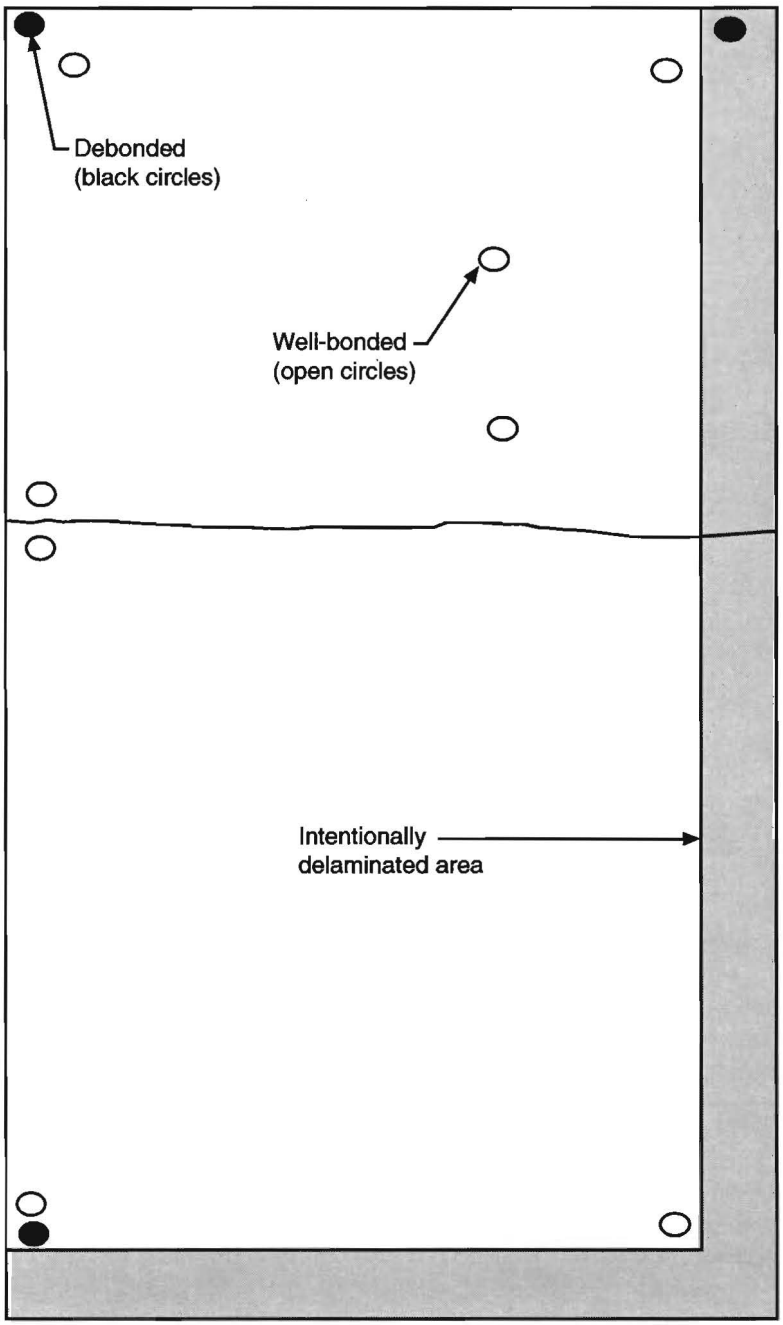

Figure 6.6 Pull-off test results in Section 8, February 1966

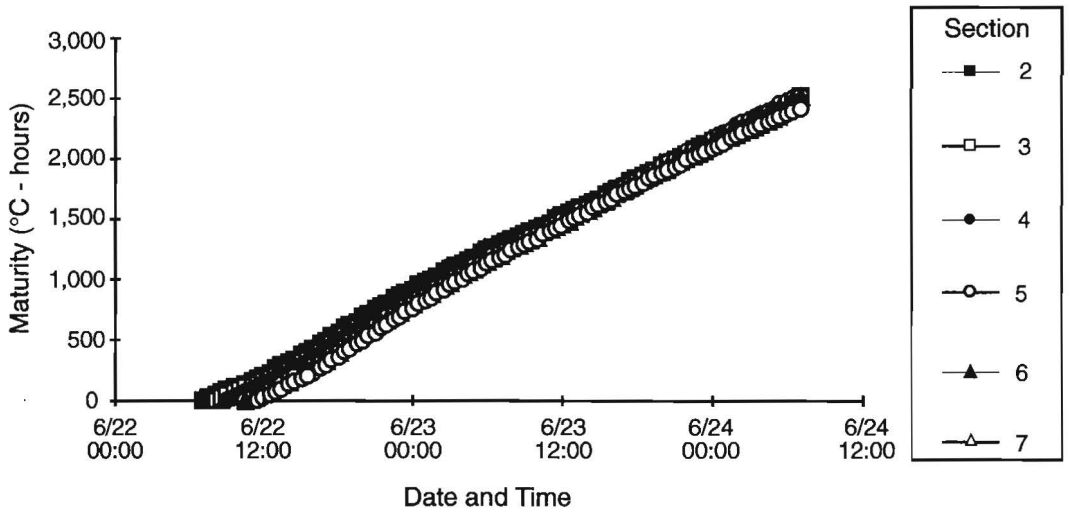

Figure 6.7 Maturity attained by Test Sections 2 through 7

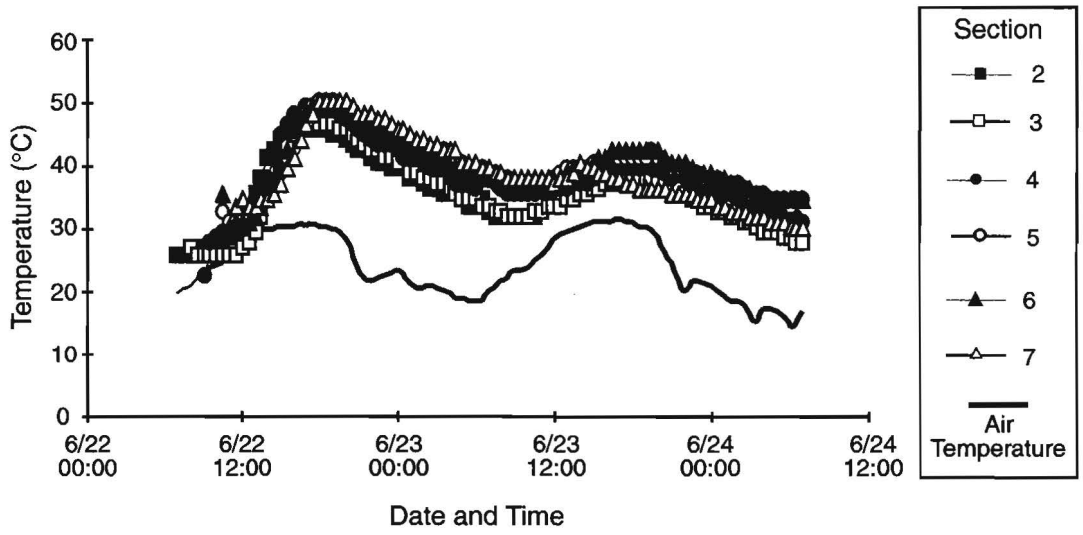

Figure 6.8 Air temperature and test section temperatures (Sections 2 through 7)

6.4.2 BCO Temperature Gradients

BCO temperature gradients, measured at different depths in the test sections, are shown in Figures 6.9 through 6.12.

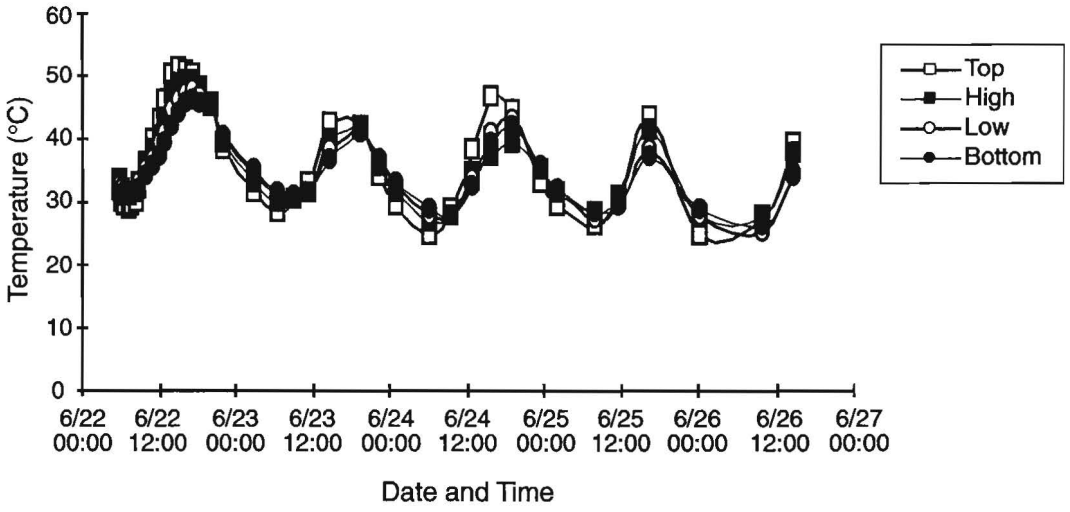

Figure 6.9 BCO temperature gradients measured by thermocouple Set 1

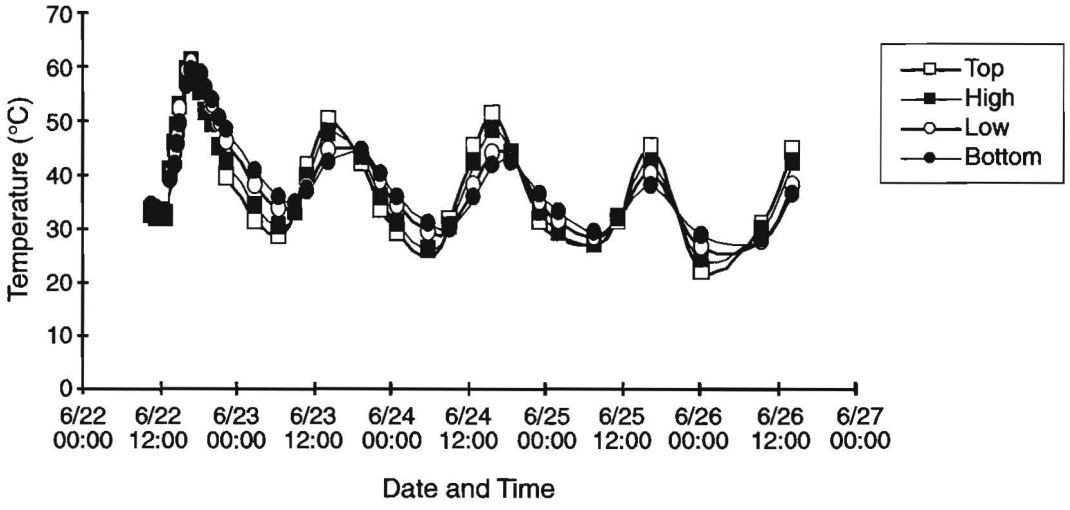

Figure 6.10 BCO temperature gradients measured by thermocouple Set 2

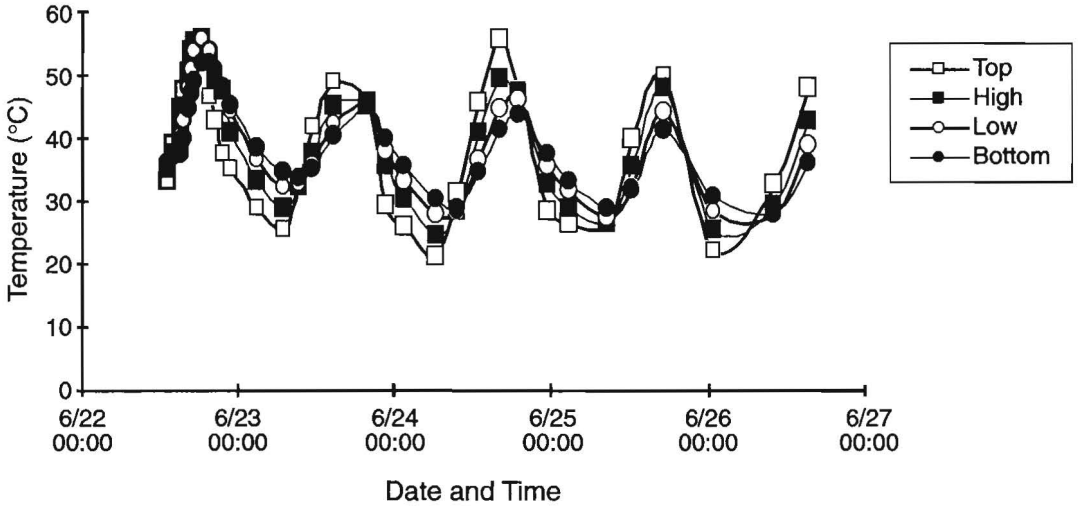

Figure 6.11 BCO temperature gradients measured by thermocouple Set 3

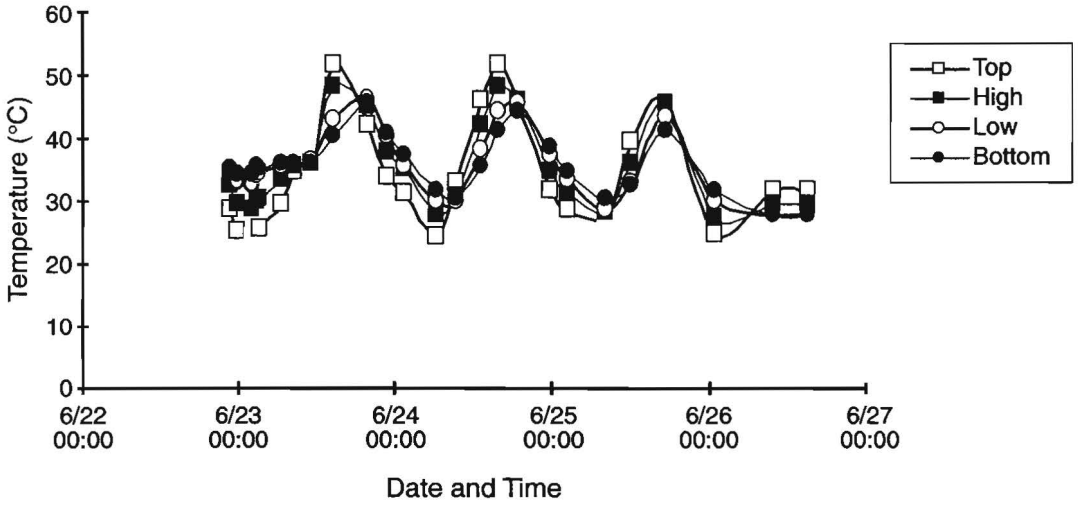

Figure 6.12 BCO temperature gradients measured by thermocouple Set 4

6.4.3 BCO Moisture Gradients

BCO moisture gradients for the first test location are shown in Figure 6.13. The second set of instruments was damaged during construction and did not yield any results.

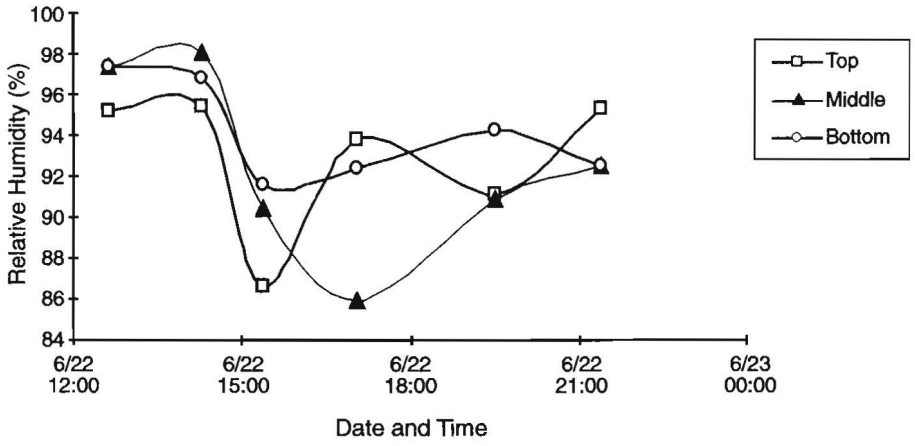

Figure 6.13 BCO moisture gradients

6.4.4 Vibrating Wire Strain Gauges

Strains and temperatures recorded by the vibrating wire strain gauges are shown in Figures 6.14 and 6.15.

6.5 WEATHER AND EVAPORATION

Weather data from the weather station and slab temperature data from the maturity meters for June 22–24, 1995, are plotted in Figures 6.8, 6.16, and 6.17. Figure 6.16 shows relative humidity and Figure 6.17 shows wind speed. After noon on June 22, rising air temperatures and wind speed and falling humidity greatly increased the potential for evaporation.

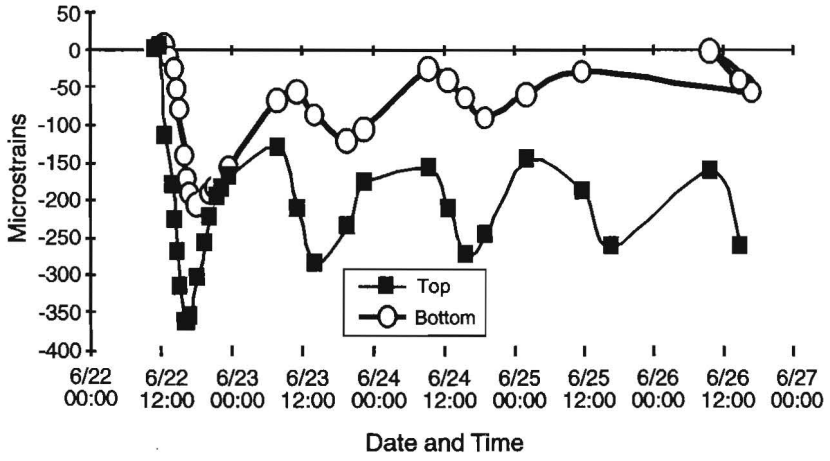

Figure 6.14 Strains measured by vibrating wire strain gauges

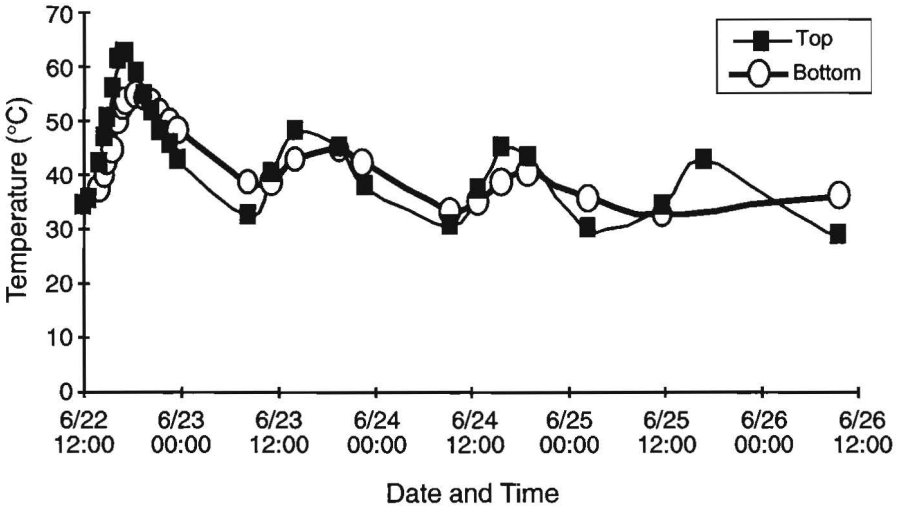

Figure 6.15 Temperatures measured by vibrating wire strain gauges

Evaporation rates predicted from Equation 3.5 using slab temperatures recorded by the maturity meters were analyzed. These data are not relevant past 1 p.m. because by this time the concrete had set, the curing compound had been applied, and bleed water was no longer evaporating from the concrete. Nevertheless, it was obvious that on June 22 at about 6 or 7 a.m. the threshold to high evaporation was crossed.

Air temperatures did not exceed 38°C during the test. The relative humidity for the most part was higher than expected — up to 60 percent. A daily cycle is apparent, with a high at 6 a.m. and a low at 6 p.m. Wind speed was lower than expected, with no obvious trends.

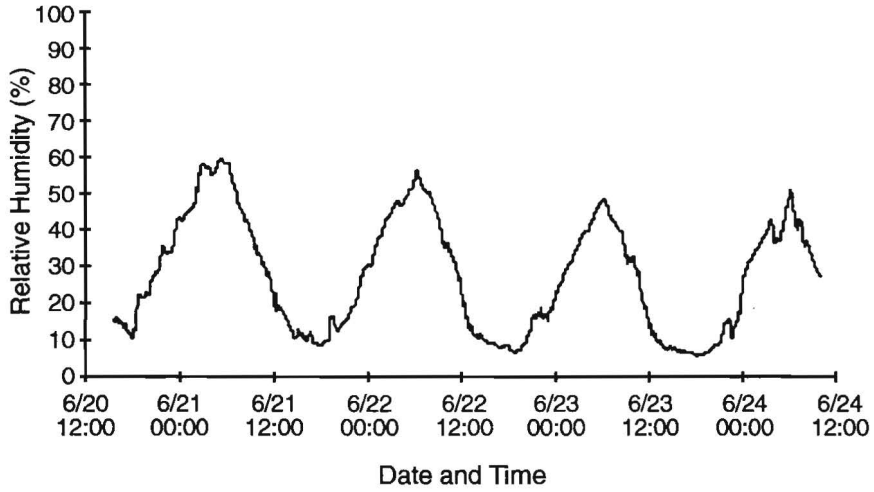

Figure 6.16 Relative humidity, June 20–24, 1995

The evaporation predictions based on an assumed concrete temperature of 41°C are plotted in Figure 6.18. This was the highest temperature reached by any section (Section 7) during the 3 hours following concrete placement. For most of this period, including the casting on the morning of the June 22, the evaporation was consistently above 1.0 kg/m^2/hr.

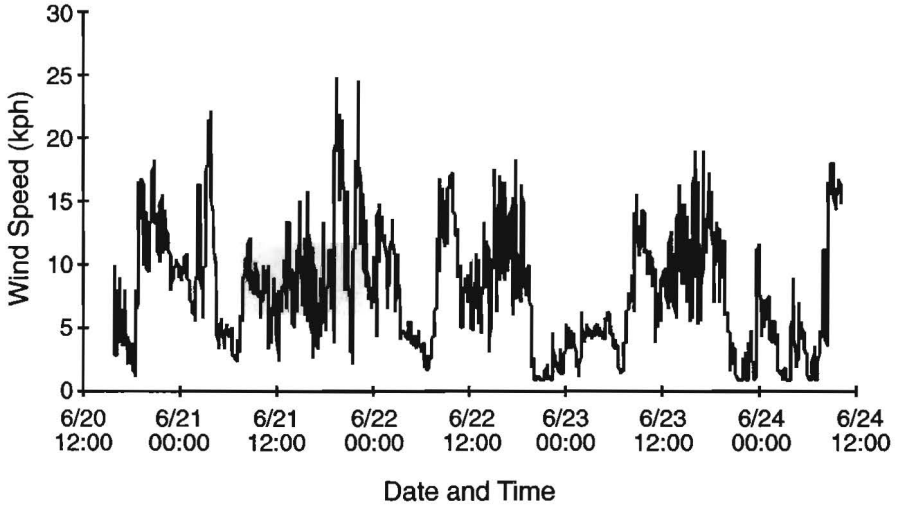

Figure 6.17 Wind speed in kph, June 20–24, 1995

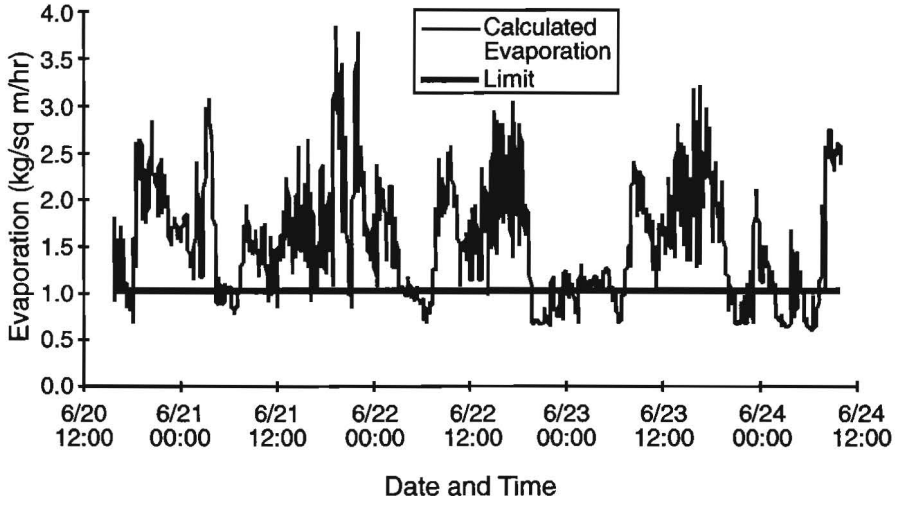

Figure 6.18 Evaporation prediction in kilograms per square meter per hour, June 20–24, 1995, assumed concrete temperature = 41°C

6.6 CRACKING

In addition to the plastic shrinkage cracking, three transverse cracks were detected on the surface of the slab on June 25, 1995. It was not possible to make a more detailed crack survey until after the formwork was removed.

Crack locations and widths in the slab were measured on July 25, August 28, and September 17, 1995. Crack widths were measured using a crack comparator. Cracks were measured in the morning (6 to 8 a.m.) when the slab was cool and cracks were widest.

Data are tabulated by section in Tables 6.10 through 6.17. Locations are given in meters from the south end of the section. A (-) in the table indicates that the crack was not observed on that date. *Closed* indicated that the crack appeared closed. Joints between sections were also measured unless they were spalled.

In some cases where particularly wide cracks were observed on July 15, cracks subsequently appeared nearby and the width of the original crack was reduced. This was observed with some of the cracks in Section 6 (Table 6.15). This may indicate redistribution of the stresses near the wider cracks.

On February 24, 1996, an attempt was made to determine if the majority of the overlay cracks were reflective. The soil was cleared away from the base slab, and eleven overlay cracks were examined. Only two were reflected from the base slab, both in Section 6. It therefore appears that the base slab had very little cracking and that the majority of the cracks that formed in the overlay were not reflective.

6.7 NONDESTRUCTIVE TESTING AND DELAMINATION DETECTION

Nondestructive testing was carried out during construction, within 48 hours following construction, and again at 3 months. SASW, impact-echo, impulse-response, and the RDD were used to attempt to detect delaminations in Sections 1, 4, 5, 6, 7, and 8 within 48 hours after casting and subsequently on 16 September 1995. Results are shown in Tables 6.19 and 6.20. The FWD was used to attempt to detect delaminations on February 26, 1996.

Table 6.10 Cracking in Section 1

Location (meters) from south end	Measured Crack Widths (in mm)		
	July 15, 1995	August 28, 1995	September 17, 1995
2.85	0.13	0.18	0.13
4.42	0.08	0.13	0.05
5.08	-	0.05	Closed
6.02	0.13	0.08	0.05
6.91	0.13	0.33	0.18
9.35	0.13	0.08	0.08
10.92	0.13	0.08	0.08
11.48	0.08	0.05	0.05
Joint 1-2	1.01	0.64	1.27

Table 6.11 Cracking in Section 2

Location (meters) from south end	Measured Crack Widths (in mm)		
	July 15, 1995	August 28, 1995	September 17, 1995
2.95	-	0.05	Closed
3.56	-	0.05	Closed
3.96	0.13	0.08	0.05
5.18	0.08	0.18	0.13
7.67	0.25	0.18	0.18
8.41	0.13	0.13	0.13
9.45	0.08	0.13	0.13
10.34	0.18	0.08	0.08
11.84	0.18	0.18	0.23
12.67	0.18	0.18	0.18
Joint 2-3	1.01	1.01	1.27

Table 6.12 Cracking in Section 3

Location (meters) from south end	Measured Crack Widths (in mm)		
	July 15, 1995	August 28, 1995	September 17, 1995
1.22	0.05	0.13	0.05
1.73	0.05	0.13	0.13
2.34	-	-	0.05
2.97	0.05	0.13	0.05
3.63	0.08	0.13	0.18
4.34	-	0.08	0.05
4.67	0.25	0.18	0.23
5.56	0.18	0.23	0.23
6.07	-	0.05	0.05
6.93	0.05	0.13	0.13
7.39	-	0.08	0.05
7.75	0.08	0.13	0.08
8.15	-	0.05	0.05
8.56	0.13	0.08	0.05
9.07	-	0.05	0.05
9.88	0.25	0.23	0.23
10.72	-	-	0.05
11.10	0.05	0.08	0.08
11.99	0.08	0.05	0.05
12.34	0.05	0.05	0.05
12.83	-	-	0.05
13.74	-	0.05	0.05
Joint 3-4	0.41	0.51	0.51

Table 6.13 Cracking in Section 4

Location (meters) from south end	Measured Crack Widths (in mm)		
	July 15, 1995	August 28, 1995	September 17, 1995
2.36	-	0.05	0.05
2.87	-	0.05	0.05
3.23	-	0.05	0.05
3.58	0.08	0.08	0.08
4.60	0.08	0.08	0.13
4.98	0.13	0.08	0.08
5.79	0.05	0.08	0.08
6.32	-	0.08	0.05
7.49	0.08	0.18	0.18
8.08	0.08	0.18	0.05
8.92	0.13	0.13	0.13
10.21	0.18	0.13	0.08
11.05	0.08	0.18	0.18
11.68	0.18	0.18	0.08
13.28	0.13	0.13	0.08
13.77	0.05	Closed	Closed
Joint 4-5	0.76	0.64	1.01

Table 6.14 Cracking in Section 5

Location (meters) from south end	Measured Crack Widths (in mm)		
	July 15, 1995	August 28, 1995	September 17, 1995
1.19	-	0.05	Closed
1.80	0.05	0.05	0.05
3.23	-	0.08	0.05
4.11	0.18	0.18	0.18
4.95	-	0.05	0.05
5.82	0.18	0.23	0.25
6.71	-	0.05	0.05
7.59	0.41	0.33	0.25
8.41	-	0.05	0.05
8.97	0.05	0.13	0.05
9.60	-	0.08	0.05
10.72	0.08	0.13	0.18
12.12	0.33	0.18	0.08
12.24	-	0.05	0.05
Joint 5-6	1.27	0.64	1.27

Table 6.15 Cracking in Section 6

Location (meters) from south end	Measured Crack Widths (in mm)		
	July 15, 1995	August 28, 1995	September 17, 1995
2.11	-	0.05	0.05
3.20	-	0.05	0.05
3.76	-	0.18	0.18
4.93	0.41	0.33	0.25
6.50	-	0.08	0.05
7.62	0.13	0.13	0.13
9.53	0.51	0.33	0.51
10.82	0.41	0.23	0.23
12.55	0.51	0.41	0.51
Joint 6-7	0.51	0.33	Spalled

Table 6.16 Cracking in Section 7

Location (meters) from south end	Measured Crack Widths (in mm)		
	July 15, 1995	August 28, 1995	September 17, 1995
1.07	0.05	0.05	0.05
1.96	-	0.05	0.05
2.69	0.18	0.23	0.33
3.53	0.08	0.08	0.18
4.37	-	0.05	0.05
4.88	0.08	0.08	0.05
6.71	0.13	0.23	0.18
8.76	0.08	0.13	0.13
9.35	0.05	0.05	0.05
10.13	0.18	0.18	0.23
10.85	0.08	0.08	0.13
11.76	0.05	0.05	0.08
12.45	0.18	0.13	0.18
13.74	0.18	0.13	0.18
Joint 7-8	0.51	0.51	Spalled

Table 6.17 Cracking in Section 8

Location (meters) from south end	Measured Crack Widths (in mm)		
	July 15, 1995	August 28, 1995	September 17, 1995
3.20	-	0.05	Closed
4.06	0.08	0.05	0.13
5.72	-	0.05	0.08
6.96	-	0.05	0.05
7.32	-	0.05	0.05
7.72	-	0.05	0.05
9.02	0.13	0.05	0.05
9.50	-	0.05	0.05
10.46	-	-	0.05
10.92	-	0.05	0.05
11.35	0.05	0.05	0.05
11.96	0.08	0.08	0.05
12.70	-	-	0.05

6.7.1 Initial Nondestructive Testing

Surface and P-wave analysis was used at the beginning of Section 1 to measure surface wave velocity in the BCO and predict overlay stiffness. Results, compared to cylinder tests when available, are shown in Table 6.18. The concrete modulus was estimated using equation 6.1 (Ref 48):

$$E_c = 4.73\sqrt{f'c} \qquad \text{(Eq 6.1)}$$

where

E_c = modulus of elasticity of concrete, GPa, and

$f'c$ = compressive strength of concrete, MPa.

The modulus predicted by nondestructive testing is at very low strain and represents an initial tangent modulus. It will thus be greater than the approximate secant modulus at a stress of 0.45 $f'c$ predicted by Equation 6.1.

Table 6.18 Stiffness development of the overlay in Section 1

Hours after casting	Modulus Predicted by Surface and P-wave analysis, GPa	Modulus Predicted by Measured $f'c$ and Equation 6.1
4	16.5	
6	22.0	
8	24.8	19.2
16		27.5

Results of SASW and impact-echo testing carried out immediately after casting the test sections are shown in Appendix C and analyzed in Table 6.19. At this time no coring had been done in debonded areas; tests shown as being in debonded areas were in regions where debonding agent had been applied. However, there was no confirmation that the overlay was in fact debonded. The RDD profile did not show any evidence of delamination, primarily because of excessive rolling noise levels due to the tined pavement surface and driving the velocity transducer beyond the linear range (Ref 66).

Table 6.19 Nondestructive testing results, June 22–24, 1995

	Tests in Debonded Areas				Tests in Bonded Areas			
Section	SASW		Impact-echo		SASW		Impact-echo	
	No. tests	No. correct	No. tests	No. correct	No. tests	No. correct	No. tests	No. correct
1	17	7	8	3	15	15	21	21
4	23	4	7	5	30	29	8	8
5	23	6	3	1	24	20	5	4
6	18	2	-	-	26	25	4	3
7	4	0	-	-	2	2	-	-
8	1	1	1	0	5	4	10	9
Totals	86	20	19	9	102	95	48	45
Percent		23 %		47 %		93 %		94 %

6.7.2 Subsequent Nondestructive Testing

On September 16, 1995, SASW, impact-echo, impulse-response, rebar sounding, and the Schmidt impact hammer were used to attempt to detect and map debonding. On September 19 and November 22, 1995, cores were taken to confirm the NDT results (Section 6.3.2). Also, the FWD was used to attempt to detect and map debonding on February 26, 1996.

6.7.2.1 Nonelectronic testing results. Rebar sounding was moderately successful. A 1- to 1.5-meter-long piece of 16 mm diameter reinforcing steel (US #5) was held vertically and dropped about 0.5 meters onto the pavement. Delaminations can be detected by listening for a hollow sound or feeling vibrations through the operator's feet.

While the process is simple and rapid, different operators have different sensitivities and operator sensitivity dulls quickly. Whereas, the method has been successfully used in the past on thinner overlays (Refs 3, 4, 20), it becomes more difficult with thicker overlays.

The Schmidt hammer was not able to differentiate between bonded and debonded sections.

6.7.2.2 Electronic methods. The three electronic methods were attempted during the day and night. It was assumed that debonding would be easier to detect when the temperature was falling and the edges of the overlay were attempting to curl up from the base slab, thus

separating the two layers in delaminated regions. Thus, the two sets of data could be used to determine how sensitive the NDT methods used were to rising or falling thermal gradients.

For SASW and impact-echo testing, it was necessary to affix steel washers to the pavement surface with epoxy to attach the magnetic accelerometers (Figure 6.19). In previous testing it had proven difficult to get contact between the accelerometers and the pavement surface due to the tined pavement surface finish. The impulse-response testing geophone only required grease to provide contact. Results are shown in Table 6.20.

6.7.2.3 FWD. The FWD tests were performed in two passes, with twenty data points taken 0.75 m from the east edge of the test sections and twenty taken 1.3 m from the west edge of the test sections. For each series of twenty points, one point was taken at the leading edge and middle of each section, and one point each was taken in Sections 5 through 8 over cracks. In Sections 5, 6, and 8 the cracks had associated delaminations; in Section 7, as noted previously, no delamination had been observed.

For each point, four tests were made by dropping the weights from different heights. These drops imposed forces on the pavement of approximately 30, 42, 54, and 72 kN, respectively. Data gathered included peak deflections at 152; 305; 610; 914; 1,219; 1,524; and 1,829 mm away from the falling weight, as well as the dynamic responses at those points.

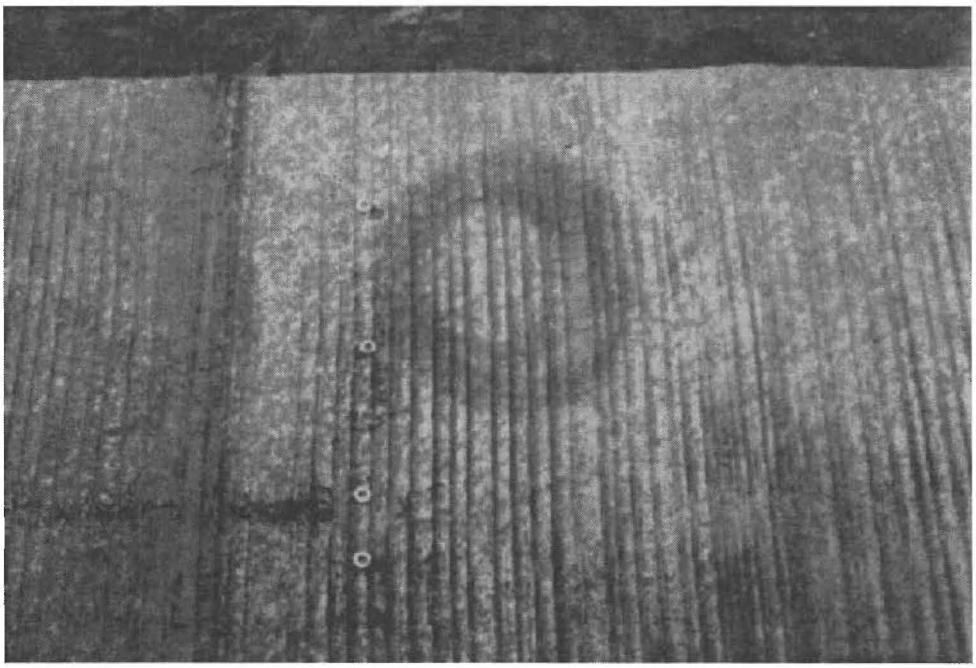

Figure 6.19 Steel washers used to attach magnetic accelerometers

The stiffness of the BCO and pavement at each data point was calculated by dividing the first deflection by the applied force for each of the four heights and averaging the results.

In all cases the COV of the four stiffnesses calculated was less than 6 percent. The stiffnesses are shown in Table 6.21.

Table 6.20 Nondestructive testing results, September 16, 1995

Location		Sec	Day			Night			Debonded area	Pull off, kPa
North (m)	West (m)		SASW	IE	IR	SASW	IE	IR		
3.4	1.7	1	B	D	B				No	-
15.1	0.3 (SASW readings at 0.15, 0.30 0.46, 0.61	1	B	D D D D	D				Yes	-
15.4	0.3 (SASW readings at 0.3, 0.46, 0.61)	2	D	D D D	D	B	B D D	B	Yes	-
30.3	3.2 (SASW Readings at 30., 3.2, 3.4)	2	D	D D D	B				No	-
30.6	3.2 (SASW readings at 30., 3.2, 3.4)	3	B	D B D	B	D	D D D	B	No	-
45.9	0.46 (SASW readings at 0.3, 0.61, 0.91, 1.2, 1.5, 1.8, 2.1, 2.4, 2.7, 3.0, night readings at 0.3, 0.46, 0.61)	4	D	D B B D D D D D D D	D	D	B D D	D	Yes	-
45.9	3.2 (SASW readings at 30., 3.2, 3.4)	4	B	D	B	D	D D D	D	Yes	-

Table 6.20 (continued) Nondestructive testing results, September 16, 1995

Location		Sec	Day			Night			Debonded area	Pull off, kPa
North (m)	West (m)		SASW	IE	IR	SASW	IE	IR		
61.1	0.46 (SASW readings at 0.3, 0.61, 0.91, 1.2, 1.5, 1.8, 2.1, 2.4, 2.7, 3.0, night readings at 0.3, 0.46, 0.61)	5	B	B B D B B D B B B B	B	B	D D B	D	No	-
61.1	3.2 (SASW readings at 30., 3.2, 3.4)	5	D	B	B	B	B D D	B	No	1,020
63.2	0.3 (SASW readings at 0.3, 0.46, 0.61)	5	D	B B B	B				No	-
63.2	3.2 (SASW readings at 30., 3.2, 3.4)	5	D	B B B	B				No	-
74.1	0.3 (SASW readings at 0.3, 0.46, 0.61)	5	B	D B B	B	B	B D D	D	No	1,510+
74.1	3.2 (SASW readings at 30., 3.2, 3.4)	5	B	B B B	B	B	D D B	D	No	1,040

Table 6.20 (continued) Nondestructive testing results, September 16, 1995

Location		Sec	Day			Night			Debonded area ?	Pull off, kPa
North (m)	West (m)		SASW	IE	IR	SASW	IE	IR		
76.4	0.46 (SASW readings at 0.3, 0.61, 0.91, 1.2, 1.5, 1.8, 2.1, 2.4, 2.7, 3.0)	6	B	B	D				Yes	0
				B						
				D						
				B						
				B						
				D						
				B						
				B						
				B						
				B						
76.4	3.2	6	B	D	B				Yes	0
85.6	3.2	6	B	B	B				No	560
85.8	3.2	6	B	B	B	D	B	B	No	390

Next, the stiffnesses calculated at the beginning of each section with a bonded edge were compared to those of the sections with debonded edges. Although the debonded edges would be expected to be less stiff than the bonded edges, there was no significant difference.

The test slabs at cracks were less stiff than at uncracked areas by 12 to 20 percent. However, there were no significant differences in stiffness between the slab near the crack in Section 7, which was bonded (Points 16 and 36), and the slabs near the cracks in Sections 5, 6, and 8, which had delaminations (Points 10, 13, 19, 30, 33, and 39). As a result, the loss of stiffness seems to be due to the cracking rather than the delamination.

Because the peak deflections did not show any obvious trends, the deflection basins for the greatest force (approximately 72 kN) were examined. In Figure 6.20, the deflection basins for bonded and unbonded edges are compared. The unbonded edges are shown with bold lines. As before, there are no obvious differences between the bonded and unbonded edges.

The deflection basins at cracked and uncracked interior locations are compared in Figure 6.21. The basins at cracked locations are shown with bold lines. There are no significant differences between deflection basins at cracked and uncracked locations.

There may be differences between dynamic responses at these locations; however, those data have not been analyzed.

Table 6.21 Pavement stiffnesses calculated from FWD testing

Data Point	Calculated Stiffness (N/mm)	Remarks
1	13.1	Start of Section 1, bonded
2	24.5	Midpoint of Section 1
3	17.1	Start of Section 2, debonded
4	24.4	Midpoint of Section 2
5	12.6	Start of Section 3, bonded
6	21.8	Midpoint of Section 3
7	10.9	Start of Section 4, debonded
8	24.2	Midpoint of Section 4
9	12.5	Start of Section 5, bonded
10	19.6	Crack in Section 5, debonded
11	24.1	Midpoint of Section 5
12	12.9	Start of Section 6, debonded
13	21.7	Crack in Section 6, debonded
14	23.2	Midpoint of Section 6
15	20.8	Start of Section 7, bonded
16	20.6	Crack in Section 7, bonded
17	27.4	Midpoint of Section 7
18	19.3	Start of Section 8, debonded
19	18.7	Crack in Section 8, debonded
20	24.3	Midpoint of Section 8
21	11.3	Start of Section 1, bonded
22	23.0	Midpoint of Section 1
23	15.5	Start of Section 2, debonded
24	21.8	Midpoint of Section 2
25	15.7	Start of Section 3, bonded
26	21.3	Midpoint of Section 3
27	9.97	Start of Section 4, debonded
28	23.4	Midpoint of Section 4
29	11.9	Start of Section 5, bonded
30	20.6	Crack in Section 5, debonded
31	23.7	Midpoint of Section 5
32	10.4	Start of Section 6, debonded
33	19.5	Crack in Section 6, debonded
34	19.7	Midpoint of Section 6
35	17.8	Start of Section 7, bonded
36	19.2	Crack in Section 7, bonded
37	25.2	Midpoint of Section 7
38	17.2	Start of Section 8, debonded
39	21.4	Crack in Section 8, debonded
40	25.1	Midpoint of Section 8

6.8 APPLICATION OF LOADING

The RDD was used to apply 51,000 cycles of an 89 kN load to Section 1 at 12 hours after casting. The loading was applied at a rate of approximately 35 Hz, avoiding resonances. After this, cracking was observed near the point of load application. Some of this cracking appeared to be related to plastic shrinkage, but some was flexural.

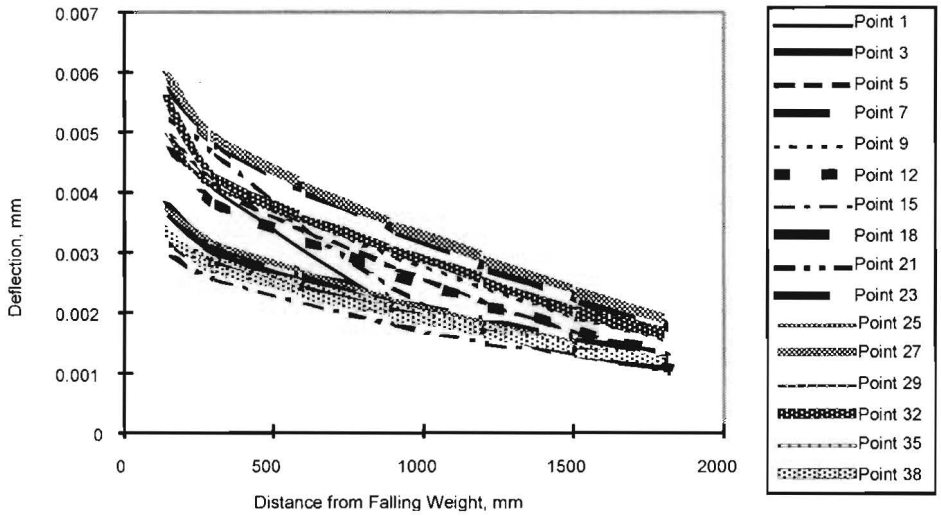

Figure 6.20 Comparison of deflection basins: Bonded and unbonded edges

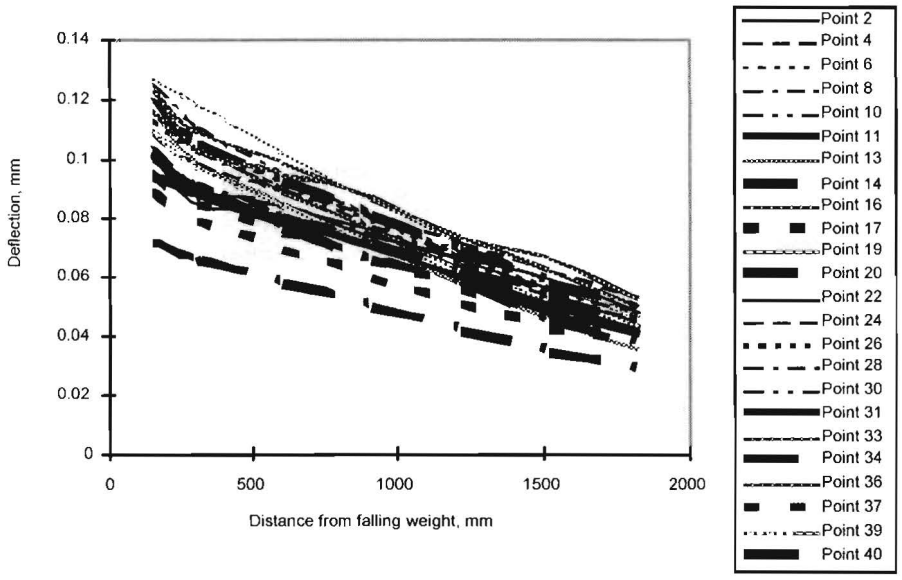

Figure 6.21 Comparison of deflection basins: Cracked and uncracked midspan locations

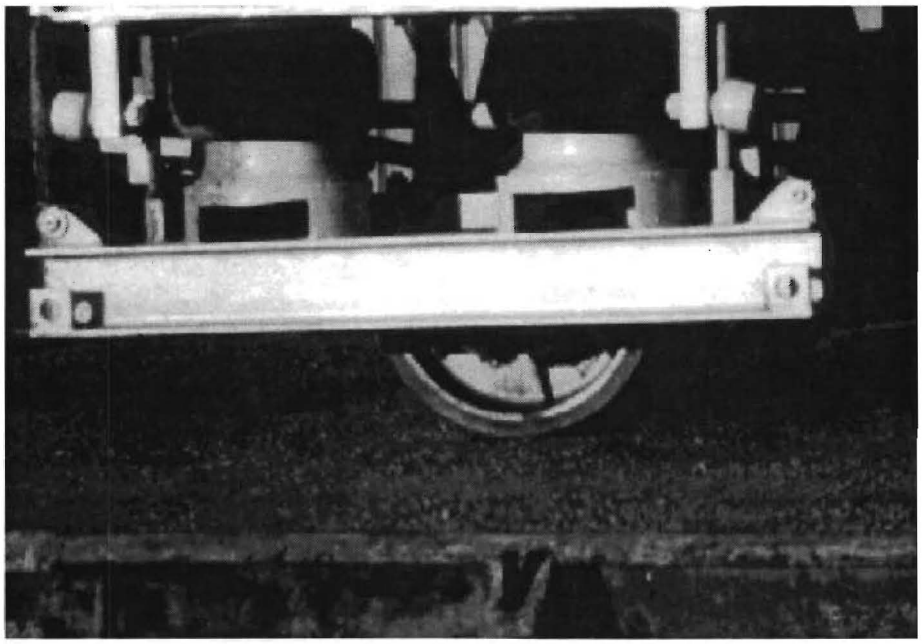

Figure 6.22 RDD loading wheel

The RDD applies load through two wheels, each with a contact area of about 5,000 mm^2 (Figure 6.22). Thus, the contact pressure was much higher than that of a truck tire. The stress concentrations may have contributed to the cracking. Subsequently, the RDD applied 60,000 cycles of an 89 kN load to Section 8, 12 hours after casting. No cracking was detected. Loading stopped when a wheel on the RDD cracked.

Aggregate trucks were allowed on the test sections on 28 June, 6 days after casting. Although traffic could have been allowed on the BCO much earlier, it was necessary to first remove the formwork to avoid damaging it. An average of 133 trucks crossed the slab 5 days a week, all loaded at or near the legal weight limit of 356 kN. On average, seventy-two trucks had two axles and sixty-one had four axles, for a total of 956 80 kN equivalent single axle loads (ESALs) calculated using axle equivalency factors (Ref 2). This is equal to 683 ESALs per day 7 days a week. Cumulative ESALs on dates cracking was surveyed are shown in Table 6.22.

Table 6.22 Approximate cumulative ESALs

Date	Cumulative ESALs
July 15, 1995	12,300
August 28, 1995	42,300
September 17, 1995	56,000

CHAPTER 7. DISCUSSION OF TEST SECTION RESULTS

7.1 CURING

Transverse cracks could not be observed on the tined surface of the substrate slab. As a result, it was not possible to compare cracking between sections. Field cylinder tests (Table 5.1) showed that wet mat curing was clearly superior, leading to compressive strengths of 20.2 MPa. Master Builders Confilm® Evaporation Reducer with curing compound and heavy applications of curing compound produced acceptable compressive strength (13.6 to 15.4 MPa). Confilm® alone and lighter applications of curing compound led to inferior cylinder strengths (7.9 to 9.4 MPa). However, Confilm® is not intended to be used alone.

The lighter application rate of the curing compound was in accordance with manufacturer's recommendations and Texas Department of Transportation (TxDOT) specifications (Ref 48). The low cylinder strength for the lighter application rates indicates that those recommendations and specifications may not be adequate for hot and dry conditions. All field-cured cylinders had much lower strength than the laboratory-cured cylinders (26.7 MPa).

Clearly, wet mats should be used if the construction schedule will accommodate them. The mats should not be allowed to dry out. The wet mats will also aid in cooling the bonded concrete overlay (BCO) through evaporation. High application rates of curing compound or curing compound with Confilm® can approach, but not equal, the curing protection afforded by wet mats. Confilm® combined with a heavy application of curing compound might also work well but was not tested.

The effectiveness of a curing compound in controlling moisture content may be evaluated by examining the moisture gradients observed on June 22 during BCO construction (Figure 6.9). In the 9 hours following concrete placement, the moisture content of the concrete fell from 95 – 97 percent to 92 – 95 percent. However, at times during the afternoon the moisture content of the top and middle of the BCO fell to approximately 86 percent, while the bottom of the BCO stayed at a minimum moisture content of 91 percent. This indicates that the curing compound was not able to keep the moisture content of the slab near 100 percent, as would be expected with wet mats. It also indicates that moisture loss into the base concrete is probably not significant.

Because it proved nearly impossible to visually detect fine cracks, in order to compare BCO sections, the north edge of the slab was left exposed after formwork was removed. This made it easy to spot cracks. Where this method is not practical, for example during actual BCO construction, a strip may be troweled smooth along the edge of the BCO.

7.2 ENVIRONMENTAL CONDITIONS

Environmental conditions during and shortly after placement of a BCO can cause distress that will substantially affect its performance. High evaporation rates can lead to plastic and drying shrinkage cracking and to discontinuities that can lead in turn to debonding. Similarly, substantial temperature drops following concrete placement can lead to thermal cracking, which also leads to increased risk of debonding.

The specification recommendations for El Paso construction (Appendix A) mandated that when evaporation exceeded 1.0 kg/m^2/hr, measures such as fogging, wet mat curing, or other methods had to be used to control the moisture content of the newly placed BCO. Furthermore, if the projected temperature drop in the 24 hours following concrete placement was expected to exceed 14°C, the day's placement had to be protected. To reduce evaporation and limit BCO temperatures, temperature of concrete was not allowed to exceed 29°C at placement.

7.2.1 Evaporation

During both series of observations, temperatures, relative humidities, and wind speeds conducive to high evaporation were recorded (Figures 5.9 and 6.14). However, the evaporation prediction (Equation 3.5) is highly dependent on concrete temperature. Figure 7.1 compares evaporation predictions for concrete temperatures of 21°C, 31°C, and 41°C. This represents the highest concrete temperature recorded during the placement of the test sections (41°C) and 10°C and 20°C cooler. The initial temperature readings recorded by the maturity meters ranged from 31°C to 39°C for Sections 2 through 7, rising by approximately 2°C before the concrete set. At a concrete temperature of 41°C, evaporation was almost always over the limit. At 21°C, it was almost always under the limit. Of course, it is probably not practical to cool concrete by 20°C. At a concrete temperature of 31°C, evaporation is below the limit for roughly half of each day.

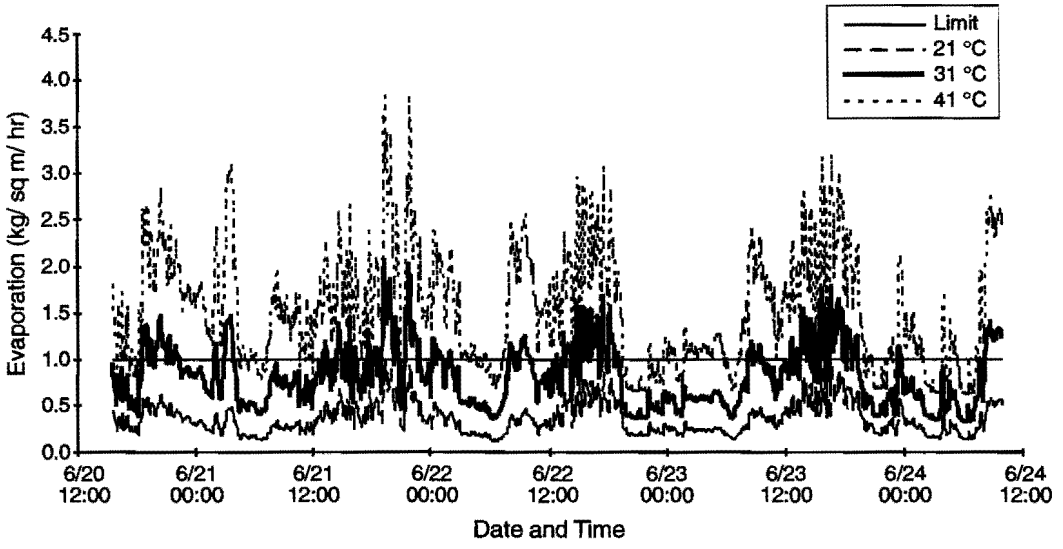

Figure 7.1 Evaporation predictions at different concrete temperatures

Figures 6.8 and 6.12 clearly show the daily variations of air temperature and humidity. Placing BCOs when air temperatures are low and humidity high can make successful construction possible even under very hot and dry conditions.

Concrete temperature can be decreased by using lower cement contents, replacing cement partially with fly ash, and using Type V cement. Thus, if high early strengths are not required, heat of hydration can be reduced using the measures above, leading to lower evaporation rates from the concrete and substantially reduced potential for plastic shrinkage cracking.

7.2.2 Thermal Differentials

The highest temperature, time to highest temperature, lowest temperature, temperature differential, and air temperature at time of casting of each test section within 24 hours after placement is shown in Table 7.1. Because data for Sections 1 and 8 were not obtained from the maturity meters, the temperatures recorded by the bottom thermocouples in sets 1 and 4 were used instead.

The highest ambient temperature in the 24 hours after casting was 36.2°C, and the lowest was 21°C. Therefore, ambient temperature differentials between time of placement and the low temperature in the following 24 hours ranged from 0°C to 9°C. This exceeds the specification of 14°C (Appendix A). In fact, on 3 of the 4 days for which ambient temperatures were recorded by the weather station (Table 7.2), the limit was exceeded. Maximum temperatures attained by the sections ranged from 45°C to 58°C, low temperatures following that high ranged from 35°C to 41°C, and temperature differentials ranged from 4°C to 17°C. Thus, the maximum temperatures and the temperature differentials of the sections were considerably higher than ambient conditions.

Table 7.1 Maximum section temperature differentials

Test Section	Time Cast	Maximum temperature, ° C	Time to maximum temperature, hours	Minimum temperature, ° C	Tem p °C	Air temperature at time of casting, ° C
1	5:30 a.m.	46	12	35	11	22
2	6:30 a.m.	53	9	37	16	21
3	8:30 a.m.	54	9	37	17	25
4	9:30 a.m.	57	8	41	16	27
5	10:30 a.m.	58	7 1/2	43	15	28
6	11:10 a.m.	57	7	42	15	30
7	11:35 a.m.	58	6 1/2	43	15	30
8	10:00 p.m.	45	21	41	4	33

Of considerable interest is the time between construction and maximum temperature for each section. For Sections 1 through 7, the time decreased from 12 hours (for Section 1) to 6 1/2 hours (for Section 7) throughout the day. For Section 8, however, the maximum

temperature was not reached until 21 hours after casting, as well as being the lowest recorded.

Table 7.2 Maximum daily ambient temperature differentials, July 20–24, 1995

Day	Low	High	Differential
June 20	-	34.4°C	13.4°C
June 21	21°C	36.2°C	15.4°C
June 22	20.8°C	35.4°C	14.5°C
June 23	20.9°C	36.3°C	19.6°C
June 24	16.7°C	-	-

There is obviously a considerable benefit to casting concrete when the temperature is falling if shrinkage and thermal cracking are to be prevented.

Examination of thermal gradients (Figures 6.9 to 6.12) shows that the top of the BCO had much larger temperature fluctuations than the bottom. Thus, the temperatures recorded by the maturity meter thermocouples placed at the BCO-substrate interface were less extreme than those expected at the top of the BCO. Furthermore, high and low temperatures at the bottom occurred slightly later than at the top, as may be seen by noting the lag in peaks and troughs in Figures 6.9 to 6.12.

The thermal gradients measured by the vibrating wire strain gauges (Figure 6.15) are similar to those recorded in the adjacent Thermocouple Set 2 (Figure 6.10). The corresponding strains, shown in Figure 6.14, reach a maximum of 360 microstrain at the top of the BCO at 4:43 p.m. and 210 microstrain at the bottom at 6:27 p.m., both on the afternoon of the day of casting.

Temperature differentials at the top and bottom of the BCO are compared in Table 7.3. For the sections cast during the day (Thermocouples 1–3), temperature fluctuations at the top of the BCO were 22°C to 30°C, those at the bottom of the BCO were 15°C to 25°C, and the top and bottom fluctuations varied by 5°C to 9°C. In contrast, for the section cast at night (Thermocouple 4) the top temperature fluctuation was only 17°C and the bottom fluctuation was only 15°C. Again, the benefit of casting a BCO when the temperature is falling may be seen.

Table 7.3 Comparison of temperature fluctuations at top and bottom of BCO

	Thermocouple Set			
	1	2	3	4
Top Readings				
High	50°C	58°C	52°C	51°C
Low	28°C	28°C	25°C	24°C
Difference	22°C	30°C	27°C	17°C
Bottom Readings				
High	46° C	59°C	52°C	45°C
Low	31° C	34°C	34°C	30°C
Difference	15° C	25°C	18°C	15°C
Top-Bottom	7° C	5°C	9°C	2°C

7.3 COMPARISON OF OBSERVED TEST SECTION CRACKING

In order to compare short-term performance and estimate long-term performance of the 8 BCO test sections, the cracking observed in the test sections (Tables 6.10 to 6.17) was compared. The comparisons are shown in Table 7.4 and Figures 7.2 to 7.5. For Section 6, with SFRC, the total crack width was the greatest although the crack spacing was relatively long.

Table 7.4 Comparison of sections (July 25, August 28, and September 17, 1995)

Sec	Total Crack Width (mm)			Average Crack Width (mm)			Number of Cracks			Average Crack Spacing (m)		
	July	Aug	Sep	July	Aug	Sep	July	Aug	Sep	July	Aug	Sep
1	0.89	1.12	0.61	0.13	0.14	0.076	7	8	8	1.91	1.69	1.69
2	1.19	1.22	1.09	0.15	0.12	0.11	8	10	10	1.69	1.39	1.39
3	1.40	2.01	1.98	0.10	0.11	0.09	14	19	22	1.09	0.76	0.66
4	1.22	1.63	1.32	0.10	0.10	0.083	12	16	16	1.17	0.90	0.90
5	1.27	1.63	1.35	0.18	0.12	0.10	7	14	14	1.91	1.01	1.01
6	1.96	1.78	1.96	0.39	0.20	0.22	5	9	9	2.54	1.52	1.52
7	1.17	1.45	1.98	0.10	0.10	0.14	12	14	14	1.17	1.01	1.01
8	0.33	0.61	0.71	0.08	0.055	0.055	4	11	13	3.05	1.27	1.09

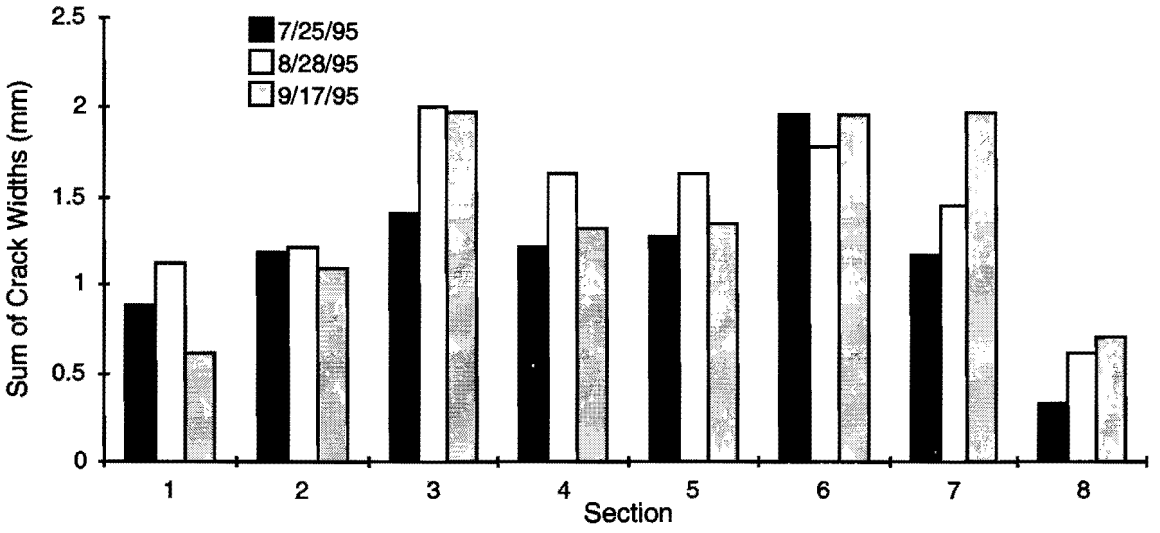

Figure 7.2 Comparison of total crack widths

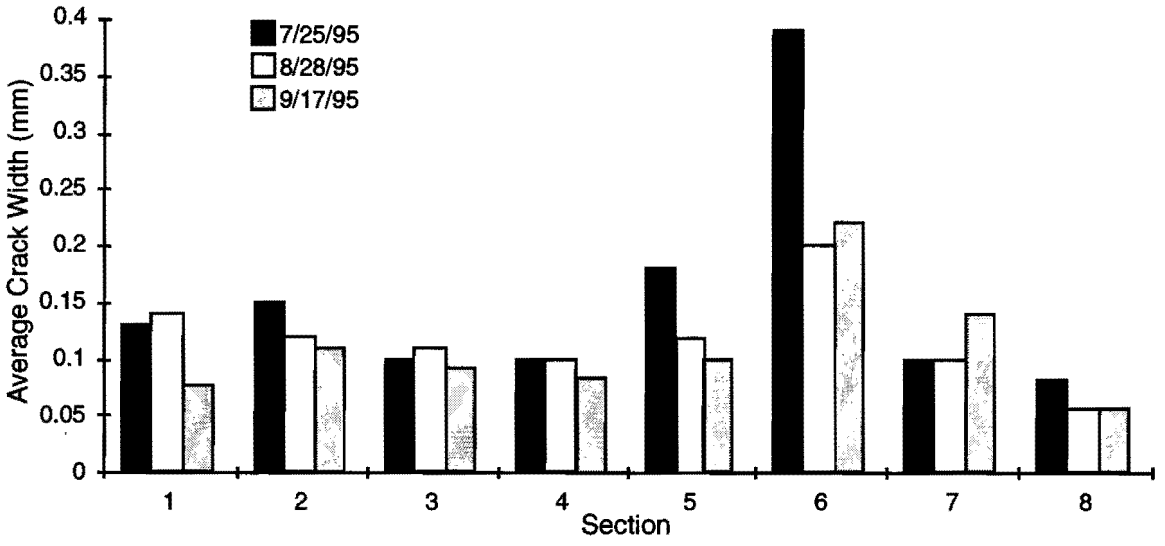

Figure 7.3 Comparison of average crack widths

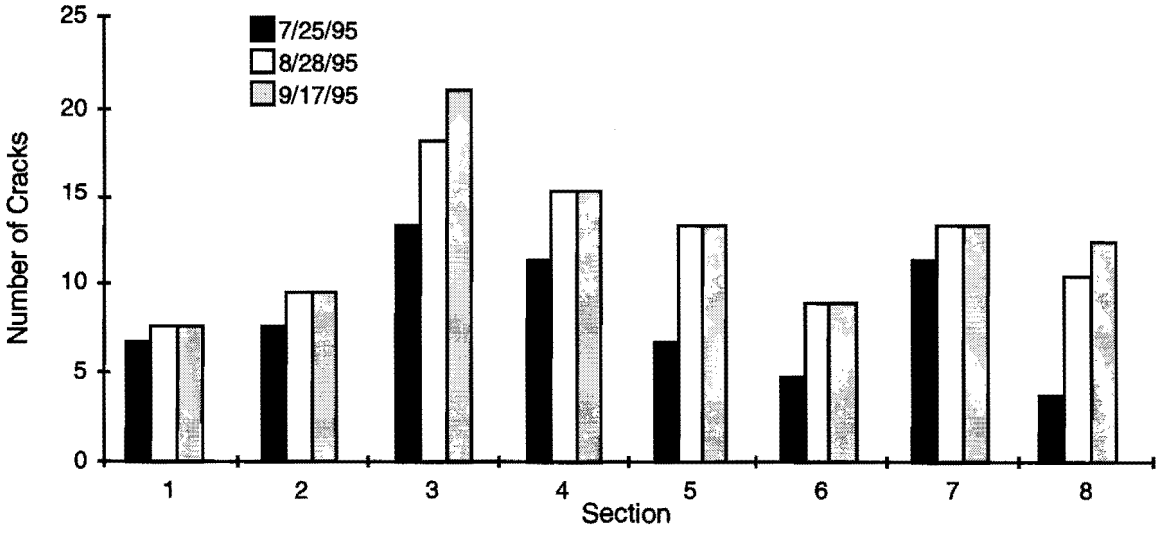

Figure 7.4 Comparison of number of cracks

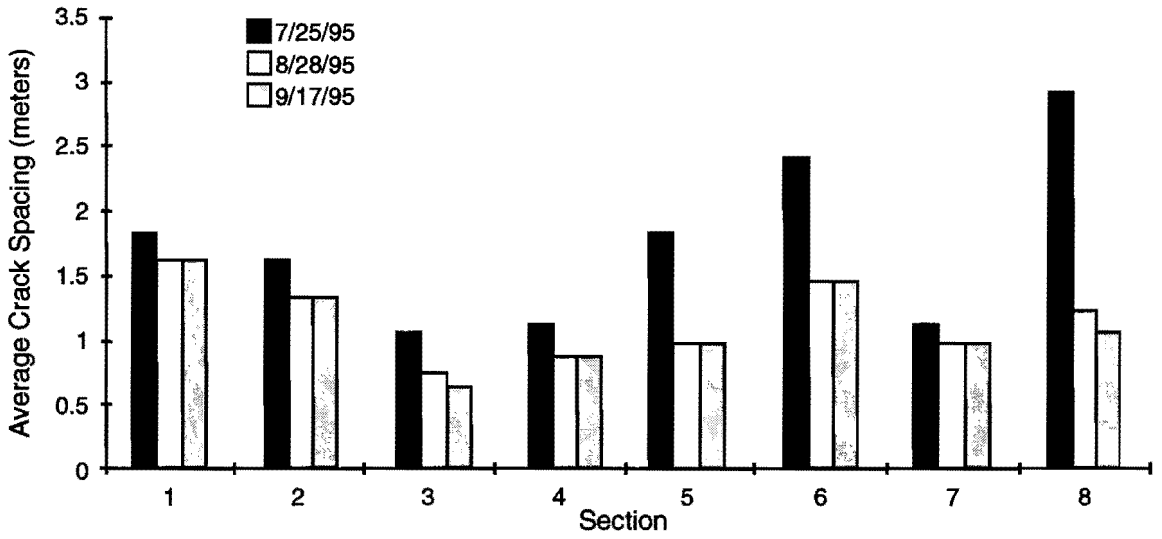

Figure 7.5 Comparison of average crack spacing

Section 8 had the greatest crack spacing and smallest total crack width and can be expected to give better performance under loading than the other sections. Crack width and spacing appears to be strongly influenced by the temperature history of the section. Sections 1 and 8, which experienced the least severe temperatures, also showed the least cracking.

7.4 COMPARISON OF PLAIN CONCRETE, SnFRC, AND SFRC

In order to compare the performance of sections made with plain concrete, SnFRC, and SFRC, it is necessary to compare sections with similar temperature histories. Because Section 1 was cast at a much lower temperature than Sections 2 or 3, and only reached a high temperature at the bottom of the BCO of 46°C, it should be compared to Section 8, which reached a high temperature of 45°C at the bottom of the BCO. Section 8 had much less cracking at 1 month, but slightly more at 3 months. It is probably more important to have less cracking at early ages to prevent delamination. Thus, the SFRC appears slightly superior to plain concrete reinforced with steel. To compare SnFRC with SFRC, Sections 2 and 3 may be compared, because both reached a maximum temperature of 53°C or 54°C, with a minimum temperature within the following 24 hours of 37°C, for a temperature differential of 16°C to 17°C.

Total crack width was greater with steel fiber reinforced concrete (SFRC) than with synthetic fiber reinforced concrete (SnFRC) (Figure 7.1). Average crack widths were approximately equal (Figure 7.2). Number of cracks was greater with SFRC than with SnFRC (Figure 7.3).

However, Section 3 contained both reinforcing steel and SFRC. Section 8, on the other hand, had only SFRC. This represents a more realistic design, since it would clearly be uneconomical to use both reinforcing steel and SFRC. Costs of SnFRC and SFRC are compared in Table 7.5. Costs are for materials or services only and do not include freight or

labor for reinforcement, or mobilization for surface preparation. The labor cost of steel is approximately 16 to 20 percent of the material cost.

7.5 SHEAR CONNECTORS

The effectiveness of shear connectors in controlling cracking can be evaluated by comparing Section 4 with Section 3 (SFRC, reinforcing steel, with and without shear connectors) and Section 5 with Section 6 (SFRC, with and without shear connectors). The total crack width in the two sections with shear connectors was always less than in the two adjacent sections by 15 percent to 54 percent (Table 7.4, Figure 7.1). Although average crack widths were roughly equal for the two sections with both SFRC and reinforcing steel (3 and 4), for the sections with SFRC only, crack widths were much larger in the section without shear connectors (Section 6) by 67 percent to 120 percent. Thus, shear connectors provide a benefit both in reducing total crack width and average crack width.

Table 7.5 Approximate costs of alternatives investigated [a]

	per square meter	per cubic meter
Concrete Reinforcement		
Polypropylene Fibers	$2.22	$13.49
Steel Fibers	$8.55	$51.99
Steel Reinforcing Bars	$4.18	$25.31
Surface Preparation		
Shotblasting	$1.50	-
Hydrocleaning	$1.50	-

[a] Cost includes only materials or, for surface preparation, only services

The comparison is complicated, however, by the fact that the high and low temperatures reached by Section 3 (54°C and 37°C) were lower than those of Sections 4, 5, and 6 (57°C to 58°C and 41°C to 43°C). The temperature differential between high and low measurements in Section 3 was 17°C, versus 15°C to 16°C in Sections 4, 5, and 6.

7.6 REINFORCEMENT

The effectiveness of steel reinforcement in controlling cracking can be evaluated by comparing Section 3 with Section 6 (SFRC, no shear connectors, with and without reinforcing steel) and Section 4 with Section 5 (SFRC, shear connectors, with and without reinforcing steel). The caveats cited above concerning the maximum and minimum temperature and temperature differentials measured in the sections also apply here.

The total crack widths measured in sections with and without reinforcing steel are roughly equivalent. Average crack widths, however, were higher in sections without steel by 20 percent to 290 percent. Thus, sections with SFRC only, had fewer but wider cracks for the same total crack width. This means that each crack in an SFRC section will have more movement, and thus a higher potential for initiating delamination. This is reflected by the

debonded cores near cracks shown in Figure 6.3. Costs are compared in Table 7.5. Cost of labor, of course, will substantially increase the cost of reinforcing steel.

7.7 SURFACE PREPARATION

Both shotblasting and hydrocleaning provided acceptable surface preparation. Hydrocleaning created a rougher surface but left fines on the pavement that had to be removed later. The hydrocleaned surface had strips along the outer edges of the nozzle path that were much rougher than others. This problem could be addressed by adjusting the nozzles on the spray bar. Production rates for the two methods were similar with the equipment used. Costs are approximately equal, as shown in Table 7.5.

Steel shotblasting has become the standard for surface preparation for BCOs. The Humble Equipment Company has considerable experience with shotblasting for BCOs, and their equipment can clean a 2-meter width on each pass. Since they could not do the work at the time required, Nelson Industrial Services was used instead. Their machine only cleans a 0.4 meter width on each pass, but several machines could be used on a job to increase production.

Hydrocleaning was investigated as an alternative technology for surface preparation. To date, it has primarily been used for cleaning old paint off runways. The equipment used was provided by Rampart. The hydrocleaner produces an uneven surface and leaves fines on the base slab. The first problem could probably be solved through experimentation with different nozzle and pressure combinations, the second by pressure washing the base slab after hydrocleaning.

Both shotblasting and hydrocleaning can provide adequate surface preparation for a BCO. Allowing both methods in specifications opens up bidding and should reduce costs to TxDOT.

7.8 DAY/NIGHT CONSTRUCTION

Paving at night is obviously superior to paving during the daytime, even with paving starting as early as 5:30 a.m. The only potential difficulty is that the concrete may require cooling to remain under the specified temperature limit of 29°C. With night paving, evaporation and the potential for plastic shrinkage cracking is substantially reduced. Therefore, it may be possible to relax the concrete temperature limit for night paving.

In Figure 7.1, it may be seen that with a concrete temperature of 31°C (slightly over the limit), evaporation was acceptable from 9 p.m. to 6 a.m. except for part of the night of June 22 and one very short period on the night of June 21. Heat buildup of the BCO is very gradual (Figure 6.12 and Table 7.1), and the high temperatures reached were considerably lower than those measured in Sections 2 through 7.

The beneficial effects of less severe environmental conditions were reflected in the cracking observed in Section 8. At 1 month, the number of cracks observed and total crack width were much less than in any other section. Section 1, which was cast at 5:30 a.m., had similar performance, although not quite as good.

7.9 STRENGTH DEVELOPMENT

The concrete mix performed well and had greater strength than required. With this mix design, the pavement met TxDOT specifications for dense concrete overlay (DC) before 16 hours (31.7 MPa compressive strength at 28 days and 4,400 kPa flexural strength at 7 days) (Ref 48). Furthermore, these strengths are probably greater than necessary before traffic is applied to the BCO.

On June 28, 1995 aggregate trucks were allowed onto the sections. The delay in traffic application was due to the need to remove the concrete formwork first; but as the RDD load testing indicated these trucks could have been allowed on the overlay on the morning of June 23.

Load testing with the RDD indicated that the pavement could sustain heavy truck traffic at 12 hours. Thus, a mix with a lower cement content could be used, which would have the advantage of lowering concrete temperatures.

Both splitting tensile strengths and compressive strengths of cores at 49 days were about 5 to 10 percent higher than the 28-day cylinder strengths, which is reasonable. Flexural strength may be predicted by Equation 7.1 (Ref 48), which would indicate a splitting tensile strength of less than 4,700 kPa.

$$f_f = 0.62\sqrt{f'c} \tag{7.1}$$

where

f_f = flexural strength, MPa, and

$f'c$ = compressive strength, MPa.

Obviously, the splitting tensile strengths measured using both cores and cylinders are substantially higher than this relationship would predict.

7.10 DELAMINATION DETECTION AND MAPPING

The most reliable method of detecting delaminations is coring, but coring is slow, expensive, and damages the pavement. Moreover, if the BCO has reinforcing steel, it is very difficult to avoid the steel. Even highly sensitive test equipment such as the Hilti Ferroscan cannot map 12.7 mm (US #4) bars at a depth of 165 mm. Cores that hit steel cannot be used to determine if the overlay was bonded because the interface is damaged when the core barrel encounters the steel.

Rebar sounding is useful, but is tedious and highly subjective. It is also more reliable with thinner overlays. As noted above, the Schmidt rebound hammer could not differentiate between bonded and unbonded areas.

Of the other nondestructive testing methods used, SASW, impact-echo, and impulse-response all showed potential for detecting delaminations. The RDD was not able to detect delaminations, although the equipment has since been modified (Ref 66). So far, the FWD has not been shown to be able to detect delaminations either. Because it is difficult to attach

accelerometers to a tined pavement surface, impulse-response is much faster and easier to use.

Results of nondestructive testing in June and September are shown in Table 6.19 and 7.6. For the June tests only SASW and impact-echo results are available. During this testing the BCO was hydrating and had a higher temperature than the base slab, so delaminations were closed. As a result, neither SASW nor impact-echo was more than 50 percent accurate in detecting delaminations. High accuracy in locating bonded regions is not particularly useful, since the entire BCO is assumed to be bonded.

Table 7.6 Comparison of nondestructive testing methods for identifying unbonded regions

		Correct Predictions		
Time of test	Bonded or debonded area	SASW	Impact-echo	Impulse-response
Day	Bonded	7 /13 (54%)	9/13 (69%)	11/13 (85%)
	Debonded	2/4 (50%)	3/4 (75%)	4/4 (100%)
Night	Bonded	4/6 (67%)	3/6 (50%)	3/6 (50%)
	Debonded	2/3 (67%)	1/3 (33%)	2/6 (67%)

More extensive testing was undertaken in September, with suspected delaminations investigated by coring. Overall, impulse-response provided the highest accuracy, particularly during the day. Owing to the lower number of tests conducted at night, these results are less conclusive. The high accuracy of impulse-response in locating delaminations is particularly useful (4 out of 4). However, this advantage was only apparent with the daytime results.

Although the night tests could be expected to be more accurate, this was not the case with impact-echo or impulse-response. SASW was slightly more accurate at night (67 percent versus 50 percent). Figure 7.6 illustrates how delaminations may be detected by impulse-response. The normalized deflection is the ratio of output deflection to the input deflection. The debonded area, which is less stiff, has an output deflection at least twice that of a bonded area over most of the frequencies considered.

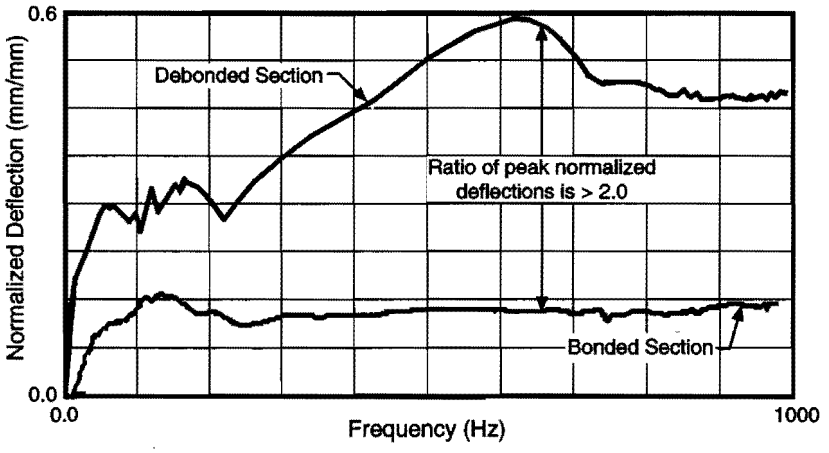

Figure 7.6 Delamination detection by impulse-response

CHAPTER 8. FACTORS AFFECTING BEHAVIOR OF BCOS AT EARLY AGES

Because delamination in bonded concrete overlays (BCOs) often occurs at early ages (Ref 8), early-age mechanical behavior is very important. After the concrete sets, it begins gaining strength. At the same time, stresses develop due to volumetric contraction and expansion of the BCO relative to the base concrete. If at any time the stresses exceed the available strength, cracking, delamination, or both will occur. Once delamination starts, it will spread until it is arrested. Spread of delamination and its effect on pavement performance will be discussed in Chapter Nine.

8.1 CURING

The early-age behavior of a BCO is greatly affected by curing. "Curing is the maintaining of a satisfactory moisture content and temperature in concrete during its early stages so that desired properties may develop" (Ref 68). For BCOs, curing has the dual role of promoting strength gain and reducing stress buildup. Maintaining moisture content and maintaining temperature are considered separately below.

8.1.1 Maintaining Moisture Content

Excessive loss of moisture from concrete may interfere with hydration and lead to undesirable shrinkage and shrinkage cracking. Common methods of curing are water curing and sealing. Water curing consists of ponding water on the surface of the concrete, spraying the concrete with water to replace moisture as it evaporates (fogging), or covering the concrete with wet burlap or cotton mats. Sealing uses plastic film or membrane-forming curing compounds to retain moisture (Ref 68).

Buch and Zollinger (Ref 69) pointed out that loss of moisture is detrimental in two respects: it interferes with the strength development of the concrete, and contributes to buildup of stress within the concrete. They noted that upper layers of concrete pavements have much quicker loss of moisture than lower layers. Using center-point beam tests, they demonstrated a considerable loss of strength with loss of moisture.

8.1.2 Maintaining Temperature

The temperature in concrete should be kept reasonably uniform to avoid stresses induced by temperature gradients. Excessively high temperatures will contribute to moisture loss through evaporation and should be avoided. Concrete will not cure unless the temperature is at least 10°C and must be protected from freezing until it reaches a compressive strength of at least 3.4 MPa (Ref 68).

The curing method may affect temperature buildup in a BCO. For example, use of wet burlap or mats will reduce temperatures through evaporative cooling. Plastic, on the other hand, will retain heat. White pigmented curing compounds are intended to keep the pavement cool by reducing absorption of solar radiation. In cold weather, insulating blankets may be used to help retain heat.

The higher heat of hydration produced by high early strength concrete mixtures exacerbates this problem. Research has shown that concrete temperature changes of 9°C to 16°C may lead to cracking (Ref 70). One study found that when high temperatures cause concrete strains of 85 to 120 microstrains, cracking occurs no matter what the age of the concrete (Ref 71).

8.2 STRENGTH DEVELOPMENT

For pavements, flexural or tensile strength is usually considered more important than compressive strength because the concrete cracks due to fatigue from flexural stresses. However, for a BCO with properly supported edges (e.g., tied shoulders), traffic loading will produce primarily compressive stresses within the overlay (Figure 8.1). Care should be taken during the design of a BCO to ensure that stresses from traffic loading will be compressive if the overlay is to be opened to traffic at early ages. This may be accomplished by preventing edge- and corner-loading conditions for example, by using tied shoulders. In this case, tensile stresses from loading will be negligible.

8.2.1 Compressive Strength

Huddleston (Ref 46) showed that a BCO could be loaded at very low strength with little risk of damage. When BCO strength is low, stiffness is also low. Thus, stresses are primarily carried by the base concrete.

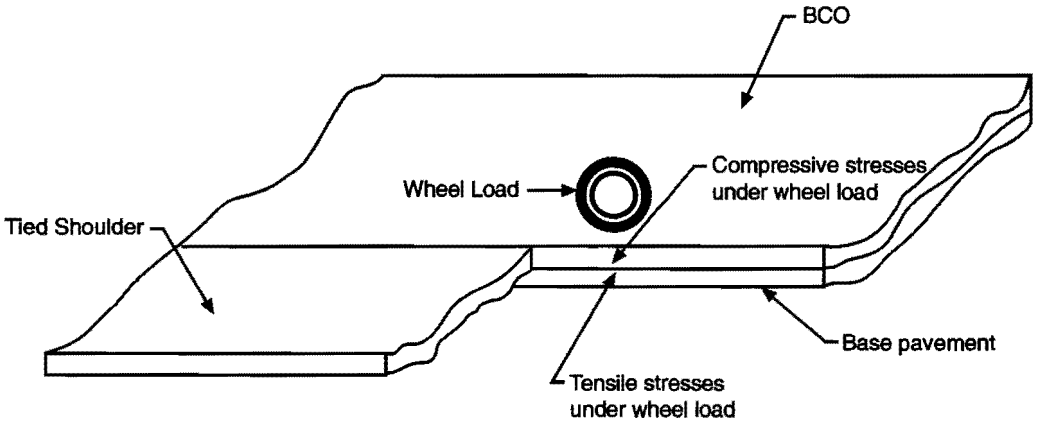

Figure 8.1 BCO Stresses from traffic loading

Factors affecting compressive strength development are shown in Table 8.1. This discussion of compressive strength development will be limited, because it is probable that other factors such as bond strength and shrinkage and thermal stresses have a much greater effect on early-age behavior and long-term performance of BCOs. Steel and synthetic fibers have little effect on compressive strength (Ref 73). Water-cement ratio and curing are the most important factors.

8.2.2 Tensile Strength

Although stresses from vehicle loading are compressive, stresses from volumetric contraction are tensile. For example, note the tensile strains in Figure 6.14, which produce tensile stresses. Thus, while traffic loading produces compressive stresses, those are likely to be low and not to affect performance of the BCO. The cracking produced by tensile stresses is more likely to govern BCO performance.

Table 8.1 Factors affecting strength development (Refs 48, 72)

Factor	Effect
Concrete Factors	
Water-cement ratio	Lower water-cement ratios lead to higher strength
Aggregate variables	
Maximum size of coarse aggregate	Larger aggregate reduces paste requirements for strength
Gradation	More uniform gradation reduces paste requirements
Particle texture	Rougher particles provide for better bond with paste
Particle shape	Shape affects bond and paste requirements
Cement composition	Variable
Admixtures	Variable
Construction factors	
Vibration/consolidation	Proper consolidation increases concrete strength
Curing	Proper curing enables concrete to achieve full potential strength
Environmental factors	
Relative humidity	Low relative humidity can disrupt curing
Age	Strength increases with age

Flexural or tensile strength of concrete is usually related to compressive strength through equations (Equation 7.1, for example) or charts. Figure 8.2 compares flexural and tensile strength to compressive strength.

However, these relationships were developed for concrete with a maximum compressive strength of about 48 MPa. Tests of cylinders and cores from the El Paso test sections showed higher splitting tensile strengths than predicted by Equation 7.1 by 40 to 45 percent. In general, the same factors that affect compressive strength also affect tensile and flexural strength (Table 8.1).

Although steel fibers have little effect on concrete flexural strength before cracking, they add considerable postcracking capacity (Refs 53, 73).

8.3 BOND DEVELOPMENT

At the interface between the BCO and the base slab, normal and shear stresses develop. Compressive normal stresses may be neglected. As the BCO contracts relative to the base slab, tensile and shear stresses develop. These stresses are highest at boundaries and corners (Figure 8.3).

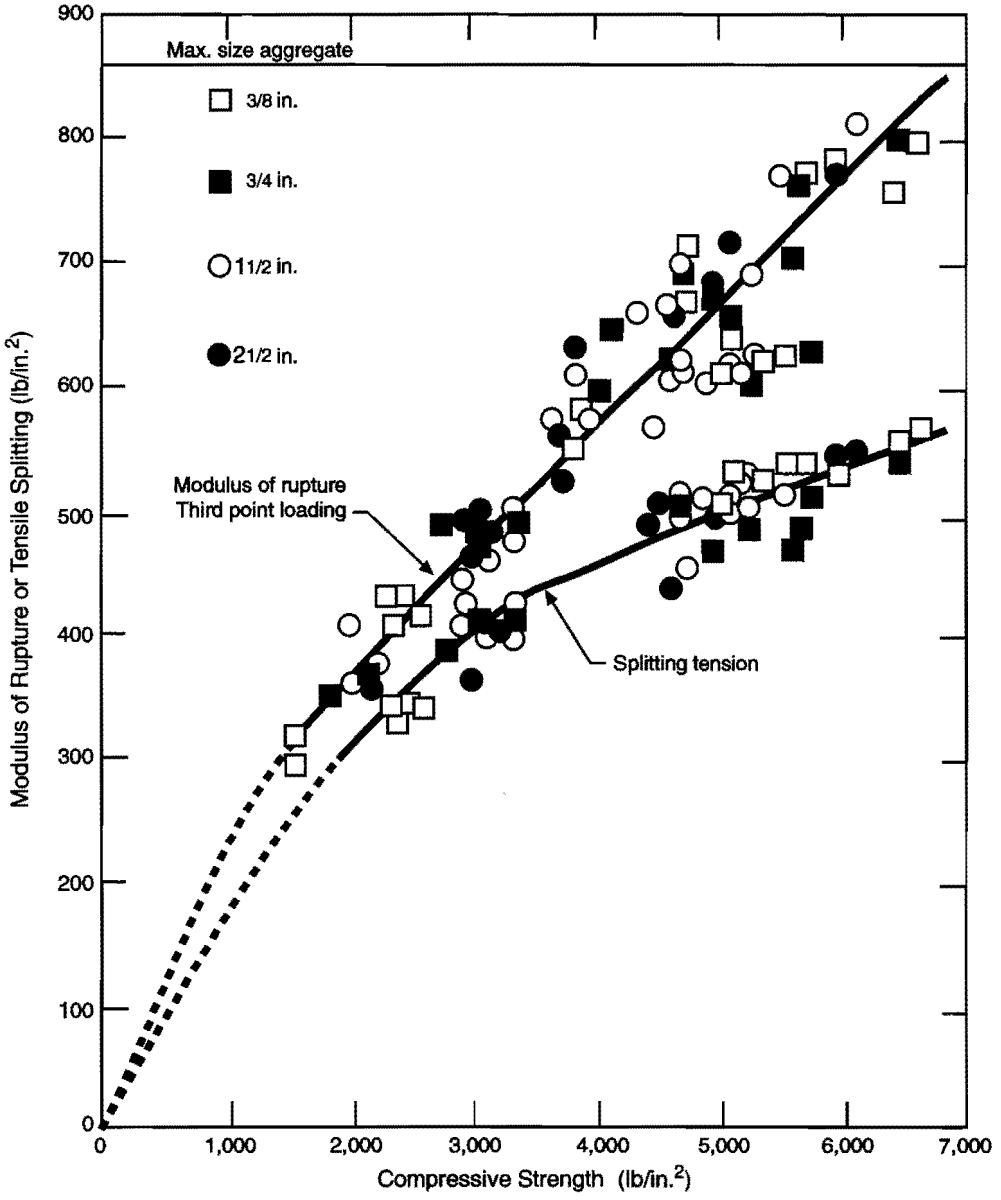

Figure 8.2 Relationship of compressive to flexural and tensile strength of concrete, (Ref 48) (1 lb/in.^{2} = 6.89 kPa)

Interface bond consists of two components—interlock and adhesion. The effectiveness of interlock is determined by the roughness of the prepared surface. Adhesion is produced by development of chemical bonds between concrete paste and the cured substrate concrete (Ref 48). Thus, adhesion is affected by the variables that normally affect paste-aggregate bond. For example, more porous aggregates will develop better adhesion (Refs 48, 72).

Whereas adhesion develops as the concrete cures, the contribution of interlock is fixed. However, improved surface roughness, in addition to improving interlock, also enhances adhesion. With a rougher surface, more area is available for the paste to adhere (Figure 8.4). Interlock considerably increases the shear capacity of the interface bond.

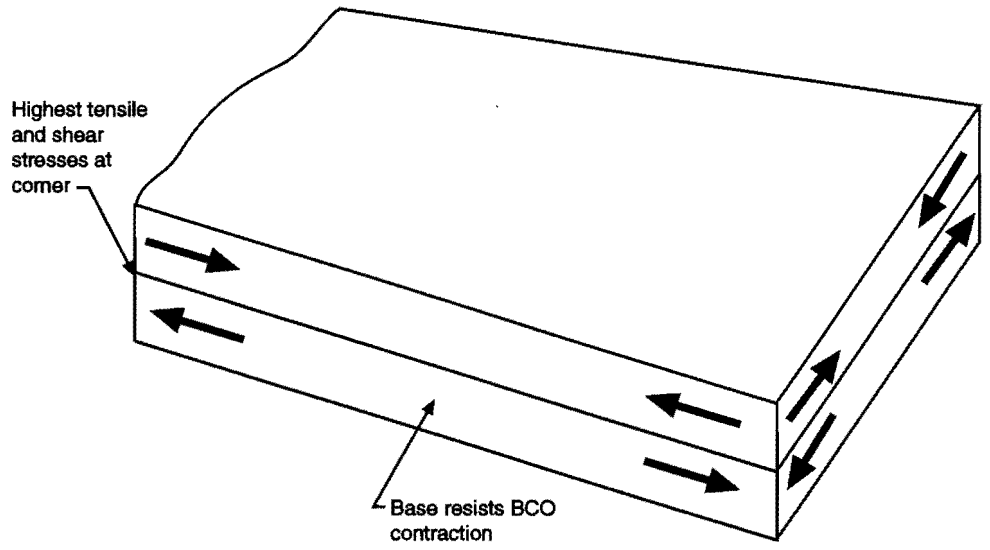

Figure 8.3 Interface stresses from BCO contraction relative to base slab

For bond between paste and aggregate, Mindess and Young note that "the bond region is weak because cracks invariably exist at the paste-coarse aggregate interface, even in continuously moist-cured concrete and before the application of any external load" (Ref 48). The same cracks, of course, will occur at the interface between the BCO paste and the base slab surface. These cracks are due to bleeding, segregation, and volume changes of cement and paste during setting and hydration (Ref 48). In addition to the cracks caused by volume changes of the cement paste, cracks may also be expected to occur due to small differential movements between the BCO and the base slab.

This may be seen by comparing pull-off test bond strength results between Sections 5 and 6 (Figures 6.3 – 6.6). The lowest bond strengths were found near wide cracks, where the highest differential movements between the BCO and base slab had occurred.

Factors affecting bond development are shown in Table 8.2. Many of the factors, such as water-cement ratio, affect compressive strength in a similar manner (Table 8.1). The most important factors are water-cement ratio, surface roughness, and curing.

Suprenant (Ref 74) noted that bond depends on surface preparation, selection and use of materials, and curing. All three must be present. Therefore, loss of one component (e.g., poor surface preparation) may lead to total loss of the bond. Each of these three may be envisioned as a link in a chain; the chain is only as strong as its weakest link (Figure 8.5).

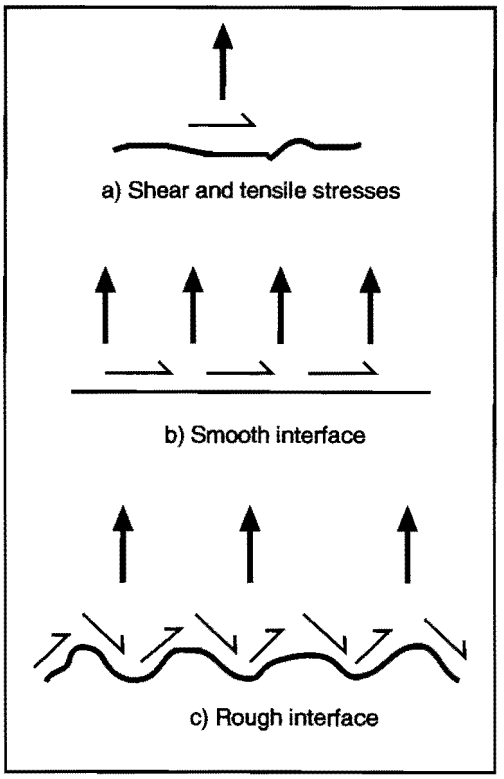

Figure 8.4 Effect of surface roughness on bond

Table 8.2 Factors affecting bond development (Refs 9, 48, 72)

Factor	**Effect**
Concrete factors	
Water-cement ratio	Lower water-cement ratios lead to higher bond strengths
Cement composition	Variable
Amount of paste	Thick paste layer may reduce strength
Construction Factors	
Vibration/consolidation	
Curing	Poor curing reduces bond strength
Surface roughness	Rougher surfaces lead to better bond
Surface cleanliness	Foreign material inhibits bond
Surface moisture	Moist surfaces may inhibit or enhance bond, based on surface roughness
Surface temperature	Substrate temperatures over 52°C damage bond
Environmental Factors	
Relative humidity	Low humidity decreases bond strength
Ambient temperature	Temperature differentials over 14°C in the 24 hours after placement damage bond
Evaporation	Evaporation over 1 kg/m^2/hr inhibits bond
Age	Bond increases with age

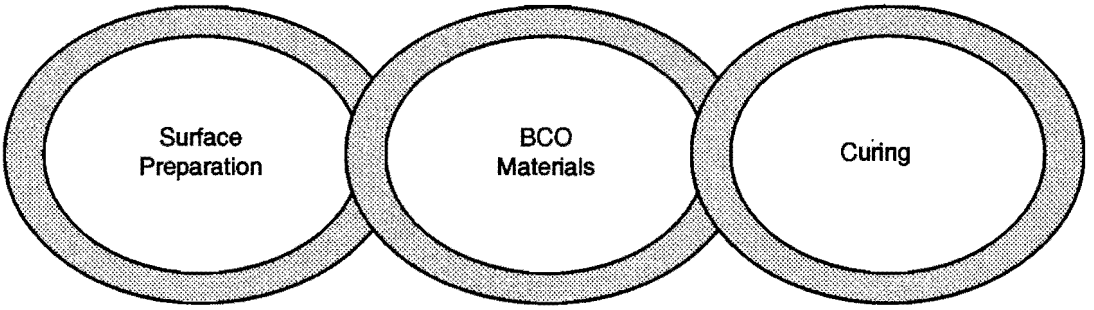

Figure 8.5 Chain model of bond strength (Ref 74)

Although this is a simple model, it may be helpful in gaining insight into poor performance of BCOs. For example, applying the model to the BCO failure on IH 80 in California, it appears that all three links of the chain were deficient.

O'Neal noted that surface preparation may have been unsatisfactory, since the sandblasting used to prepare the surface may have not roughened it enough, and dried grout may have interfered with adhesion. The BCO concrete had high shrinkage due to highly absorptive aggregate. Finally, the curing did not adequately protect against moisture loss (because the fogging spray blew away) nor protect against the 28°C temperature differential (Ref 20). Under these conditions, it is not at all surprising that the BCO delaminated.

The model may also be used to explain the greater cracking and lower bond strengths observed in Section 6 compared with Sections 7 and 8. In all three sections the material (SFRC) was the same. However, the surface preparation in Section 7 was superior due to the greater roughness produced by the hydrocleaning equipment (a mean sand patch roughness of 1.71 mm versus 1.5 mm for shotblasting). Thus, the average crack width was narrower, and bond strengths were higher. Section 8 had better curing because it was cast in the evening. Thus, Sections 7 and 8 illustrate the effects of superior surface preparation or curing on early age BCO behavior.

Emmons and Vaysburd (Ref 75) offer a model of a surface repair system consisting of the repair material, a transition zone (interface zone), and existing concrete (Figure 8.6). This is similar to the chain model in Figure 8.5, if the existing concrete and transition zone are assumed to comprise surface preparation. The surface repair system emphasizes the importance of removing unsound existing concrete.

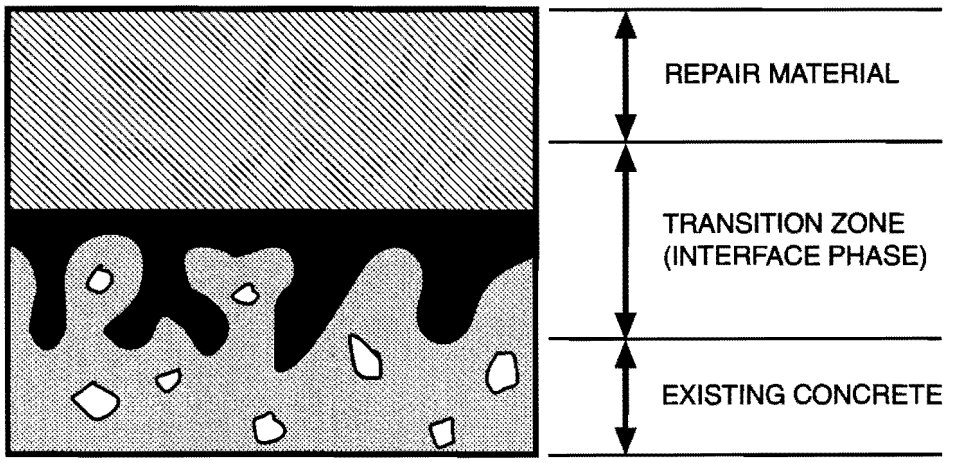

Figure 8.6 Idealized model of a surface repair system (Ref 75)

Silfwerbrand (Ref 76) compared jackhammering, sandblasting, and water-jetting (also known as hydrodemolition, hydrojetting, and hydroblasting) as the means of surface preparation for bridge deck overlays. Water-jetting produced the roughest surface, followed by jackhammering. The sandblasted surface was considerably smoother. He pointed out that jackhammering produced much more microcracking in the surface of the base concrete than the other two methods. Of the pull-off tests made of overlays on water-jetted surfaces in this study, 93 percent broke below the interface. The average strength was 2,250 kPa. For jackhammered surfaces, 69 percent of the tests pulled off below the interface, with a mean strength of 900 kPa. With sandblasting, 62 percent of breaks were below the surface, at an average of 1,700 kPa. In this study, water-jetting was clearly shown to be superior for this application. However, shotblasting was not considered in the study, so these data cannot be used to predict bond strengths on shotblasted surfaces.

Pull-off test failures in the base concrete are desirable because they indicate that the interface is at least as strong as the base concrete. Silfwerbrand suggested that when the interface strength is at least 1,500 kPa, 80 percent of pull-off tests will break in the base concrete.

It has been found in investigations using slant-shear concrete specimens and masonry prisms that thicker layers of paste at an interface lead to lower bond strengths. For example, in slant-shear specimens, increasing a layer of portland cement mortar bonding agent (with a water-cement ratio of 0.35) from 3.2 mm to 6.4 mm reduced bond strength from 44.4 MPa to 34.9 MPa, a difference of 21 percent (Ref 77). The reason was not explained, but the reduction may be due to more microcracking occurring due to shrinkage in the thicker mortar layer.

This suggests that use of portland cement grouts or concretes with too much paste, which may lead to thicker bond layers, may in turn lead to lower bond strength. The slant-shear tests also indicated that specimens with no bonding agent had good bond strength (43.5 MPa) and a wet surface gave slightly higher bond strengths (46.0 MPa versus 41.7 MPa, an increase of about 10 percent) (Ref 77).

With pull-off tests, Whitney et al. found that for lightly shotblasted surfaces, wet substrates gave the best bond. However, for severely shotblasted surfaces, dry substrates gave better bond (Ref 9). Thus, for rougher surfaces, a dry substrate is preferred.

In the present study, very few well-bonded cores failed at the interface. In most cases, the interface proved to be stronger than the concrete on the surface of the BCO. Six test results that failed at the interface ranged from 1,020 kPa to 1,980 kPa with a mean of 1,350 kPa, a standard deviation of 370 kPa, and a COV of 0.28. This compares favorably with specifications used previously in other states of 670 kPa (Ref 40) to 1,380 kPa (Ref 13).

8.4 SHRINKAGE

Volume changes in concrete due to loss of moisture are referred to as shrinkage. Shrinkage is usually divided into plastic shrinkage, which occurs in fresh concrete, and drying shrinkage, which occurs in hardened concrete (Ref 48).

8.4.1 Plastic Shrinkage

Water leaves the surface of fresh concrete due to evaporation and is replaced by water bleeding to the surface. If the rate of evaporation exceeds the rate of bleeding, plastic shrinkage cracking occurs. In theory, it is possible to prevent plastic shrinkage cracking by either reducing evaporation or increasing bleeding. However, excessive bleeding can lead to weakness, porosity, and lack of durability of the concrete surface due to a high water-cement ratio. Also, water pockets may form under large aggregate particles (Ref 48). Thus, it is preferable to control plastic shrinkage cracking by controlling evaporation (Section 3.8) and proper curing. In addition to evaporation, water may also be lost into the dry base concrete under the BCO.

The overall volumetric contraction due to plastic shrinkage is on the order of 1 percent (Ref 72). Since a BCO is restrained in all horizontal dimensions by friction at the interface, most of this volumetric contraction probably occurs through the thickness of the BCO, unless plastic shrinkage cracking occurs. Plastic shrinkage is greater with higher cement content and earlier setting (Table 8.3).

Table 8.3 Factors affecting plastic shrinkage (Refs 48, 72)

Factor	Effect
Cement content	High cement content increases shrinkage
Setting time	Earlier setting increases shrinkage
CFP fibers	CFP fibers decrease plastic shrinkage

Shaeles and Hover (Ref 78) studied the influence of mix proportions and construction operations on plastic shrinkage cracking using thin slabs of mortar (20 mm thick by 0.61 meters by 0.91 meters). Evaporation rates were high, at least 1.22 kg/m^2/hr. Temperatures were 25°C to 35°C, relative humidities were 10 to 25 percent, and wind speeds were 11 to 13 Kph. Fans were used to produce the wind. Cracking generally began 45 to 100 minutes after

the fans were started, and continued to develop for up to 2 1/2 hours. Water-cement ratios studied were 0.50 to 0.70. Mixes with higher paste content had a greater tendency to crack.

Cracks formed parallel to the screed and perpendicular to the directions of screeding. Faster screeding (10 m/minute) produced more cracking than slower screeding (1 m/minute). Proper finishing also reduced cracking.

The study found that the severity of cracking did not depend on the rate of evaporation as long as it was over 1.0 kg/m^2/hr. Considerable cracking was observed, in one case, at a rate of 1.27 kg/m^2/hr, whereas in another case, none was observed at 2.10 kg/m^2/hr.

The authors pointed out that high plastic shrinkage may not lead to extensive cracking if the material is able to accommodate the volume change or develops tensile capacity rapidly.

Collated fibrillated polypropylene (CFP) fiber manufacturers claim that SnFRC made with CFP has reduced plastic shrinkage and bleeding and superior resistance to plastic shrinkage cracking (Ref 79). Soroushian et al. (Ref 80) studied the effect of CFP fibers on plastic shrinkage cracking, using Shaeles and Hover's testing method. Experimental variables were synthetic fiber content (0 percent and 0.1 percent), screeding speed (3 m/minute and 12 m/minute), and screeding direction. Thirty-eight mm thick slabs were used. SnFRC set faster than plain concrete and had 18 percent less bleeding. Initial setting time was reduced by 9 percent with SnFRC, and setting time was reduced by 27 percent. The synthetic fibers significantly reduced maximum crack width, as well as reducing the crack area by 95 percent.

Nanni et al. (Ref 81) used a proposed ASTM testing procedure to investigate the effects of steel and synthetic fibers on plastic shrinkage cracking. Each specimen had a stress riser to cause a crack to occur in the center of the specimen, and all samples cracked. A temperature of 35°C, a relative humidity of 40 percent, and a wind of 18.4 Kph were used to induce an evaporation rate of 1 kg/m sq/hr. All of the fibers except for one (a synthetic monofilament) reduced cracking by an average of 30 to 70 percent.

Therefore, plastic shrinkage cracking may be reduced by lowering the evaporation rate, reducing paste content, and use of steel and synthetic fibers. Slower screeding and proper finishing will also lower the probability of plastic shrinkage cracking.

8.4.2 Drying Shrinkage

Loss of water from concrete leads to both reversible and irreversible shrinkage. Loss of adsorbed water is much more significant than loss of free water (Ref 72). The mechanisms of reversible and irreversible shrinkage are discussed in detail in References 48 and 72. Factors affecting drying shrinkage are shown in Table 8.4. The two most important influences are aggregate and water-cement ratio. Other important factors are the environment, time, admixtures, and steel and synthetic fibers.

8.4.2.1 Aggregate. Shrinkage is affected by the amount and modulus of the aggregate. Usually aggregate is viewed as resisting the shrinkage of the cement paste. The effect of aggregate content on shrinkage is shown by an empirical equation (Ref 48):

$$\varepsilon_{sh} = \varepsilon_p (1 - A)^n \tag{8.1}$$

where

ε_{sh} = concrete shrinkage strain,

ε_p = paste shrinkage strain, for paste hydration products having the same water/ cement ratio as the concrete,

A = aggregate content, and

n = an exponent varying from 1.2 to 1.7.

For example, Equation 8.1 predicts that increasing aggregate content from 65 percent to 70 percent will decrease shrinkage by 17 percent to 23 percent for the same paste shrinkage strain.

A more detailed model for ultimate shrinkage, based on elastic and composite theory, is given by Hansen and Almudaiheem (Ref 82):

$$\varepsilon_{sh} = 0.5\varepsilon_p (1 - V_d)\left[\frac{1}{1 - V_d + kmV_d} + (1 - V_d) + \frac{V_d}{km}\right] \tag{8.2}$$

where

V_d = relative restraining volume of the dispersed particle phase (i.e., aggregate and unhydrated cement),

m = modulus ratio = E_d / E_p,

E_d = elastic modulus of dispersed particle phase,

E_p = elastic modulus of hydration products;

k = $\frac{1 - 2\nu_p}{1 - 2\nu_d}$, and

ν_p = Poisson's ratio of paste, and

ν_d = Poisson's ratio of the dispersed particle phase, and other variables are as previously defined.

Table 8.4 Factors affecting drying shrinkage (Refs 48, 72, 82)

Factor	Effect
Concrete Factors	
Aggregate content	High aggregate content decreases shrinkage
Aggregate modulus	High aggregate content decreases shrinkage
Clay coatings on aggregate	Presence of clay increases shrinkage
Use of shrinking aggregates (often possessing high absorption)	Use increases shrinkage
Fine aggregate content	Higher fine aggregate content versus coarse aggregate increases shrinkage
Water-cement ratio	Low water-cement ratio decreases shrinkage
Cement content	Higher cement contents lead to more shrinkage
Cement composition	Different cements may have different paste shrinkage strains; finer cements have more shrinkage
Air content	Higher air content increases shrinkage
Admixtures	Various
Fiber reinforcement	Fiber reinforcement decreases shrinkage and resists shrinkage cracking
Construction Factors	
Surface area/ volume ratio of member	High surface area/ volume ratio increases shrinkage
Member thickness	Thinner members have more shrinkage
Curing temperature	Elevated curing temperatures may decrease shrinkage
Environmental Factors	
Age	Shrinkage increases with age
Relative humidity	Low relative humidity increases shrinkage

V_d may be estimated by:

$$V_d = \left[\frac{1-h}{1+(w/c)\left(\frac{\rho_c}{\rho_w}\right)}\right]\left(\frac{V_p}{V_c}\right)+\frac{V_a}{V_c} \tag{8.3}$$

where

h = relative degree of hydration,

w/c = water-cement ratio,

ρ_c = density of cement,

ρ_w = density of water,

V_p = volume of paste,

V_a = volume of aggregate, and

V_c = volume of concrete.

For $E_d = E_p$ and $\nu_d = \nu_p$, equation 8.2 becomes:

$$\varepsilon_{sh} = \varepsilon_p (1 - A) \tag{8.4}$$

which is the same as equation 8.1 with n = 1. The model gives good agreement with experimental results. The model predicts a difference of about 18 percent for an increase in aggregate content from 65 percent to 75 percent, for water-cement ratios of 0.35 to 0.5 (Ref 82).

These models clearly illustrate the influence of aggregate modulus and volume on drying shrinkage. To reduce drying shrinkage, aggregates with high modulus and the highest possible volume of aggregate should be used, and clay coatings should be removed from the aggregate. Some aggregates are subject to shrinkage; this is often indicated by high absorption (Ref 72). Such aggregates should not be used.

8.4.2.2 Water-cement ratio and cementitious material content. Drying shrinkage is lower at lower water-cement ratios. The effect is more pronounced for lower aggregate contents (Ref 72).

Research by Smadi, Slate, and Nilson (Ref 83) established that high strength concrete (HSC, 59 to 69 MPa compressive strength) and medium strength concrete (MSC, 35 to 41 MPa) had lower shrinkage than low strength concrete (LSC, 21 to 24 MPa) by about 45 percent. The HSC had greater shrinkage at early ages than MSC, possibly due to greater heat of hydration. However, ultimate shrinkage was approximately the same. They suggested that "drying shrinkage of concrete decreases as water-cement ratio decreases, down to a certain limit of water-cement ratio, below which the shrinkage might increase slightly depending on the drying period. The value of this water-cement ratio appears to lie between 0.65 and 0.32 (by weight)" (p. 232, Ref 83).

Sennour and Carrasquillo (Ref 84) studied the effect of partial replacement of cement with Class C and F fly ash on shrinkage and creep of concrete. In all cases the shrinkage was increased. It was suggested that shrinkage may depend on the CaO content of the fly ash.

The effects of water-cement ratio and cementitious material content on shrinkage are complex; however, high cement contents with low water-cement ratios, as used in high performance concrete, may lead to shrinkage within acceptable limits. Gardner and Zhao (Ref 85) noted that high strength concretes (with water-cement ratios below 0.35) may exhibit shrinkage due to self-desiccation.

8.4.2.3 Environment. Relative humidity has been shown to have a great effect on paste shrinkage. The ACI relative humidity correction factor γ_H is (Ref 86):

$$\gamma_H = 3.00 - 0.03(RH) \text{ for } 80 \text{ percent} \leq RH \leq 100 \text{ percent} \tag{8.5}$$

or

$$\gamma_H = 1.40 - 0.01(RH) \text{ for } 40 \text{ percent} \leq RH \leq 80 \text{ percent} \quad (8.6)$$

where

RH = relative humidity, percent (Ref 49).

Hansen and Almudaiheem proposed a different correction factor K_H (Ref 82):

$$K_H = 1.80 - 0.018(RH) \text{ for } 50 \text{ percent} \leq RH \leq 100 \text{ percent} \quad (8.7)$$

or

$$K_H = 1.34 - 0.0083(RH) \text{ for } 11 \text{ percent} \leq RH \leq 50 \text{ percent} \quad (8.8)$$

The prediction of Equation (8.8) is lower than that of Equations 8.5 and 8.6 where 50 percent ≤ RH ≤ 100 percent, but gives better agreement with experimental results (Ref 82). These coefficients are compared in Figure 8.6. Equation 8.8 covers a range of lower relative humidities that Equation 8.6 does not address.

Relative humidities as low as 11 percent were measured in El Paso during the test (Figure 6.12). Humidities this low can increase drying shrinkage by 25 percent (Figure 8.7).

Shrinkage predictions may also be adjusted for curing, average member thickness, volume-surface area ratio, slump, fine aggregate percentage, cement content, and air content using ACI formulas (Ref 86).

8.4.2.4 Time. The rate of shrinkage also decreases with time. Approximately 14 to 34 percent of ultimate (20 year) shrinkage occurs within 2 weeks, 40 to 80 percent within 3 months, and 66 to 85 percent within 1 year. This may be delayed by prolonged moist curing, but ultimate shrinkage may be higher (Ref 68). However, at later ages the effect of shrinkage strains on BCO performance may be mitigated by creep and by the greater strength of the concrete.

Drying shrinkage is exacerbated by the high surface area to volume ratio of a BCO. The effect of drying shrinkage is also substantially influenced by the moisture gradient between the top and bottom of a BCO.

ACI predicts shrinkage at time t ($\varepsilon_{sh}(t)$) using an equation (Ref 86):

$$\varepsilon_{sh}(t) = \frac{t}{t+35}\varepsilon_{sh} \quad (8.9)$$

Where t = time in days. This formula is only valid after 7 days, however, and thus is not useful for predicting early-age behavior. The ultimate shrinkage strain ε_{sh} may range from

415 to 1,070 x 10^{-6}; ACI suggests using 780 x 10^{-6}, for 40 percent relative humidity, in the absence of better data (Ref 86).

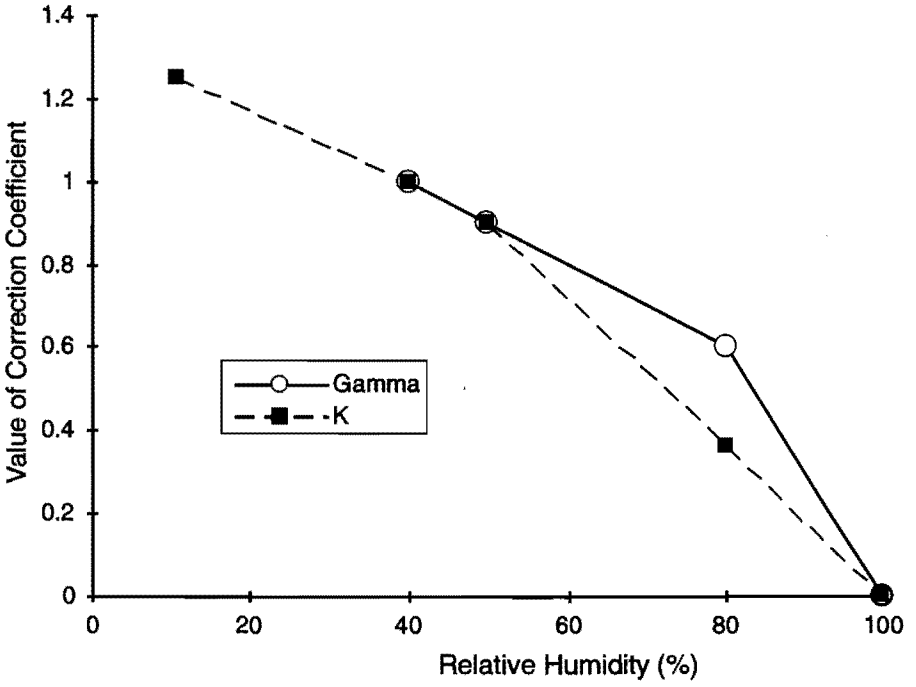

Figure 8.7 Comparison of ACI (Gamma) and Hansen and Almudaiheem (K) relative humidity drying shrinkage correction coefficients (Ref 82)

Another shrinkage prediction is given by the Comité Euro-International du Béton (CEB-FIP) (Ref 87) formula:

$$\varepsilon_{sh}(t) = \varepsilon_{sh}\left[\beta_s(t) - \beta_s(t_0)\right] \tag{8.10}$$

where ε_{sh} and β_s are given by standard tables and graphs, and t is given by:

$$t = \frac{1}{30}\sum\left[\left(T(t_m) + 10\right)\Delta t_m\right] \tag{8.11}$$

where

t_m = concrete temperature, °C, and

Δt_m = number of days at temperature $T(t_m)$.

Thus, Equation 8.10, unlike Equation 8.9, is a function of maturity and not time only (Ref 49).

Gardner and Zhao (Ref 84) claim that the ACI formula overestimates early-age shrinkage and underestimates later-age shrinkage, and the CEB formula underestimates shrinkage by a factor of 2.

The Bazant-Panula (BP) shrinkage model (Ref 88) uses more parameters but is claimed to be more accurate:

$$\varepsilon_{sh} = \varepsilon_{\infty}\left[1+\left(\frac{\tau_{sh}}{\$ t}\right)^{r}\right]^{-\frac{1}{2r}} \tag{8.12}$$

where

$\$ t = t - t_0$ = duration of drying,

t = age of concrete, and

t_0 = age when drying started, and $\varepsilon_{\infty}, \tau_{sh}, r$ are material parameters. τ_{sh} is directly proportional to the effective thickness of the cross section, and ε_{∞} is affected by environmental humidity.

Since shrinkage is highly variable, statistical analysis was applied by Bazant et al. to the three models discussed above (Ref 89). The coefficient of variation of deviations of shrinkage strain from the ACI formula (Equation 8.9) was found to be 52.5 percent. The corresponding COVs for the CEB-FIP model (Equation 8.10) and BP model (Equation 8.12) were 71.7 percent and 16.5 percent, respectively.

Although curing at elevated temperatures can decrease irreversible shrinkage by two-thirds (Ref 48), it is probably not economically feasible to achieve the required temperature of 65°C in a BCO. For example, even with high ambient temperatures and a high cement content in the concrete, the highest temperature measured by Thermocouple Set 2 (Figure 6.7) was approximately 60°C. Moreover, the elevated temperatures would exacerbate thermal expansion and contraction.

8.4.2.5 Admixtures. Use of superplasticizers has not been shown to substantially reduce shrinkage (Ref 75). Shrinkage reducing admixtures have been found to reduce free shrinkage and shrinkage cracking, at some loss of strength (Ref 90). Air entrainment, by reducing the stiffness of concrete, would be expected to increase shrinkage.

8.4.2.6 Steel and synthetic fibers. Steel and polypropylene fiber reinforcement reduces drying shrinkage and shrinkage cracking. Tests with Novocon Xorex™ steel fibers at 0.25 percent to 1.5 percent by volume (20 to 120 kg/m^3) showed a significant reduction of average crack width with increasing steel fiber volume (Ref 73). This does not agree with the

large average crack width observed in Section 6 during the El Paso test (Figure 7.2); however, as discussed earlier, the fault may not lie with the SFRC, but with the surface preparation or curing.

Chern and Young (Ref 91) found a 30 to 40 percent reduction in drying shrinkage at 2 percent steel fibers, by volume. Increasing fiber volume to 4 percent provided no additional reduction of shrinkage. Also, the shrinkage reduction at early ages was not as great.

Padron and Zollo (Ref 92) observed that monofilament polypropylene fibers prevented shrinkage cracking more than they reduced shrinkage, because the actual degree of shrinkage reduction was too small to account for the decrease in cracking.

Grzybowski and Shah (Ref 93) used ring-shaped restrained shrinkage specimens to study the effect of steel and CFP fibers on shrinkage cracking. Specimens had a water-cement ratio of 0.5 and were tested at a relative humidity of 40 percent at 20°C.

Only slight (5 to 10 percent) reductions in free shrinkage were observed at 1 percent steel or CFP fibers by volume. Total free shrinkage was approximately 1,000 microstrains.

Cracks were measured using a microscope. Total crack width from the plain concrete specimen was 0.900 mm. For SFRC, total crack width ranged from 0.345 mm at 0.25 percent by volume to 0.03 mm at 1.5 percent. CFP total crack widths were 0.875 mm at 0.1 percent by volume to 0.215 mm at 1.0 percent. Steel fibers were more effective than CFP fibers at the same volumes, and CFP at less than 0.25 percent had very little effect. A theoretical model to predict shrinkage cracking was developed as part of the study.

All of these studies suggest that drying shrinkage cracking may be considerably reduced by using steel or synthetic fibers. Little research has been done on use of both types of fiber in the same concrete.

8.4.3 Shrinkage Data with El Paso Materials

As part of the present study, the plastic and drying shrinkage of concrete made with El Paso materials was investigated with two types of specimens. For one type, both plastic and drying shrinkage were measured. For the second set of specimens, only drying shrinkage was measured.

8.4.3.1 Plastic and drying shrinkage specimens. Plots of early-age plastic and drying shrinkage of concrete made with El Paso aggregates and Type II and V cements, using the mix design from Chapter 3, are shown in Figures 8.8 – 8.11. Although several series of tests were performed, only representative results are shown below.

Specimens were cast in steel molds 75 mm by 75 mm by 300 mm, with the bottom and sides sealed with plastic to prevent moisture loss and reduce friction with the mold. The top of each specimen was left open in the laboratory, with a relative humidity of approximately 40 to 60 percent. The shrinkage of the specimen was measured every 2 hours between aluminum angles cast into the concrete 228 mm apart. Measurements were made for 7 days. The temperature of each specimen was also recorded, so that drying shrinkage could be calculated by subtracting thermal strain from total shrinkage. The thermal coefficient of the concrete at early ages was assumed to be the same as that at later ages at a relative humidity of approximately 60 percent (discussed in Section 8.6).

The initial plastic shrinkage was highly variable, ranging from 200 to 900 microstrains. Plastic shrinkage is shown by the jump occurring in the first 4 hours of each plot. This measurement is probably lower than the actual plastic shrinkage, because some shrinkage may have taken place before the instrument began recording.

Of course, since the plastic shrinkage occurs while the concrete has little or no stiffness, its contribution to concrete stress (if restrained) is small. Drying shrinkage is much more useful for predicting stresses. Drying shrinkage for the specimens shown in Figures 8.8 – 8.11 was approximately 350 to 450 microstrains over the first 7 days. The fluctuations in these curves, as well as those for drying shrinkage, are due to experimental error, because very small quantities were measured.

8.4.3.2 Drying shrinkage specimens. Several specimens with steel studs cast in the ends were made to measure drying shrinkage. Each of these specimens was 50 mm by 50 mm by 300 mm long, with a gauge length of 250 mm between the ends of the steel studs.

Three specimens each were made of concrete with Type V cement contents of 181 and 326 kg/m^3 (with 98 and 176 kg/m^3 of fly ash, respectively), and two specimens were made with a cement content of 254 kg/m^3, with 137 kg/m^3 of fly ash. These will be referred to as low, high, and medium cement content (LCC, HCC, and MCC), respectively.

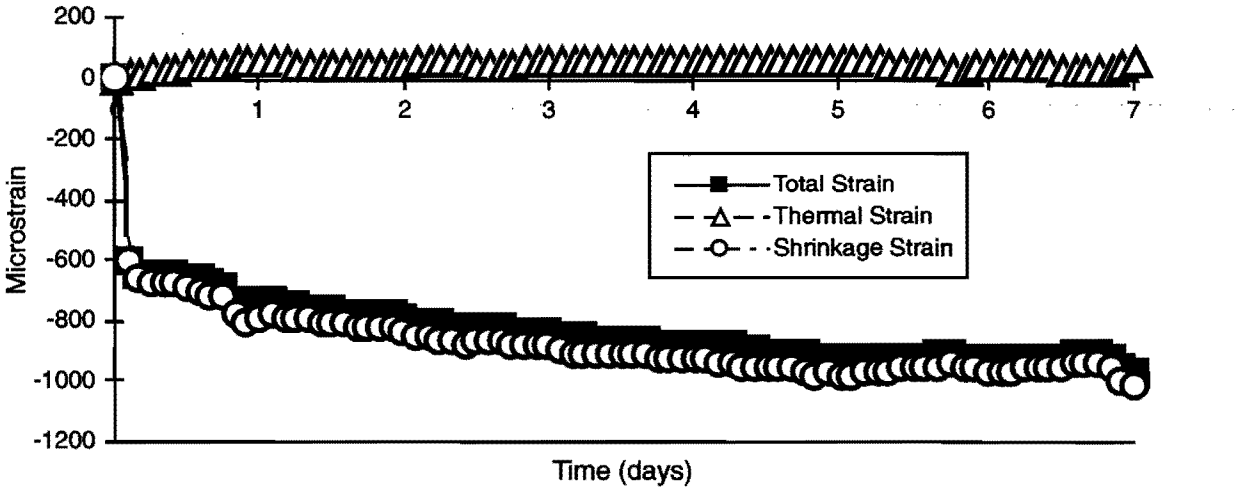

Figure 8.8 Shrinkage, Type II cement, 520 kg/cubic meter

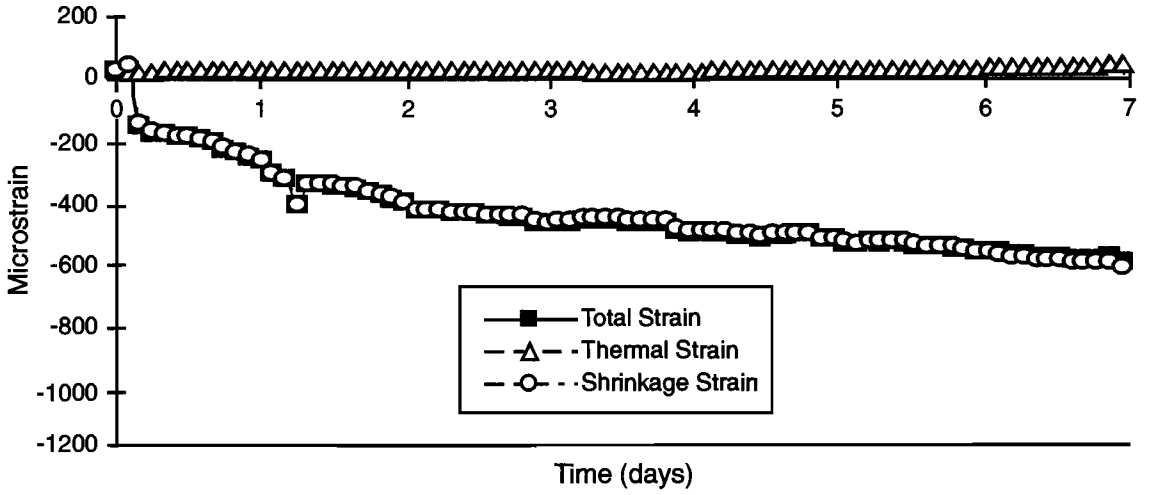

Figure 8.9 Shrinkage, Type V cement, 520 kg/cubic meter, specimen 1

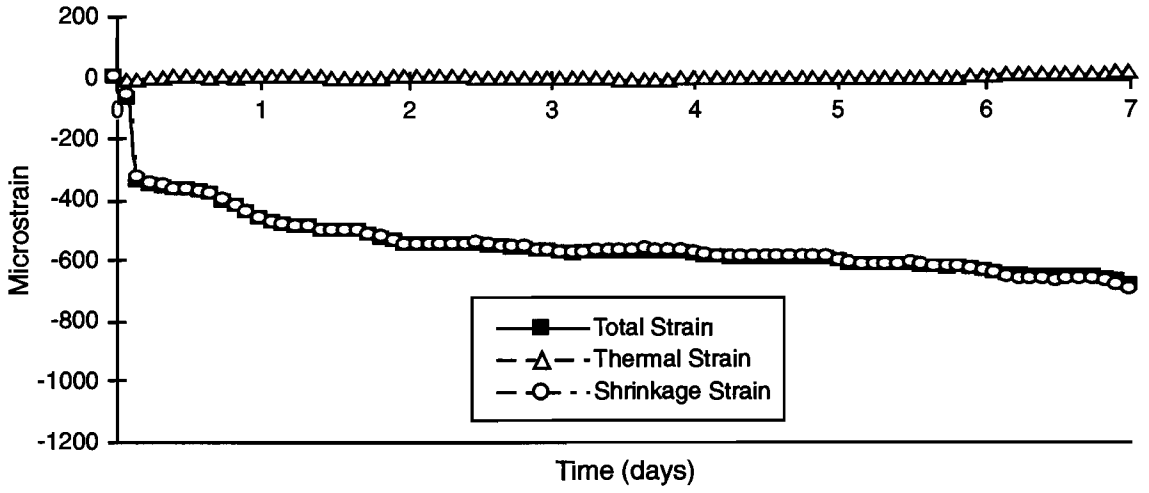

Figure 8.10 Shrinkage, Type V cement, 520 kg/cubic meter, specimen 2

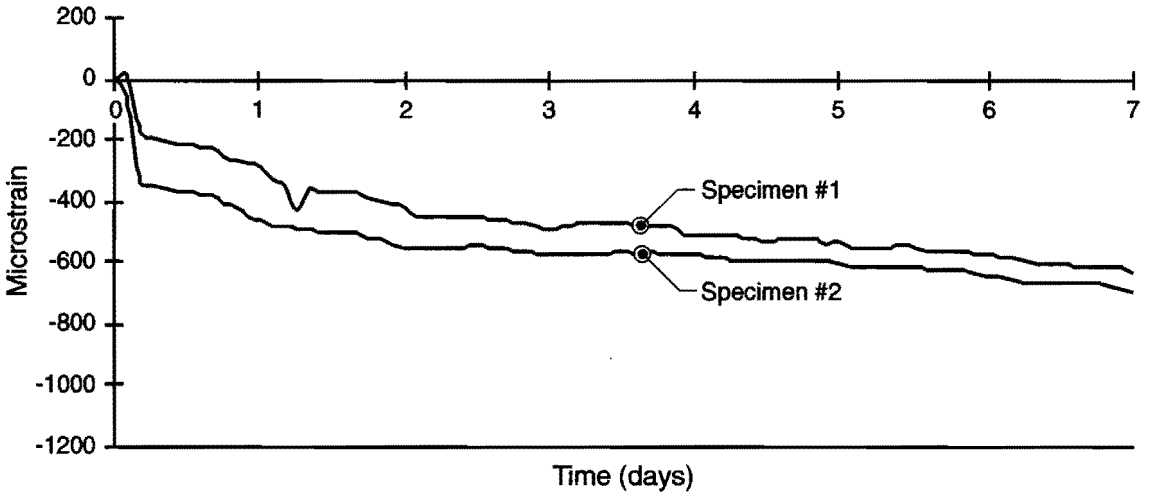

Figure 8.11 Comparison of shrinkage, specimens 1 and 2, Type V cement

After moist curing, the LCC specimens were demolded at 3 days, the MCC at 2 days, and the HCC at 1 day, and exposed on all four sides to the atmosphere. The relative humidity was 40 to 60 percent, and the temperature was 18°C to 24°C. Drying shrinkage was observed for 28 days, after which the specimens were used for thermal coefficient testing. The drying shrinkage of these specimens during the first week was slightly less than that of the specimens observed previously. The drying shrinkage strain at 28 days was approximately 280 to 380 microstrains for all specimens. The initial rate of shrinkage was lowest for the HCC specimens.

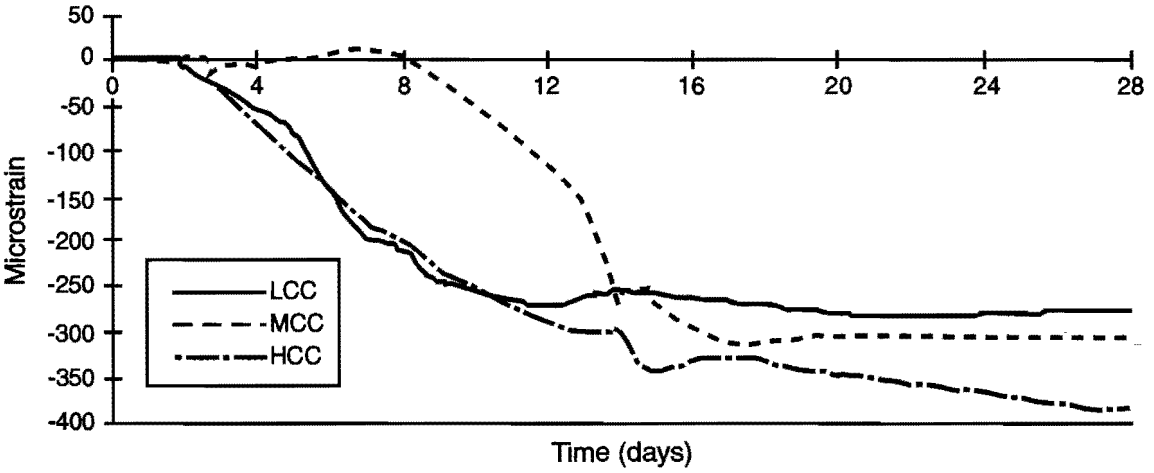

Figure 8.12 Drying shrinkage of LCC, MCC, and HCC specimens

8.5 CREEP

For many structural applications, such as prestressed concrete, shrinkage and creep are considered together because both effects are detrimental. Under imposed and sustained stress, creep adds strain to the initial elastic strain. Under an imposed strain, however, creep relaxes the stress caused by resistance to the strain. Therefore, for BCOs, creep is beneficial because it relaxes the tensile stresses induced by shrinkage. The effect of creep in reducing tensile stresses and cracking may be seen in Figure 8.13. Thus, when engineering concretes for BCO applications, it would be desirable to minimize drying shrinkage and maximize creep.

However, many of the same factors that affect drying shrinkage (Table 8.4) affect creep in much the same manner (Table 8.5). Thus, concretes with low drying shrinkage will also, in general, have low creep.

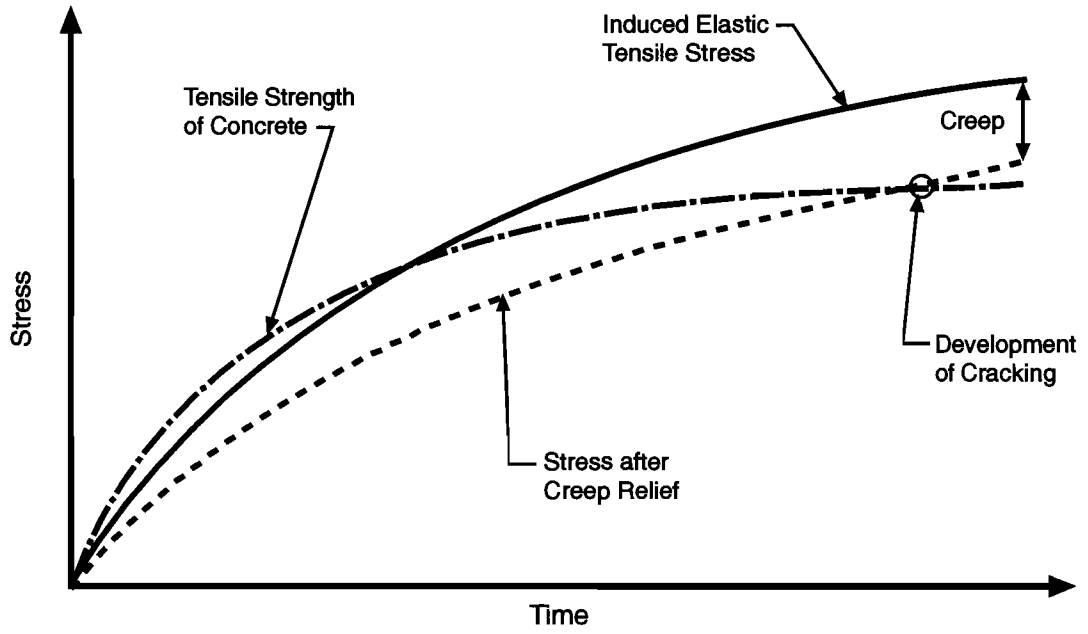

Figure 8.13 Effect of creep on drying shrinkage cracking (Ref 72)

ACI (Ref 86) predicts creep using either a creep per unit stress (δ_t) or creep coefficient (ν_t), which is a ratio of creep strain to initial strain. The latter method is used here. Creep strain is given by:

$$\varepsilon_c = \varepsilon_i \nu_t \tag{8.13}$$

where

ε_c = creep strain,

ε_i = instantaneous applied strain, and

ν_t = creep coefficient for loading at 7 days. ν_t is given by:

$$\nu_t = \frac{t^{0.60}}{10 + t^{0.60}} \nu_u \tag{8.14}$$

where

t = time after loading, days, and

ν_u = ultimate creep coefficient. The normal range for ν_t is 1.30 to 4.15.

Table 8.5 Factors affecting creep (Refs 48, 72, 83)

Factor	Effect
Concrete Factors	
Aggregate content	High aggregate content decreases creep
Aggregate modulus	High aggregate content decreases creep
Use of shrinking aggregates (often possessing high absorption)	Use increases creep
Fine aggregate content	Higher fine aggregate content versus coarse aggregate increases creep
Water-cement ratio	Low water-cement ratio decreases creep
Cement composition	Different cements may have different paste creep strains
Air content	Higher air content increases creep
Admixtures	Various
Construction Factors	
Surface area/volume ratio of member	High surface area/volume ratio increases creep
Member thickness	Thinner members have more creep
Environmental Factors	
Applied stress	Higher applied stress increases creep
Duration of load	Longer load duration increases creep
Time of initial load application	Later initial load application decreases creep

Creep decreases with increasing loading age and increases with increasing loading duration. Creep also increases with increasing surface area/volume ratio of the member, temperature slump, fine aggregate content, and air content. The effect of cement content is negligible. Creep decreases with increasing relative humidity and member thickness (Refs 48, 72, 83, 94). Smadi, Slate, and Nilson (Ref 83) found that the creep coefficient was much lower for HSC than MSC or LSC.

8.6 THERMAL EXPANSION AND CONTRACTION

Concrete expands when heated and contracts when cooled. Within the range of normal temperatures for construction and service conditions (0°C to 60°C), the relationship is linear (Ref 75):

$$\varepsilon_T = \alpha(\Delta T) \tag{8.15}$$

where

ε_T = thermal strain,

α = coefficient of thermal expansion, mm/mm/°C, and

ΔT = change in temperature, °C, = $T - T_0$,

T = temperature, °C, and

T_0 = reference temperature, °C.

Both α and ΔT may be influenced by concrete composition. Factors affecting thermal expansion and contraction are shown in Table 8.6.

8.6.1 Coefficient of Thermal Expansion

The coefficient of thermal expansion of concrete is often considered approximately equal to 10×10^{-6} mm/mm/°C (Ref 94).

Table 8.6 Factors affecting thermal expansion and contraction (Refs 48, 72)

Factor	Effect
Concrete Factors	
Aggregate	Higher aggregate α increases concrete α
Water-cement ratio	Affects moisture and heat
Construction Factors	
Curing	Affects moisture and heat
Environmental Factors	
Relative Humidity	α high for RH from 40 to 80 percent
Age	α decreases with increasing age and loss of moisture
Temperature	Expansion increases with increasing temperature

The two most important factors affecting the coefficient of thermal expansion of concrete are the coefficient of thermal expansion of the aggregate (Table 8.7) and the relative humidity of the concrete. The effect of moisture (hygrothermal expansion) depends on water/cement ratio and age, since these govern the porosity of the paste. The actual coefficient of thermal expansion is:

$$\alpha_{actual} = \alpha_{true} + \alpha_{hygro} \tag{8.16}$$

where

α_{actual} = measured coefficient of thermal expansion,

α_{true} = that measured in the absence of hygrothermal change, and

α_{hygro} = coefficient of hygrothermal expansion (Ref 48).

As may be seen in Figure 8.14, this effect is important for relative humidities from 40 percent to 80 percent.

Table 8.7 Thermal coefficient of aggregates and cement paste (Refs 48, 72)

Material	Coefficient of thermal expansion, strain x 10^{-6}/°C
Granite	7 - 9
Basalt	6 - 8
Limestone	6
Dolomite	7 - 10
Sandstone	11- 12
Quartzite	11 - 13
Marble	4 - 7
Cement Paste	11 - 20

The only practical way to ensure concrete with a low coefficient of thermal expansion is to select aggregates with low thermal coefficients. The El Paso specification recommendations (Appendix A) limit concrete α to 9.9 mm/mm/°C, tested dry. It will, in general, be impossible to control ambient relative humidity.

The coefficient of thermal expansion of various concretes made with El Paso materials, as measured in the present study, is shown in Table 8.8. A slag aggregate was tested and found to have a coefficient of thermal expansion considerably higher than the limestone. The effect of the coefficient of hygrothermal expansion may be considerable, as may be seen in the difference between the thermal coefficients of the BCO test section and slag aggregate concretes at 0 and 60 percent relative humidity. The thermal expansion of concrete made with El Paso dense dolomitic limestone is approximately 70 percent of that of most concrete, making this material very useful for BCO construction.

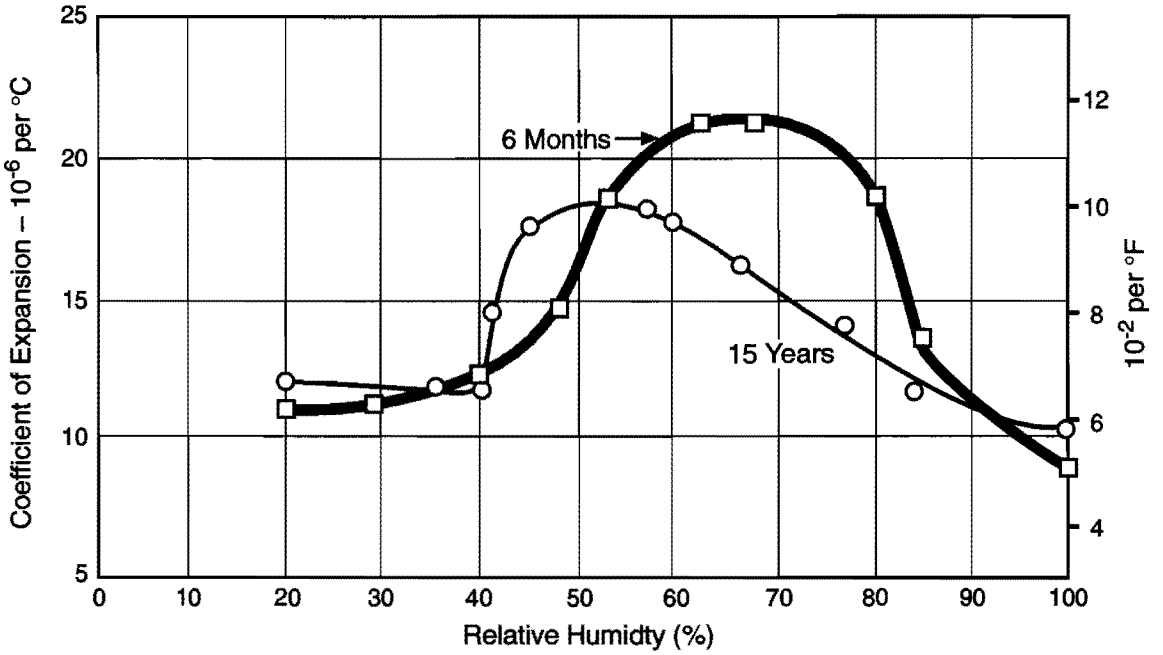

Figure 8.14 Variation of coefficient of thermal expansion with moisture content of cement paste (Ref 72)

Table 8.8 Thermal coefficient of concretes made with El Paso materials

Concrete	Relative humidity	Coefficient of thermal expansion, x 10^{-6} mm/mm/°C
Original pavement	60 percent	7.6
BCO test sections	60 percent	6.9
Slag aggregate	60 percent	9.5
BCO test sections	0 percent	6.3
Slag aggregate	0 percent	8.1
Medium cementitious content (MCC)	0 percent	7.2
High cementitious content (HCC)	0 percent	6.8

8.6.2 Temperature Differential

Thermal expansion and contraction depend on the temperature differential as well as the coefficient of thermal expansion (Equation 8.15). The temperature differential must be measured in terms of a reference temperature T_0, usually the set or curing temperature (Ref 75). At $T = T_0$, there is no thermal expansion or contraction and no thermally induced stress.

Emborg and Bernander (Ref 95) noted that temperature rise and differentials may be mitigated by using low-heat cements and fly ash, reducing cement content, reducing placing temperature, and using cooling techniques. They pointed out that the most important

parameters that affect early-age thermal stresses in concrete are the temperature development in the element being cast, the temperature in the adjoining structure (e.g., the base slab on which a BCO is cast), the mechanical behavior of the young concrete, and the degree of restraint imposed on the element.

"The temperature development in the element is dependent on (1) dimensions and geometry of the structure; (2) the thermal properties of the young concrete (heat of hydration, specific heat, etc.); (3) the conditions at concreting (placing temperature, formwork, insulation, cooling, etc.); and (4) the environmental conditions (ambient air temperature, temperature of neighboring structures, etc.)" (Ref 95). The properties of young concrete considered important were elasticity and creep, strength development, thermal expansion/contraction, and tensile behavior.

In one example, stress levels for a initial concrete temperature of 20°C and air temperature of 5°C were shown to be much lower than for either an initial concrete temperature of 20°C and air temperature of 20°C, or an initial concrete temperature of 10°C and an air temperature of 20°C, even though the temperature difference in the concrete was substantially higher in the first case. Thus, using temperature differential limits for quality control may not prevent thermal cracking.

8.7 MODELING EARLY–AGE BCO BEHAVIOR

The BCO strains induced by traffic loading, thermal expansion and contraction, and creep may be expressed as follows:

$$\varepsilon = \varepsilon_{el} + \varepsilon_{sh} + \varepsilon_T - \varepsilon_c \tag{8.17}$$

where

ε = total strain,

ε_{el} = elastic strain from externally imposed loading,

ε_{sh} = drying shrinkage strain,

ε_T = thermal strain, and

ε_c = creep strain,

where positive strains are tensile.

For early-age behavior, before traffic is allowed on the overlay, the elastic strain is zero, and Equation 8.16 becomes:

$$\varepsilon = \varepsilon_{sh} + \varepsilon_T - \varepsilon_c \tag{8.18}$$

where all variables are as previously defined.

The total strain may be measured, as in Figure 6.14, but the shrinkage, thermal, and creep strains in a BCO test section cannot be measured, because the sources of the strains cannot be isolated. Shrinkage strain may be estimated from laboratory specimens (e.g., Figures 8.8 – 8.12). Thermal strain may be estimated using measured thermal gradients (e.g., Figures 6.9 – 6.12 and 6.15) and thermal coefficients measured from laboratory specimens (Table 8.8). Creep strain, then, may be calculated by subtracting total strain from the sum of shrinkage and thermal strain. This estimate, however, is likely to have considerable error, due to the errors in measuring the other three strains.

The sign of creep strain is opposite to that of shrinkage and thermal strain because it will tend to relax those strains. For computing stresses at early ages, therefore, it will be conservative to neglect creep. It is therefore possible to write:

$$\varepsilon \leq \varepsilon_{sh} + \varepsilon_T \tag{8.19}$$

that will give an upper bound to early-age strains and stresses.

Horizontal strains are resisted by the BCO, producing stresses:

$$\sigma = E\varepsilon \tag{8.20}$$

where

σ = stress, kPa, and

E = modulus of elasticity, kPa.

Since strains and elastic modulus vary with time, stress will also vary with time. Equation 8.20 may be written for any stress at a time t_1:

$$\sigma(t_1) = \int_0^{t_1} d\varepsilon(t) E(t) dt \tag{8.21}$$

to emphasize the time-dependent nature of σ, E, and ε.

8.6.1 Crack Formation in BCOs

Although $\sigma(t)$ may be tensile or compressive, because concrete is much weaker in tension than compression, only tensile stresses will be considered. If the tensile stress, $\sigma(t)$, at any point exceeds the tensile strength of the concrete, $f_t(t)$,

$$\sigma(t) > f_t(t) \tag{8.22}$$

the concrete will crack. Once a crack occurs, the opening of the crack will relieve stresses in the immediate vicinity of the crack.

The CRCP on which the BCO is placed is cracked, and those cracks close and open as the pavement heats and cools. The pavement contracts and a crack opens; this causes a high tensile stress concentration in the BCO directly over the crack. This leads to the often observed phenomenon of reflective cracking where cracks appear in a BCO directly over old cracks in the base concrete (Figure 8.15).

Cracks in the CRCP on IH-10 in El Paso are approximately 2 meters apart (Ref 7), thus, reflective cracks would be expected to appear approximately 2 meters apart in a BCO. In some cases (Refs 8, 28, 40), not all cracks reflected through, particularly with BCOs made with SFRC. Reinforcement in the BCO and CRCP keeps cracks closed tightly.

If cracks occurred at precisely the same places in the CRCP and BCO, and if the expansion and contraction of the CRCP and BCO were the same, there would be no stresses at the interface. However, even if the coefficients of thermal expansion of the BCO and CRCP concrete were the same, this would not be the case for the following two reasons:

1) The BCO is contracting from drying shrinkage, whereas the CRCP is no longer subject to drying shrinkage.
2) The BCO experiences greater temperature differentials than the CRCP because the BCO is exposed to the air and solar radiation, and the CRCP is insulated by the BCO.

As a result, when the ambient temperature is low, the BCO contracts, causing shear and tensile interface stresses between the BCO and CRCP (Figure 8.3).

Shrinkage and thermal contraction in the BCO, if great enough, may cause cracks in the BCO between reflective cracks (Figure 8.16). Interface stresses also develop at these cracks. In fact, the stresses at cracks in the BCO that are not reflective cracks will be higher because the uncracked CRCP is stiffer.

8.6.2 Observed Pavement and Overlay Strains

Early-age thermal and shrinkage strains have been observed in the field. In studies by Nagataki (Ref 96), laboratory tests and field tests of model concrete pavements were used to measure drying shrinkage and thermal strains.

Nagataki divided shrinkage strain into mean and warping strain. Mean shrinkage strain increased from approximately 35 microstrains at 15 days to 130 microstrains at 1 year. Warping strain increased from approximately 50 microstrains at 15 days to 160 microstrains at 1 year. Greater contraction due to daily temperature cycles was observed at the top of pavement rather than the bottom; this approached 200 microstrains. The observed distribution of restrained strain caused by daily temperature cycling and drying shrinkage is shown in Figure 8.17.

To calculate stresses, Nagataki adjusted the elastic modulus to account for creep and found that the highest tensile stress (approximately 2,900 kPa) occurred when the concrete was 30 to 50 days old.

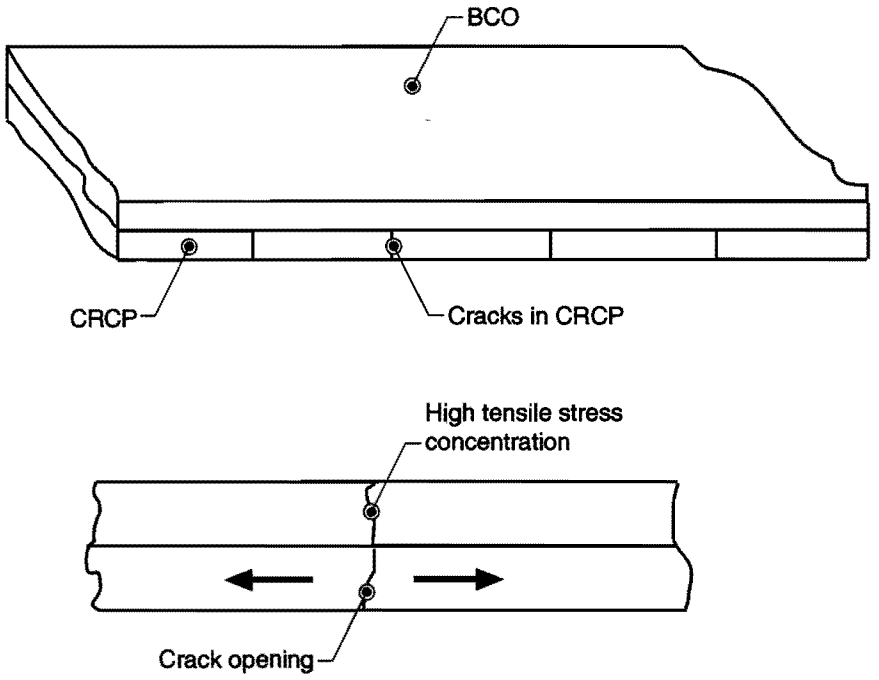

Figure 8.15 Reflective cracking

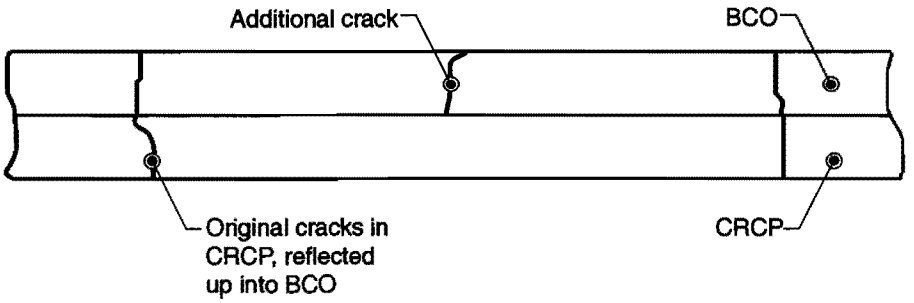

Figure 8.16 Crack forming in BCOs between reflective cracks

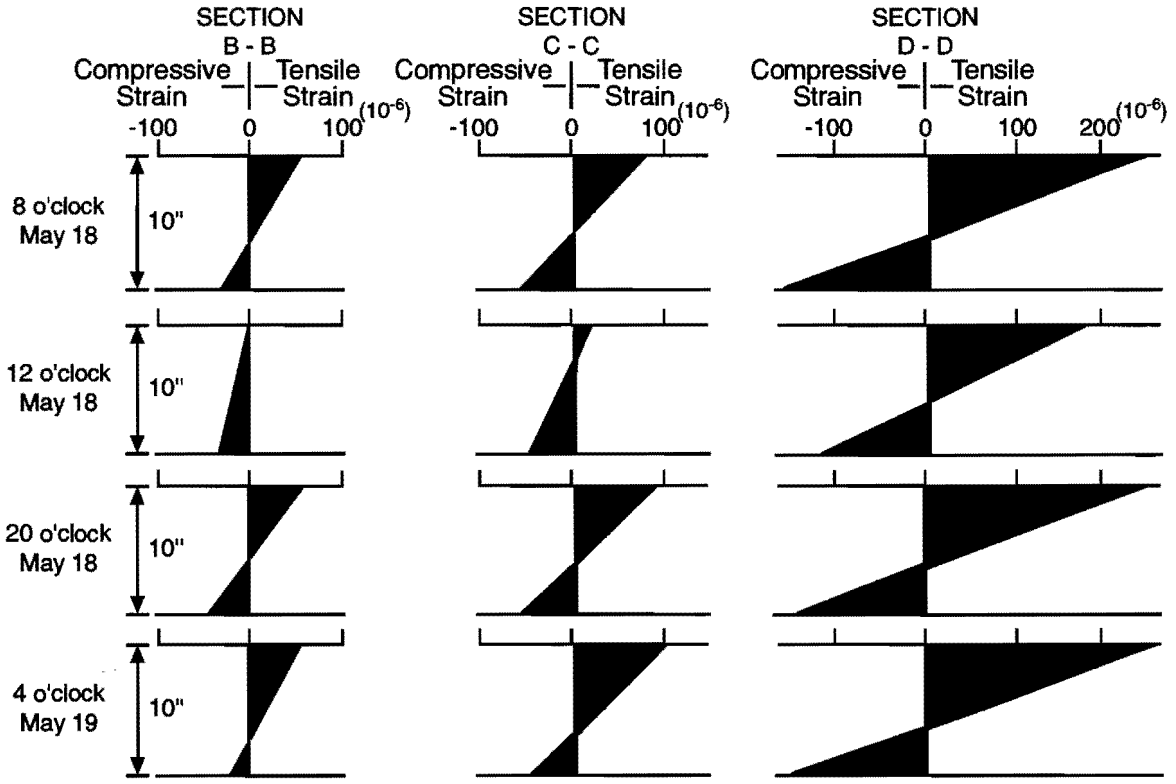

Figure 8.17 Distribution of restrained strain due to daily temperature cycle and drying shrinkage (Ref 96)

In the present study, strains of approximately 360 microstrains at the top of the BCO and 200 microstrains at the bottom were measured 6 to 8 hours after the concrete was cast at the location of the vibrating wire strain gauges, approximately 5 p.m. (Figure 6.14). The corresponding elastic modulus of the concrete at that time was approximately 20 to 25 GPa, based on SASW and extrapolation from compression cylinders (Table 6.18).

Using Equation 6.21 and assuming that the development of strain and modulus of elasticity is linear, this equates to tensile stress of 3,600 to 4,500 kPa at the top of the BCO, and 2,000 to 2,500 kPa at the bottom of the BCO. At the time the splitting tensile strength of the concrete was only 2,100 kPa (Table 6.2); therefore, it is easy to see why cracking occurred. The drop in strain at 5 p.m. on June 22 (Figure 6.14) may be due to a crack opening at a location a short distance from the strain gauge relieving the stress. This stress calculation, however, does not account for the effect of creep.

8.6.3 Modeling of Interface Stresses

Interface stresses may be calculated using the following algorithm:

1) Estimate moisture and temperature gradients in the BCO (Figure 8.18a).

2) Using moisture and temperature gradients, estimate the strain distribution in the BCO (Figure 8.18b).
3) Convert the strain distribution to stress distribution using Equation 8.19.

This procedure may be used to calculate interface stresses using finite element or boundary element methods. The segment of BCO and CRCP chosen for analysis should be between two consecutive cracks in the BCO. In the case of two reflected cracks, this is shown in Figure 8.19a. Because the problem is symmetrical in the longitudinal and transverse directions, only one quarter of the segment to be analyzed needs to be modeled (Figure 8.19b). The boundaries along the axes of symmetry are fixed against translation or rotation.

Calculation of stresses at concentrations at the corner may be easier with the boundary element method, since the finite element method may require an extremely fine mesh at that point (Ref 98). For a BCO crack occurring between reflective cracks, the CRCP at the crack should be fixed against rotation and longitudinal translation, but not against vertical translation (Figure 8.20).

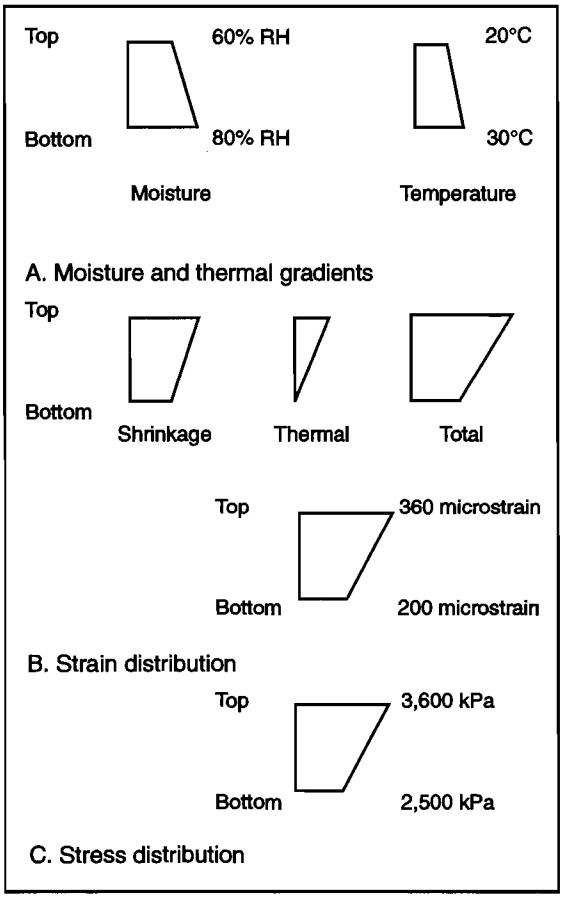

Figure 8.18 Strain and stress distribution

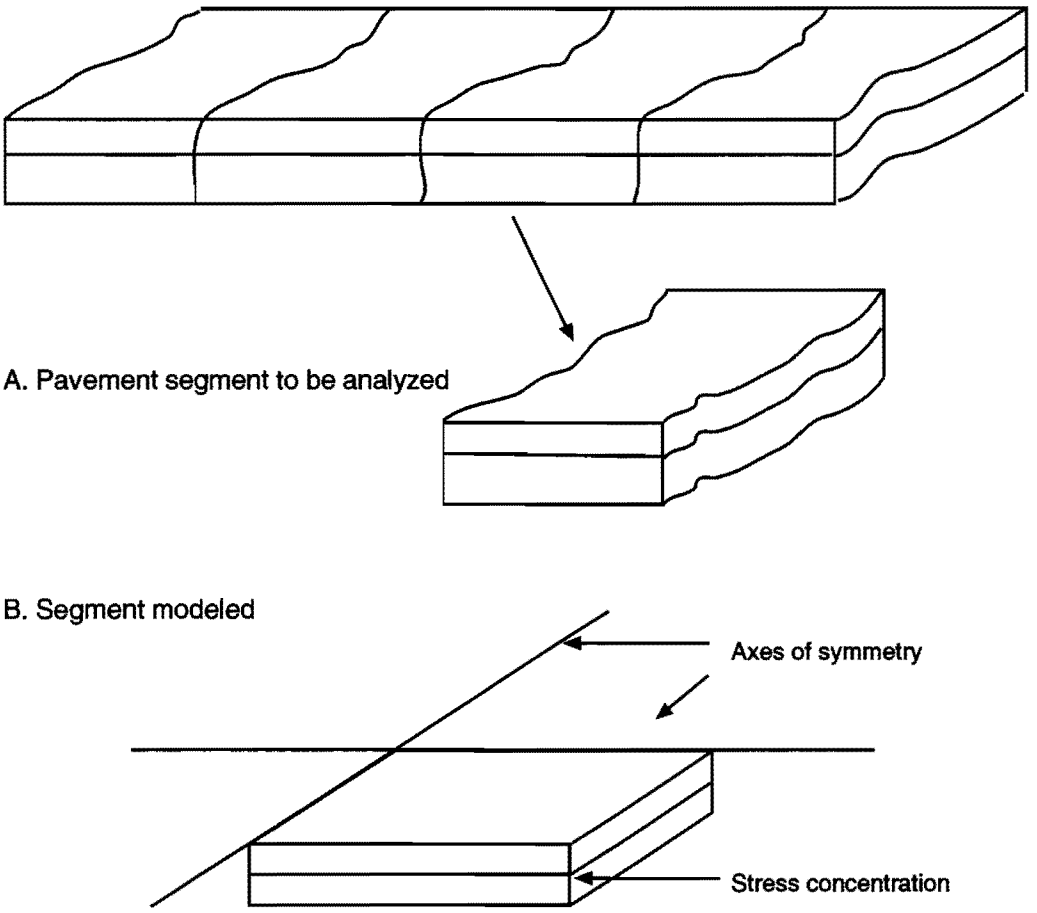

Figure 8.19 Modeling a segment of BCO and CRCP

Of course, the edge of the segment of CRCP adjacent to the next segment is not free as implied in Figure 8.19, but restrained by the reinforcing steel crossing the crack at middepth of the CRCP. The effect of this restraint will be to increase interface stresses. If the BCO is reinforced with steel bars or steel fibers, the reinforcement will reduce interface stresses.

8.6.4 Two-Dimensional Solutions

BCO contraction is clearly three dimensional, as may be seen in Figures 8.1 and 8.3. However, due to the difficulty of modeling the problem in three dimensions, most solutions have been two-dimensional.

Lundy, van Metzinger, et al., (Refs 4, 8, 33) used the two-dimensional finite element program NSLIP to calculate BCO interface stresses from shrinkage, thermal effects, and traffic loading. Shear stresses calculated were much lower than the shear and tensile bond strengths usually measured. The highest stresses predicted during these studies were only 220 kPa in shear and 960 kPa in tension under environmental conditions typical of Houston

(Ref 8). Since the concrete rapidly develops interface bond strengths higher than these values, delamination would have to occur very early in the life of the pavement if it were to occur at all.

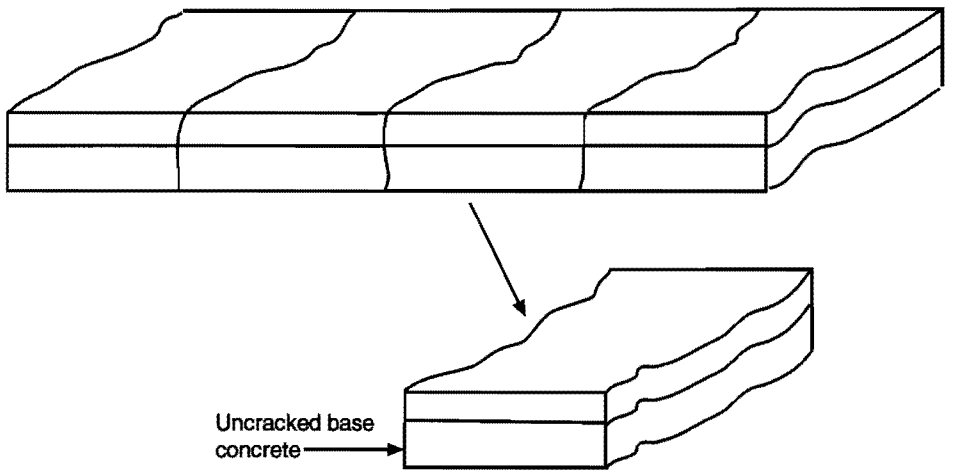

A. Pavement segment to be analyzed

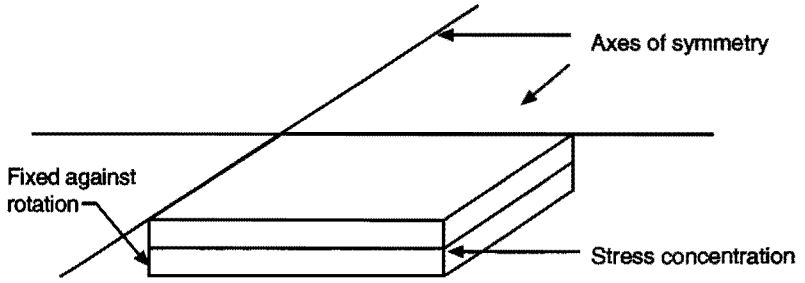

B. Segment modeled

Figure 8.20 Modeling interfaces at a BCO crack between reflective cracks

Choi (Ref 97) developed an analytical solution for interface stress development with polymer concrete overlays on portland cement concrete substrates. Choi's solution for an overlay thickness 45 percent of that of the base concrete, with both layers having the same modulus, and an imposed thermal strain in the interface of 500 microstrains, gave considerably higher stresses. The interface stresses were 1,700 kPa in tension and 3,000 kPa in shear. Furthermore, the stresses increase with increasing overlay thickness, so stresses in a 165 mm thick overlay would be even higher. On the other hand, the imposed shrinkage was more typical of polymer concrete, and it is highly unlikely that BCO strains due to the combination of shrinkage and thermal contraction could reach 500 microstrains.

To obtain stresses for higher or lower shrinkage strain, the stresses calculated in Ref 97 should be multiplied by the ratio of the actual strain to 500 microstrains. The solutions assume the same temperature exists in all layers of the base and overlay.

Choi's procedure is extremely useful for solving two-dimensional overlay problems when the base concrete is unrestrained. The stresses predicted by Choi are of the same order of magnitude as the strength of the bond layer. They are highly concentrated at the boundary and dissipate rapidly in the interior of the beam. These results suggest that delaminations are likely to occur, but are unlikely to propagate far from the boundary.

8.6.5 Prediction of Interface Stresses Using Fictitious Compressive Stress Distribution

Interface stresses may be calculated by modeling the tensile stresses within the BCO during BCO contraction (Figure 8.18) as compressive stresses imposed on the boundary of the BCO (Figure 8.21). Interface stresses and stresses in the CRCP will be of the correct sign and magnitude. Stresses in the BCO will be of the correct magnitude, but wrong sign (compressive rather than tensile).

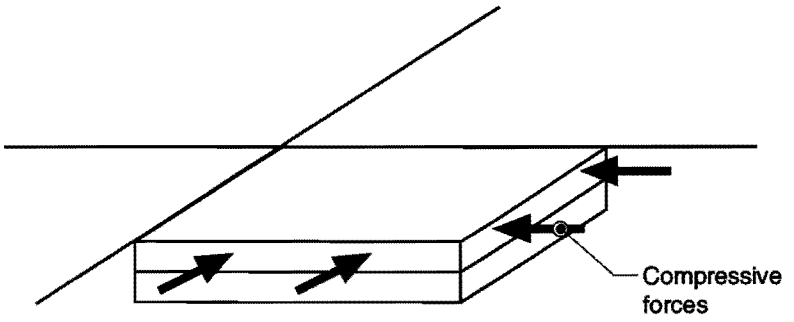

Figure 8.21 Modeling BCO contraction with a fictitious compressive force

Vertical displacements in the BCO will not be correct because the Poisson effect will cause dilation rather than contraction of the BCO, thus upward rather than downward displacements. However, since these deformations are not restrained, they do not induce stresses. The important results of the analysis will be interface stresses to determine if delamination occurs or progresses, and tensile strains in the BCO to determine if additional cracks form.

This allows the investigation of the potential effect of different reinforcement schemes on delamination. For example, if the contraction of the BCO is modeled by an equivalent compressive stress imposed on the boundary of the BCO, the reinforcement may be modeled by a tensile force imposed on the boundary (Figure 8.21). The reinforcing steel in the CRCP is modeled by a tensile force at the midpoint of the CRCP; uncracked CRCP

may be modeled by increasing the magnitude of the tensile force to account for the contribution of the concrete in tension.

8.6.5.1 Position of reinforcing steel bars in the BCO. The reinforcing steel in the BCO is modeled by a tensile force in the BCO. Positioning the reinforcing bars at the interface between the BCO and CRCP is the least effective position for resisting the upward curling of the CRCP; the most effective position would be at the top of the CRCP. However, this would add considerably to the cost and difficulty of construction.

8.6.5.2 Use of SFRC. Steel fibers should be modeled as a tensile stress distribution on the boundary of the BCO. The magnitude of the tensile stress depends upon the crack opening. As the crack width increases, the tensile stress carried by the steel fibers increases. Thus, steel fibers are more effective than reinforcing bars placed directly on the base concrete, because the fibers are better placed to resist the upward curling of the BCO.

8.6.6 Implications for Pavement Performance

The effects of cracking and delamination on pavement performance will be discussed in Chapter 9. Wide cracks with large movement increase the potential for delamination. At early ages, it is important to (1) promote the development of tensile and bond strength, and (2) reduce differential drying shrinkage and thermal strains between the BCO and CRCP.

CHAPTER 9. LONG-TERM PERFORMANCE OF BCOS

The purpose of placing a bonded concrete overlay (BCO) on continuously reinforced concrete pavement (CRCP) is to return the pavement to its original, or better, level of serviceability. The long-term performance of a BCO may be adversely affected by poor durability of concrete, delamination, and fatigue cracking. These problems are not independent; poor durability or delamination can greatly increase potential for fatigue cracking.

9.1 DURABILITY

Durability in concrete may be defined as resistance to physical attack, such as freezing and thawing, or chemical attack (Ref 94). Mechanisms of chemical attack include sulfate attack, alkali-aggregate reactions, and delayed ettringite formation. All of these mechanisms of attack require water; thus, concrete with low permeability is more durable. Concretes with low water-cement ratios have low permeability. Proper curing also makes concrete less permeable (Ref 48). Proper curing may reduce capillary porosity of concrete by 80 percent or more (Ref 99). All of these mechanisms can cause progressive destruction of a concrete pavement even in the absence of traffic loading (Ref 2). If concrete can get dry and stay dry, it will generally not have durability problems (Ref 100). However, with pavements this is impossible.

9.1.1 Freezing and Thawing

Concrete can be badly damaged by cyclic freezing and thawing. Water migrates into small voids in concrete, then freezes and expands, damaging the structure of the concrete and providing larger voids for further freezing (Refs 48, 72, 94).

Mather (Ref 100) has suggested that freeze-thaw damage will not occur if the environment is favorable, if there are no pores in the concrete to hold freezable water, if any pores with water are no more than 91 percent full, or if there is an adequate air void system.

Freeze-thaw resistance in concrete is primarily provided by air entrainment. In addition, lower water-cement ratios aid freeze-thaw resistance by making the concrete stronger and more resistant to cracking, and by decreasing the air void bubble spacing (Ref 48). Thus, it may be possible to reduce air entrainment for concretes with low water-cement ratios, which is useful because air entrainment may cause losses of 10 to 20 percent of concrete strength.

9.1.2 Sulfate Attack

Sulfates may attack concrete, with chemical reactions that convert monosulfoaluminate to ettringite. The reaction is expansive and causes internal cracking of the concrete. Ettringite is formed by the reaction of C_3A with sulfate ions supplied by the gypsum in cement. This occurs early in hydration before the expansion of the ettringite can damage the concrete. If the sulfate from the gypsum is consumed before the C_3A is totally hydrated, monosulfoaluminate is formed instead. If sulfates later attack the

monosulfoaluminate, ettringite is formed. Because the concrete has now hardened, the expansion of the ettringite cracks the hardened cement paste.

Sulfate attack is very often associated with exposure to seawater; however, when large amounts of clay are present in soil, the groundwater flowing through the soil may contain sulfates.

The water-cement ratio of the concrete, by influencing permeability, greatly affects susceptibility to sulfate attack. Also, cements with low amounts of C_3A, such as Type II or V cements, are effective in combating sulfate attack (Ref 48). Day (Ref 101) points out that the water-cement ratio of concrete should be kept to 0.45 or lower for sulfate resistant concrete, and the cement content should be at least 391 kilograms per cubic meter. Proper curing and consolidation, use of air-entraining admixtures, and use of a pozzolan to lower permeability also aid sulfate resistance. Day referred to a case study of a concrete slab built directly on silty clay with a high sulfate content that was beginning to disintegrate after only a few years in service.

9.1.3 Alkali-Aggregate Reactions

Some reactions between alkalis in hardened cement paste and certain aggregates form expansive products and damage concrete. The two main types are alkali-silica reactions and alkali-aggregate reactions (Refs 48, 94).

Alkali-silica reaction (ASR) occurs between alkali in cement and certain reactive forms of silica in aggregate, such as opal, silica glass, tridymite, and microcrystalline or highly strained quartz. These reactions may be prevented by avoiding these aggregates, using low alkali cements ($\leq$ 0.60 percent), or using low water-cement ratios to reduce permeability. Swamy and Al-Asali (Ref 102) investigated the engineering properties of concrete that were affected by alkali-silica reaction. The greatest effect was a loss of flexural strength, which would considerably affect the performance of pavements and BCOs.

In a similar manner, alkali-carbonate reactions occur with some dolomitic limestones. Possible remedies include not using the aggregate, using cement with no more than 0.40 percent alkali, and using a low water-cement ratio.

9.1.4 Delayed Ettringite Formation

Another recently documented form of pavement deterioration is delayed ettringite formation (DEF). In the past, DEF has been mistaken for ASR; however, use of scanning electron microscopes has revealed that the reaction products are more consistent with DEF than ASR (Ref 103). The mechanism is similar to sulfate attack.

Ettringite forms in plastic concrete without creating any problems. Normally, all of the available sulfates react with gypsum. If, however, sulfate later becomes available for reaction, the formation of ettringite after the concrete has hardened causes the damage.

Day (Ref 104) prefers the term secondary ettringite formation to DEF. He has pointed out that the phenomenon usually occurs either in precast concrete members cured at high temperatures or when cements with high sulfate and alumina contents are used. Mather (Ref 100) notes that cement manufacturers now recycle kiln dust back into the kiln, which may increase alkali and sulfate contents.

The problem has been observed in pavements in Iowa (Ref 103); however, to date it has not appeared in pavements in Texas. There does not as yet appear to be any consensus on how to write specifications to address the problem.

9.2 DELAMINATION

The processes by which delaminations initiate at early ages were discussed in Chapter Eight. To date, no delaminations initiating more than 48 hours after the BCO has been placed have been documented. The California study by Neal (Ref 20) measured the progress of delaminations in test overlays. That study identified cyclic heating and cooling as the main mechanism of delamination progression.

Another possible mechanism of delamination progression is ice lens formation, similar to the ice lenses observed in soils. This mechanism requires large voids and a supply of water to form the lenses (Ref 48). The prying action of ice lenses could easily spread delaminations. There are, however, no observations that directly support this hypothesis. Nevertheless, where conditions for ice lens formation are favorable, it would be prudent to ensure that the pavement is well drained.

A finite element study of the effect of overlay debonding in airports (Ref 105) found increases in pavement deflections of 19.4 to 33.9 percent with loss of bond. For a 152 mm thick overlay over 203 mm thick pavement, debonding also less to stress increases of 51 to 63 percent.

In general, where debonding has been observed in the field, it has been swiftly remedied, usually by removal and replacement of the overlay (Refs 20, 21, 34). As a result, progression of delamination under field conditions is not well understood, nor is the effect of traffic loading, if any, on delamination progression.

9.3 FATIGUE

Concrete pavements (rigid pavements) are designed to achieve a specified service life on the basis of the resistance of concrete to fatigue. A maximum stress in the pavement is calculated, and this is divided by the flexural strength (also called modulus of rupture) to calculate a stress ratio:

$$SR = \frac{\sigma}{f_t} \qquad \text{(Eq 9.1)}$$

where

SR = stress ratio,

σ = tensile stress, kPa, and

f_t = flexural strength of the concrete.

At stress ratios less than or equal to 0.50, the fatigue life of the concrete is assumed to be infinite. The allowable load repetitions decrease from 400,000 at a stress ratio of 0.51 to 650 at a stress ratio of 0.74 (the percentage stress increase discussed for delamination in Section 9.2), according to charts developed by the Portland Cement Association (Ref 2).

Thus, a 51 percent stress increase will, in theory, reduce pavement life from 400,000 loads to less that 650. Moreover, the greatest tensile stress may be in the BCO, leading to premature failure of the overlay. For a Boeing 727 loading in the example cited above (Ref 104), loss of bond with a 229 mm thick overlay over a 203 mm thick base concrete reduced allowable load repetitions from 6,000 to 267.

However, for a BCO-CRCP pavement, reaching the fatigue strength of the concrete may not necessarily lead to failure of the structure. If the base concrete is cracked, the steel in the CRCP can still take tensile stress (Figure 9.1). Therefore, because the steel can hold the crack closed to provide shear transfer, the pavement will not fail structurally until the steel fractures in fatigue. This implies that a BCO will add even more life to a CRCP than would be assumed based on current computer models, particularly if the stresses in the steel are low enough.

Furthermore, the high stresses calculated analytically assume that there is no composite action between the BCO and the CRCP. If only small areas of the BCO debond, the loss of pavement stiffness may not be great. This may account for the inability of the FWD to detect significant differences between bonded and unbonded areas in the present study.

If adhesion is lost, the interface will no longer be able to transfer tensile stresses. It will, however, still be possible to transfer shear stresses through interlock and friction. Thus, the assumption of no stress transfer across the interface, while conservative, is incorrect.

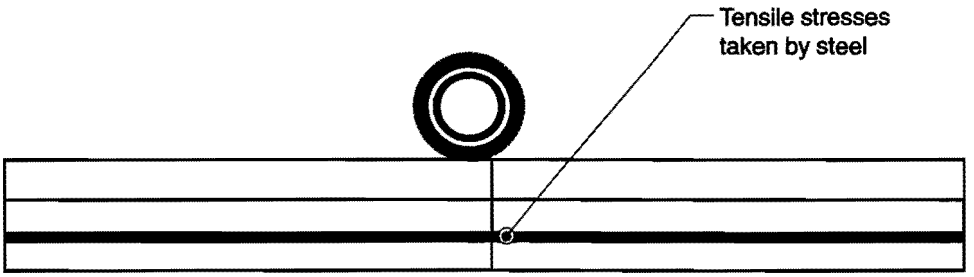

Figure 9.1 Fatigue of a BCO over CRCP

CHAPTER 10. MATERIALS SELECTION

Mather has suggested that "the way to obtain satisfactory concrete is to know what to avoid and to take proper steps to avoid it" (Ref 100). This is particularly applicable to bonded concrete overlays BCOs, although it should be pointed out that among the acceptable materials, some will lead to better performance than others.

10.1 CEMENTITIOUS MATERIALS

Cementitious materials should be selected on the basis of desired strength gain, limiting heat of hydration, and avoidance of durability problems.

10.1.1 Cement

For El Paso conditions Type II and V cements are desirable because they are resistant to sulfate attack and have lower heat of hydration than other cements. Strength gain and set time may be regulated with admixtures and mix proportioning.

Although expansive cement may seem to be useful for offsetting drying shrinkage, concrete with expansive cement is very difficult to design and control. Because expansive cement relies on ettringite formation for expansion, too little ettringite formation will result in less expansion than anticipated, while too much ettringite formation may damage the concrete (Ref 94). Therefore, it should not be used.

10.1.2 Fly Ash

Cement may be partially replaced with fly ash. Use of Class C fly ash leads to higher ultimate concrete strengths and lower permeability. Although heat of hydration is reduced with the use of fly ash, strength gain is also reduced. It has been shown (Ref 105) that fly ash with an available alkali content of 1.5 percent or less used to replace cement can prevent expansion due to alkali-aggregate reaction.

Concrete made with Class C fly ash has been shown to be more durable than concrete made without fly ash. Shrinkage is similar to or lower than that of concrete without fly ash. Workability is equal or better (Ref 107).

It is, however, important to ensure that the fly ash is of good and uniform quality (Ref 107). Fly ash costs less than cement, so that concrete made with fly ash is more economical.

Tikalsky and Carrasquillo (Refs 108, 109) found that concrete made with low calcium fly ash may is more sulfate resistant than ordinary concrete. Class F fly ash with low calcium provided excellent sulfate resistance. Class C fly ash with high calcium content does not (Ref 108).

Fly ash with less than 10 percent bulk CaO can be used without problems. Fly ash with more than 25 percent bulk CaO should not be used where sulfate attack is a concern. Between these limits, sulfate exposure tests should be performed (Ref 109).

10.1.3 Other Cementitious Materials

Silica fume has been investigated as a partial replacement for cement (about 5 percent) to decrease permeability for 32 mm thick bridge deck overlays. Permeability was reduced, and strength and durability were satisfactory (Ref 110). Polymer concretes have also been used. For thinner overlays or special conditions, these materials may merit consideration.

10.2 AGGREGATES

Aggregates should be selected on the basis of strength, modulus of elasticity, absence of high absorptivity and shrinkage, thermal coefficient, and susceptibility to alkali-aggregate reactions. However, since aggregates form the bulk of concrete, cost will often dictate which aggregates may be considered for construction in a given area.

10.2.1 Coarse Aggregate

As a minimum, coarse aggregate must be sound and non-reactive. The modulus of elasticity of the aggregate should be as high as possible, and the coefficient of thermal expansion should be as low as possible. Fortunately, the dense dolomitic limestone available in El Paso meets these criteria and has been shown to produce concrete with satisfactory strength. The maximum size of the aggregate (MSA) should be consistent with the production of high performance concrete, 12.5 mm to 19 mm, and it should be well graded to reduce paste demand. Aggregate should also be less than one-third to one-fourth of the thickness of the BCO; however, strength development will often require a smaller maximum size of aggregate.

Current TxDOT DC and CO overlay concrete specifications (Ref 49) mandate a 12.5 mm MSA. However, this may be too restrictive for thicker overlays. The present limitation is appropriate for overlay thicknesses up to 50 mm. For overlays 80 mm thick and thicker, 19 mm MSA should be allowed.

10.2.2 Fine Aggregate

Fine aggregate must also be sound and nonreactive. The gradation of the sand will affect mix proportioning.

10.3 ADMIXTURES

BCO concrete will require air-entraining admixtures for freeze-thaw resistance. Superplasticizers will probably also be necessary to produce workable high-performance concrete. In many high-performance concrete applications, superplasticizers are used to achieve slumps of 150 mm or more. These slumps are not necessary for BCO applications; however, superplasticizers may still be necessary to achieve any workability at all at very high cement factors and low water-cement ratios. By dispersing cement particles, superplasticizers also increase the rate of hydration of high-performance concretes. Low

superplasticizer dosages may be used at the batch plant, with more used at the job site to maintain or regain workability. In very hot weather, superplasticizers with retarder may be necessary to prevent premature setting of the concrete.

10.4 FIBERS

Although different fiber types and contents are normally compared on the basis of toughness, the toughness test may not say much about the performance of fibers in BCOs. However, it is satisfactory for use until either more field data are available, or more relevant tests are developed.

10.4.1 Steel

Bekaert Dramix® fibers have performed very well in toughness tests and field applications. At equivalent dosage rates they seem to be superior to other fibers that are currently available. It would be useful, however, to compare them directly to other fibers such as Novocon Xorex™ in BCO test sections.

10.4.2 Synthetic

Collated fibrillated polypropylene (CFP) fibers should be used for synthetic fiber reinforced concrete (SnFRC). Synthetic fibers and steel fibers may be combined to improve both early-age and long-term performance.

Recently, another type of synthetic fiber, nonmetallic or polyolefin, has been developed by 3M. Up to 1.6 percent by volume of these fibers may be used without the workability problems of steel fibers. Identical performance to both SnFRC at early ages and SFRC at later ages is claimed.

An experimental bridge deck overlay was cast in South Dakota using nonmetallic fibers. The concrete had a high cement content and low slump. The deck has had no cracking or debonding after nine months in service (Ref 111). These fibers may be suitable for expedited BCO construction.

CHAPTER 11. MIX DESIGN

This chapter discusses the proportioning of high-performance concrete for bonded concrete overlays (BCOs) using the absolute volume method (Refs 47, 51). In the absolute volume method of mix design, a water content is first selected based on workability requirements. Cementitious material content is then selected based upon the water-cement ratio. Next, the coarse aggregate content is selected. Finally, the fine aggregate volume is selected as the volume of a cubic meter of concrete minus the volume of the other mix constituents.

11.1 CEMENTITIOUS MATERIAL CONTENT

The cement content of the BCO concrete must be high enough to ensure that adequate paste is available to achieve bond at the interface (thus eliminating the need for a bonding agent) and to meet strength and permeability requirements. The requirement for paste may be reduced by using well-graded coarse aggregates.

TxDOT specifications (Ref 49) usually mandate a minimum cement content for concrete, such as 390 kilograms per cubic meter for CO class overlay concrete and 490 kilograms per cubic meter for DC class dense overlay concrete. Five field tests of high-performance concrete for rapid highway repairs used 516 kilograms per cubic meter (Ref 112). The El Paso full-scale test sections (Chapters 3 and 4) used 520 kilograms per cubic meter; however, the specifications only required 390 kilograms per cubic meter.

Concrete made with 520 kilograms of cementitious material per cubic meter has been shown to produce a BCO with excellent bond and high strength. It may be possible to produce high early strength BCO concrete with lower cementitious material contents, and research is currently underway to investigate this possibility. Until this is shown to be possible, the higher cementitious material contents should be used. Higher contents have the disadvantage of increasing heat of hydration. This may be mitigated by using Type V or II cements, fly ash replacement, use of retarders, lowering concrete temperatures, and proper environmental controls (e.g., constructing BCOs at night). Fly ash should be used to replace 35 percent of the cement by weight, to improve ultimate strength, reduce heat of hydration, and improve durability.

11.2 WATER–CEMENT RATIO

The water-cement ratio of the concrete is determined by strength and durability (permeability) requirements. Mather has suggested that the optimum water-cement ratio is 0.4 by weight, because at lower ratios there is not enough water to completely hydrate the cement (Ref 100). However, lower water-cement ratios may be desirable for faster hydration.

Concrete with a water-cement ratio of 0.4 or less has very low permeability. The BCO test section concrete had a water-cement ratio of 0.29. The TxDOT class CO and DC overlay specifications require water-cement ratios of 0.4 and 0.32, respectively (Ref 49). A minimum water-cement ratio of 0.35 should be specified for high early strength BCO concrete. This will achieve the desired early strength and durability requirements.

11.3 AGGREGATES

The main criterion for determining aggregate content is workability. Paving concretes usually use more coarse aggregate, as compared to fine aggregate, than concretes for other applications. Furthermore, high-performance concretes often use less fine aggregate because the higher paste content and fly ash help lubricate the concrete, reducing the importance of the fine aggregate in determining workability.

The paste requirement for a concrete may be reduced and workability improved by improving overall aggregate gradation as suggested by Shilstone (Ref 113). It may be useful to incorporate an intermediate aggregate, particularly when using steel fibers (Ref 73). A suggested combined aggregate gradation is shown in Figure 11.1. For the El Paso specification recommendations, a Grade 9 aggregate was used, which required the incorporation of an intermediate aggregate (Appendix A).

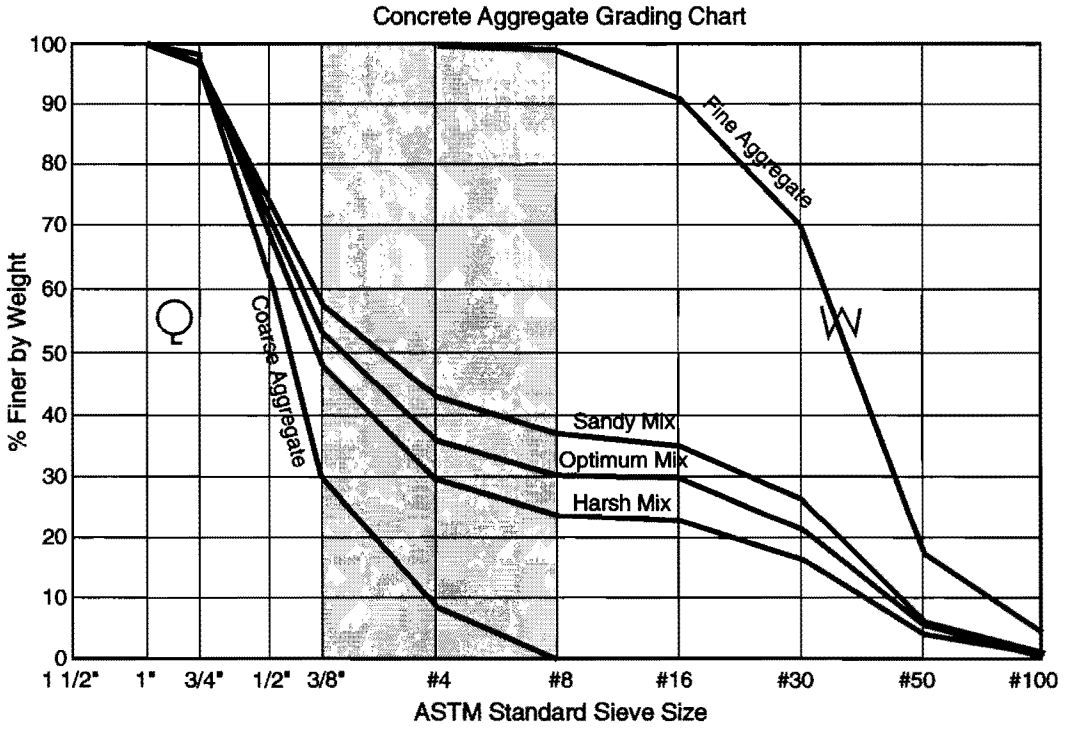

Figure 11.1 Suggested combined aggregate gradation (Ref 113)

11.4 ADMIXTURES

Previous research conducted for TxDOT has suggested that air contents as low as 3 percent may provide sufficient durability for high-performance concrete containing fly ash (Ref 50). Nevertheless, it is probably prudent to require an air content of at least 5 percent, given the severe exposure that may be experienced by BCOs in certain locations. Use of fly

ash may require greater dosages of air-entraining agent to achieve the same percentage of entrained air (Ref 107). An air content of 4 to 6 percent was used for the BCO test section concrete and recommended for El Paso construction.

Selection of the amount of superplasticizer must be based on trial batches. During this study, the quantity of superplasticizer required in the laboratory was much less than usual manufacturer recommendations. However, during field testing, it was necessary to add more superplasticizer at the job site. Also, use of a superplasticizer with retarder helped preserve workability until the concrete could be placed, without affecting strength development.

11.5 FIBER REINFORCEMENT

Steel fiber content should be selected on the basis of crack control and drying shrinkage cracking. Because synthetic fibers should be used in conjunction with reinforcing bars or steel fibers for crack control, only plastic and drying shrinkage need to be considered.

Normal steel fiber contents for steel fiber reinforced concrete (SFRC) are approximately 1 to 1.5 percent by volume. In this study, a fiber content of approximately 1.1 percent by volume was used for test sections. It is likely that certain fibers require higher contents than others for satisfactory results, e.g., a higher content of Novocon Xorex™ may be necessary, compared to Bekaert Dramix®. The research reviewed in Section 8.4 suggests that an optimum steel fiber content to reduce shrinkage cracking is 1.5 to 2 percent by volume. Bekaert has developed a chart to determine the appropriate steel fiber volume for replacement of welded wire fabric (WWF) with steel fibers. Other manufacturers can probably provide similar information.

Collated fibrillated polypropylene (CFP) fibers should be used at a minimum of 0.25 percent by volume, with significant benefits noted at 1 percent by volume. Little research is available on concrete made with both steel and synthetic fibers.

CHAPTER 12. RECOMMENDATIONS FOR IH-10 CONSTRUCTION

Based upon the full-scale test section results (Chapter Seven) and analysis of bonded concrete overlay (BCO) early-age behavior and long-term performance (Chapters Eight and Nine), recommendations were made for El Paso IH-10 construction. The full text of the specification recommendations is given in Appendix A. They are described below, as well as the test section recommendations.

12.1 EL PASO BCO CONSTRUCTION

The following recommendations were made for El Paso BCO construction specifications:

12.1.1 Surface Preparation

Either shotblasting or hydrocleaning should be allowed for surface preparation. Surface roughness must be at least 1.5 mm, as measured by the sand patch method. The surface must be prepared not more than 8 hours before paving.

12.1.2 Evaporation Rate Limits

The evaporation rate from the concrete should be limited to 1.0 $kg/m^2/hr$. If evaporation exceeds this limit for more than 20 minutes, fogging, wet mat, or similar curing methods should be required. The entire day's placement should be protected for a minimum of 36 hours.

12.1.3 Temperature Differential Limits

The maximum temperature differential in the 24 hours following BCO placement should be limited to 14°C. If the temperature differential is expected to exceed this value, the BCO should be placed no later than noon the preceding day and 18 hours before the expected low.

12.1.4 Night Paving

These measures should encourage the contractor to pave at night, but this should not be specifically required.

12.1.5 Concrete Temperature Limits

The concrete temperature should not exceed 29°C when the BCO is placed.

12.1.6 Membrane Curing

Membrane curing compound should be applied in two passes of at least 5.9 square meters per liter each. Care should be taken to ensure all sides of the tines are coated.

12.1.7 Opening to Traffic

The BCO may be opened to traffic when it is at least 12-hours old and has achieved a splitting tensile strength of at least 3,450 kPa.

12.1.8 Concrete

SnFRC should be used with reinforcing steel. The minimum cement content should be 390 kilograms per cubic meter, and the maximum water-cement ratio should be 0.35. A minimum 7-day splitting tensile strength of 6,200 kPa should be required.

12.1.9 Thermal Coefficient

The thermal coefficient of the concrete should be limited to a maximum of 9.9×10^{-6} mm/mm/°C, tested dry.

12.2 EL PASO BCO TEST SECTIONS

Recommended experimental variables were reinforcing steel, nails, polypropylene fibers, and steel fiber content (none, 30 kg/m^3, and 45 kg/m^3). Recommended test sections and proposed test section numbers are shown in Table 12.1.

Table 12.1 Test section recommendations

		Steel:	Yes			No		
		Steel Fibers:	None	30 kg/m^3	45 kg/m^3	None	30 kg/m^3	45 kg/m^3
Poly Fibers:	Nails:							
Yes	Yes		4				1	2
	No		5					
No	Yes		3					
	No							

A full factorial would require twenty-four test sections. With the sections recommended, direct comparisons may be made between:

1) Different steel fiber contents (Sections 1 and 2);
2) Steel fiber and reinforcing steel (Sections 1, 2, and 4);
3) With and without polypropylene fibers (Sections 3 and 4); and
4) With and without nails (Sections 4 and 5). Section 5 is a control, and is the same as the rest of the BCO.

Test sections should be located in the outer one and one-half lanes in the westbound direction. Transitions will have reinforcing steel. Test section locations are shown in Table 12.2.

Table 12.2 Test section locations

	Station	
Section	Starting	Ending
Transition	372+12.50	371+50
1	371+50	369+50
Transition	369+50	369+00
2	369+00	367+00
Transition	367+00	366+50
3	366+50	364+50
Transition	364+50	364+00
4	364+00	362+00
Transition	362+00	361+50
5	361+50	359+50

CHAPTER 13. SUMMARY, CONCLUSIONS, AND RECOMMENDATIONS

13.1 SUMMARY

This research has clearly demonstrated the feasibility and benefits of using high-performance concrete for high early strength bonded concrete overlays. Following the initial mix design, the bond and fatigue strength characteristics of the proposed concrete were investigated and documented. Using this information, eight different bonded concrete overlay designs and construction methods were tested under field conditions in El Paso. Average and total crack widths as well as bond strengths were used to compare the performance of the sections. Experimental variables for these sections were type of concrete (plain, synthetic fiber reinforced concrete [SnFRC], or steel fiber reinforced concrete [SFRC]), shear connectors, reinforcement, surface preparation, and day/night construction.

Eight different methods were used to attempt to detect and map delaminations. Some delaminations had been included in the test sections during construction. Although several methods proved to be able to detect delaminations, all were too slow to be used for quality control.

Next, early-age behavior and long-term performance of bonded concrete overlays (BCOs) were analyzed to interpret test section results and make recommendations for El Paso construction. Materials selection and mix design considerations were also reviewed. The El Paso specification recommendations were summarized and discussed.

13.2 CONCLUSIONS

The conclusions of this research are divided into the areas of surface preparation, shear connectors, materials selection and mix design, reinforcement, environmental effects and curing, and delamination detection and mapping. All components of the overlay system (surface preparation, BCO materials, and curing) must perform well if the overlay is to perform well.

13.2.1 Surface preparation

Proper surface preparation is critical to BCO performance.

1) Rougher surface preparation substantially improved performance of BCOs for the range of roughnesses investigated. The rougher surface preparation of Section 7 (mean roughness of 1.71 mm versus a mean roughness of 1.30 mm for the shotblasted sections) considerably reduced average crack width as well as delamination when compared to Section 6. The improvement occurred in spite of the fact that Section 7 reached similar temperatures.
2) Both shotblasting and hydrocleaning may be used to prepare existing pavement for BCO construction. These methods preferentially erode the paste and expose aggregate, leading to a rough surface with only sound material remaining on the surface of the substrate. However, hydrocleaning left debris on the pavement that

had to be removed with a pressure washer. The costs of the two methods were found to be similar.

3) No bonding agent should be used. Satisfactory bond was achieved without using any bonding agent.

13.2.2 Shear Connectors

Shear connectors function in a manner similar to rougher surface preparation in decreasing crack width and preventing delamination.

1) Shear connectors reduced average and total crack widths. Section 4, with shear connectors, had fewer cracks than and similar crack widths to Section 3, which was cast earlier but had no shear connectors. Section 5, with shear connectors, had smaller total crack width and considerably smaller average crack width than Section 6, without shear connectors. Section 5 reached higher temperatures similar to Section 6.
2) The effect of shear connectors in preventing delamination did not seem to have been as great as that of rougher surface preparation. The delamination indicated by coring in Section 5 (shear connectors) is similar to that in Section 6 (no shear connectors), whereas no delamination was found in Section 7 (rougher surface preparation, no shear connectors).

13.2.3 Materials Selection and Mix Design

High-performance concrete is an appropriate material for expedited BCO construction. BCO materials should be selected and proportioned for early strength development, minimum shrinkage, and minimum coefficient of thermal expansion. Concrete meeting the TxDOT DC overlay specification is appropriate for high early strength BCOs.

1) At early ages, the strengths achieved by the BCO test section concrete were considerably higher than required to carry stresses from traffic loading. However, analysis of the thermal and shrinkage strains in the BCO concrete indicates that bond and tensile strength are much more important at early ages. Therefore, high-performance concrete is important to prevent early cracking and debonding.
2) High-performance concrete improves long-term BCO performance by increasing durability and fatigue strength.
3) The high heart of hydration produced by high-performance concrete may be addressed by use of fly ash and lower-heat cements, such as Type II or Type V.
4) Concrete aggregates should be selected to result in concrete with a minimum coefficient of thermal expansion (less than or equal to 9.9×10^{-6} mm/mm/°C).

13.2.4 Reinforcement

Steel and synthetic fibers offer promising alternatives to reinforcing steel bars for BCO construction.

1) For thicker overlays (over 100 mm) steel fibers should replace reinforcing steel. Inclusion of steel fibers requires adjustments to the mix design, and batching and workability issues must be addressed. However, if the base concrete is not in good condition, some steel may be needed to hold wide reflective cracks together.
2) CFP synthetic fibers considerably reduce plastic shrinkage cracking and may be introduced into the concrete without adjusting the mix design. Nonmetallic (polyolefin) fibers may provide another alternative, but were not tested in this study.

13.2.5 Curing

Proper curing is essential.

1) For hot and dry conditions, the best curing alternative is wet mats. Field cylinders cured with wet mats and plastic developed considerably greater strength (20.2 MPa compressive strength versus 7.9 to 15.4 MPa for the other alternatives).
2) Membrane curing is acceptable under less severe conditions.
3) Under more severe conditions, night placement of the BCO may avoid excessive concrete heat buildup and evaporation.

13.2.6 Delamination Detection and Mapping

Detection of delamination is important for evaluating the performance of BCOs.

1) Delaminations occurred in at least three sections (Sections 5, 6, and 8), probably shortly after the BCO was cast. All delaminations occurred at intersections of cracks and edges or intersections of edges.
2) Where observed, delaminations did not progress more than 250 mm from the intersection of cracks and edges or intersections of edges.
3) None of the delamination detection methods tested was appropriate for rapid large-scale surveying of a newly cast BCO.
4) Coring may be used to determine overlay thickness, but should not be relied upon to verify bond, particularly for thicker (over 100 mm) overlays containing reinforcing steel.
5) Of the nondestructive delamination detection methods tested, impulse-response had the greatest success in detecting delaminations.

6) For cases where the delaminations significantly decrease the stiffness of the BCO, the falling weight deflectometer (FWD) and rolling dynamic deflectometer (RDD) should be able to sample the pavement rapidly for that loss of stiffness. The delaminations installed in the test sections probably did not decrease BCO stiffness enough for this equipment to detect them.

13.3 RECOMMENDATIONS FOR FUTURE RESEARCH

1) Analytical modeling should be undertaken to determine what compressive, tensile, and bond strengths are required of BCO concrete at early ages to prevent delamination and ensure satisfactory long-term performance. This information would be useful for refining specifications for BCO concrete. The effects of different curing methods and BCO thicknesses should be considered.
2) Analytical modeling should be used to investigate the progress of delamination with daily temperature cycling and traffic loading, and to determine the effect of partial delamination on long-term BCO performance.
3) The possibility of using shear connectors to achieve composite action between a BCO and base pavement without any other method of surface preparation should be considered. This method, if successful, would allow extremely rapid BCO construction.
4) Test sections should be used to investigate early-age behavior and long-term performance of BCOs made with different amounts and designs of steel and synthetic fibers.
5) Nondestructive delamination detection using impulse-response, FWD, and RDD should be investigated further, particularly for thinner overlays.

REFERENCES

1. McGhee, K. H., *Portland Cement Concrete Resurfacing*, Synthesis of Highway Practice 204, National Cooperative Highway Research Program, Washington, D. C., 1994.
2. Yoder, E. J., and Witczak, M. W., *Principles of Pavement Design*, Second Edition, John Wiley & Sons, New York, 1975.
3. Lundy, J. R., and McCullough, B. F., "Delamination in Bonded Concrete Overlays of Continuously Reinforced Pavement," *Proceedings, 4th International Conference of Concrete Pavement Design and Rehabilitation*, pp. 221–229, April 1989.
4. Lundy, J. R., McCullough, B. F., and Fowler, D. W., "Delamination of Bonded Concrete Overlays at Early Ages," Research Report 1205-2, Center for Transportation Research (CTR) The University of Texas at Austin, January 1991.
5. Dietert, M., McCullough, B. F., and Fowler, D. W., "Bonded Concrete Overlay (BCO) Experience and Project Selection," *Proceedings, Texas Regional Concrete Pavement Conference*, May 1995.
6. Whiting, D., Todres, A., Nagi, M., Yu, T., Peshkin, D., Darter, M., Holm, J., Andersen, M., and Geiker, M., *Synthesis of Current and Projected Concrete Highway Technology,* SHRP-C-345, Strategic Highway Research Program, National Research Council, Washington, D.C., 1993.
7. Allison, B. T., McCullough, B. F., and Fowler, D.W., "Feasibility Study for a Full-Scale Bonded Concrete Overlay on IH-10 in El Paso, Texas," Research Report 1957-1F, CTR, The University of Texas at Austin, January 1993.
8. van Metzinger, W. A., Lundy, J. R., McCullough, B. F., and Fowler, D. W., "Design and Construction of Bonded Concrete Overlays," Research Report 1205-4F, CTR, The University of Texas at Austin, January 1991.
9. Whitney, David P., Polykarpos, Isis, McCullough, B. F., and Fowler, David W., "An Investigation of Various Factors Affecting Bond in Bonded Concrete Overlays," Research Report 920-5, CTR, The University of Texas at Austin, June 1992.
10. "Fast Track Concrete — The Construction Material with a Conscience," Concrete Pavement Progress Special Report SR-809.3, American Concrete Pavement Association, Arlington Heights, Ill.
11. *Technical Bulletin 004.0 IT, Fast Track Concrete Pavements*, American Concrete Pavement Association, Arlington Heights, Ill., 1989.
12. Thompson, T., "Portland Cement Concrete Alternatives for Fast-Track Paving," Department of Civil Engineering, University of New Brunswick, Frederickton, New Brunswick, Canada, April 1993.

13. McGhee, K. H. and Ozyildirim, C., "Construction of Thin-Bonded Portland Cement Concrete Overlay Using Accelerated Paving Techniques," Report No. FHWA/VA-IR2, Virginia Transportation Research Council, January 1992.

14. Husbands, T. B., Malone, P. G., and Wakely, L. D., "Performance of Concretes Proportioned with Pyrament Blended Cement," Final Report CPAR-SL-94-2, Construction Productivity Advancement Research (CPAR) Program, U.S. Army Corps of Engineers Waterways Experiment Station, April 1994.

15. Okamoto, P. A., and Whiting, D., "Use of Maturity and Pulse Velocity Techniques to Predict Strength Gain of Rapid Concrete Pavement Repairs during the Curing Period," Paper No. 940122, 73rd Annual Meeting, Transportation Research Board (TRB), January 1994.

16. *Accelerated Rigid Paving Techniques, State of the Art Report,* Special Project 201, U.S. Department of Transportation, Federal Highways Administration, FHWA-SA-94-080, December 1994.

17. Cole, L. W., and Voight, G. F., "Fast-track concrete paving: More Than Just High-Early-Strength," pp. 32–35, *Concrete International*, May 1995.

18. Cole, L. W., and Okamoto, P. A., *Flexural Strength Criteria for Opening Concrete Roadways to Traffic*, Paper No. 950222, 74th Annual Meeting, TRB, January 1995.

19. Hutchinson, R. L., "Resurfacing With Portland Cement Concrete," *National Cooperative Highway Research Program Synthesis of Highway Practice 99*, TRB, December 1982.

20. Neal, B. F., "California's Thin Bonded PCC Overlay," Report No. FHWA/CA/TL-83-04, June 1983.

21. Temple, W. H., and Cumbaa, S. L., *Thin Bonded PCC Resurfacing*, Louisiana Department of Transportation and Development, Report No. FHQA/LA-85/181, July 1985.

22. Kailasananthan, K., McCullough, B. F., and Fowler, D. W., "A Study of the Effects of Interface Condition on Thin Bonded PCC Overlays," Research Report 357-1, CTR, The University of Texas at Austin, December 1984.

23. Bagate, M., McCullough, B. F., Fowler, D. W., and Muthu, M., "An Experimental Thin-Bonded Concrete Overlay Pavement," Research Report 357-2F, CTR, The University of Texas at Austin, November 1985.

24. Solanki, A. I., Fowler, D. W., and McCullough, B. F., "A Study of the Effect of Construction Variables on the Bond Behavior of CRCP Overlays," Research Report 457-4, CTR, The University of Texas at Austin, October 1987.

25. Suh, Y-C, Lundy, J. R., McCullough, B. F., and Fowler, D. W., "A Summary of Studies of Bonded Concrete Overlays," Research Report 457-5F, CTR, The University of Texas at Austin, November 1988.

26. Reilley, K., Saraf, C., McCullough, B. F., and Fowler, D. W., "A Laboratory Study of the Fatigue of Bonded PCC Overlays," Research Report 457-2, CTR, The University of Texas at Austin, September 1986.

27. American Society for Testing and Materials, *1994 Annual Book of ASTM Standards,* 1994.

28. Tayabji, S. D., and Ball, C. G., "Field Evaluation of Bonded Concrete Overlays," *Pavement Evaluation and Rehabilitation*, pp. 179–192, Transportation Research Record 1196, TRB, 1988.

29. Koesno, K., and McCullough, B. F., "Evaluation of the Performance of Bonded Concrete Overlay on Interstate Highway 610 North, Houston, Texas," *Pavement Evaluation and Rehabilitation*, pp. 201–211, Transportation Research Record 1196, TRB, 1988.

30. Koesno, K., and McCullough, B. F., "Evaluation of the Performance of the Bonded Concrete Overlay on Interstate Highway 610 North, Houston, Texas," Research Report 920-2, CTR, The University of Texas at Austin, December 1987.

31. Bagate, M., McCullough, B. F., and Fowler, D. W., "A Mechanistic Design for Thin-Bonded Concrete Overlay Pavements," Research Report 457-3, CTR, The University of Texas at Austin, September 1987.

32. Teo, K. J., Fowler, D. W., and McCullough, B. F., "Monitoring and Testing of the Bonded Concrete Overlay on Interstate Highway 610 North in Houston, Texas," Research Report 920-3, CTR, The University of Texas at Austin, February 1989.

33. van Metzinger, W. A., McCullough, B. F., and Fowler, D. W., "An Empirical-Mechanistic Design Method Using Bonded Concrete Overlays for the Rehabilitation of Pavements," Research Report 1205-1, CTR, The University of Texas at Austin, January 1991.

34. Chanvillard, G., Aitcin, P. C., and Lupien, C., *Thin Concrete Overlay with Steel-Fibre-Reinforced Concrete*, Paper No. 880666, 68th Annual Meeting, TRB, January 1989.

35. Ibukiyama, S., Kokubun, S., and Ishikawa, K., "Introduction of Recent Thin Bonded Concrete Overlay Construction and Evaluation of Those Performances in Japan," *Proceedings, 4th International Conference of Concrete Pavement Design and Rehabilitation*, pp. 193–203, April 1989.

36. Verhoeven, K., "Thin Overlays of Steel Fiber Reinforced Concrete and Continuously Reinforced Concrete, State of the Art in Belgium" *Proceedings, 4th International Conference of Concrete Pavement Design and Rehabilitation*, pp. 205–219, April 1989.

37. Marks, V. J., "A Fifteen Year Performance Summary of Fibrous PC Concrete Overlay Research in Greene County, Iowa," *Fifteen Year Report for Iowa Highway*

Research Board, Research Project HR-165, Iowa Department of Transportation, August 1989.

38. Marks, V. J., "Thin Bonded Portland Cement Concrete Overlay," Final Report for Iowa Department of Transportation Project HR-521, Federal Highway Project DTFH71-83-3502-IA-11, November 1990.
39. Harris, G., "Performance of a Nongrouted Thin Bonded PCC Overlay," Report No. HR-291, Iowa Department of Transportation, January 1992.
40. King, W. M., "Design and Construction of a Bonded Fiber Concrete Overlay of CRCP (Louisiana, Interstate Route 10, August 1990)," Report No. FHWA/LA-92/266, Louisiana Transportation Research Center, January 1992.
41. Campbell, R. L., "Overlays on Horizontal Concrete Surfaces: Case Histories," Technical Report REMR-CS-42, U.S. Army Corps of Engineers, Waterways Experiment Station, February 1994.
42. Calvert, G., Lane, O. J., and Anderson, C., *Thin Bonded Concrete Overlay with Fast Track Concrete,* Final Report for Project HR-531, Iowa Department of Transportation, November 1990.
43. Wade, D. M., Fowler, D. W., and McCullough, B. F., "Concrete Bond Characteristics for a Bonded Concrete Overlay on IH-10 in El Paso," Research Report 2911-2, CTR, The University of Texas at Austin, July 1995.
44. Rasmussen, R. O., McCullough, B. F., and Weissmann, J., "Development of a Bonded Concrete Overlay Computer-Aided Design System," Research Report 2911-1, CTR, The University of Texas at Austin, January 1995.
45. Choi, D. U., *An Experimental Investigation of Interface Bond Strength of Concrete Using Large Power-Driven Nails,* Dissertation Presented in partial fulfillment of the requirements for the degree of Doctor of Philosophy, The University of Texas at Austin, February 1996.
46. Huddleston, J. L., Fowler, D. W., and McCullough, B. F., "Effects of Early Traffic Loading on a Bonded Concrete Overlay," Research Report 2911-3, CTR, The University of Texas at Austin, September 1995.
47. Kosmatka, S. H., and Panarese, W. C., *Design and Control of Concrete Mixtures*, Portland Cement Association, Thirteenth Edition, 1992.
48. Mindess, S., and Young, J. F., *Concrete,* Prentice Hall, Inc., Edgewood Cliffs, New Jersey, 1981.
49. *Standard Specifications for Construction of Highways, Streets, and Bridges*, Texas Department of Transportation, 1995.
50. Ernzen, J. J., and Carrasquillo, R.L., "Resistance of High Strength Concrete to Cold Weather Environments," Research Report 481-7, CTR, The University of Texas at Austin, July 1992.
51. *ACI 211.1-81 Standard Practice for Selecting Proportions for Normal, Heavyweight, and Mass Concrete*, American Concrete Institute (ACI), 1980.

52. Rabalais, N., *Evaluation of Fiber Reinforced Concrete (Final Report)*, Louisiana Transportation Research, May 1991.

53. Zellers, R. C., "A Discussion of the Evolution of the Use of Synthetic Fiber as a Reinforcement for Concrete," Paper presented at Materials Symposium on Concrete for the 1990's, Ohio State University, April 13, 1994.

54. Temple, M., Meyer, A. H., and Fowler, D. W., "Evaluation of Fiber Reinforced Rapid-Setting Materials for Highway Repair," Research Report 311-5, CTR, The University of Texas at Austin, November 1984.

55. Menzel, C. A., "Causes and Prevention of Crack Development in Plastic Concrete," *Proceedings*, Portland Cement Association, Annual Meeting, 1954.

56. National Ready Mix Concrete Association (NRMCA), "Plastic Cracking of Concrete," *Engineering Information,* July 1960.

57. Lerch, W., "Plastic Shrinkage," *Journal of the American Concrete Institute*, Vol. 53, 1957.

58. Hover, K. C., "Evaporation of Surface Moisture: A Problem in Concrete Technology and Human Physiology," *Concrete in Hot Climates.*

59. Murray, F. W., "On the Computation of Saturation Vapor Pressure," *Journal of Applied Meteorology*, pp. 203–204, January 1967.

60. "Hot Weather Concreting-ACI 305R-91," *ACI Manual of Concrete Practice, 1994,* Part 2, American Concrete Association, 1994.

61. Bloem, D. L., *Plastic Cracking of Concrete,* Technical Information Letter No. 171, National Ready Mixed Concrete Association, July 1960.

62. Stokoe, K. H., Nazarian, S., Rix, G. J., Sanchez-Salinero, I., Sheu, J-C., and Mok, Y-J., "In Situ Seismic Testing of Hard-to-sample Soils by Surface Wave Method," *Proceedings,* American Society of Civil Engineers, Specialty Conference on Earthquake Engineering and Soil Dynamics II- Recent Advances in Ground Motion Evaluation, Park City, Utah, June 1988.

63. Nazarian, S., Stokoe, K.H. II, Briggs, R. C., and Rogers, R., "Determination of Pavement Layer Thicknesses and Moduli by SASW Method," *Pavement Evaluation and Rehabilitation,* pp. 133–150, Transportation Research Record 1196, TRB, 1988.

64. Sheu, J. C., Stokoe, K.H. II, and Roesset, J. M., "Effect of Reflected Waves in SASW Testing of Pavements," *Pavement Evaluation and Rehabilitation*, pp. 51–61, Transportation Research Record 1196, TRB, 1988.

65. Sansalone, M., and Carino, N. J., "Impact-Echo Method," *Concrete International,* April 1988.

66. Stokoe, K. H. II, and Bay, J. A., "Rolling Dynamic Deflectometer Testing at the El Paso Overlay Prototype Facility," Unpublished, February 20, 1996.

67. Hasan, S., Meyer, A.H., and Fowler, D. W., "Establishment of Acceptance Limits for 4-Cycle MSS and Modified Wet Ball Mill Tests for Aggregates Used in Seal Coats and HMAC Surfaces," Research Report 1222-1F, CTR, The University of Texas at Austin, November 1991.

68. "Standard Practice for Curing Concrete- ACI 308-92," *ACI Manual of Concrete Practice* 1994, Part 2, ACI, 1994.

69. Buch, Neeraj, and Zollinger, D. G., "Preliminary Investigation on Effects of Moisture on Concrete Pavement Strength and Behavior," Transportation Research Record 1382, pp. 26–31, 1993.

70. Tritsch, S. L., *Temperature Management of PCC Slabs,* Paper No. 950119, 74th Annual Meeting, TRB, January 1995.

71. Hughes, Barry P., and Mahmood, A. T., "Laboratory Investigation of Early Thermal Cracking of Concrete," *ACI Materials Journal*, pp. 164–171, May–June 1988.

72. Neville, A. M., *Properties of Concrete*, Third Edition, Pitman Publishing, Inc., Marshfield, Massachusetts, 1981.

73. Smith, Rick E., "The Mechanical Properties of Steel Fiber Reinforced Concrete," Paper prepared for a Materials Symposium on Concretes for the 1990's, Ohio State University, April 13, 1994.

74. Suprenant, Bruce, "Bonding New Concrete to Old," *Concrete Construction*, July 1988, pp. 676–680.

75. Emmons, Peter H., Vaysburd, Alexander M., *Performance Criteria for Concrete Repair Materials, Phase I*, Technical Report REMR-CS-47, U.S. Army Corps of Engineers, Waterways Experiment Station, April 1995.

76. Silfwerbrand, Johan, "Improving Concrete Bond in Repaired Bridge Decks," *Concrete International*, September 1990, pp. 61–66.

77. Wall, J. S., and Shrive, N. G., "Factors Affecting Bond Between New and Old Concrete," *ACI Materials Journal*, pp. 117–125, March–April 1988.

78. Shaeles, Cristos A., and Hover, Kenneth C., "Influence of Mix Proportions and Construction Operations on Plastic Shrinkage Cracking in Thin Slabs," *ACI Materials Journal*, November–December 1988, pp. 495–504.

79. "FORTA® CR® Three-Dimensional Fibrous Polypropylene Reinforcement for Concrete, FORTA Corporation.

80. Soroushian, Parvis, Mirza, Faiz, and Alhozaimy, Abdulrahman, "Plastic Shrinkage Cracking of Polypropylene Fiber-Reinforced Concrete Slabs," Transportation Research Record 1382, 1993, pp. 64–68.

81. Nanni, Antonio, Ludwig, Dennis A., and McGillis, Michael T., "Plastic Shrinkage Cracking of Restrained Fiber-Reinforced Concrete," Transportation Research Record 1382, 1993, pp. 69–72.

82. Hansen, Will, and Almudaiheem, Jamal A., "Ultimate Drying Shrinkage of Concrete-Influence of Major Parameters," *ACI Materials Journal,* pp. 217–223, May–June 1987.

83. Smadi, Mohammed M., Slate, Floyd O., and Nilson, Arthur H., "Shrinkage and Creep of High-, Medium-, and Low-Strength Concretes, Including Overloads," *ACI Materials Journal*, pp. 224–234, May–June 1987.

84. Sennour, Mohand L., and Carrasquillo, Ramon L., "Creep and Shrinkage Properties in Concrete Containing Fly Ash," Research Report 481–6, CTR, The University of Texas at Austin, November 1989.

85. Gardner, N. J., and Zhao, J. W., "Creep and Shrinkage Revisited," *ACI Materials Journal*, May–June 1993, pp. 236–246.

86. "Prediction of Creep, Shrinkage, and Temperature Effects in Concrete Structures-ACI 209R-92," *ACI Manual of Concrete Practice, 1994*, Part 1, ACI, 1994.

87. "Model Code for Concrete Structures," Comité Euro-International du Béton, April 1978.

88. Bazant, Z. P., Wittman, F. H., Kim, J. K., and Alou, F., "Statistical Extrapolation of Shrinkage Data- Part I: Regression," *ACI Materials Journal*, January–February 1987, pp. 20–34.

89. Bazant, Z. P., Kim, J. K., Wittman, F. H., and Alou, F., "Statistical Extrapolation of Shrinkage Data-Part II: Bayesian Updating," *ACI Materials Journal*, March–April 1987, pp. 83–91.

90. Shah, S. P., Karaguler, M. E., and Sarigaphuti, "Effects of Shrinkage-Reducing Admixtures on Restrained Shrinkage Cracking of Concrete," *ACI Materials Journal*, May–June 1992, pp. 289–299.

91. Chern, Jenn-Chaun, and Young, Chin-Huai, "Study of Factors Influencing Drying Shrinkage of Steel Fiber Reinforced Concrete," *ACI Materials Journal*, pp. 123–129, March–April 1990.

92. Padron, Isabel, and Zollo, Ronald F., "Effect of Synthetic Fibers on Volume Stability and Cracking of Portland Cement and Mortar, *ACI Materials Journal*, pp. 327–332, July–August 1990.

93. Grzybowski, Miroslaw, and Shah, Surendra P., "Shrinkage Cracking of Fiber Reinforced Concrete," *ACI Materials Journal*, March–April 1990, pp. 138–148.

94. Illston, J. M., Dinwoodie, J. M., and Smith, A. A., *Concrete, Timber, and Metals*, Van Nostrand Reinhold, 1979.

95. Emborg, Mars, and Bernander, Stig, "Assessment of Risk of Thermal Cracking in Hardening Concrete," *Journal of Structural Engineering*, Vol. 120, No. 10, October 1994, pp. 2893–2912.

96. Nagataki, Shigeyoshi, "Shrinkage and Shrinkage Restraints in Concrete Pavements," *Journal of the Structural Division, Proceedings of the American Society of Civil Engineers*, July 1970, pp. 1333–1358.

97. Choi, Dong Uk, *An Analytical Investigation of Thermally-Induced Stresses in Polymer Concrete-Portland Cement Concrete Composite Beams*, Thesis presented in partial fulfillment of the requirements for the degree of Master of Science, The University of Texas at Austin, May 1992.

98. Brebbia, C. A., *The Boundary Element Method for Engineers*, Pentech Press, 1984.

99. Senbetta, E., and Malchow, G., "Studies on Control of Durability of Concrete Through Proper Curing," *Concrete Durability, Katherine and Bryant Mather International Conference, Volume 1*, ACI SP-100, 1987, pp. 73–88.

100. Mather, Bryant, "Concrete in Transportation: Desired Performance and Specifications," Transportation Research Record 1382, 1993, pp. 5–10.

101. Day, Robert W., "Damage to Concrete Flatwork from Sulfate Attack," *Journal of the Performance of Constructed Facilities*, Vol. 9, No. 4, November 1995, pp. 302–310.

102. Swamy, R. N., and Al-Asali, M. M., "Engineering Properties of Concrete Affected by Alkali-Silica Reaction," *ACI Materials Journal*, September–October 1988, pp. 367–374.

103. Marks, Vernon J., Dubberke, Wendell G., *A Different Perspective for Investigation of PCC Pavement Deterioration,* Interim Report for Iowa DOT Research Project HR-2074, 74th Annual Meeting, TRB, January 23, 1995, Washington, D.C.

104. Day, Robert L., "The Effect of Secondary Ettringite Formation on the Durability of Concrete: A Literature Analysis," PCA Research and Development Bulletin RD108T, 1992.

105. Van Dam, Thomas, Blackmon, Eleanor, and Shahin, M. Y., "Effect of Concrete Overlay Debonding on Pavement Performance," Transportation Research Record 1136, 1987, pp. 119–129.

106. Carrasquillo, Ramon L., and Snow, Peter G., "Effect of Fly Ash on Alkali-Aggregate Reaction in Concrete," *ACI Materials Journal*, July–August 1987, pp. 299–305.

107. Tikalsky, P. J., Carrasquillo, P. M., and Carrasquillo, R. L., "Strength and Durability Considerations Affecting Mix Proportioning of Concrete Containing Fly Ash," *ACI Materials Journal,* November–December 1988, pp. 505–511.

108. Tikalsky, P. J., and Carrasquillo, R.L., "The Effect of Fly Ash on the Sulfate Resistance of Concrete," Research Report 481-5, CTR, The University of Texas at Austin, August 1989.

109. Tikalsky, P. J., and Carrasquillo, R. L., "Fly Ash Evaluation and Selection for Use in Sulfate Resistant Concrete," *ACI Materials Journal,* November–December 1993, pp. 545–551.

110. Ozyildirim, Celik, "Laboratory Investigation of Concrete Containing Silica Fume for Use in Overlays," *ACI Materials Journal*, January–February 1987, pp. 3–7.

111. Ramakrishnan, V., and Kakodkars, S., *Evaluation of Non-Metallic Fiber Reinforced Concrete in PCC Pavements and Structures*, Study SD 94-04 Interim Report, SD Department of Transportation Office of Research, September 1995.

112. Schemmel, John J., and Leming, Michael L., "Use of Higher-Performance Concrete for Rapid Highway Pavement Repairs: An Overview of Five Field Installations," Transportation Research Record 1382, 1993, pp. 20–25.

113. Shilstone, James M., Sr., "Concrete Mixture Optimization," *Concrete International*, June 1990, pp. 33–39.

APPENDIX A:

PROJECT 2911 RECOMMENDED SPECIFICATIONS

The following recommendations for special provisions to Items 360 and 421 were made.

SPECIAL PROVISION
TO
ITEM 360
CONCRETE PAVEMENT

For this project, Item 360, "Concrete Pavement" of the Standard Specifications is hereby amended with respect to the clauses cited below and no other clauses or requirements of this Item are waived or changed hereby.

Article 360.1. Description is voided and replaced by the following:

360.1 Description. This Item shall govern for the construction of portland cement concrete pavement and bonded concrete pavement overlay with or without monolithic curbs on a prepared subgrade, base course, or previously placed concrete pavement in accordance with the typical sections shown on the plans, the lines and grades established by the engineer and the requirements herein.

Article 360.4. Equipment is supplemented by the following:

(15) Existing Concrete Pavement Surface Preparation Equipment. Shotblasting equipment shall be power operated and shall be capable of propelling steel shot against the pavement surface in a uniform manner so that the entire concrete surface is uniformly prepared. The shotblasting equipment shall include means of collecting used shot that may be reused, and of collecting and disposing of dust. The shotblasting equipment shall be capable of removing all dirt, oil, paint, membrane cure compound, and other foreign material, as well as any laitance or loose concrete from the surface on which the new concrete is to be placed. Hydrocleaning equipment may be substituted for shot blasting equipment providing the required surface texture and cleanness can be achieved.

Article 360.6. Subgrade, Subbase and Forms, Subarticle (1) Preparation of Subgrade or Subbase is supplemented by the following:

Where shown on the plans, the entire existing concrete pavement surfaces to be overlaid with bonded concrete pavement shall be prepared by shotblasting or hydrocleaning. All dirt, oil, paint, membrane cure compound, laitance and loose concrete shall be removed from the existing surface. The size shot used in shotblasting shall be appropriate for blasting concrete. All foreign material remaining on the existing concrete pavement after operating the shotblasting equipment shall be removed by sweeping, air blasting, or other methods approved by the engineer. The entire surface shall be saturated surface dry and air blasted just prior to the paving operation.

To minimize the possibility of contamination of the cleaned surface, the bonded concrete paving operation shall begin within eight (8) hours following the shotblasting or hydrocleaning operation unless otherwise directed by the engineer. If for any reason the cleaned surface becomes contaminated, reblasting or recleaning shall be required.

The surface texture of the cleaned, blasted concrete pavement shall have a minimum texture depth of 1.52 mm as measured by Test Method Tex 436-A. The number and location of the tests will be as directed by the engineer.

Article 360.8.Concrete Mixing and Placing, Subarticle (3) Placing is supplemented by the following:

At those times when the evaporation rate exceeds 1.0 kilograms/square meter/hour for a period of time as specified by the engineer, or greater than 20 minutes, measures shall be taken to control the moisture content of the newly placed bonded concrete overlay. Fogging, wet mat curing, or other approved methods shall be used to control the moisture content. The entire day's placement shall be protected and the protection shall remain in place for 36 hours or until such time as directed by the engineer. These measures are in addition to the membrane curing required.

At those times when the difference in the ambient temperature at the time of placement versus the expected low temperature in a 24-hour period is expected to exceed 14°C, special measures shall be taken. The bonded concrete overlay shall be placed no later than 12 noon the preceding day or a minimum of 18 hours prior to the time the maximum temperature difference is expected. At those times when the difference in the ambient temperature at the time of placement verses the expected low temperature in a 24-hour period exceeds 14°C, the entire day's placement shall be protected by wet mat curing or other methods approved by the engineer. The protection shall remain in place for a minimum of 36 hours, or until such a time as directed by the engineer.

The contractor will not be restricted from paving at night.

The temperature of all paving concrete shall not exceed 29°C when placed.

There shall be no free water on the surface of the existing concrete at the time of the placement of the concrete for the bonded overlay pavement, but will be in an SSD condition.

Article 360.11.Curing, Subarticle (3) Membrane Curing. is voided and replaced by the following:

(3) Membrane Curing. After final finish and immediately after the free surface moisture has disappeared, the concrete surface shall be sprayed uniformly with a Type 2, Class A curing compound in accordance with Article 526.5 except that the membrane curing compound shall be applied in two applications of approximately 5.9 square meters per liter each. A metering device to measure the rate of application shall be required. Should the membrane be damaged

from any cause before the expiration of 72 hours after the final application, the damaged portions shall be repaired immediately with additional compound.

Special care shall be taken to insure that the sides of the tining groves are coated with curing compound.

Article 360.12.Protection of Pavement and Opening to Traffic, Subarticle (2) Opening Pavement to Traffic. is voided and replaced by the following:

(2) Opening Pavement to Traffic. The pavement shall be closed to all traffic, including vehicles of the contractor, until the last concrete placed is at least twelve (12) hours old and has been determined to meet either a splitting tensile strength of 2,100 kPa (350 psi) or a flexural strength of 3,800 kPa (550 psi).

At the end of this period the pavement may be opened for use by vehicles of the contractor or the public. Such opening, however, shall in no manner relieve the contractor from his responsibility for the work in accordance with Item 7, "Legal Relations and Responsibilities to the Public." On those sections of the pavement to be opened to traffic, all joints shall first be sealed and the pavement cleaned. Unless otherwise shown on the plans, stable material shall be placed against the pavement edges before permitting vehicles thereon.

Article 360.13. Deficient Pavement Thickness, (A) Coring. The first paragraph is voided and replaced by the following:

(A) Coring. To determine thickness acceptability, the contractor shall drill 100 mm minimum diameter cores after all required profile corrective work and prior to final acceptance. Locations of core tests will be selected by the engineer; however, the spacing interval for core tests, as specified herein, is to be maintained. The engineer will determine the core thickness by measurement of the cores in accordance with Test Method Tex-424-A. The contractor shall mark each core for identification as specified by the engineer. The thickness of cores removed from the bonded concrete pavement overlay will be measured by making four measurements on each core at the estimated line of bonding and averaging the four measurements. The measurements will be equally spaced around the periphery of the core.

Article 360.13. Deficient Pavement Thickness, (A) Coring. The first sentence of paragraph four is voided and replaced by the following:

One (1) core will be taken by the contractor at the location selected by the engineer in each unit.

Article 360.14. Ride Quality is voided and replaced by the following:

360.14. Ride Quality. Unless otherwise shown on the plans, ride quality will be required in accordance with special specification, "Ride Quality for Pavement Surfaces."

Article 360.15. Measurement, Subarticle (1) Measurement by the Square Yard. is voided and replaced by the following:

When provided by the plans, concrete pavement and bonded concrete pavement overlay will be measured by the square yard of surface area of completed and accepted work. The surface area will include that portion of the pavement slab extending beneath the curb. When concrete pavement is to be measured by the square yard and monolithic curb is required, measurements for "Monolithic Curb" will be by the linear foot complete in place.

Article 360.15. Measurement, Subarticle (3) is voided and replaced by the following:

(3) Ride Quality. Ride quality will be measured as described in special specification, "Ride Quality for Pavement Surfaces."

Article 360.16. Payment. is voided and replaced by the following:

The work performed and materials furnished in accordance with this Item and measured as provided under "Measurement" will be paid for at the adjusted unit price bid as provided under Article 360.13 for "Concrete Pavement" of the type, reinforcement and depth specified, and for "Monolithic Curb" of the type specified. This price shall be full compensation for furnishing, loading, unloading, storing, hauling and handling of all concrete ingredients, including all freight and royalty involved; for placing and adjusting forms, including supporting material or preparing track grade; for shot blasting or hydrocleaning for preparing concrete surfaces prior to the placement of bonded concrete pavement overlay; for furnishing and installing all reinforcing steel, polypropylene fibers, steel fibers; for installing anchorage nails or other shear reinforcement at the edges of the bonded pavement; for furnishing all material for sealing joints and placing longitudinal, expansion and weakened-plane joints, including all steel dowel caps and load transmission devices required; for mixing, placing, finishing, curing and sawing concrete; for cleaning and sealing concrete joints; and for all manipulations, labor tools, equipment and incidentals necessary to complete the work.

When surface Test Type-B, as specified in Item 585, "Ride Quality for Pavement Surfaces," is used, a bonus or deduction for each 0.16 km section of each travel lane will be calculated in dollars and cents.

SPECIAL PROVISION

TO

ITEM 421

PORTLAND CEMENT CONCRETE

For this project, Item 421, Portland Cement Concrete of the Standard Specifications is hereby amended with respect to the clauses cited below and no other clauses or requirements of this Item are waived or changed hereby.

Article 421.9. Quality of Concrete is supplemented by the following:

Concrete shall have a thermal coefficient less than 9.9 x 10^{-6} mm/mm/°C when tested according to Corps of Engineers Test Method for Coefficient of Linear Thermal Expansion CRD C 39-81. The following additional requirements shall also apply:

Steel studs shall be cast into specimens for determining length measurements.

Specimens shall have a minimum dimension at least three times the nominal size of the coarse aggregate.

Specimens shall have a minimum aspect ratio of 2:1.

Specimens shall be tested in a dry condition after curing a minimum of 28 days.

APPENDIX B:

TESTING AND MONITORING PLAN

1. Materials testing will be conducted before, during, and after test section construction.

2. Before construction, the quality of surface preparation shall be measured.

a. Purpose — To compare actual roughness to specified roughness, investigate variability of roughness, and correlate substrate roughness to subsequent BCO performance.

b. Methods and sampling frequency — four measurements on each test section using the Sand Patch Method or the Mini Texture Meter (MTM).

3. During construction, the following measurements will be made: development of splitting tensile strength, development of compressive strength, maturity, temperature gradient, pavement strains, weather data, and thermal coefficient. None of this testing shall supersede normal TxDOT sampling and testing or any supplemental testing carried out under the QC/QA program. Data gathered by TxDOT should be compared to data gathered by CTR.

a. Purpose — Development of splitting tensile strength will be used to investigate splitting tensile strength criteria for opening BCOs to traffic, to correlate splitting tensile to compressive strength, and to correlate splitting tensile strength with subsequent BCO performance. Development of compressive strength will be used to investigate compressive strength criteria for opening BCOs to traffic and to correlate compressive strength with subsequent BCO performance. Maturity data will be used to develop procedures to open BCOs to traffic based on maturity readings. Temperature gradients, pavement strains, weather data, and thermal coefficients will be used to calibrate Finite Element Models (FEM) to predict BCO behavior and performance. Weather data will also be used to provide warning to TxDOT and contractor personnel when evaporation limits may be exceeded.

b. Methods and sampling frequency —

i. Development of splitting tensile strength — cast fifteen 152 by 305 mm cylinders from each test section. Test two cylinders each at 12 hours, 24 hours, 3 days, 7 days, and 28 days. Test a third cylinder if the values are more than 5 percent from their mean.

ii. Development of compressive strength — cast eighteen 152 by 305 mm cylinders from each test section. Test two cylinders each at 12 hours, 24 hours, 3 days, 7 days, 28 days, and 56 days. Test a third cylinder if the values are more than 5 percent from their mean.

iii. Maturity — insert four thermocouples for a four-channel maturity meter into each test section (5 meters total).

iv. Temperature gradient — insert four thermocouples distributed through the depth of the BCO at one test point in each test section. It may be possible to use maturity meters for this (5 additional meters).

v. Pavement strains — insert vibrating wire strain gauges in each test section, depending on equipment availability.

vi. Weather data — sample at 30-minute intervals using the Campbell Scientific weather station

vii. Thermal coefficient — cast four specimens per test section with embedded steel studs to be tested at CMRG.

4. After construction, test section cracking and the surface texture of the newly constructed BCO will be measured, and cores will be taken. Sampling should also be undertaken with the FWD, supplemented by rebar sounding.

a. Purpose — Test section cracking will be measured to compare the different crack widths and spacings in the test sections and correlate cracking to subsequent BCO performance. Texture of the BCO will be measured to evaluate smoothness of BCO surface and correlate with performance. Cores will be taken to measure core pulloff strength and compare to cylinder splitting tensile and/or compressive strength. The FWD will be used to compare pavement stiffness among test sections and attempt to detect any delaminations. Delamination detection may be supplemented by rebar sounding.

b. Methods and sampling frequency —

i. Cracking — visually detect, mark, and measure cracks in the troweled strip along each test section. Cracking should be surveyed just after sunrise at 1, 3, 7, and 28 days after section construction

ii. Texture of BCO — the Mini Texture Meter should be run down each section.

iii. Cores — drill 100 mm cores, epoxy steel caps, and pull off with pulloff tester. Drill eight cores per test section.

iv. FWD — test in each test section every 10 m at all four heights. Store dynamic responses for possible analysis.

APPENDIX C:

RESULTS OF SASW AND IMPACT–ECHO TESTING

Appendix C: Results of SASW and impact-echo testing carried out immediately after casting the test sections. The symbols for "sasw deb" and "sasw bon" indicate that SASW predicted that those areas were debonded and bonded, respectively. The symbols for "ie bon" and "ie deb" indicate that impact-echo predicted that those areas were bonded and debonded, respectively.

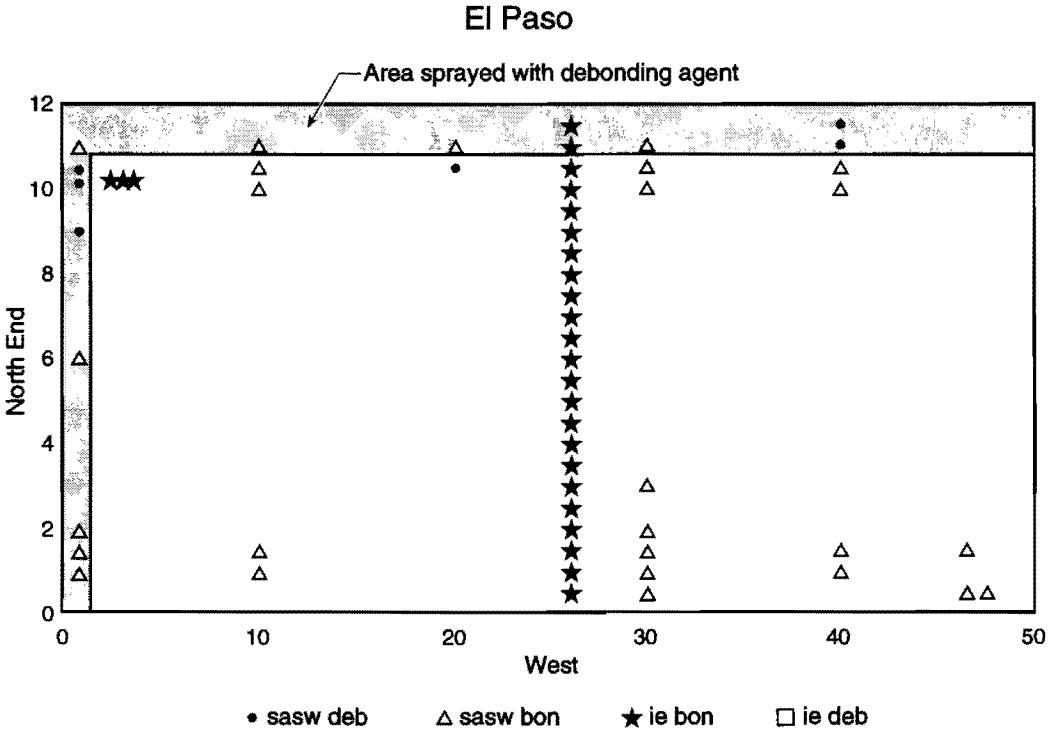

Figure C.1: Nondestructive Testing Results, Section 1

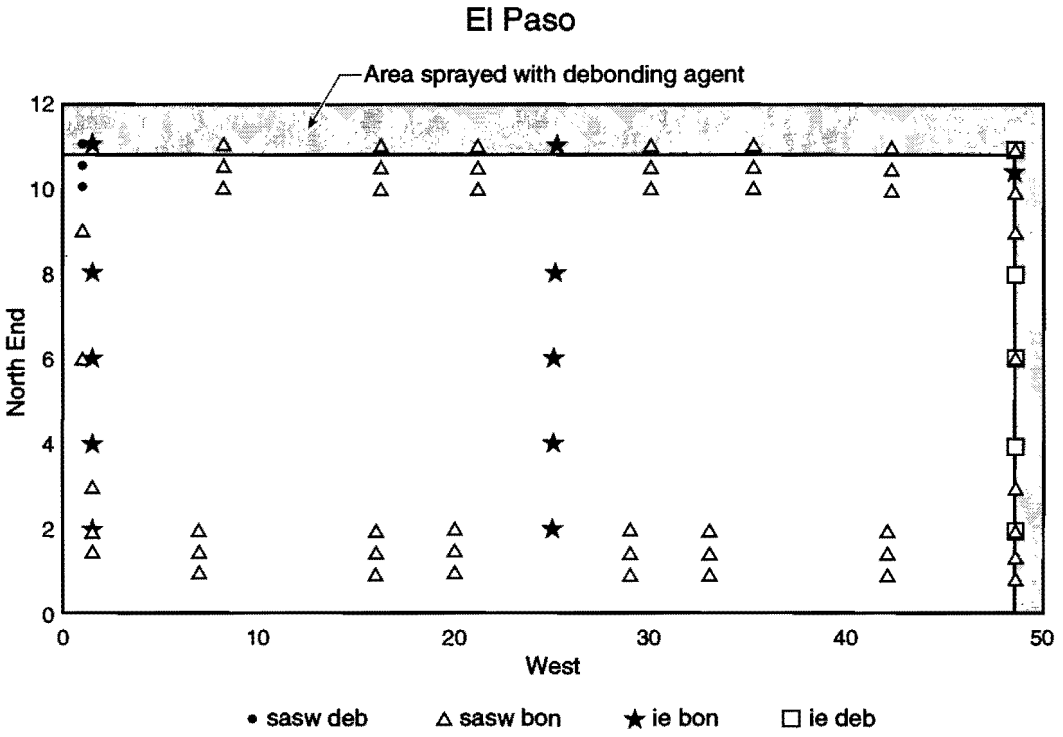

Figure C.2: Nondestructive Testing Results, Section 4

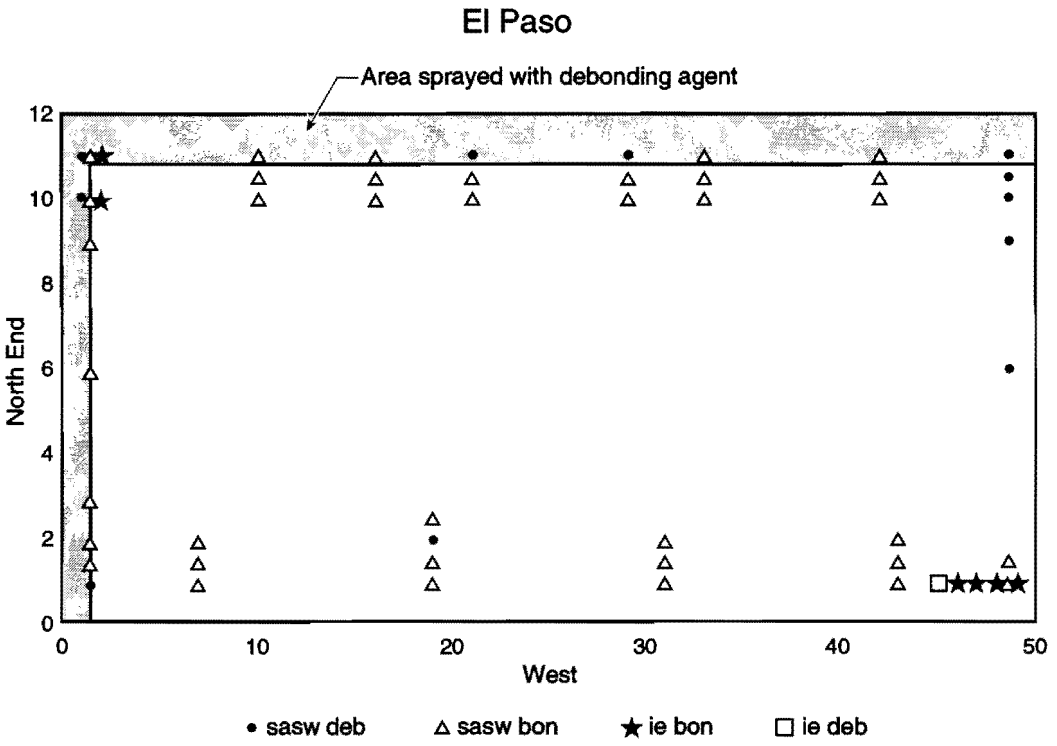

Figure C.3: Nondestructive Testing Results, Section 5

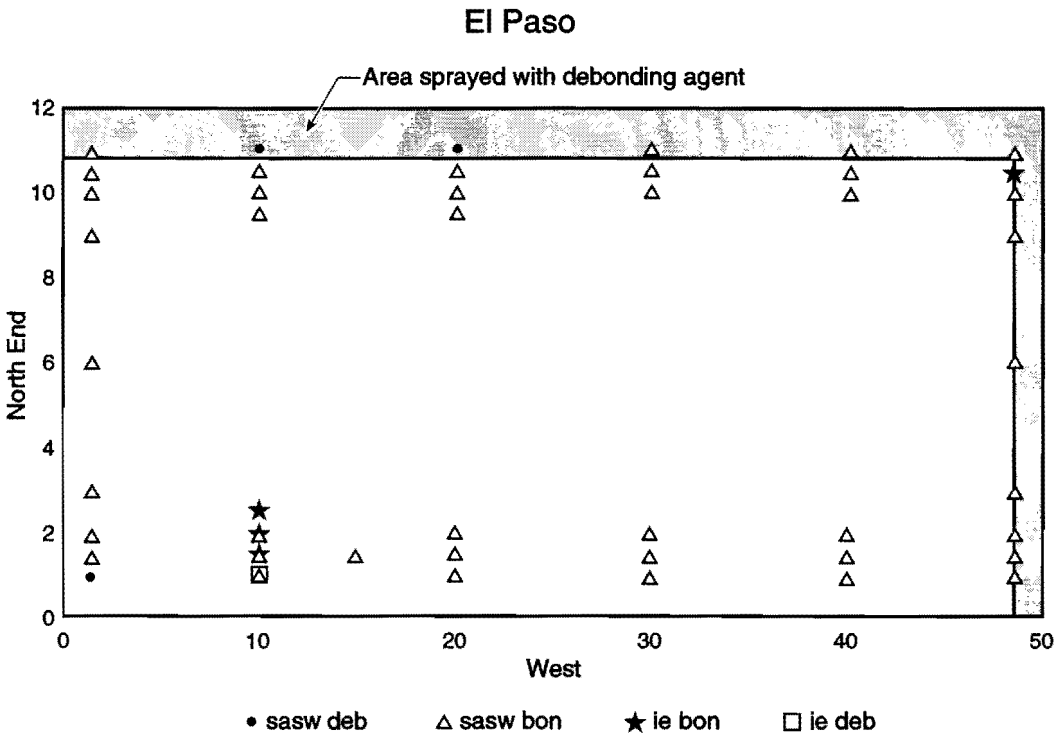

Figure C.4: Nondestructive Testing Results, Section 6

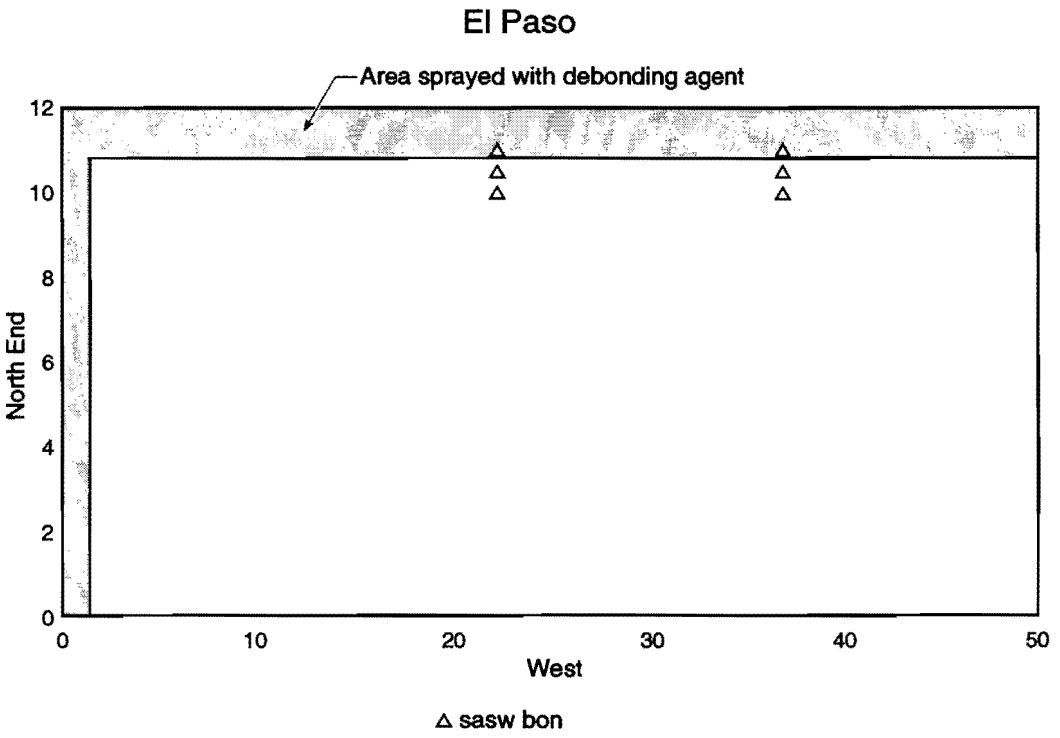

Figure C.5: Nondestructive Testing Results, Section 7

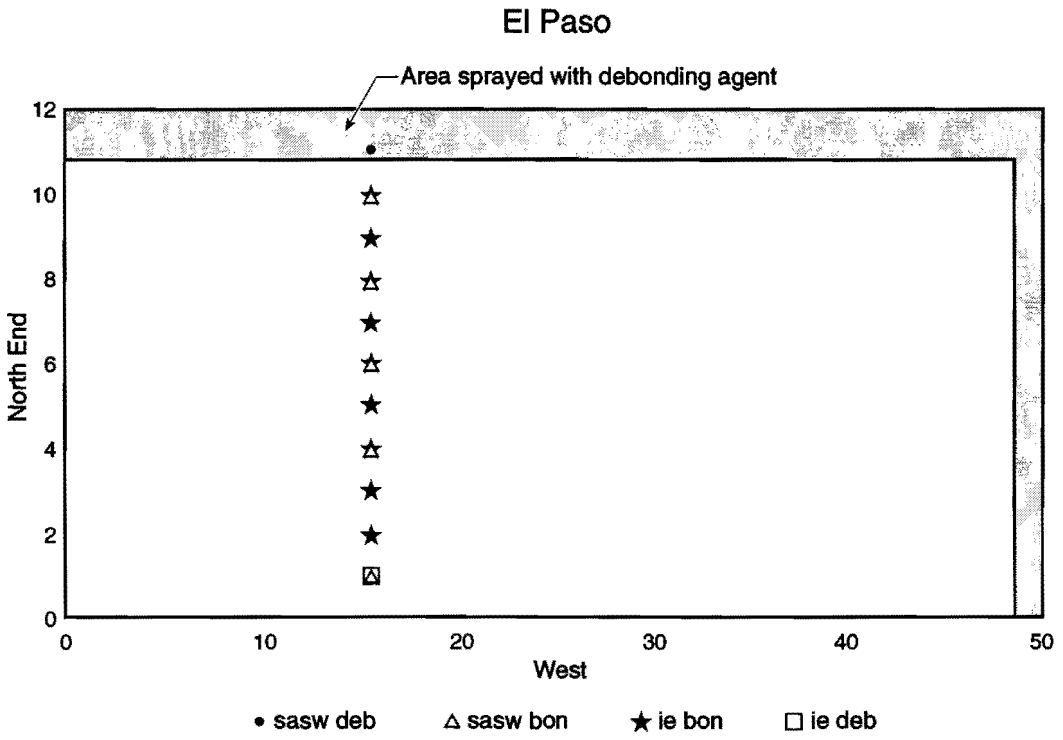

Figure C.6: Nondestructive Testing Results, Section 8

APPENDIX D:

LIST OF ACRONYMS

AASHTO	American Association of State Highway and Transportation Officials
ACI	American Concrete Institute
ACPA	American Concrete Pavement Association
ARAN	Automated Road Analyzer
ASTM	American Society for Testing and Materials
BCO	Bonded Concrete Overlay
BCOCAD	Bonded Concrete Overlay Computer Aided Design
CFP	Collated Fibrillated Polypropylene
COV	Coefficient of Variation
CTB	Cement Treated Base
CTR	Center for Transportation Research
CRC	Continuously Reinforced Concrete
CRCP	Continuously Reinforced Concrete Pavement
DOCter	Defect Orientation Confirmation Tester
ESAL	Equivalent Single Axle Load
FHWA	Federal Highways Administration
FWD	Falling Weight Deflectometer
HES	High Early Strength
JCP	Jointed Concrete Pavement
NCHRP	National Cooperative Highway Research Program
PBC	Pyrament Blended Cement
PCC	Portland Cement Concrete
RDD	Rolling Dynamic Deflectometer
RPRDS	Rigid Pavement Rehabilitation Design System
SASW	Spectral Analysis of Surface Wave
SFRC	Steel Fiber Reinforced Concrete
SHRP	Strategic Highway Research Program
SnFRC	Synthetic Fiber Reinforced Concrete
SRG	Siliceous River Gravel
TBCO	Thin Bonded Concrete Overlay
TxDOT	Texas Department of Transportation
WWF	Welded Wire Fabric